THE UNIVERSITY of KANSAS CENTER FOR RESEARCH, INC.
2291 Irving Hill Drive-Campus West
Lawrence, Kansas 66045

Design, Analysis and Control of Large Transports so that Control of Engine Thrust can be Used as a Back-up of the Primary Flight Controls

Final Technical Report
Grant # NAG 2-789

Prepared for
National Aeronautics and Space Administration
Ames Research Center
Moffett Field, California

Jan Roskam, Principal Investigator
Deane E. Ackers Professor of Aerospace Engineering
University of Kansas Center for Research, Inc.
Flight Research Laboratory
2291 Irving Hill Road
Lawrence, Kansas 66045

April 1995

Gerren, Donna S. (Ph.D., 1995)

Department of Aerospace Engineering, University of Kansas

Design, Analysis, and Control of a Large Transport Aircraft Utilizing Selective Engine Thrust as a Backup System for the Primary Flight Controls

A propulsion controlled aircraft (PCA) system has been developed at NASA Dryden Flight Research Center at Edwards Air Force Base, California, to provide safe, emergency landing capability should the primary flight control system of the aircraft fail.

As a result of the successful PCA work being done at NASA Dryden, this project investigated the possibility of incorporating the PCA system as a backup flight control system in the design of a large, ultra-high capacity megatransport in such a way that flight path control using only the engines is not only possible, but meets MIL-Spec Level 1 or Level 2 handling quality requirements.

An 800 passenger megatransport aircraft was designed and programmed into the NASA Dryden simulator. Many different analysis methods were used to evaluate the flying qualities of the megatransport while using engine thrust for flight path control, including:

- Bode and root locus plot analysis to evaluate the frequency and damping ratio response of the megatransport
- analysis of actual simulator strip chart recordings to evaluate the time history response of the megatransport
- analysis of Cooper-Harper pilot ratings by two NASA test pilots.

Some of the design variables which were investigated included engine location and engine time constant.

Analysis of these data showed that engine location did not appear to be as important a parameter as the time required for the megatransport/PCA system to achieve the commanded input. In looking at the MIL-Spec flying qualities requirements for large transport aircraft, the megatransport/PCA system satisfied Level 1 flying quality requirements based upon the frequencies, damping ratios, and time constants of the longitudinal and lateral-directional modes. In addition, both project test pilots consistently rated the megatransport/PCA system either Level 1 (test pilot B) or Level 2 (test pilot A) on the Cooper-Harper pilot rating scale.

The megatransport/PCA system fell short of satisfying Level 1 requirements, however, for the time required for the aircraft to achieve a 30 degree bank angle (Level 2 requirements were satisfied) and the time for the aircraft to respond to a control input (Level 3 requirements were not met).

ACKNOWLEDGEMENTS

I would first like to thank my advisor, Dr. Jan Roskam, and my committee members, Dr. David Downing, Dr. Saeed Farokhi, Dr. Edward Lan, Dr. Francis Thomas, and Mr. Bill Burcham for their support of this work.

I would next like to thank the personnel of NASA Dryden Flight Research Center for not only making it possible for me to perform my research work at that facility, but also for the assistance and friendship given me during my eighteen months there.

Many thanks go to Bill Burcham for being my sponsor at NASA Dryden and to Einar Enevoldson and Gordon Fullerton for contributing their time and effort by participating as the project test pilots.

My thanks to the propulsion and performance branch, without whose assistance this work would not have been possible - Lauren Ford, Kimberly Ennix, Tim Conners, and Kevin Walsh for their help with engine performance; Trindel Maine for her assistance as system administrator in helping me to utilize the various workstations and programs; Dr. Stephen Corda for his help with ground effects; Lisa Neufeld for all her administrative assistance; and most especially Gerard Schkolnik, Peter Schafer, John Orme, and Glenn Gilyard for their invaluable help with control system design, analysis, and testing.

Outside the propulsion and performance branch, my thanks to Alex Sim for his help with aerodynamics; John Burken for his assistance with turbulence models and frequency analysis methods; Jeanette Le, Tom Wolf, Marlin Pickett, and Martha Evans for their help in teaching me to program and operate the

NASA Dryden simulator; Dave Rait and Rich Wheaton for coming to my rescue when the simulator malfunctioned; library staff Rita Romanick and Dennis Ragsdale for their help in procuring numerous reference materials; and my posthumous thanks to NASA Dryden chief engineer and my friend, Milt Thompson, for his support and encouragement.

I would also like to thank the staff in the Aerospace Engineering Department and the Dean's Office in the School of Engineering at the University of Kansas for their administrative assistance.

Many thanks to my family and friends for their patience and understanding during the completion of this degree and to my parrot, Topper, for keeping a smile on my face even during the worst of times.

Finally, I would like to dedicate this dissertation to my loving husband and best friend, Dr. Richard A. Gerren. This work would most certainly have not been possible without his encouragement and understanding. The continual support, advice, and help he has given me throughout this entire endeavor can never be adequately acknowledged or my thanks adequately expressed. Thank you, Rick.

TABLE OF CONTENTS

LIST OF SYMBOLS

Symbol	Definition	Dimension
A	Area	ft^2
A, AR	Aspect ratio	---
alpha	Angle of attack	deg or rad
b	Span	ft
C, c	Chord	ft
$\bar{c}$	Mean aerodynamic chord	ft
C.G., c.g.	Center of gravity	---
C_D	Drag coefficient	---
$C_{D_{BASE}}$, C_{D_o}	Drag coefficient for zero angle of attack and zero longitudinal control surface deflection	---
C_{D_u}	Variation of drag coefficient with speed	---
C_{D_α}	Variation of drag coefficient with angle of attack	rad^{-1}
$C_{D_{\delta E}}$	Variation of drag coefficient with elevator angle	rad^{-1}
$C_{D_{\delta H}}$	Variation of drag coefficient with stabilizer angle	rad^{-1}
CGR	Climb gradient	rad
C_{ℓ_p}	Variation of rolling moment coefficient with roll rate	rad^{-1}
C_{ℓ_r}	Variation of rolling moment coefficient with yaw rate	rad^{-1}

C_{ℓ_β}	Variation of rolling moment coefficient with sideslip angle	rad^{-1}
$C_{\ell_{\delta_A}}$	Variation of rolling moment coefficient with aileron angle	rad^{-1}
$C_{\ell_{\delta_R}}$	Variation of rolling moment coefficient with rudder angle	rad^{-1}
C_L	Lift coefficient	----
$C_{L_{BASE}}$	Lift coefficient for zero angle of attack and zero longitudinal control surface deflection	----
C_{L_q}	Variation of lift coefficient with pitch rate	rad^{-1}
C_{L_u}	Variation of lift coefficient with speed	----
C_{L_α}	Variation of lift coefficient with angle of attack	rad^{-1}
$C_{L_{\dot{\alpha}}}$	Variation of lift coefficient with rate of change of angle of attack	rad^{-1}
$C_{L_{\delta E}}$	Variation of lift coefficient with elevator angle	rad^{-1}
$C_{L_{\delta H}}$	Variation of lift coefficient with stabilizer angle	rad^{-1}
C_m	Pitching moment coefficient	----
C_{m_q}	Variation of pitching moment coefficient with pitch rate	rad^{-1}
C_{mT}	Thrust pitching moment coefficient	----
C_{mT_α}	Variation of thrust pitching moment coefficient with angle of attack	----
C_{mT_u}	Variation of thrust pitching moment coefficient with speed	----
C_{m_u}	Variation of pitching moment coefficient with speed	----

C_{m_α}	Variation of pitching moment coefficient with angle of attack	rad^{-1}
$C_{m_{\dot{\alpha}}}$	Variation of pitching moment coefficient with rate of change of angle of attack	rad^{-1}
$C_{m_{\delta E}}$	Variation of pitching moment coefficient with elevator angle	rad^{-1}
$C_{m_{\delta H}}$	Variation of pitching moment coefficient with stabilizer angle	rad^{-1}
C_{n_p}	Variation of yawing moment with roll rate	rad^{-1}
C_{n_r}	Variation of yawing moment with yaw rate	rad^{-1}
C_{nT_β}	Variation of thrust yawing moment with sideslip angle	rad^{-1}
C_{n_β}	Variation of yawing moment with sideslip angle	rad^{-1}
$C_{n_{\dot{\beta}}}$	Variation of yawing moment with rate of change of sideslip	rad^{-1}
$C_{n_{\delta A}}$	Variation of yawing moment with aileron angle	rad^{-1}
$C_{n_{\delta R}}$	Variation of yawing moment with rudder angle	rad^{-1}
C_{TX}	Thrust force coefficient	----
C_{TX_u}	Variation of thrust force with speed	----
C_{y_p}	Variation of side force with roll rate	rad^{-1}
C_{y_r}	Variation of side force with yaw rate	rad^{-1}
C_{y_β}	Variation of side force with sideslip angle	rad^{-1}
$C_{y_{\dot{\beta}}}$	Variation of side force with rate of change of sideslip angle	rad^{-1}

$C_{y_{\delta A}}$	Variation of side force with aileron angle	rad^{-1}
$C_{y_{\delta R}}$	Variation of side force with rudder angle	rad^{-1}
D	Diameter	ft
D	Drag	lb
DGEAR	A logical variable set equal to one if the gear is extended, zero if the gear is retracted	----
e	Oswald's efficiency factor	-----
f	Equivalent parasite area	ft^2
$F_{X_{\delta T}}$	Force along x-axis due to change in thrust	lb
$F_{Z_{\delta T}}$	Force along z-axis due to change in thrust	lb
g	Acceleration due to gravity	ft/sec^2
GAMMA	Flight path angle	deg
H, h	Altitude	ft
$\dot{h}$	Rate of change of altitude	ft/sec
i	Incidence angle	deg
I_{xx}	Moment of inertia about X-body axis	$slug\text{-}ft^2$
I_{xz}	Product of inertia	$slug\text{-}ft^2$
I_{yy}	Moment of inertia about Y-body axis	$slug\text{-}ft^2$
I_{zz}	Moment of inertia about Z-body axis	$slug\text{-}ft^2$
j	Square root of -1	----
K	Gain constant	----
k	Factor of proportionality	----
L	Length	ft
L	Lift	lb
$L_{Z_{\delta T}}$	Force due to asymmetric thrust along z-axis	lb

$L_{\delta A}$	Dimensional variation of rolling moment with aileron angle	sec^{-2}
$L_{\delta R}$	Dimensional variation of rolling moment with rudder angle	sec^{-2}
$L_{\delta T}$	Dimensional variation of rolling moment with asymmetric thrust	sec^{-2}
M	Mach number	——
m	Mass	slugs
$MX_{\delta T}$	Force due to symmetric thrust along x-axis	lb
$MZ_{\delta T}$	Force due to symmetric thrust along z-axis	lb
$M_{\delta E}$	Dimensional variation of pitching moment with elevator angle	sec^{-2}
$M_{\delta T}$	Dimensional variation of pitching moment with change in thrust	sec^{-2}
N	Number of engines	——
n	Load factor or Laplace variable	-----
nm	Nautical miles	nm
$NX_{\delta T}$	Force due to asymmetric thrust along x-axis	lb
$N_{\delta A}$	Dimensional variation of yawing moment with aileron angle	sec^{-2}
$N_{\delta R}$	Dimensional variation of yawing moment with rudder angle	sec^{-2}
$N_{\delta T}$	Dimensional variation of yawing moment with asymmetric thrust	sec^{-2}
p	Perturbed roll rate	rad/sec
PHI	Bank angle	deg
Q, q	Perturbed pitch rate	rad/sec
$\bar{q}$	Dynamic pressure	lb/ft^2

R, r	Perturbed yaw rate	rad/sec
r	Weight relief factor	-----
RC	Rate of climb	ft/min or ft/sec
R_C	Cantilever ratio	-----
S	Area	ft^2
s	Laplace variable	sec^{-1}
S_{FL}	Landing field length distance	ft
S_{TOFL}	Takeoff field length distance	ft
T	Thrust	lb
TC	Time constant	sec
T_{eng}	Time constant of engine	sec
T_R	Time constant of roll mode	sec
T_S	Time constant of spiral mode	sec
u	Perturbed forward velocity	ft/sec
U_1	Steady-state aircraft speed	ft/sec
V	True airspeed	miles/hr or ft/sec
v	Perturbed side velocity	ft/sec
V_{CAS}	Calibrated airspeed	kts
W	Weight	lb
w	Perturbed downward velocity	ft/sec
X, x	Distance along X	ft
$X_{\delta E}$	Dimensional variation of X-force with elevator angle	ft/sec^2
$X_{\delta T}$	Dimensional variation of X-force with change in thrust	ft/sec^2
Y, y	Distance along Y	ft

$Y_{\delta A}$	Dimensional variation of Y-force with aileron angle	ft/sec^2
$Y_{\delta R}$	Dimensional variation of Y-force with rudder angle	ft/sec^2
$Y_{\delta T}$	Dimensional variation of Y-force with asymmetric thrust	ft/sec^2
Z, z	Distance along Z	ft
$Z_{\delta E}$	Dimensional variation of Z-force with elevator angle	ft/sec^2
$Z_{\delta T}$	Dimensional variation of Z-force with change in thrust	ft/sec^2

Greek Symbol	Definition	Dimension
α	Angle of attack	rad or deg
$\dot{\alpha}$	Rate of change of angle of attack	rad/sec or deg/sec
β	Sideslip angle	rad or deg
$\dot{\beta}$	Rate of change of sideslip angle	rad/sec or deg/sec
δ	Control surface deflection	-----
δ, Δ	Incremental value	-----
Φ	Turbulence spectral form	-----
ϕ	Bank (roll) angle	rad or deg
Γ	Dihedral angle	rad or deg
γ	Flight path angle	rad or deg
η	Engine cant angle	rad or deg
η	Nondimensional lateral coordinate	-----
Λ	Sweep angle	deg
λ	Taper ratio	-----

π	Constant (3.14159)	-----
θ	Pitch attitude angle	rad or deg
ρ	Density	slugs/ft^3
σ	Density ratio	-----
σ	Mean square value of gust velocity	ft/sec
$\overline{\sigma}$	Mean normal stress	lb/ft^2
τ	1/Time constant	sec^{-1}
$\overline{\tau}$	Mean shear stress	lb/ft^2
Ω	Spatial frequency	ft^{-1}
ω	Frequency	rad/sec or deg/sec
ω_n	Undamped natural frequency	rad/sec or deg/sec
ψ	Heading angle	rad or deg
ζ	Damping ratio	----

Subscripts	Definition
1	Steady state
A	Aileron
A	Approach
BASE	Base
cg	Center of gravity
cl	Climb
clean	Clean
cp	Center of pressure
cr	Cruise
crew	Crew

D	Dutch roll
den	Denominator
E	Elevator
E	Empty
e	Equivalent
e, eng	Engine
F	Fuel
fan	Fan
FL	Field length
fus	Fuselage
g	gust
GEAR	Gear
H, h	Horizontal tail
IL	Inboard left
in	Inboard
IR	Inboard right
L	Landing
LE	Leading edge
max	Maximum
num	Numerator
OL	Outboard left
OR	Outboard right
out	Outboard
P	Phugoid
p	Pilot
PL	Payload

R	Roll
R	Rudder
r	Root
ref	Reference
reqd	Required
S	Spiral
S	Stall
SIL	Inboard left spoiler
SIR	Inboard right spoiler
SOL	Outboard left spoiler
SOR	Outboard right spoiler
SP	Short-period
t	Tip
T_{asym}	Asymmetric thrust
TE	Trailing edge
tfo	Trapped fuel and oil
TO	Takeoff
T_{sym}	Symmetric thrust
v	Vertical tail
w	Wing
wind	Wind

Acronyms	Definition
AAA	Advanced Aircraft Analysis
AGL	Above Ground Level

AIAA	American Institute of Aeronautics and Astronautics
CAS	Control Augmentation System
DAC	Douglas Aircraft Company
FAA	Federal Aviation Administration
FAR	Federal Aviation Regulations
HUD	Heads-Up Display
MIL	Military
MSL	Mean Sea Level
NASA	National Aeronautics and Space Administration
NTSB	National Transportation Safety Board
OEI	One Engine Inoperative
PCA	Propulsion Controlled Aircraft
PIO	Pilot Induced Oscillation
PLA	Power Lever Angle
PLF	Power for Level Flight
Spec	Specifications
USAF	United States Air Force

LIST OF TABLES

LIST OF FIGURES

CHAPTER 1

INTRODUCTION

1.1. DOUGLAS DC-10 UNITED AIRLINES ACCIDENT [Refs. 1,2,3,4,5,6]

United Airlines Flight 232 from Denver to Chicago was cruising above Iowa at 37,000 feet on July 19, 1989. About one hour into the flight, the flight crew heard an explosion and the DC-10 (see Figure 1.1) began to shudder. The instruments showed that the tail-mounted engine had failed.

As the captain and the first officer struggled to control the aircraft, the flight engineer reported that all the hydraulic gauges were reading zero. There was no fluid and no pressure in any of the three independent hydraulic systems.

Primary flight controls on the DC-10 consist of inboard and outboard ailerons, two-section elevators, and a two-section rudder. Secondary flight controls consist of leading edge slats, spoilers, inboard and outboard flaps, and a dual-rate movable horizontal stabilizer. Flight control surfaces are segmented to achieve redundancy. Each primary and secondary control surface is powered by two of three independent hydraulic systems.

The three independent, continuously operating hydraulic systems are intended to provide power for full operation and control of the airplane in the event that one or two of the hydraulic systems are rendered inoperative. System integrity of at least one hydraulic system is required - fluid present

and the ability to hold pressure - for continued flight and landing. There are no provisions for reverting to manual flight control inputs.

Loss of hydraulic fluid in all three hydraulic systems made control of the aircraft using the flight control systems impossible. At this time the pilot declared an emergency. The aircraft was re-routed to Sioux City municipal airport due to the 8,999 foot long runway.

The passengers were told of the engine failure and the flight attendants were instructed to prepare the cabin for an emergency landing. Among the passengers was an off-duty United Airlines training check pilot, who had logged 3,000 of his 23,000 flight hours in DC-10s. He offered his help and was immediately invited up to the cockpit.

The check pilot was asked to go back into the cabin and inspect the wings. The inboard ailerons were displaced slightly upwards, the spoilers were locked down, and there was no movement of the flight control surfaces. The first officer would later perform a cabin check and report that, in addition, the horizontal stabilizers were badly damaged.

The captain directed the check pilot to take control of the throttles to free the captain and first officer to try once more to manipulate the flight controls. The check pilot attempted to use engine power to control pitch and roll. Control of the aircraft was extremely difficult. It took anywhere from 20 to 40 seconds after a thrust adjustment for the intended change in attitude to occur.

The pilots jettisoned as much fuel as possible and extended the landing gear by means of a backup system. The flight crew said that they made visual contact with the airport about nine miles out. Though they had planned on landing on Runway 31 due to its length, the aircraft was lined up with shorter

Runway 22. Because of the difficulty in making turns, the crew decided to land on Runway 22.

The check pilot worked the throttles continuously during final approach. The flaps and slats could not be extended since their operation required the hydraulic system. Visual cues and the first officer's airspeed indicator were used to determine the flight path and the need for thrust changes. The aircraft was fairly well aligned with the runway, but was descending at a high rate.

On final approach, the nose pitched down and the right wing dropped. First ground contact was made by the right wing tip followed by the right main landing gear. The airplane skidded to the right of the runway and rolled to an inverted position. The airplane cartwheeled and ignited in flame, coming to rest after crossing Runway 17.

Fire fighting and rescue operations began immediately, but the aircraft was destroyed by impact and fire. There were 296 passengers and crewmembers aboard Flight 232 - 185 of them survived the crash.

The FAA determined that the tail-mounted engine experienced an uncontained failure of the stage 1 fan rotor disk assembly. The engine fragments severed the Number 1 and Number 3 hydraulic system lines. In addition, the forces of the engine failure fractured the Number 2 hydraulic system, rendering the three hydraulic-powered flight control systems inoperative. Typical of all wide-body transport aircraft, there are no alternate power sources for the flight control systems.

Because of the loss of the three hydraulic systems, the flight crew was confronted with a unique situation that left them with very limited control of the airplane. The only means available to fly the airplane was manipulation of

thrust available from the remaining two wing-mounted engines. The primary task confronting the flight crew was controlling the flight path. This task was extremely difficult to accomplish because of the need to manipulate the engine throttles asymmetrically to maintain lateral roll control while also manipulating the throttles symmetrically to maintain pitch control. The flight crew found that despite their best efforts, they could not maintain a stabilized flight condition.

Douglas Aircraft Company, the FAA, and United Airlines considered the total loss of hydraulic-powered flight controls so remote that no procedure to counter such a situation was ever conceived. The simulator reenactment of the events leading to the crash landing revealed that landing under these conditions involves many variables that affect the extent of controllability during the approach and landing such as airspeed, ground effect, aircraft attitude, and rate of descent. While any one of these parameters might be controllable by the flight crew, it was virtually impossible to control all parameters simultaneously.

The National Transportation Safety Board concluded that the damaged DC-10 aircraft was marginally flyable using throttle controls to control the thrust on the remaining two engines. However, a safe landing on a runway was determined to be virtually impossible with the loss of all hydraulic flight controls. The Safety Board ruled that under the circumstances, the United Airlines flight crew performance was highly commendable and greatly exceeded reasonable expectations.

1.2. NATIONAL TRANSPORTATION SAFETY BOARD RECOMMENDATIONS

[Ref. 2]

As a result of the United Airlines DC-10 accident at Sioux City, the National Transportation Safety Board reviewed alternate flight control system design concepts for wide-body airplanes. The concept of three independent hydraulic systems, as installed on the DC-10, is not unique. Boeing and Airbus have three such systems on some of their most recently certified models. Lockheed and Boeing have also provided four independent systems on some of their wide-body airplanes.

The Safety Board could find no inherent safety advantage to the installation of additional independent hydraulic systems for flight controls beyond those currently operating in today's fleet. However, the Safety Board believes that backup systems to the primary hydraulic systems should be developed and included in the initial design for certification. Such backup systems are particularly important for the coming generation of wide-body airplanes. Manual reversion flight control systems are quite likely impractical because of the power requirements to deflect large control surfaces that are heavily loaded. Therefore, the Safety Board recommended that the FAA encourages continued research and development into backup flight control systems for newly certificated wide-body airplanes that employ an alternate source of motive power separate than that used for the conventional control system.

1.3. STUDIES REGARDING USE OF THROTTLES FOR EMERGENCY FLIGHT CONTROL [Refs. 7,8,9,10,11]

The NASA Dryden Flight Research Center (NASA Dryden) at Edwards Air Force Base, California, has been the site for conducting preliminary flight, ground simulator, and analytical studies regarding the use of throttles for emergency flight control of a multi-engine aircraft. This investigation was begun as a result of the relatively successful attempted landing of the United Airlines DC-10 at Sioux City. The objective has been to determine the degree of control power available with the throttles for various classes of airplanes and to investigate the development of possible control modes for future airplanes.

The research work performed thus far at NASA Dryden appears to indicate that control of an aircraft with partial or total flight control system failure using throttles-only control is feasible. Based on simulator and flight results, all of the airplanes studied at NASA Dryden to date have exhibited some control capability with throttles-only control. All airplanes could be controlled in a gross manner, although it was very difficult to achieve precise control with manual throttle control. Landings using manual throttles-only control were extremely difficult.

As a result of these studies, an augmented control system has been developed at NASA Dryden. The control mode uses pilot controlled pitch and roll thumbwheel inputs, with appropriate gains and feedback parameters, to drive the throttles. Performance in the augmented mode was greatly improved. Figure 1.2 shows the F-15 simulation landing results for the manual throttles-only mode and for the augmented throttles-only mode. The

distance from the runway centerline, distance from the runway threshold, and sink rate and roll angle are plotted in a three-dimensional representation. As is graphically demonstrated, the augmented throttles-only control mode resulted in safe and survivable landings, whereas the manual throttles-only control mode resulted primarily in nonsurvivable crashes. Based on simulation results, it appears that the augmented control system makes runway landings practical using throttles-only control.

1.4. PURPOSE AND OBJECTIVES [Refs. 12,13,14,15,16,17]

The world's civil aircraft manufacturers are studying, and even marketing in some cases, next generation ultra-high capacity jet transports. Current trends predict that by the year 2015, there will be a need in the international market for more than 400 aircraft seating between 400 to 600 passengers , and more than 350 aircraft with a seating capacity above 600 passengers.

Boeing, Airbus, and McDonnell Douglas are currently evaluating preliminary designs of superjumbo transports carrying up to 670 passengers (see Figure 1.3). The possibility that one of these large transports might crash due to total failure of the flight control system is not unthinkable, particularly in light of the Sioux City accident. In view of the work already done at NASA Dryden, it seems reasonable to ask the following questions regarding these large megatransports:

• Is it possible to arrange the engines in a large passenger transport in such a way that flight path control using only the engines is not only possible, but meets Level 1 or Level 2 handling quality requirements?

• Since total failure of the primary flight control system can be caused by the failure of an engine, can the number of engines and their arrangement be selected such that flight path control with one engine inoperative is still possible with Level 1 or Level 2 handling quality requirements?

• Can one or more levels of primary flight control system redundancy be eliminated in an airplane equipped with a Level 1 or Level 2 engine control system, allowing the engine thrust to be used as a backup flight control system?

This dissertation will present a procedure which will answer these important questions. Chapter 2 contains the background information pertinent to this project. Chapter 3 presents the preliminary megatransport design, while the megatransport simulation is described in Chapter 4. Chapters 5 and 6 contain the test description and data analysis sections, respectively. The conclusions and recommendations are covered in Chapter 7.

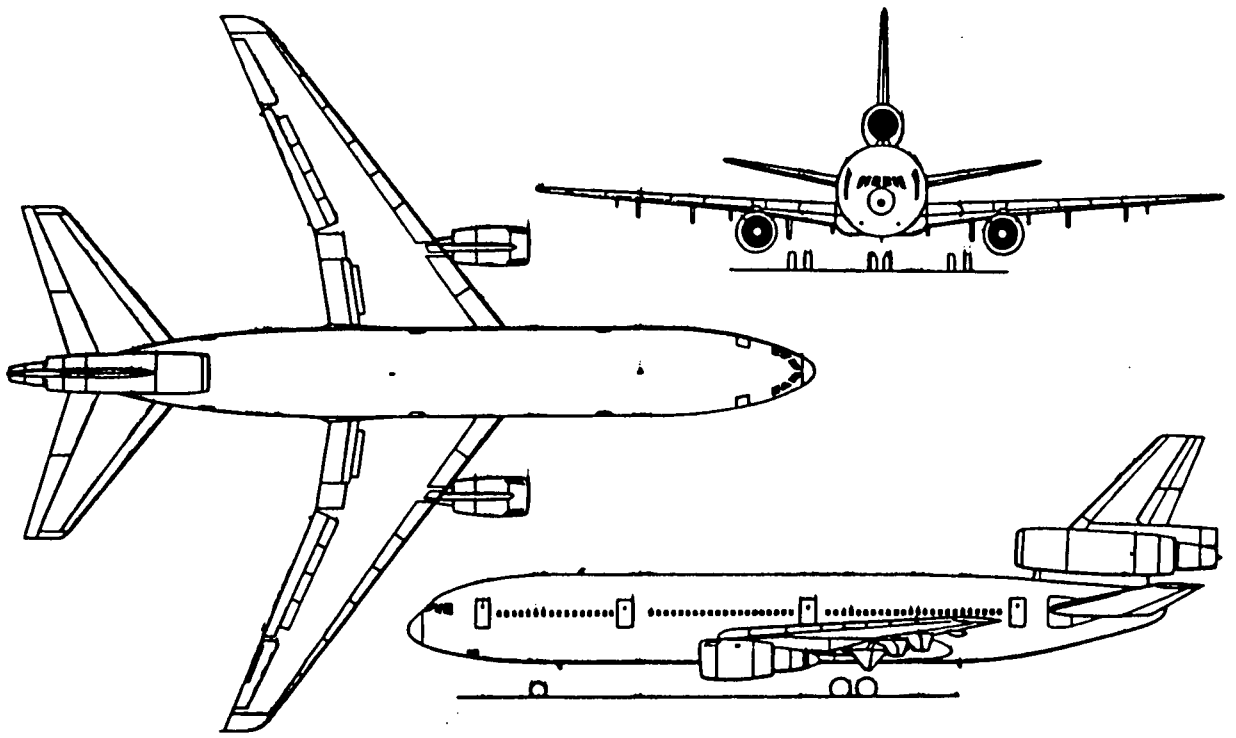

Figure 1.1 The DC-10 Commercial Jet Transport (Ref. 1)

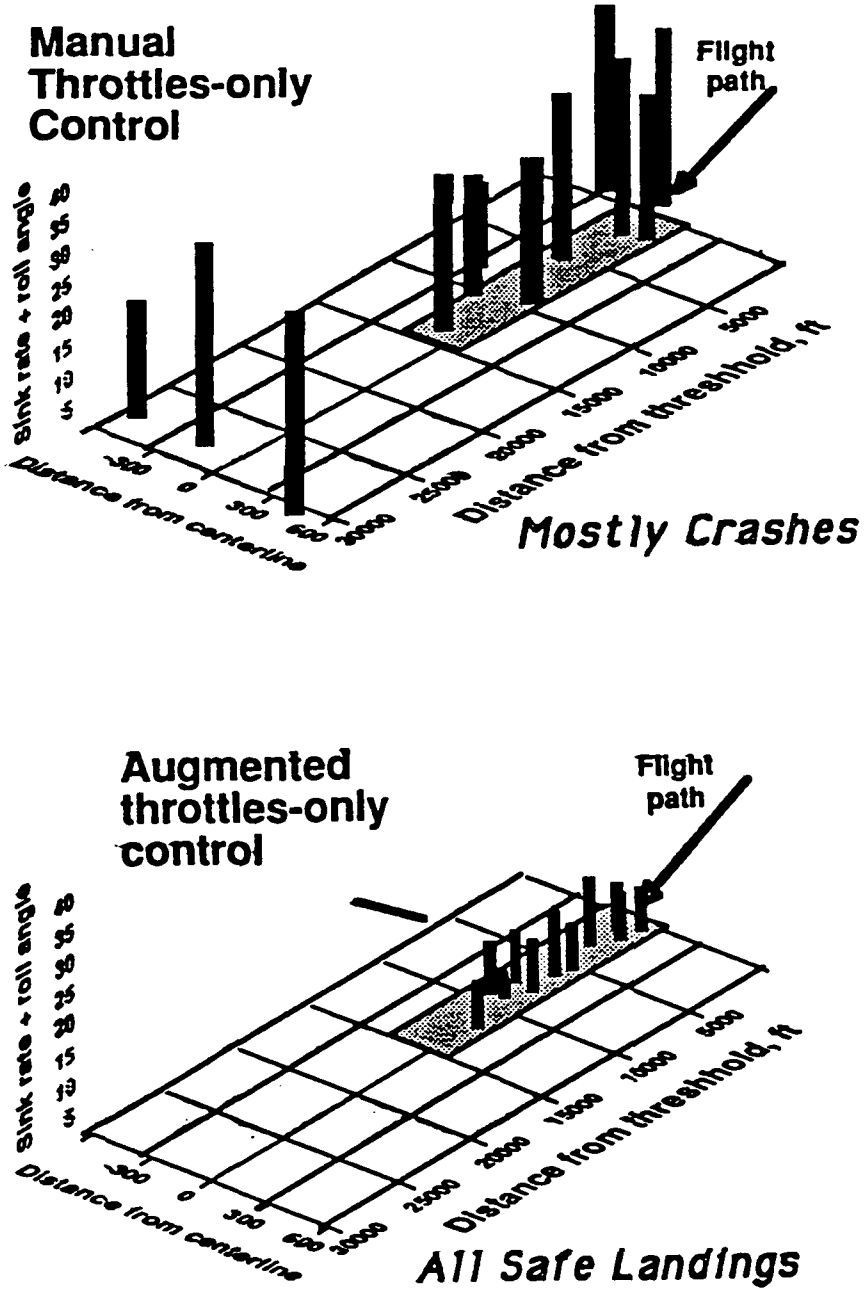

Figure 1.2 Landing Results, F-15 Simulation
(Refs. 10 and 11)

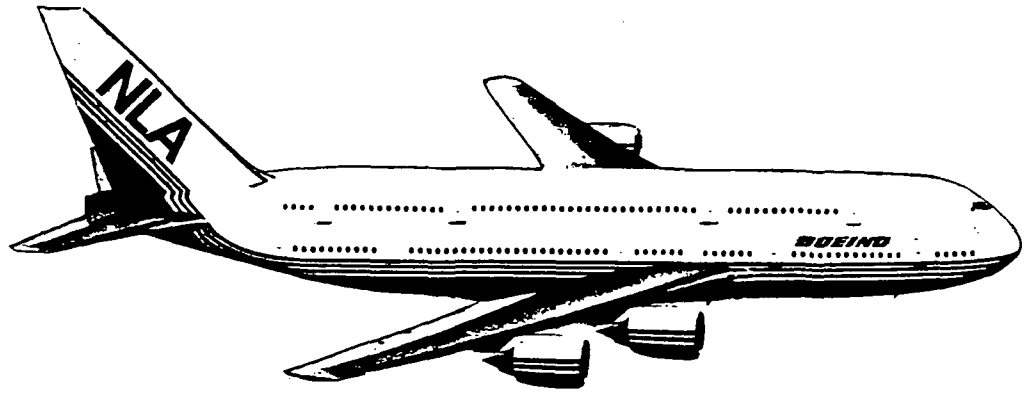

Figure 1.3(a) Boeing's 606 - Seat New Large Airplane Passenger Transport Concept (Refs. 14 and 15)

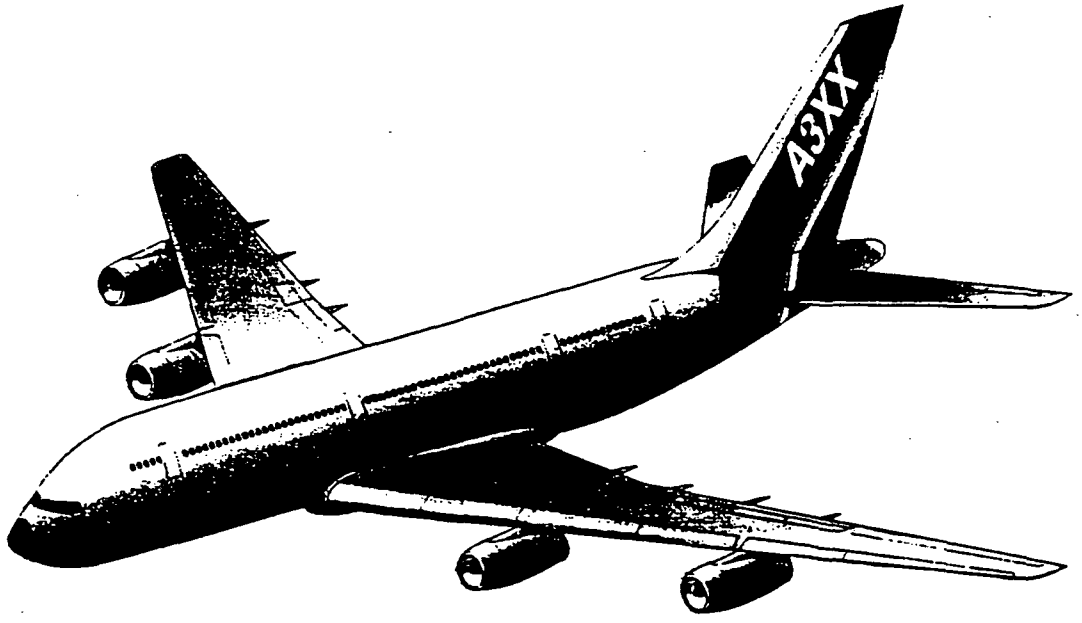

Figure 1.3(b) Airbus' 530 - 670 Seat A3XX Ultra-High Capacity Aircraft Concept (Ref. 16)

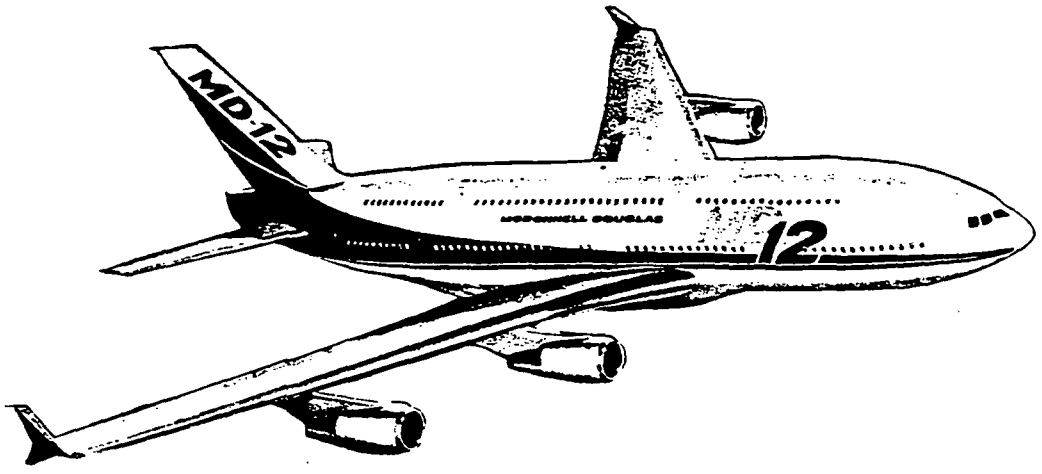

Figure 1.3(c) McDonnell Douglas' 481 - 579 Seat MD-12 Superjumbo Aircraft Concept (Ref. 12)

CHAPTER 2

BACKGROUND INFORMATION

2.1. INTRODUCTION [Refs. 2,9]

Current generation aircraft rely on multiple, independent flight control systems so that any single failure of an aircraft component will not disable more than one system, thus leaving the aircraft with satisfactory flight control capability. Despite these design objectives, failures have occurred where aerodynamic control surface effectiveness has been significantly impaired or completely lost. This can result from impairment and failures in the electrical, hydraulic, and hardware systems. Such problems can be the result of internal aircraft system failures (due to engine failure, fatigue, corrosion, improperly executed repairs, or terrorist damage) or external damage (due to bird strikes, mid-air collision, or tactical battle damage). In such cases, selective engine thrust can be used as the primary means of controlling the aircraft. Several examples are described in Appendix A.

2.2 PRINCIPLES OF ENGINES-ONLY CONTROL [Refs. 2,9]

Steady level cruise flight is attained when the forces and moments acting on the airplane are in a state of equilibrium; that is, thrust equals drag and the weight of the airplane is balanced by the lift forces produced primarily

by the wing and horizontal stabilizer. Lift, drag, and thrust vary with airspeed, angle of attack, and atmospheric conditions.

Transient changes from the steady cruise condition are achieved by manipulating the cockpit controls to move the longitudinal controls (stabilizer, elevator, canard, or canardvator) or the lateral-directional controls (aileron, spoiler, differential stabilizer, or rudder). The deflection of the longitudinal control surface causes a change in the attitude, angle of attack, and airspeed of the aircraft. In routine flight, the pilot will change both thrust and longitudinal control surface position to attain a new steady flight path. Lateral-directional control is normally achieved by using the lateral-directional control surfaces to produce a bank angle that will result in a turn or change in the direction of the flight heading.

An inability to reposition the control surfaces severely restricts the pilot's control over such flight path and heading changes by eliminating the essential means of changing the normal force and moment balance. The primary flight control system is one of the most crucial systems on an aircraft. The aircraft incidents described in Chapter 1 and Appendix A all experienced partial or total flight control system failure and all exhibited an ability to use engine thrust for emergency control. Selective engine thrust can be used to control the heading and flight path of a multi-engine airplane. This section presents the principles of engine-only flight control.

2.2.1. YAW-ROLL CONTROL [Refs. 7,10,18,19]

Differential thrust, a difference in thrust between the engines on the right side of the fuselage and the left side of the fuselage, generates sideslip. Through the normal dihedral effect present on most airplanes, this results in roll. Roll from differential thrust is controlled to establish a bank angle, which results in a turn rate and a change in aircraft heading.

Some aircraft will exhibit a coupled mode between roll and yaw called dutch roll. The dutch roll mode consists of a lightly damped, moderately low frequency oscillation. An example of what a complete three-degrees-of-freedom dutch roll motion looks like to an outside observer is shown in Figure 2.1.

Attempting to control dutch roll using throttles alone can cause roll and heading control difficulties for the pilot. The dutch roll frequency during low altitude cruise flight for a Boeing 747 aircraft is 1.05 radians/second. The control system time delay in response to throttles is approximately one second. During that one second, the 747 has completed 1.05 radians, or 60 degrees, of the dutch roll cycle. Therefore, there is a 60 degree phase lag that the pilot must attempt to anticipate. The F-15 fighter aircraft, during low altitude slow flight, has an even larger 112 degree phase lag in the dutch roll.

2.2.2. PITCH CONTROL [Refs. 7,10]

Pitch control caused by throttle changes is more complex. The desired result is to stabilize and control the vertical flight path. There are several effects that may be present which are described in the following subsections. One of these effects may dominate, depending on the aircraft characteristics and flight conditions.

2.2.2.1. PHUGOID OSCILLATIONS [Refs. 2,7,10,18]

The airplane will continuously seek the airspeed and flight path angle at which the forces balance for the existing longitudinal control surface position and the existing thrust level. This produces an approximately constant angle of attack motion in which kinetic and potential energies (airspeed and altitude) are traded. This longitudinal oscillation is called the phugoid mode. An example of what the phugoid motion looks like to an outside observer is shown in Figure 2.2.

The phugoid produces a long period of pitch oscillation and will produce speed variations about the trim speed. If the speed varies from the trim speed, the airplane will change pitch and either climb or descend to recover to the trim speed. For example, if the speed falls below the trim speed while the airplane is in level flight, the lift produced by the wing is not sufficient to maintain altitude. The airplane will start to descend and pick up speed. Normally, the airspeed will increase beyond the trim speed and the

airplane lift will become greater than required, resulting in an increase in vertical velocity and subsequent climb. During the climb, the airspeed will fall toward the trim speed and the cycle continues.

The time to complete one oscillation is called the period of the phugoid. The period of the phugoid is directly proportional to the forward velocity and is typically about one minute for large jet transports, but may be as long as several minutes for some airplanes. The period is a function primarily of speed and not of aircraft design.

Whenever elevator control is present, the phugoid is easily damped and is not noticeable to the pilot. In a situation involving control surface failure, however, the control surfaces are 'frozen' at the time of failure and, therefore, the trim speed is set. Phugoid damping becomes a critical factor during approach and landing. A landing which occurs on the down slope of the phugoid sinusoidal curve will have an extremely high rate of descent.

Properly sized and timed throttle inputs to control pitch can be used to damp unwanted phugoid oscillations, but the phugoid is difficult to damp with changes in thrust alone without prior experience flying throttles-only flight control. One reason for this difficulty is that pitch rate, shown in Figure 2.3, is a function of both speed and of whether the throttles are being commanded to go from high thrust to lower thrust, or from low thrust to higher thrust.

2.2.2.2 PITCHING MOMENT RESULTING FROM THRUST LINE OFFSET

[Refs. 7,10]

If the engine thrust line does not pass through the c.g., there will be a pitching moment introduced by thrust change. For many transport aircraft,

the thrust line is below the c.g. Increasing thrust results in a nose-up pitching moment, with the magnitude being a linear function of the thrust change. This is the desirable geometry for throttles-only control, because a thrust change immediately starts the nose in the same direction needed for the long-term flight path angle change. High-mounted engines result in just the opposite effect and thrust changes then fight the speed stability effects. The pitching moment caused by the thrust will cause a change in the trimmed angle of attack and airspeed as well as changing the long-term flight path angle.

2.2.2.3. FLIGHT PATH ANGLE CHANGE RESULTING FROM THE VERTICAL COMPONENT OF THRUST [Refs. 7,10]

If the thrust line is inclined to the flight path, an increase in thrust will cause a direct increase in vertical velocity, that is, rate of climb. For a given aircraft configuration, this effect will increase as angle of attack increases.

2.2.3. SPEED CONTROL [Refs. 7,10]

Once the flight control surfaces become locked at a given position, the trim airspeed of most airplanes is affected only slightly by engine thrust. Retrimming to a different speed may be achieved by other techniques. These techniques include moving the c.g., lowering the flaps and landing gear, and by using stabilizer trim, if available. In general, the speed will need to be

reduced to an acceptable landing speed, implying the need to develop nose-up pitching moments. Methods for accomplishing this include moving the c.g. aft and selective lowering of flaps. In aircraft with more than two engines, speed can be reduced by increasing the thrust of low-mounted engines. The retrimming capability varies widely between airplanes.

2.2.4. THRUST RESPONSE [Refs. 7,10]

Most turbine engines respond faster at higher thrust levels than at lower thrust levels. High-bypass turbofans are particularly slow to respond at flight idle. A high-bypass ratio engine takes as long as three seconds to go from flight idle to 30 percent thrust, then three more seconds to go from 30 to 100 percent thrust. Turbojet and low-bypass ratio turbofan engines typical of fighter airplanes and older transports are faster in response, in some cases as fast as 2.5 seconds from idle to full thrust.

2.2.5. EFFECTS OF SPEED ON PROPULSIVE CONTROL POWER [Refs. 7,10]

For turbine-powered airplanes, engine thrust is not a strong function of airspeed. However, the stabilizing effects of vertical and horizontal stabilizers are a function of dynamic pressure, which is proportional to the square of the airspeed. Consequently, the propulsive forces and moments become more effective as the airspeed, and hence the aerodynamic forces, decrease. For example, at high airspeed differential thrust develops a yawing moment that is

small compared to the restoring moment produced by the vertical tail. Therefore, the sideslip is small and the roll rate resulting from differential thrust is low. At low speed, the differential thrust moment may be the same as at high speed. The aerodynamic restoring moment will be much smaller and larger sideslip will develop, producing higher roll rates. A similar effect occurs in the pitch axis, where speed stability increases as speed decreases.

2.3. HISTORICAL REVIEW [Refs. 7,8,10]

The NASA Dryden Flight Research Center at Edwards Air Force Base, California, has been the site for conducting preliminary flight, ground simulator, and analytical studies regarding the use of throttles for emergency flight control of a multi-engine aircraft. This investigation was begun by Frank W. Burcham, Jr., chief of NASA Dryden's propulsion and performance branch, as a result of the relatively successful attempted landing of the United Airlines DC-10 at Sioux City, Iowa, in July 1989. The objective has been to determine the degree of control power available with the throttles for various classes of airplanes and to investigate the development of possible control modes for future airplanes.

Several airplanes, including a light twin-engine piston-powered airplane, jet transports, and a high performance fighter were studied during flight and piloted simulations. Simulation studies used the B-720, B-727, MD-11, and F-15 aircraft. Flight studies used the Lear 24, Piper PA-30, and F-15 airplanes. Some physical characteristics of these airplanes are given in Table 2.1.

2.3.1. FLIGHT RESEARCH STUDIES

Some preliminary flight research studies were conducted on three airplanes: the F-15, the Lear 24, and the PA-30 aircraft.

2.3.1.1. F-15 AIR SUPERIORITY FIGHTER [Refs. 7,10]

The F-15 airplane (see Figure 2.4) is a high performance fighter with a maximum speed of Mach 2.5. It has a high wing with 45 degrees of leading-edge sweep and twin vertical tails. It is powered by two F100 afterburning turbofan engines mounted close together in the aft fuselage. The thrust-to-weight ratio is very high, approaching one at low altitudes. The engine response is fast - 3 seconds from idle to intermediate power. The F-15 has a mechanical flight control system augmented with a high-authority electronic control augmentation system. Hydraulic power is required for all flight control surfaces.

In flight tests using the NASA F-15 airplane, three pilots evaluated the controllability of the F-15 airplane with throttles only, leaving the stick and rudder centered. Using only manual throttle control, pilots could roll the airplane, hold a bank angle, and hold an assigned heading.

If the airplane was trimmed at 170 knots, adequate pitch control was available to hold altitude within approximately 100 feet. If a flight control failure occurred at higher speeds, some method would be necessary to retrim the F-15 to lower speeds. Use of fuel transfer to move the c.g. aft would be one

way to develop nose-up pitching moments, which would slow the F-15. The ramps of the variable capture inlets are also useful in generating nose-up moments. Extension of the landing gear results in almost no change in speed on the F-15 airplane.

2.3.1.2. LEAR 24 EXECUTIVE JET TRANSPORT [Refs. 7,10]

The Lear 24 airplane (see Figure 2.5) is a twin-engine business jet. The low-mounted wing has 13 degrees of sweep. The engines, GE CJ610 turbojets with 2,900 pounds of thrust each, are mounted high on the aft fuselage. The airplane has a T-tail arrangement. Maximum weight is 11,800 pounds. The Lear 24 has a thrust-to-weight ratio of approximately 0.5. The turbojet engines respond rapidly to throttle changes, 2.5 seconds from idle to full thrust.

The airplane used in this evaluation was the Calspan variable stability airplane. It is equipped with the basic Lear 24 mechanical control system, including an electric stabilizer pitch trim capability. In addition, there are hydraulic actuators that add electric inputs from the variable stability system to the mechanical system.

The Lear 24 characteristics with throttles-only control were investigated at a speed of approximately 200 knots. Roll control power is quite large. The basic Lear 24 pitch control capability was also investigated. In contrast to the roll axis, pitch control with thrust was very difficult. Because of the high engine placement, a thrust increase caused a nose-down pitch. Eventually, the speed stability would bring the nose back up. The phugoid was very difficult

to damp with throttle inputs. Despite these difficulties, the Lear 24 was flown for 20 minutes using only the throttles. Roll and heading were controlled precisely and altitude was maintained within 500 feet.

2.3.1.3. PA-30 PISTON-POWERED LIGHT TWIN-ENGINE PLANE [Refs. 7,10]

The Piper PA-30 airplane (see Figure 2.6) is a light, twin-engine, four-place airplane. It has a low-mounted unswept wing, and the engines are mounted ahead of the wing in nacelles. Maximum weight is 3,600 pounds. The engines are the Lycoming IO-320 model, rated at 160 horsepower each.

The PA-30 when flown with throttles-only had significant control power. The roll control of the PA-30 using engine thrust for flight control is highly nonlinear, however. It appears that the major rolling moment is caused by reducing the throttle on one side until the blowing over the wing is sharply reduced. The linear response to differential thrust seen on other jet-powered airplanes was not present. Pitch control is difficult. There is adequate control power available from speed stability, but the longitudinal phugoid is hard to damp. Overall, it was possible to maintain gross control of heading and altitude, but landing on a runway would be extremely difficult.

2.3.2. SIMULATOR STUDIES

Piloted simulator studies of engines-only flight control capability were conducted on the B-720, B-727, MD-11, and the F-15 aircraft. One task

evaluated was 'up-and-away' control. This is the ability to control heading to within a few degrees, and to control altitude to within +/- 200 feet. The other task was landing on a runway.

2.3.2.1. B-720 COMMERCIAL JET TRANSPORT [Refs. 7,10]

The Boeing 720 airplane (see Figure 2.7) is a four-engine transport designed in the late 1950's. It has a 35 degree swept wing mounted low on the fuselage, the four engines mounted on pods below and ahead of the wing. The engines are Pratt and Whitney JT3C-6 turbojets. The airplane is equipped with a conventional flight control system incorporating control cables and hydraulic boost. It also incorporates a slow-rate electric stabilizer trim system. The flaps are electrically controlled.

The pilot of the B-720 simulation flew manually using the throttles only. Good roll capability was evident. Good pitch capability was also found, with some pitching moment caused by the thrust line being below the c.g., and some pitching moment caused by speed stability.

It was possible for a pilot to maintain gross control, hold heading and altitude, and make a controlled descent. However, it was extremely difficult for a pilot to make a landing on a runway. There was a one second lag in pitch and roll before the airplane began to respond to the throttles. Judging the phugoid damping was difficult, and the lightly damped dutch roll was a major problem in roll and heading control. Although a few pilots did develop techniques for successful landings using manual throttles, most were unable to make repeatable successful landings.

2.3.2.2. B-727 COMMERCIAL JET TRANSPORT [Refs. 7,10]

The Boeing 727 three-engine transport (see Figure 2.8) has a swept wing and a T-tail. The three Pratt and Whitney low-bypass ratio turbofan engines are mounted in the aft fuselage. The two outboard engines are mounted on short pylons, while the center engine is located in the aft fuselage and has an inlet above the fuselage. The engine response was slow from idle to an engine pressure ratio of 1.2, then fast until full thrust was reached.

Pitch control power was evaluated. There is significant pitching authority with thrust on the B-727. The roll capability, while much less than the F-15 or B-720 airplanes, was surprisingly large considering the fuselage-mounting of the engines.

The airplane was flown using differential engine thrust for bank angle and electric stabilizer trim in pitch, and gross control was possible. Precise control of the flight path angle using throttles was more difficult, however. Landings were attempted using differential throttle and electric trim. Neither of the evaluation pilots could successfully land the airplane on the runway by themselves. The low roll rate and roll control lag made it nearly impossible to remain lined up with the runway.

Improved roll control was achieved by reducing the center engine throttle to idle; the higher thrust and the faster thrust response of the outboard engines improved directional control. Splitting the control task between two pilots also helped. One pilot would fly pitch with electric trim, while the other pilot used differential throttles for roll and heading control.

Even with this technique, it was not possible to make consistent landings on the runway.

2.3.2.3. F-15 AIR SUPERIORITY FIGHTER [Refs. 7,10]

A simulator study was performed on the NASA F-15 airplane (see Figure 2.4). It was flown in a simulator cockpit with actual F-15 stick and throttles. A visual scene, including the Edwards dry lake bed runways, was provided on a video monitor.

The piloted F-15 simulation was used in a landing study. The pilots used throttles-only control to fly approaches and landings using the video display of the 15,000 foot-long Edwards Runway 22. During the initial landing attempts, control was extremely difficult. The phugoid mode was excited close to the ground and was a constant problem throughout touchdown. Throttle inputs to damp the phugoid were hard to judge. Roll control, while adequate in rate, had a troublesome one second lag. Most landings had such a high sink rate that they were categorized in the 'certain damage' category; many were not survivable landings.

2.3.2.4. MD-11 COMMERCIAL JET TRANSPORT [Refs. 7,10,20]

The MD-11 airplane (see Figure 2.9) is a large, long-range commercial transport. It has a 35 degree sweep, low-mounted wing. It is powered by three high-bypass turbofan engines, two mounted in underwing pods and the third

mounted in the base of the vertical tail. The engines are slow to respond at low thrust levels, but respond well above 30 percent thrust.

Simulator results of throttles-only flight showed that altitude could be maintained, heading could be held within reasonable limits and, with practice, manual landings were possible. These results were substantiated with flight data.

2.3.3. OVERALL FLYING QUALITIES [Refs. 7,10]

Based on simulator and flight results, all the airplanes exhibited some control capability with throttles. All airplanes could be controlled in a gross manner (heading and altitude could be maintained) although pilot workload was very high. Because of the phugoid characteristics and the lag associated with the engine thrust response, it was very difficult to achieve precise control with manual throttle control. Landings using manual throttles-only control were extremely difficult; landing at a predetermined point and airspeed on a runway was a highly random event.

2.3.3.1. AUGMENTED CONTROL SYSTEM [Refs. 7,9,10]

An augmented control system, called the propulsion controlled aircraft (PCA) system, was developed by Glenn B. Gilyard and Joseph L. Conley, both engineers at NASA Dryden, for the B-720 simulation. The control mode uses

pilot stick inputs, with appropriate gains and feedback parameters, to drive the throttles.

In the pitch axis, a flight path angle command loop was implemented. The command was designed to act through the forward and aft motion of the stick and have a command capability of +/-10 degrees of flight path angle. In addition to flight path angle feedback, pitch rate is also fed back to augment the damping (see Figure 2.10).

The control for the roll axis was mechanized using differential throttle to command sideslip, and hence, through dihedral effect, roll. Bank angle was commanded by lateral stick position and was designed to have a command capability of +/-45 degrees of bank. The damping of the augmented dutch roll mode is very light despite roll rate and sideslip feedback (see Figure 2.11). However, the mean bank angle holds well if care is taken not to excite the dutch roll.

Using the augmented control mode, it was possible for a pilot to make successful landings. Pilot proficiency improved rapidly with time, as the lead time required to compensate for slow engine response was learned. Landings without turbulence or with light turbulence were generally good. With moderate turbulence, pilot ratings degraded, but most landings were still successful.

The augmented mode developed for the B-720 airplane was incorporated into the F-15 simulator. Gain changes were made to account for the differences in throttle range and thrust, but the basic control concept remained the same.

As testing was begun on evaluating pilot performance while flying the augmented mode F-15 simulation, suggestions were made by some of the pilots

to develop thumbwheel controllers to command bank angle and pitch attitude directly. The augmented mode aircraft performance was sluggish and slow to respond compared to flight using conventional flight control surfaces which the pilots were used to flying. Several pilots had some difficulty in flying the augmented mode with the control stick due to overcompensation and tendencies for pilot induced oscillation (PIO).

Pitch attitude and bank angle thumbwheels were developed for the simulator and are shown in Figure 2.12. The pitch thumbwheel has a command capability of +/-10 degrees of flight path angle and can be positioned at half-degree intervals. Although the bank angle thumbwheel does not have discrete settings like the pitch thumbwheel, the bank angle indicator is marked at every 10 degrees of bank and has been calibrated up to +/-30 degrees of bank.

Currently, both methods of flying the augmented mode are available in the simulator. The advantage of the control stick is that it enables the pilot to control the disabled aircraft with conventional control methods (moving the stick forward and aft to control pitch and from side to side to control roll). The advantages of the thumbwheel are:

- the pilot is reminded that the system is a slow-response, low-authority system
- good resolution (incremental commands are easily attained)
- the pilot is not required to hold the thumbwheel to maintain command (thumbwheels remain where set)
- pitch and roll control are separate (the control stick has virtually no pitch/roll isolation)

- similar controls are used in transport aircraft to command the autopilot.

The evaluation of both control systems thus far indicates a pilot preference for thumbwheel control of the thrust.

The augmented control provided two important improvements over manual throttles-only control. First, the augmented control system enabled the pilot to command flight variables rather than throttle position. Second, feedback of key pitch and roll parameters was provided automatically to stabilize the flight path. In the pitch axis, flight path angle and pitch rate feedback are provided. The pitch rate feedback provides phugoid damping. In the roll axis, bank angle feedback was used for roll control.

By using the augmented system, performance of the thrust-controlled F-15 was greatly improved. The augmented modes effectively damped the phugoid and improved the roll characteristics. Figure 2.13 demonstrates the time history of a throttles-only manual landing of the F-15 simulation. As can be seen from the figure, the pilot landed well short and to the right of the runway with a rate of sink of 20 feet per second. With the augmented system, however, it was possible to make repeatable landings on a runway and inexperienced pilots were able to make good landings on their first tries as was seen in Figure 2.14. Based on simulation results, it appears that the augmented control system makes runway landings practical using throttles-only control.

2.4. CURRENT RESEARCH [Refs. 11,21,22,23,24,25,26,27,28,29,30,31]

Douglas Aircraft Company (DAC), in conjunction with NASA Dryden, is currently performing an evaluation of the augmented throttles-only control concept for the MD-11 on their MD-11 Flight Deck Simulator. In addition to the simulator studies, manual throttles-only control was flown on an actual MD-11 aircraft in September 1992. Although no throttles-only landings were attempted, an approach was made within 70 feet above the runway. The preliminary evaluation by both DAC and NASA pilots is that the results are "very promising".

In addition to the work being done on the MD-11, an augmented propulsion controlled aircraft system has been designed and installed on the NASA F-15 HIDEC aircraft. The first F-15 PCA flight was flown January 22, 1993. Several small problems in the control system were noted, but the performance was judged "good." Subsequent flights allowed NASA to refine the PCA control system gains and fly additional test points in the flight envelope, investigating effects such as different fuel weights, different speeds, and different attitudes.

On February 5, 1993, the F-15 was flown within 10 feet above the runway under PCA control. Sink rate was well within acceptable limits and bank angle was less than one degree. The first PCA landings were accomplished April 21, 1993. With its flight controls deliberately locked, the F-15 HIDEC demonstrated the ability to be flown and landed safely using only engine power for control. The control was excellent during both landings, the F-15 touching down within 10 feet of the runway centerline in each case.

Since the first PCA landings, several additional PCA flights have included unusual attitudes (90 degree bank plus 20 degree nose down attitude) and a series of guest pilots to evaluate the PCA system. In all cases, the F-15 PCA performance was exceptional and the guest pilots flew precision approaches on their first PCA flights. The last NASA F-15 PCA flight occurred October 26, 1993, after which the NASA F-15 HIDEC aircraft was officially retired from service October 29.

Table 2.1 Physical Characteristics of the Airplanes Studied at NASA Dryden (Ref. 7)

	Airplane					
	F-15	Lear 24	B-720	B-727	MD-11	PA-30
Typical mid-fuel weight, lb	35,000	11,000	140,000	160,000	359,000	3,000
Wing quarter chord sweep, deg	45	13	35	32	35	0
Wing span, ft	43	36	130	108	169.6	35.98
Wing area, ft^2	608	231	2,433	1,700	3,958	178
Length, ft	64	43	137	153	192	25.16
Number of engines	2	2	4	3	3	2
Maximum thrust/engine, sea level static, lb	13,000*	2,900	12,500	15,000	60,000	(160 hp)

*F-15 engine at intermediate power

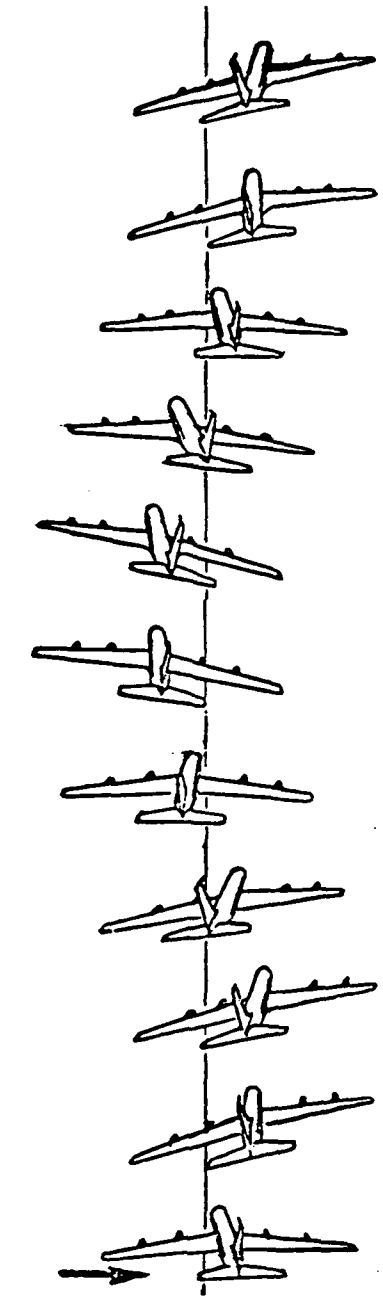

Figure 2.1 Dutch Roll Mode as Seen by an Outside Observer (Ref. 18)

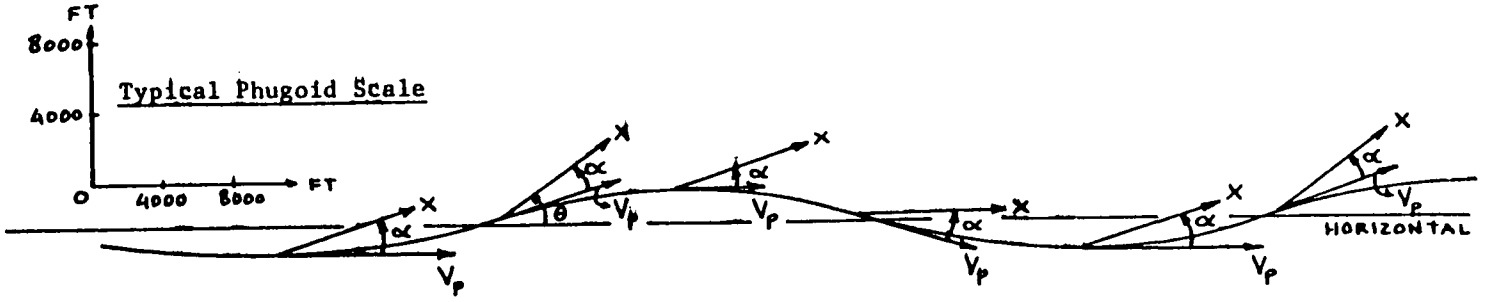

Figure 2.2 Phugoid Mode as Seen by an Outside Observer (Ref. 18)

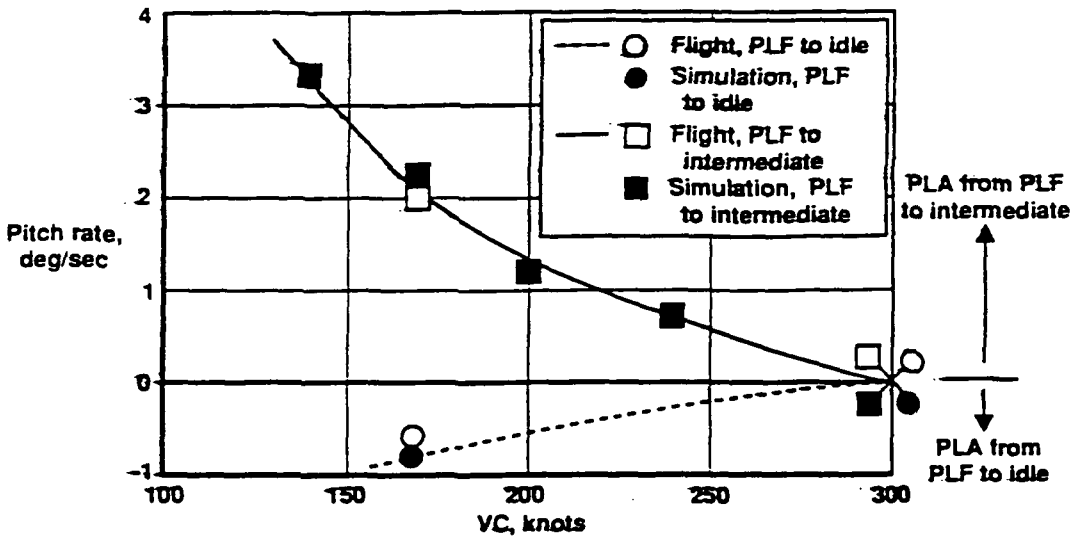

Figure 2.3 Effect of Speed on F-15 Flight and Simulation Maximum Pitch Rates (CAS Off) (Ref. 7)

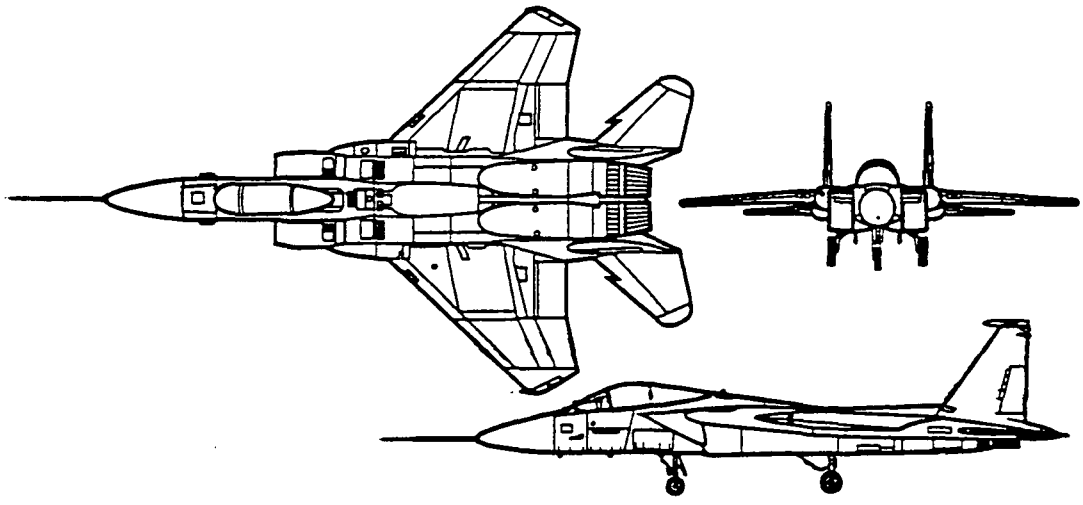

Figure 2.4 The F-15 Air Superiority Fighter (Ref. 7)

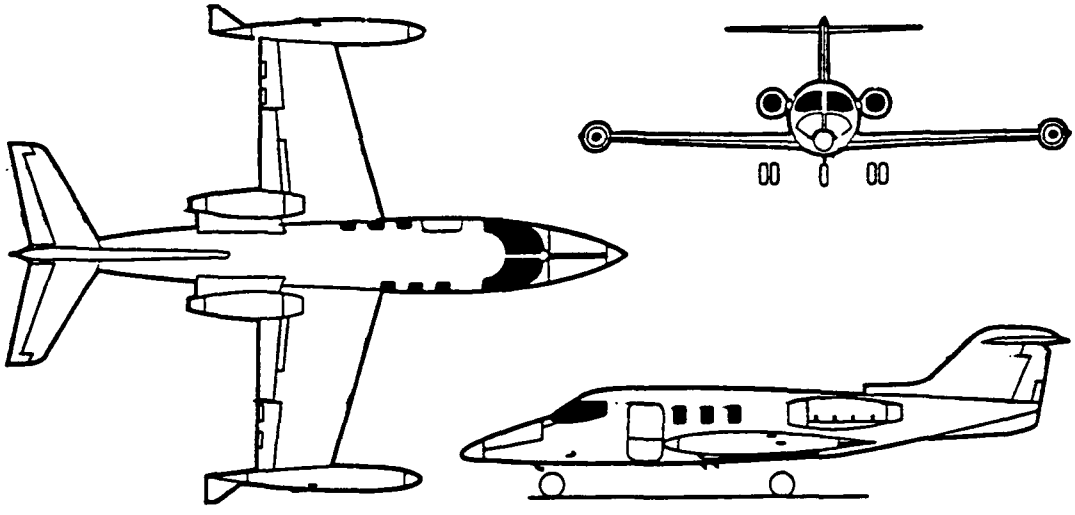

Figure 2.5 The Lear 24 Executive Jet (Ref. 7)

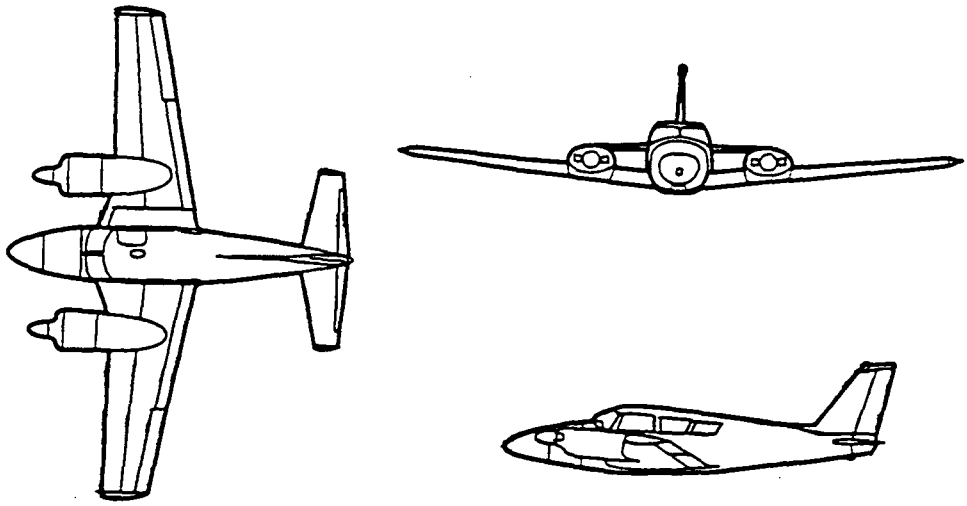

Figure 2.6 The PA-30 Light, Twin-Engine Airplane (Ref. 7)

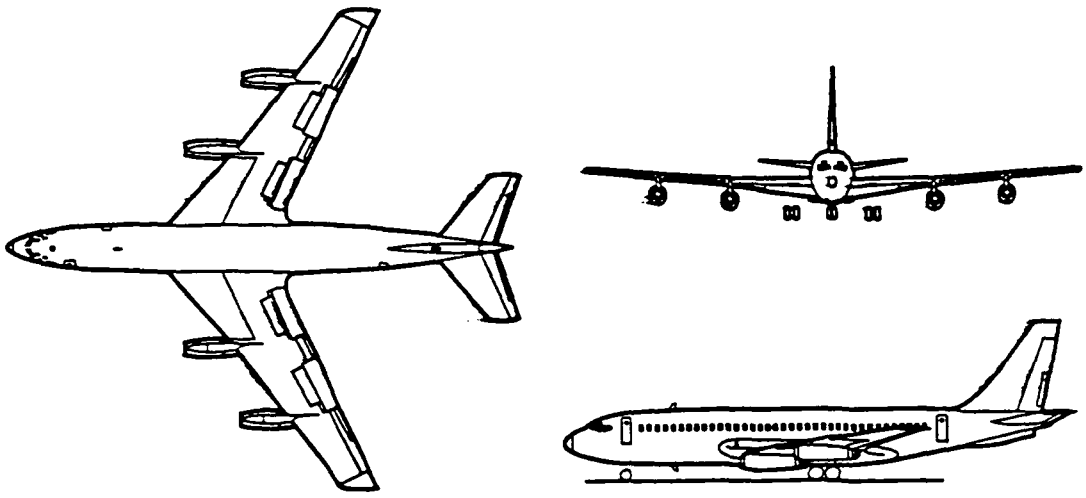

Figure 2.7 The B-720 Commercial Jet Transport (Ref. 7)

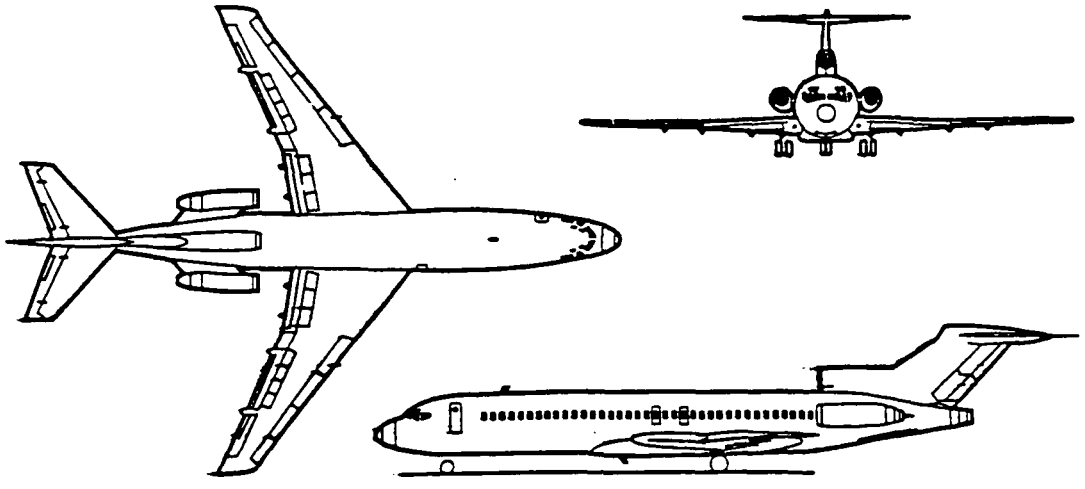

Figure 2.8 The B-727 Commercial Jet Transport (Ref. 7)

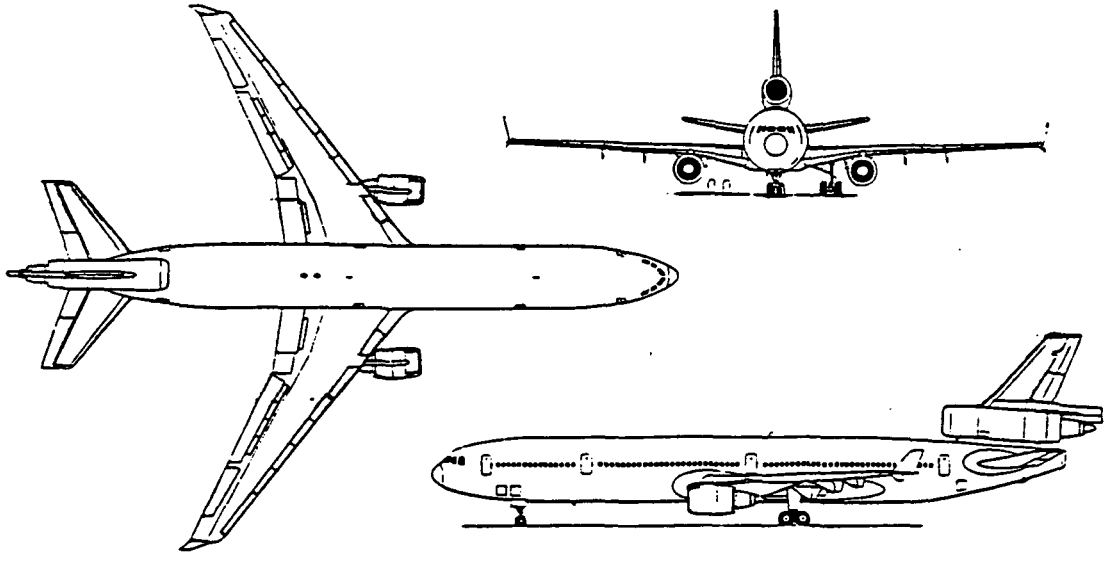

Figure 2.9 The MD-11 Commercial Jet Transport (Ref. 20)

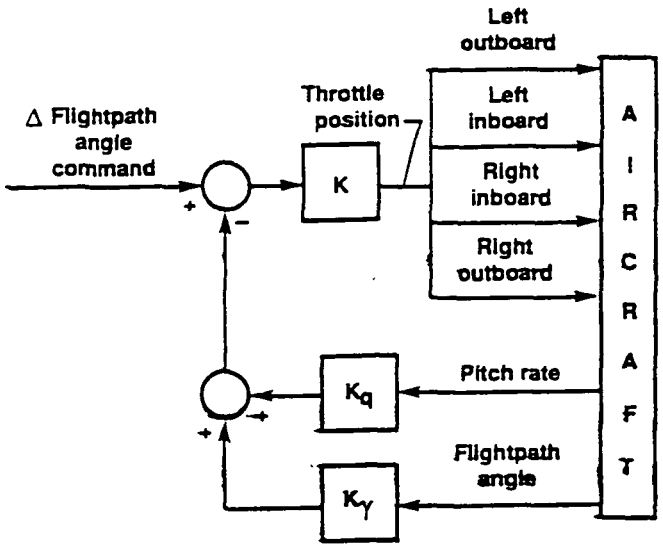

Figure 2.10 B-720 Longitudinal Block Diagram - Flight Path Angle Control (Ref. 9)

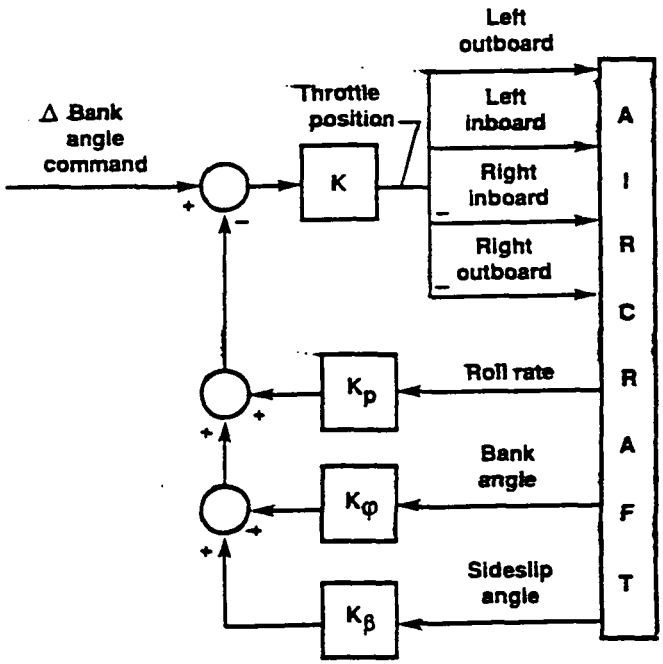

Figure 2.11 B-720 Lateral-Directional Block Diagram - Bank Angle and Heading Control (Ref. 9)

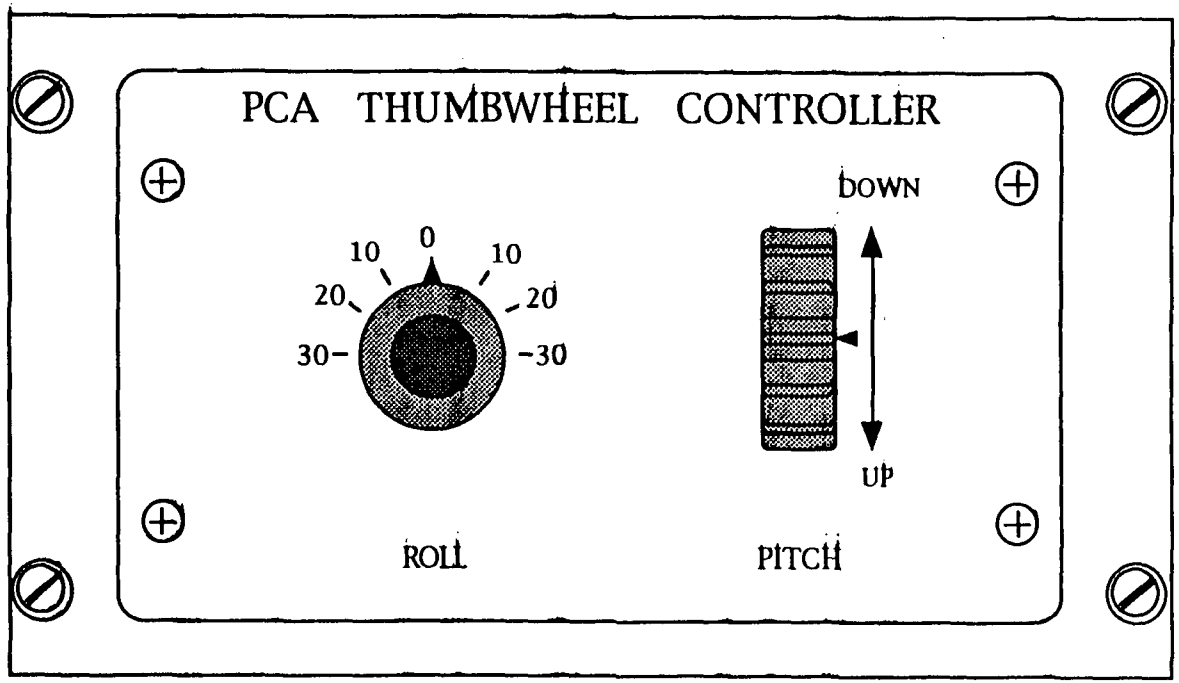

Figure 2.12 NASA Dryden Simulator PCA Thumbwheel Controller Panel

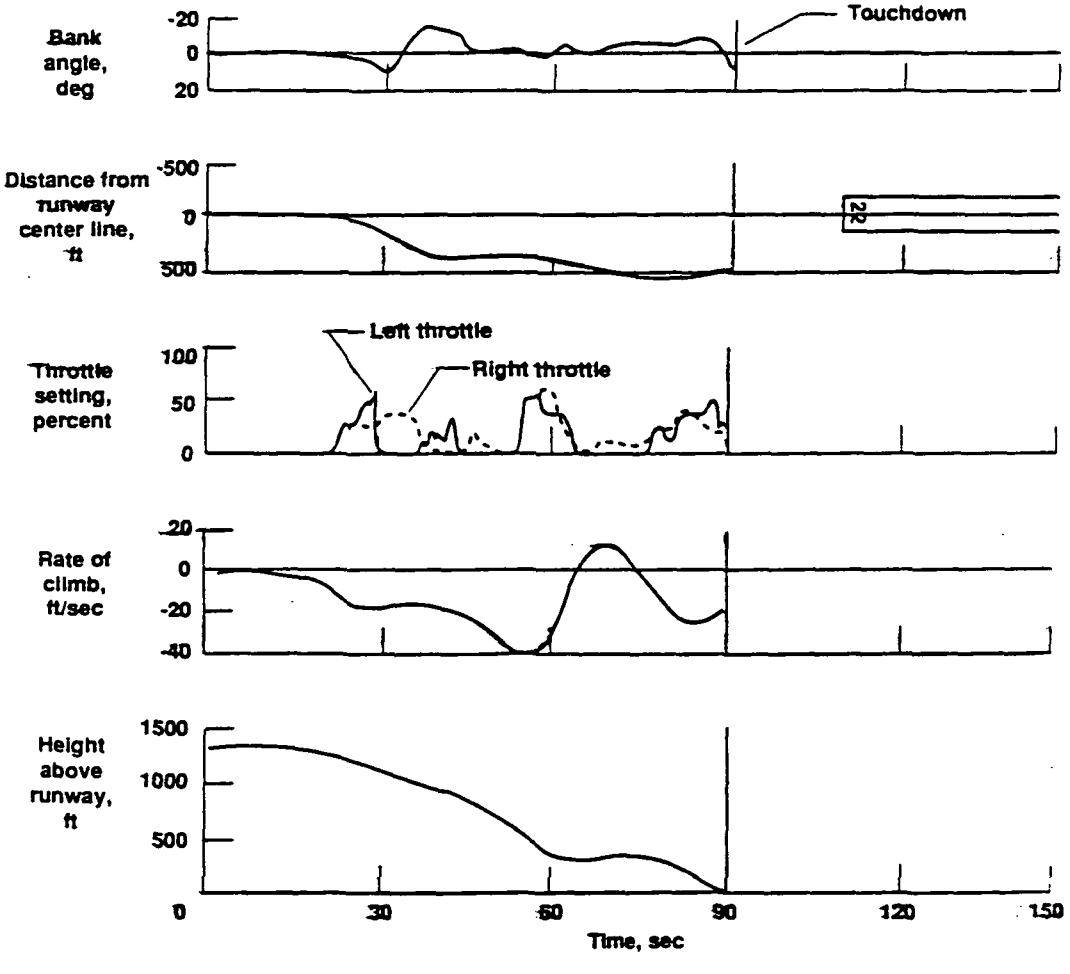

Figure 2.13 Time History of Throttles-Only Manual Landing of the F-15 Simulation (Trim Airspeed 170 knots - Pilot Inexperienced with Manual Throttles-Only Control) (Ref. 7)

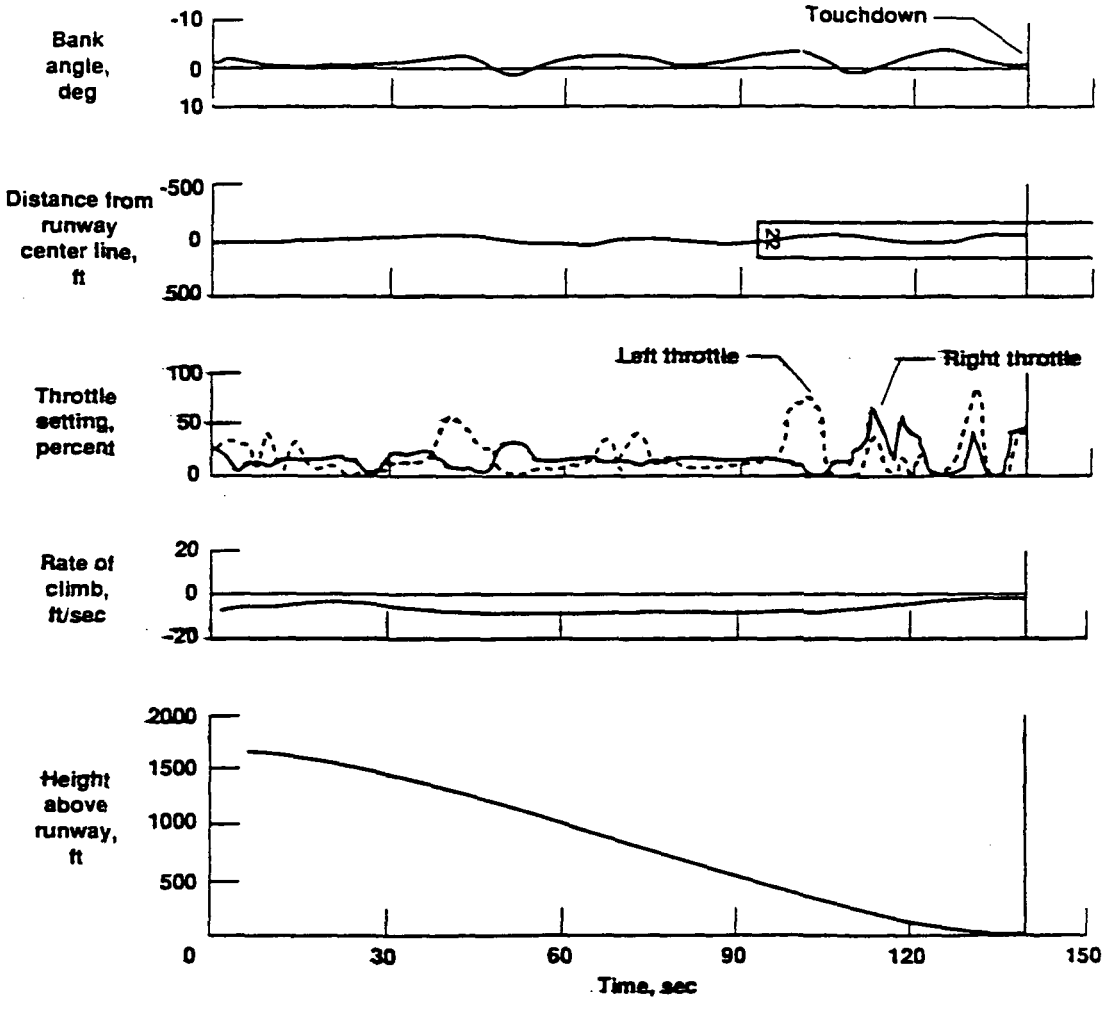

Figure 2.14 Time History of Augmented Throttles-Only Landing of the F-15 Simulation (Trim Airspeed 170 knots - Inexperienced Pilot's First Landing Using System) (Ref. 7)

CHAPTER 3

PRELIMINARY MEGATRANSPORT DESIGN

3.1. INTRODUCTION

An ultra-high capacity aircraft, or megatransport, was designed using References 32 through 45 and the Advanced Aircraft Analysis program (Reference 46). AAA is an interactive computer program which was developed by Design, Analysis and Research Corporation in conjunction with the University of Kansas to perform preliminary design and analysis functions for fixed wing aircraft.

The megatransport was designed to meet the mission specifications and mission profile which are presented in the following sections.

3.2. MISSION SPECIFICATIONS [Refs. 17,32,33]

- Role
  - 800 passenger capacity commercial jet transport aircraft
- Crew
  - 2 flight crews - each flight crew consisting of 1 pilot and 1 co-pilot
  - 16 flight attendants

- Payload
  - Each crewmember is allowed 30 lb of baggage
  - Each passenger is allowed 40 lb of baggage
- Performance
  - Range : 5,000 nautical miles
  - Cruise Speed : M = 0.85 at 35,000 ft
  - Cruise Altitude : 35,000 ft
  - Service Ceiling : 40,000 ft
  - Field Length : 10,000 ft @ 5,000 ft field elevation, 95° F day
  - Climb : Direct climb to cruise altitude
- Powerplant
  - 4 turbofan engines
- Certification
  - FAR 25
- Fuel Reserves
  - Must meet FAR 121.645 fuel supply requirements for turbine-engine-powered flag carrier operations.

3.3. MISSION PROFILE [Refs. 17,33]

FAR 121.645 states, in part, that no turbine-engine-powered flag carrier may be dispatched unless it has enough fuel:

- to fly and land at the airport to which it is released;

- after that, to fly for a period of 10 percent of the total time required to fly from the airport of departure to, and land at the airport to which it was released;
- after that, to fly to and land at the most distant alternate airport specified in the flight release, if an alternate is required; and
- after that, to fly for 30 minutes at holding speed at 1,500 feet above the alternate airport under standard temperature conditions.

The conditions of the FAR 121.645 fuel requirements determine the mission profile of the megatransport as follows. The mission profile consists of the following 14 mission segments:

- Warmup
- Taxi
- Takeoff to destination airport
- Climb to cruise altitude
- Cruise to destination airport
- Loiter for a time period equal to 10 percent of the total time required to fly from the airport of departure to, and land at the airport to which it was released
- Descent
- Land/Taxi
- Takeoff to alternate airport
- Climb to intermediate altitude
- Cruise to alternate airport

- Loiter for a time period of 30 minutes at holding speed at 1,500 feet above the alternate airport
- Descent
- Land/Taxi.

The mission profile of the megatransport is shown in Figure 3.1.

3.4. PRELIMINARY SIZING [Refs. 32,33,34]

Airplanes must meet very stringent range, endurance, and speed requirements while carrying a given payload. It is important to be able to accurately predict the takeoff weight of the airplane, wing area, and maximum takeoff thrust required to meet the mission specifications. Preliminary sizing is the process by which these design parameters may be calculated.

3.4.1. WEIGHT SIZING

The takeoff weight can be broken down as follows:

$$W_{TO} = W_E + W_F + W_{PL} + W_{tfo} + W_{crew} \qquad \text{[Eqn. 3.1]}$$

where:

- W_{TO} is the gross takeoff weight
- W_E is the empty weight
- W_F is the fuel weight
- W_{PL} is the payload weight

- W_{tfo} is the trapped fuel and oil weight
- W_{crew} is the weight of the crewmembers.

A summary of the weight data for the megatransport can be found in Table 3.1.

3.4.2. PERFORMANCE SIZING

Airplanes are usually required by the FAA or the customer to meet performance objectives in the following areas:

- stall speed
- takeoff distance
- climb rate
- cruise speed
- maneuvering
- landing distance.

Satisfying one of these performance objectives will determine a range of takeoff thrust-to-weight ratios, $(T/W)_{TO}$, and takeoff wing loading values, $(W/S)_{TO}$, for which the airplane will satisfy the particular performance objective being evaluated. Satisfying these performance objectives simultaneously results in a range where values of $(T/W)_{TO}$ and $(W/S)_{TO}$ may be selected in which all the performance objectives of the airplane are met.

It usually follows that the combination of the highest possible wing loading and the lowest possible thrust loading which still meets all performance requirements results in an airplane with the lowest weight.

In the United States, large commercial transport aircraft such as the megatransport are required to meet the performance objectives specified by FAR 25 regulations. The following sections will summarize the FAR 25 performance requirements and determine the range of takeoff thrust-to-weight ratios and wing loading values required by the megatransport to achieve these performance objectives.

3.4.2.1. STALL SPEED PERFORMANCE

There are no FAR 25 stall speed requirements.

3.4.2.2. TAKEOFF DISTANCE PERFORMANCE

The takeoff field length, S_{TOFL}, relates the thrust-to-weight ratio and the wing loading in the following equation:

$$S_{TOFL} = 37.5(W/S)_{TO}/\{\sigma C_{L_{maxTO}}(T/W)_{TO}\} \qquad \text{[Eqn. 3.2]}$$

A plot of the takeoff distance constraints for three different takeoff lift coefficients is found in Figure 3.2.

3.4.2.3. CLIMB PERFORMANCE

3.4.2.3.1. FAR 25 CLIMB REQUIREMENTS

FAR 25 climb requirements stipulate both takeoff and landing climb gradients for the following six flight segments:

- initial climb segment - one engine inoperative
- transition segment climb - one engine inoperative
- second segment climb - one engine inoperative
- enroute climb - one engine inoperative
- balked landing - all engines operating
- balked landing - one engine inoperative.

For jet powered airplanes with one engine inoperative, Equation 3.3 is used:

$$(T/W)_{TO} = \{N/(N-1)\}\{(L/D)^{-1} + CGR\} \qquad \text{[Eqn. 3.3]}$$

For jet powered airplanes with all engines operating, Equation 3.4 is used:

$$(T/W)_{TO} = \{(L/D)^{-1} + CGR\} \qquad \text{[Eqn. 3.4]}$$

As can be seen from the equations, the climb performance is independent of the wing loading. A plot of the FAR 25 climb requirements is shown in Figure 3.3. As can be seen in the figure, the most critical climb constraint is that imposed by the second segment climb requirement.

3.4.2.3.2. TIME-TO-CLIMB AND CEILING REQUIREMENTS

In addition to satisfying FAR 25 climb performance criteria, the megatransport was also sized to satisfy time-to-climb requirements, where a direct climb to cruise altitude is desired, and ceiling requirements, where the rate of climb at the service ceiling (40,000 ft) is specified as 500 feet per minute.

The rate of climb, RC, may be determined by simultaneously solving Equations 3.5 and 3.6:

$$RC = RC_0[1 - (h_{cruise}/h_{ceiling})] \qquad \text{[Eqn. 3.5]}$$

$$RC = V\{(T/W)_{TO} - (L/D)^{-1}\} \qquad \text{[Eqn. 3.6]}$$

where:

$$V = [2(W/S)_{TO}/\{\rho(C_{D_0}\pi Ae)^{1/2}\}]^{1/2} \qquad \text{[Eqn. 3.7]}$$

The ceiling requirement may be determined by substituting in a value of 500 feet per minute for the rate of climb at the service ceiling in Equation 3.6.

Figure 3.4 shows a plot of the time-to-climb and ceiling requirements of the megatransport. The time-to-climb requirement is by far the most critical constraint of the two as can be seen in the figure.

3.4.2.4. CRUISE SPEED PERFORMANCE

The cruise speed of the megatransport was specified in the mission specifications to be M = 0.85 at 35,000 ft. This is equivalent to a cruise airspeed of 490 knots. The equation for determining the cruise speed requirements is:

$$(T/W)_{CR} = C_{D_0}(1/2)\rho(V_{CR})^2(S/W)_{CR} + (W/S)_{CR}/[(1/2)\rho(V_{CR})^2\pi Ae] \qquad \textit{[Eqn. 3.8]}$$

where:

$$(T/W)_{TO} = (T/W)_{CR}(T_{TO}/T_{CR})(W_{CR}/W_{TO}) \qquad \text{[Eqn. 3.9]}$$

$$(W/S)_{TO} = (W/S)_{CR}(W_{TO}/W_{CR}) \qquad \text{[Eqn. 3.10]}$$

Figure 3.5 shows a plot of the cruise speed requirements for the megatransport.

3.4.2.5. MANEUVERING PERFORMANCE

The FAA specifies the lateral control requirements for an airplane with four or more engines in FAR 25.147. The regulation states, in part, that the airplane must be able to make 20 degree banked turns under the following conditions:

- with and against the two critical engines inoperative
- from steady flight at a speed equal to 1.4 V_{S_1}

- with maximum continuous power
- the center of gravity must be in the most forward position
- the flaps must be in the most favorable climb position
- landing gear retracted
- maximum landing weight.

The relationship between the thrust-to-weight ratio and the takeoff wing loading is given by the following equation:

$$(T/W)_{TO} = \left[\bar{q}C_{D_0}/(W/S)_{TO}\right] + \left[(W/S)_{TO}(n)^2/(\pi A e \bar{q})\right] \qquad \text{[Eqn. 3.11]}$$

A plot of the megatransport maneuvering requirements is shown in Figure 3.6.

3.4.2.6. LANDING DISTANCE PERFORMANCE

The landing field length, S_{FL}, is related to the takeoff wing loading through the following equations:

$$S_{FL} = 0.3V_A^2 \qquad \text{[Eqn. 3.12]}$$

$$V_A = 1.3V_{S_L} \qquad \text{[Eqn. 3.13]}$$

$$V_{S_L} = \{2(W/S)_L/\rho C_{L_{max_L}}\}^{1/2} \qquad \text{[Eqn. 3.14]}$$

$$(W/S)_{TO} = (W/S)_L(W_{TO}/W_L) \qquad \text{[Eqn. 3.15]}$$

Figure 3.7 shows the plot of the landing distance constraints. As can be seen from the equations and the figure, the landing distance performance is independent of the thrust-to-weight ratio.

3.4.2.7. DETERMINATION OF TAKEOFF THRUST-TO-WEIGHT RATIO AND TAKEOFF WING LOADING FOR THE MEGATRANSPORT

Figure 3.8 plots the thrust loading and wing loading requirements for the following performance parameters:

- takeoff distance
- climb rate
    - FAR 25 second segment climb requirement
    - time-to-climb requirement
- cruise speed
- maneuvering.

Only the most critical climb constraint, the second segment climb requirement, was plotted for the FAR 25 climb requirements. The ceiling requirement was not plotted since it was determined to be a non-critical parameter as compared to the time-to-climb requirement.

The landing distance requirements were not plotted because all of the $(W/S)_{TO}$ constraints were well above 200 lb/ft^2, as can be seen in Figure 3.7. These values were not considered to be of critical importance compared with the $(W/S)_{TO}$ constraints shown in Figures 3.2 through 3.6.

Point 'P', shown in Figure 3.8, lies in the area which satisfies all the performance requirements, provided the value of the maximum lift coefficient is 2.3 or less, and provides an acceptable combination of the highest possible takeoff wing loading with the lowest possible thrust-to-weight ratio. The selected values are:

- $(T/W)_{TO} = 0.28$
- $(W/S)_{TO} = 120$ lb/ft^2

Using these values it is then possible to determine T_{TO} as:

$$T_{TO} = W_{TO}(T/W)_{TO} \qquad \text{[Eqn. 3.16]}$$

$$= (1{,}421{,}900)(0.28)$$

$$= 398{,}132 \text{ lb}$$

and S_W as:

$$S_W = W_{TO}/(W/S)_{TO} \qquad \text{[Eqn. 3.17]}$$

$$= (1{,}421{,}900)/(120)$$

$$= 11{,}849 \text{ ft}^2$$

So the takeoff thrust and the wing area for the megatransport have been performance sized to be, respectively:

- $T_{TO} = 400{,}000$ lb

  $= 100{,}000$ lb per engine

- $S_W = 11{,}900$ ft^2

3.5. MEGATRANSPORT GEOMETRY [Refs. 20,32,33,35,36,37,40,42]

The geometry of the megatransport depends, in large part, on its mission specifications (number of passengers, payload, range, cruise speed), as well as the requirements of federal regulating agencies (FAA mandated number of exits, width of aisles) and the physical limitations of airports (maximum runway or ramp weight, maximum wing span allowed at terminal gate).

The following sections will describe the design criteria which shaped the design of the megatransport. A three-view of the megatransport can be found in Figure 3.9.

3.5.1. FUSELAGE GEOMETRY

The fuselage must be wide enough and long enough to hold 800 passengers and their baggage, 20 crewmembers and their luggage, plus aisles, exits, galleys, lavatories, storage and cargo space.

Because of its large capacity, the megatransport was designed to have three decks - the upper two decks for passenger seating and the lower deck for cargo and baggage. A cross-section of the fuselage is shown in Figure 3.10. The fuselage geometry data are listed in Table 3.2.

3.5.2. WING GEOMETRY

The wing must be large enough to:

- generate sufficient lift for the megatransport
- carry the bulk of the fuel required to complete the mission task
- provide adequate area for the attachment of the ailerons, spoilers, flaps, and leading edge slats.

The wing area needed to achieve the FAR 25 performance objectives was previously determined in the preliminary sizing section. The airfoil that was selected was the NACA 64A411 cambered airfoil (11% thickness-to-chord ratio) at the wing root and the NACA 64A409 cambered airfoil (9% thickness-to-chord ratio) at the wing tip.

The type of flaps which were chosen for the megatransport were Fowler flaps. The megatransport wing was also equipped with full-span leading-edge slats. The wing geometry data are listed in Table 3.2.

3.5.3. EMPENNAGE GEOMETRY

The empennage consists of both the horizontal and vertical tails. The horizontal tail must be large enough to:

- provide adequate area for the attachment of the elevator
- provide sufficient longitudinal control.

The vertical tail must be large enough to:

- provide adequate area for the attachment of the rudder
- provide sufficient directional control.

The airfoil that was selected for both the horizontal and vertical stabilizers was the NACA 0009 symmetrical airfoil (9% thickness-to-chord ratio) throughout the entire span. Geometry data for the horizontal and vertical tails are listed in Table 3.2.

3.5.4. CONTROL SURFACE GEOMETRY

The megatransport achieves longitudinal and lateral-directional control with the following control surfaces:

- longitudinal control
  - horizontal stabilizer
  - elevator
- lateral-directional control
  - inboard ailerons
  - outboard ailerons
  - spoilers
  - rudder.

The horizontal stabilizer and elevator geometry can be seen in Figure 3.11, while the vertical tail and rudder geometry are shown in

Figure 3.12. The layout of the inboard and outboard ailerons, spoilers, flaps, and leading edge slats on the wing is detailed in Figure 3.13.

3.5.5. ENGINE GEOMETRY

In the megatransport performance sizing calculations, it was found that the required takeoff thrust was 100,000 pounds of thrust per engine. At present, there is no commercial transport engine that produces this much thrust, although the Pratt & Whitney PW4084 and General Electric GE90 turbofan engines come the closest rated at 84,000 pounds thrust and 87,000 pounds thrust, respectively.

NASA Dryden Flight Research Center was given a static engine deck of the Pratt & Whitney PW4084 turbofan engine by the Pratt & Whitney division of United Technologies Corporation (UTC). Since the PW4084 engine thrust is not rated high enough for the thrust levels required for the megatransport engine, the PW4084 thrust data were extrapolated for use in the megatransport simulator. The engine model which was used for the megatransport, including engine time lag and time constants, is described in detail in Appendix B.

Because the PW4084 engine was used as a model for the megatransport engine, the megatransport engine geometry is based on the physical dimensions of the PW4084 engine. The fan diameter and overall length of the megatransport engine are listed in Table 3.2. The engine can be seen to scale in the megatransport three-view shown in Figure 3.9.

C-2

3.5.6. LANDING GEAR GEOMETRY

The landing gear must be designed to:

- absorb impact loads upon landing
- distribute the weight of the aircraft so that runway damage such as impact punctures or surface deformations do not occur
- satisfy longitudinal and lateral-directional tip-over criteria
- satisfy longitudinal and lateral-directional ground clearance criteria.

The megatransport was designed to have one nose gear, consisting of a single bogey with four wheels in a twin tandem arrangement, and four main landing gear bogeys, each bogey having a tri-twin tandem arrangement of the six wheels. A view of the landing gear arrangement can be seen in Figure 3.14. The two inboard bogeys retract into the fuselage, while the two outboard bogeys retract into the wing structure.

Any spray caused by the nose gear on a wet runway or any gravel thrown up by the nose gear must not enter the engine inlets. The placement of the nose gear satisfies the spray and foreign object ingestion angle criteria of Reference 37.

The placement of the main gear bogeys satisfies both the longitudinal and lateral tip-over criteria as well as the longitudinal and lateral ground clearance requirements of Reference 35. The landing gear can be seen in the megatransport three-view shown in Figure 3.9.

3.6. DRAG POLARS [Ref. 34]

Assuming a parabolic drag polar, the drag coefficient of an airplane can be written as:

$$C_D = C_{D_O} + C_L^2/(\pi Ae) \qquad \text{[Eqn. 3.18]}$$

where C_{D_O}, the zero-lift drag coefficient, can be expressed as:

$$C_{D_O} = f/S \qquad \text{[Eqn. 3.19]}$$

where f is the equivalent parasite area and S is the wing area.

The value of C_{D_O} will vary depending on whether the configuration is clean (no extended gear, no flaps) or whether takeoff flaps (0° - 20° flaps), landing flaps (30° - 50° flaps), or landing gear are extended.

The low speed drag polars for the following five configurations were calculated:

- takeoff, gear down
- takeoff, gear up
- clean configuration
- landing, gear up
- landing, gear down.

Table 3.3 presents a summary of the drag polar equations for the five configurations listed above. A drag polar plot of the megatransport in the clean configuration is shown in Figure 3.15.

3.7. WEIGHT AND BALANCE [Refs. 34,35,38,43]

3.7.1. EMPTY WEIGHT

The empty weight of the megatransport was divided into the ten major weight component groups listed below:

- fuselage group
- wing group
- emmpenage group 1 (horizontal tail)
- emmpenage group 2 (vertical tail)
- landing gear group 1 (nose gear bogey)
- landing gear group 2 (main gear bogies)
- engine group 1 (right and left inboard engines)
- engine group 2 (right and left outboard engines)
- fixed equipment group 1 (equipment between nose and mid-fuselage point)
- fixed equipment group 2 (equipment between mid-fuselage point and tail).

The AAA design program was used to estimate the weight of the groups listed above. The methodology used relies on the estimation of the weight of these various groups as a percentage of the gross takeoff weight. These percentages are obtained from actual weight data for existing airplanes.

The procedure is to average these percentages for a number of airplanes similar to the one being designed. These averaged percentages are

multiplied by the takeoff weight to obtain a first estimate of the weight of each major component. The estimated weights for these major components of the megatransport are listed in Table 3.4.

One of the variables under investigation in this project was the location of the engine with respect to the wing. Several of the test points run in the megatransport simulator involved changing the engine location on the wing (see Chapter 5). The wing weight is a function of many factors such as shear forces, bending moments, stress levels, and material properties. These, in turn, depend upon the placement of the engines.

Torenbeek (Ref. 43) has developed a design-sensitive weight prediction method for wing structures which was used to modify the wing weight, and therefore the total airplane weight, according to the engine location on the wing. If one of these engine location test points was to be run, the weight of the airplane was changed and entered into the simulator. The methodology used for calculating the wing weight is found in Appendix C.

3.7.2. FUEL AND PAYLOAD WEIGHTS

The center of gravity of the megatransport was calculated by breaking down the gross fuel and payload weights into more detailed components and determining the x-, y-, and z-direction moment-arms of these smaller components.

The takeoff weight of the megatransport, consisting primarily of the aircraft empty weight, payload weight, and fuel weight, has been divided into the thirteen major components listed below:

- empty weight (consisting of the ten weight groups discussed previously)
- crew (2 flight crews plus crew baggage)
- trapped fuel and oil
- mission fuel group 1 (inboard fuel tanks)
- mission fuel group 2 (outboard fuel tanks)
- passenger group 1 (passengers between nose and mid-fuselage point on the lower passenger deck)
- passenger group 2 (passengers between nose and mid-fuselage point on the upper passenger deck)
- passenger group 3 (passengers between mid-fuselage point and tail on the lower passenger deck)
- passenger group 4 (passengers between mid-fuselage point and tail on the upper passenger deck)
- baggage group 1 (passenger carry-on baggage)
- baggage group 2 (passenger baggage stowed on cargo deck)
- cargo group 1 (cargo between nose and mid-fuselage point on the cargo deck)
- cargo group 2 (cargo between mid-fuselage point and tail on the cargo deck).

These component weights and their x- and z-direction moment-arms are listed in Table 3.5. Moment-arms were not listed for the y-direction as the aircraft is assumed to be loaded symmetrically on each side of the xz-plane of the aircraft, resulting in a net moment-arm of zero in the y-direction. The resulting megatransport center of gravity is:

- x_{cg} = 135.15 ft (from nose of aircraft)
- y_{cg} = 0 ft (from centerline of aircraft)
- z_{cg} = 19.94 ft (from ground level)

3.7.3. CENTER OF GRAVITY EXCURSION

It is important to know how the center of gravity of the aircraft changes not only in the air as fuel is burned, but also on the ground as cargo and passengers are loaded or unloaded.

A c.g. diagram has been made for the megatransport in the x- and z-directions as can be seen in Figures 3.16 and 3.17, respectively. From Figure 3.16 it is noted that the c.g. shift between the most fore and aft c.g. location in the x-direction is only 1.71% and 1.86%, respectively. Figure 3.17 shows that the c.g. shift between the lowest and highest c.g. location in the z-direction is only 1.91% and 0.32%, respectively.

3.7.4. INERTIAS

The following equations were used to calculate the megatransport body-axis moments of inertia, I_{xx}, I_{yy}, and I_{zz}, and the product of inertia, I_{xz}:

$$I_{xx} = \sum_{i=1}^{n} m_i \left\{ \left(y_i - y_{cg}\right)^2 + \left(z_i - z_{cg}\right)^2 \right\} \qquad \text{[Eqn. 3.20]}$$

$$I_{yy} = \sum_{i=1}^{n} m_i \left\{ \left(x_i - x_{cg} \right)^2 + \left(z_i - z_{cg} \right)^2 \right\} \qquad \text{[Eqn. 3.21]}$$

$$I_{zz} = \sum_{i=1}^{n} m_i \left\{ \left(x_i - x_{cg} \right)^2 + \left(y_i - y_{cg} \right)^2 \right\} \qquad \text{[Eqn. 3.22]}$$

$$I_{xz} = \sum_{i=1}^{n} m_i \left\{ \left(x_i - x_{cg} \right)\left(z_i - z_{cg} \right) \right\} \qquad \text{[Eqn. 3.23]}$$

where 'i' represents the summation of the components listed in Table 3.5.

The moments and products of inertia of the megatransport are:

- I_{xx} = 57,995,453 sl-ft^2
- I_{yy} = 59,538,365 sl-ft^2
- I_{zz} = 114,154,212 sl-ft^2
- I_{xz} = 3,154,588 sl-ft^2

For a symmetric aircraft, the products of inertia I_{xy} and I_{yz} are zero.

As was mentioned in Section 3.7.1, one of the variables under investigation in this project was the location of the engine with respect to the wing. Several of the test points run in the megatransport simulator involved changing the engine location on the wing.

If one of these engine location test points was to be run, the *x*-, y-, and z-coordinates of the new engine location would be entered into the simulator, along with the new values for the airplane I_{xx}, I_{yy}, I_{zz}, and I_{xz} inertias which had changed due to the new engine location. The inertias for each of the test points run in the simulator are listed in Table C1.

3.8. STABILITY AND CONTROL DERIVATIVES [Refs. 18,39,44,45]

Aircraft dynamic properties are defined, in general, by the aircraft equations of motion. These force and moment equations consist of aircraft nondimensional stability derivative terms, along with information such as the velocity, altitude, angle of attack, geometry, weight, inertias, and thrust of the aircraft. The aerodynamic force and moment coefficient equations which were used in the megatransport simulator are covered in Section 4.2.

Since the primary purpose of this project was to evaluate the controllability of the megatransport using the throttles-only control system during approach and landing, stability derivatives were calculated only for a limited flight envelope. The altitude limits of the limited flight envelope ranged from zero to 5,000 feet, the velocity limits ranged from zero to 330 knots (corresponding to Mach numbers of approximately zero to 0.5 throughout this altitude range), and the angle of attack varied from -4 to 14 degrees.

Because these stability and control derivatives are nondimensional, comparison between different flight conditions or between different aircraft are possible. Tables 3.6 and 3.7 list the primary longitudinal and lateral-directional stability and control derivatives, respectively, for the megatransport, B-747, C-5A, and DC-8 in a power approach condition. As can be seen from the data, the megatransport derivatives compare reasonably well with the derivatives of the other aircraft.

3.9. MEGATRANSPORT DYNAMICS [Refs. 18,41]

3.9.1. DYNAMIC STABILITY REQUIREMENTS

It is generally agreed that airplanes must be able to meet certain dynamic stability and flying quality requirements. In the United States, commercial aircraft operating under ordinary flight conditions are required to meet FAR 25 regulations. From an aircraft designer's viewpoint, these regulations can be considered to be met if the airplane meets Level 1 flying qualities as defined in the current USAF Military Specification - Flying Qualities of Piloted Airplanes (MIL-Specs) document.

The MIL-Specs specify requirements for response characteristics as a function of time (such as time required to achieve 30 degrees of bank angle) or requirements for specific frequency responses or damping characteristics (such as dutch roll or phugoid frequencies and damping ratios). These specifications are given in numerical tables and graphs, thereby establishing analytical criteria by which to measure whether or not the aircraft achieves the desired handling qualities.

In specifying handling quality criteria, it is necessary to recognize differences in types of aircraft, in types of flying maneuvers to be performed during some phase of flight, and in failure states of airplane systems. These differences are recognized in the flying quality specifications and are defined in Tables 3.8 through 3.11.

The megatransport, being a very large commercial transport aircraft, falls into the Class III classification of airplanes as can be seen from Table 3.8.

Of the three categories listed in Table 3.9, Category C flight phase requirements are of the most interest since this project is concerned primarily with the flying characteristics of the megatransport during the approach and landing phases.

The flying quality levels as defined in Table 3.10 are tied in with the Cooper-Harper pilot rating scale. This scale represents a very successful attempt to relate pilot comments about the ease or difficulty with which airplanes can be controlled in certain flight situations to a numerical rating. The Cooper-Harper scale is shown in Figure 3.18. The tie-in with the flying quality levels as previously defined is indicated in the table.

The Cooper-Harper pilot rating scale was the primary method used by the test pilots to evaluate the flying qualities of the various test runs flown in the megatransport simulator. Cooper-Harper pilot ratings are covered further in Chapters 5 and 6.

3.9.2. LONGITUDINAL DYNAMICS

As was previously mentioned in Section 3.8, aircraft dynamic properties are generally defined by the aircraft equations of motion. The dynamic properties contained in the aircraft equations of motion can best be represented by a series of transfer functions that relate output quantities (various aircraft motions) to input variables (control surface motions). These transfer functions are readily obtained from the linearized Laplace-transformed aircraft equations of motion as sets of ratios between transformed aircraft output and input quantities or initial conditions. The ratios consist of

numerators and denominators expressed as rational polynomials in the Laplace transform variable, 's'. The various polynomial coefficients are composed of combinations of dimensional stability derivatives and aircraft speed and attitude data.

The standard longitudinal transfer functions relate the output quantities angle of attack, speed, and pitch attitude to the elevator deflection input. The longitudinal stability behavior of the airplane depends entirely upon the roots which are obtained when setting the denominator equal to zero. The (α/δ_E), (u/δ_E), and (θ/δ_E) longitudinal transfer function equations are presented in Table 3.12.

The denominator has four complex roots - two pairs of complex conjugates. Each pair of complex conjugates can be factored into a form which yields a frequency and a damping ratio. One pair consists of a highly damped, high frequency oscillation and the other pair consists of a very lightly damped, low frequency oscillation. The first is called the short-period (SP) mode of motion while the second is called the phugoid (P) mode of motion. The short-period and phugoid frequencies and damping ratios for the megatransport in the approach flight condition are listed below:

- $\omega_{nSP} = 1.2419$ rad/sec
- $\zeta_{SP} = 0.7840$
- $\omega_{nP} = 0.1335$ rad/sec
- $\zeta_P = 0.1503$

According to the MIL-Specs, for a Class III aircraft in the Category C flight phase, the phugoid damping ratio, as well as the short-period frequency and damping ratio, all satisfy Level 1 requirements (there is no phugoid

frequency requirement) as can be seen in Figure 3.19. A graph showing the megatransport short-period frequency plotted against the MIL-Spec short-period frequency requirements for Category C flight phase is found in Figure 3.20.

3.9.3. LATERAL-DIRECTIONAL DYNAMICS

The standard lateral-directional transfer functions relate the output quantities sideslip, bank angle, and heading angle to either the aileron or rudder deflection input. The (β/δ_A), (φ/δ_A), (ψ/δ_A), (β/δ_R), (φ/δ_R), and (ψ/δ_R) lateral-directional transfer function equations are presented in Table 3.13.

The denominator has five complex roots - one pair of complex conjugates, two real roots, and one root equal to zero. The zero root is due to the fact that the airplane has neutral heading stability. The pair of complex conjugates can be factored into a form which yields a frequency and a damping ratio. This lightly damped, moderately low frequency oscillation is called the dutch roll (D) mode of motion. The two real roots consist of a slowly divergent term, called the spiral (S) mode of motion, and a highly stable term, called the rolling (R) mode of motion. The spiral and rolling mode time constants, as well as the dutch roll frequency and damping ratio for the megatransport in the approach flight condition, are listed below:

- $T_S = 70.4270$ sec
- $T_R = 0.4890$ sec
- $\omega_{nD} = 0.8941$
- $\zeta_D = 0.2375$

According to the MIL-Specs, for a Class III aircraft in the Category C flight phase, the spiral time constant, as well as the dutch roll frequency and damping ratio, all satisfy Level 1 requirements as can be seen in Figure 3.21. A graph showing the megatransport dutch roll frequency and damping ratio plotted against the MIL-Spec dutch roll frequency and damping ratio requirements is found in Figure 3.22.

The roll time and roll performance levels are shown in Figure 3.23. The roll performance is defined as the minimum bank angle reached in some specified time after initiation of lateral cockpit control motion. By making measurements from actual megatransport simulator strip chart recordings, the time for the megatransport to achieve a 30 degree bank angle using all the lateral-directional control surfaces was found to be 2.4 seconds. This falls within the MIL-Spec Level 1 requirements for Category C flight phase. The megatransport design satisfies all Level 1 requirements using the conventional flight control system for flight path control.

Table 3.1 Summary of Weight Data for the Megatransport

W_{TO}	1,421,900 lb
W_E	683,400 lb
W_F	541,400 lb
W_{PL}	186,500 lb
W_{tfo}	7,100 lb
W_{crew}	3,500 lb

Table 3.2 Summary of Geometry Data for the Megatransport

Wing

S_W, wing area	11,900 ft^2
b_W, wing span	318.0 ft
AR_W, wing aspect ratio	8.5
λ_W, wing taper ratio	0.30
$\Lambda_{W_{C/4}}$, wing quarter-chord sweep	30 deg
C_W, wing mean geometric chord	41.0 ft
C_{r_W}, wing root chord	57.6 ft
C_{t_W}, wing tip chord	17.3 ft
i_W, wing incidence angle	3 deg
Γ_W, wing dihedral angle	4 deg

Horizontal Tail

S_h, horizontal tail area	2,800 ft^2
b_h, horizontal tail span	105.8 ft
AR_h, horizontal tail aspect ratio	4.0
λ_h, horizontal tail taper ratio	0.34
$\Lambda_{h_{C/4}}$, horizontal tail quarter-chord sweep	35 deg
C_h, horizontal tail mean geometric chord	28.6 ft
C_{r_h}, horizontal tail root chord	39.5 ft
C_{t_h}, horizontal tail tip chord	13.4 ft
Γ_h, horizontal tail dihedral angle	6 deg

Table 3.2 Summary of Geometry Data for the Megatransport (cont.)

Vertical Tail

S_V, vertical tail area ..... 2,019 ft^2

b_V, vertical tail span ..... 56.8 ft

AR_V, vertical tail aspect ratio 1.6

λ_V, vertical tail taper ratio 0.35

$\Lambda_{V_{C/4}}$, vertical tail quarter-chord sweep ..... 37 deg

C_V, vertical tail mean geometric chord ..... 38.3 ft

C_{r_V}, vertical tail root chord ..... 52.6 ft

C_{t_V}, vertical tail tip chord ..... 18.4 ft

Fuselage

L_{fus}, fuselage length ..... 277 ft

D_{fus}, average fuselage diameter ..... 25 ft

Engine

D_{fan}, fan diameter ..... 10.0 ft

L_{eng}, overall engine length ..... 16.7 ft

η, engine cant angle ..... 2 deg

Table 3.3 Summary of Megatransport Drag Polar Equations

Configuration	Equation
Takeoff, Gear Down	$C_D = 0.0464 + 0.0468\ C_L^2$
Takeoff, Gear Up	$C_D = 0.0264 + 0.0468\ C_L^2$
Clean Cofiguration	$C_D = 0.0124 + 0.0441\ C_L^2$
Landing, Gear Up	$C_D = 0.0764 + 0.0499\ C_L^2$
Landing, Gear Down	$C_D = 0.0964 + 0.0499\ C_L^2$

Table 3.4 Empty Weight Breakdown for the Megatransport

Component	Weight
Fuselage Group	132,663 lb
Wing Group	162,585 lb
Empennage Group 1	19,083 lb
Empennage Group 2	12,722 lb
Landing Gear Group 1	7,046 lb
Landing Gear Group 2	55,309 lb
Engine Group 1	64,605 lb
Engine Group 2	64,605 lb
Fixed Equipment Group 1	82,391 lb
Fixed Equipment Group 2	82,391 lb

Table 3.5 Weight and Balance Center of Gravity Excursion for the Fully Loaded Megatransport

Component	Weight (lb)	x (ft) (from nose of aircraft)	z (ft) (from ground level)
Empty Weight	683,400	136.89	19.70
Crew	1,300	24.93	28.96
Trapped Fuel and Oil	7,100	121.02	16.03
Mission Fuel Group 1	378,980	121.02	18.03
Mission Fuel Group 2	162,420	164.64	23.59
Passenger Group 1	35,700	81.72	19.08
Passenger Group 2	35,700	81.72	27.33
Passenger Group 3	35,700	176.50	19.08
Passenger Group 4	35,700	176.50	27.33
Baggage Group 1	8,000	81.72	28.21
Baggage Group 2	24,000	176.50	13.92
Cargo Group 1	6,950	81.72	13.92
Cargo Group 2	6,950	176.50	13.92
Total Takeoff Weight	1,421,900	135.15	19.94

Table 3.6 Longitudinal Nondimensional Stability and Control Derivatives for the Megatransport, B-747, C-5A, and DC-8 (Refs. 44,45)

	Power Approach Condition			
Longitudinal Nondimensional Derivatives	Megatransport	B-747	C-5A	DC-8
C_{m_u}	0.036	0.067	-	-0.001
C_{m_α} (rad^{-1})	-1.127	-1.260	-0.827	-1.478
$C_{m_{\dot{\alpha}}}$ (rad^{-1})	-5.177	-3.200	-8.300	-3.840
C_{m_q} (rad^{-1})	-18.372	-20.800	-23.200	-0.001
$C_{m_{T_u}}$	-0.062	0.000	-	-
$C_{m_{T_\alpha}}$ (rad^{-1})	0.000	0.000	-	-
C_{L_u}	0.045	-0.202	-	0.004
C_{L_α} (rad^{-1})	4.850	5.700	6.080	4.810
$C_{L_{\dot{\alpha}}}$ (rad^{-1})	1.723	-6.700	-	0.000
C_{L_q} (rad^{-1})	6.589	5.400	-	-
C_{D_α} (rad^{-1})	0.458	0.660	0.622	0.487
C_{D_u}	0.023	0.000	-	0.004
$C_{m_{\delta_e}}$ (rad^{-1})	-1.536	-1.340	-1.600	-
$C_{L_{\delta_e}}$ (rad^{-1})	0.511	0.338	0.385	0.328
$C_{D_{\delta_e}}$ (rad^{-1})	0.000	0.000	-	0.000

Table 3.7 Lateral-Directional Nondimensional Stability and Control Derivatives for the Megatransport, B-747, C-5A, and DC-8 (Refs. 44,45)

	Power Approach Condition			
Lateral-Directional Nondimensional Derivatives	Megatransport	B-747	C-5A	DC-8
C_{ℓ_β} (rad^{-1})	-0.229	-0.221	-0.123	-0.158
C_{ℓ_p} (rad^{-1})	-0.609	-0.450	-0.458	-0.385
C_{ℓ_r} (rad^{-1})	0.400	0.101	0.290	0.248
$C_{\ell_{\delta_a}}$ (rad^{-1})	0.062	0.046	0.089*	-0.086
$C_{\ell_{\delta_r}}$ (rad^{-1})	0.017	0.007	0.021	0.022
C_{n_β} (rad^{-1})	0.137	0.150	0.075	0.163
C_{n_p} (rad^{-1})	-0.174	-0.121	-0.098	-0.087
C_{n_r} (rad^{-1})	-0.155	-0.300	-0.293	-0.196
$C_{n_{\delta_a}}$ (rad^{-1})	0.009	0.006	0.009*	-0.011
$C_{n_{\delta_r}}$ (rad^{-1})	-0.072	-0.109	-0.106	-0.083
C_{y_β} (rad^{-1})	-0.618	-0.960	-0.770	-0.873
C_{y_p} (rad^{-1})	-0.090	0.000	-	-
C_{y_r} (rad^{-1})	0.386	0.000	-	-
$C_{y_{\delta_a}}$ (rad^{-1})	0.000	0.000	-0.004*	0.000
$C_{y_{\delta_r}}$ (rad^{-1})	0.190	0.175	0.211	0.187

* Spoiler effects included

Table 3.8 Classification of Airplanes (Ref. 41)

- Class I

  Small, light airplanes such as:

  Light utility
  Primary trainer
  Light observation

- Class II

  Medium weight, low-to-medium maneuverability airplanes such as:

  Heavy utility/search and rescue
  Light or medium transport/cargo/tanker
  Early warning/electronic countermeasures/airborne command, control, or communications relay
  Antisubmarine
  Assault transport
  Reconnaissance
  Tactical bomber
  Heavy attack
  Trainer for Class II

- Class III

  Large, heavy, low-to-medium maneuverability airplanes such as:

  Heavy transport/cargo/tanker
  Heavy bomber
  Patrol/early warning/electronic countermeasures/airborne command, control, or communications relay
  Trainer for Class III

- Class IV

  High maneuverability airplanes such as:

  Fighter/interceptor
  Attack
  Tactical reconnaissance
  Observation
  Trainer for Class IV

Table 3.9 Flight Phase Categories (Ref. 41)

Nonterminal Flight Phases

- Category A

  Those nonterminal flight phases that require rapid maneuvering, precision tracking, or precise flight path control. Included in this Category are:

  a) Air-to-air combat (CO)
  b) Ground Attack (GA)
  c) Weapon delivery/launch (WD)
  d) Aerial recovery (AR)
  e) Reconnaissance (RC)
  f) In-flight refueling (receiver) (RR)
  g) Terrain following (TF)
  h) Antisubmarine search (AS)
  i) Close formation flying (FF)

- Category B

  Those nonterminal flight phases that are normally accomplished using gradual maneuvers and without precision tracking, although accurate flight path control may be required. Included in this Category are:

  a) Climb (CL)
  b) Cruise (CR)
  c) Loiter (LO)
  d) In-flight refueling (tanker) (RT)
  e) Descent (D)
  f) Emergency descent (ED)
  g) Emergency deceleration (DE)
  h) Aerial delivery (AD)

Table 3.9 Flight Phase Categories (cont.)

Terminal Flight Phases

- Category C

  Terminal flight phases are normally accomplished using gradual maneuvers and usually require accurate flight path control. Included in this Category are:

  a) Takeoff (TO)
  b) Catapult takeoff (CT)
  c) Approach (PA)
  d) Wave-off/go-around (WO)
  e) Landing (L)

Table 3.10 Levels of Flying Qualities (Ref. 41)

- Level 1

  Flying qualities clearly adequate for the mission flight phase.

- Level 2

  Flying qualities adequate to accomplish the mission flight phase, but some increase in pilot workload or degradation in mission effectiveness, or both, exists.

- Level 3

  Flying qualities such that the airplane can be controlled safely, but pilot workload is excessive or mission effectiveness is inadequate, or both. Category A flight phases can be terminated safely, and Category B and C flight phases can be completed.

Table 3.11 Allowable Probability of Certain System Failures (Ref. 18)

- At Least Level 1 - for airplane normal (no failure) state

- At Least Level 2 - after failures that occur less than once per 100 flights

- At Least Level 3 - after failures that occur less than once per 10,000 flights

Flying quality levels below Level 3 are not allowed except under special circumstances.

Table 3.12 Longitudinal Transfer Functions of the Megatransport in the Approach Flight Condition

a) Angle of Attack to Elevator Transfer Function

$$\left(\frac{\alpha}{\delta_E}\right) = \frac{-0.0671 \cdot (s + 18.4902) \cdot \left(s^2 + 0.0362s + 0.0317\right)}{\left(s^2 + 1.9473s + 1.5424\right) \cdot \left(s^2 + 0.0401s + 0.0178\right)}$$

b) Speed to Elevator Transfer Function

$$\left(\frac{u}{\delta_E}\right) = \frac{-1.7805 \cdot (s - 6.2113) \cdot (s + 2.2436)}{\left(s^2 + 1.9473s + 1.5424\right) \cdot \left(s^2 + 0.0401s + 0.0178\right)}$$

c) Pitch Attitude to Elevator Transfer Function

$$\left(\frac{\theta}{\delta_E}\right) = \frac{-1.2453 \cdot (s + 0.5657) \cdot (s + 0.0940)}{\left(s^2 + 1.9473s + 1.5424\right) \cdot \left(s^2 + 0.0401s + 0.0178\right)}$$

Table 3.13. Lateral-Directional Transfer Functions of the Megatransport in the Approach Flight Condition

a) Sideslip to Aileron Transfer Function

$$\left(\frac{\beta}{\delta_A}\right) = \frac{0.0321s \cdot (s + 6.9045) \cdot (s + 0.0335)}{s \cdot (s - 0.0142) \cdot (s + 2.0465) \cdot \left(s^2 + 0.4248s + 0.7994\right)}$$

b) Bank Angle to Aileron Transfer Function

$$\left(\frac{\phi}{\delta_A}\right) = \frac{0.4089s \cdot \left(s^2 + 0.2538s + 0.3519\right)}{s \cdot (s - 0.0142) \cdot (s + 2.0465) \cdot \left(s^2 + 0.4248s + 0.7994\right)}$$

c) Heading Angle to Aileron Transfer Function

$$\left(\frac{\psi}{\delta_A}\right) = \frac{-0.0356 \cdot (s - 0.2386) \cdot (s + 5.1667) \cdot (s + 0.3419)}{s \cdot (s - 0.0142) \cdot (s + 2.0465) \cdot \left(s^2 + 0.4248s + 0.7994\right)}$$

d) Sideslip to Rudder Transfer Function

$$\left(\frac{\beta}{\delta_R}\right) = \frac{0.0254s \cdot (s - 0.0549) \cdot (s + 9.2092) \cdot (s + 2.4696)}{s \cdot (s - 0.0142) \cdot (s + 2.0465) \cdot \left(s^2 + 0.4248s + 0.7994\right)}$$

e) Bank Angle to Rudder Transfer Function

$$\left(\frac{\phi}{\delta_R}\right) = \frac{0.1183s \cdot (s - 3.5424) \cdot (s + 0.7655)}{s \cdot (s - 0.0142) \cdot (s + 2.0465) \cdot \left(s^2 + 0.4248s + 0.7994\right)}$$

f) Heading Angle to Rudder Transfer Function

$$\left(\frac{\psi}{\delta_R}\right) = \frac{-0.2419 \cdot (s + 2.2619) \cdot \left(s^2 - 0.0147s + 0.0599\right)}{s \cdot (s - 0.0142) \cdot (s + 2.0465) \cdot \left(s^2 + 0.4248s + 0.7994\right)}$$

MISSION PHASES

1) Warmup
2) Taxi
3) Takeoff to destination airport
4) Climb to cruise altitude
5) Cruise to destination airport
6) Loiter
7) Descent
8) Land/Taxi
9) Takeoff to alternate airport
10) Climb to intermediate altitude
11) Cruise to alternate airport
12) Loiter
13) Descent
14) Land/Taxi

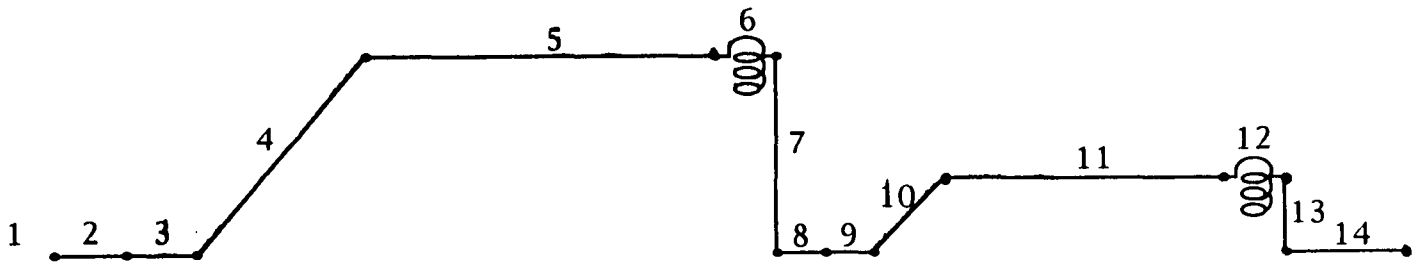

Figure 3.1 Mission Profile of the Megatransport

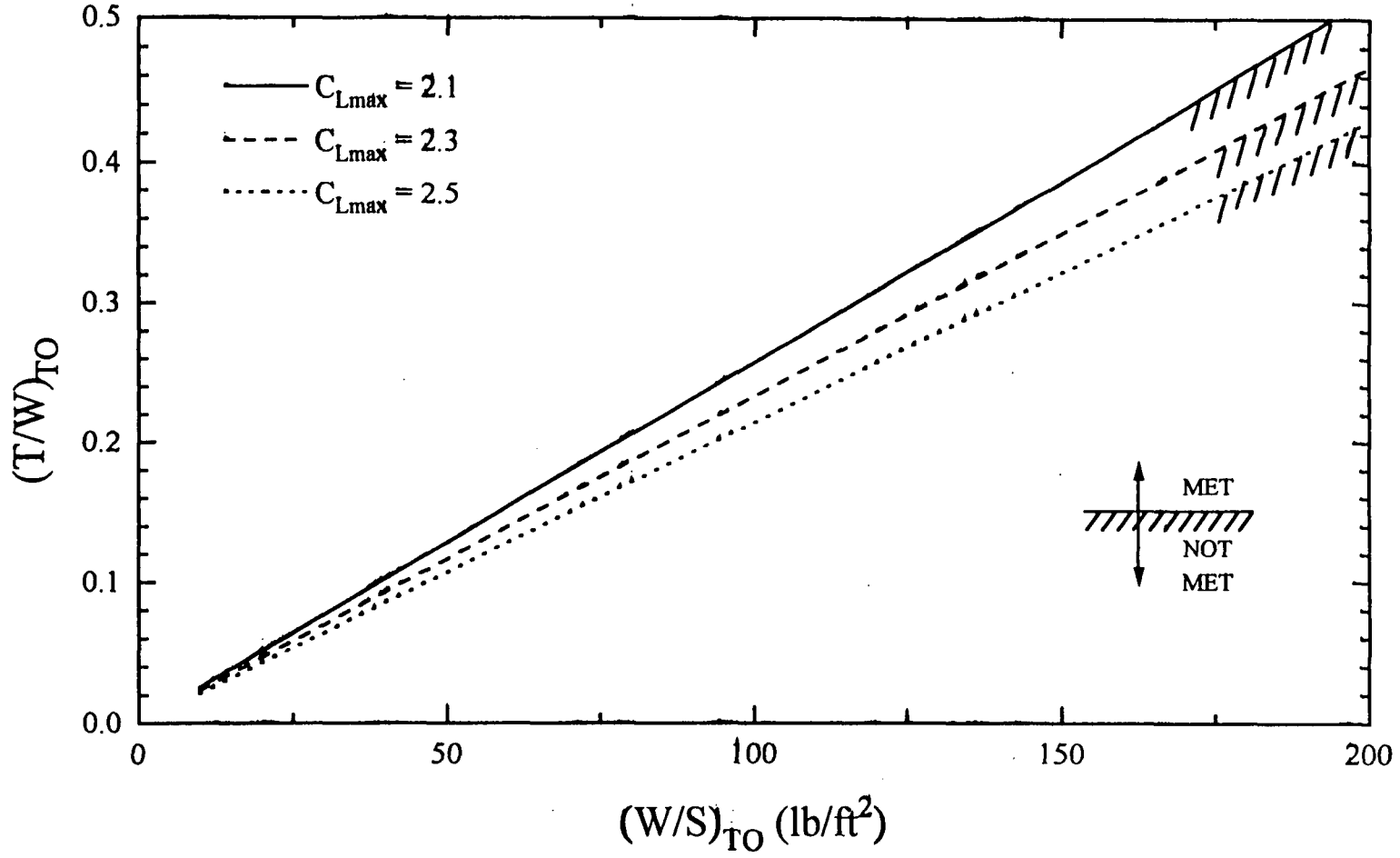

Figure 3.2 Megatransport Performance Sizing, Takeoff Distance Requirements

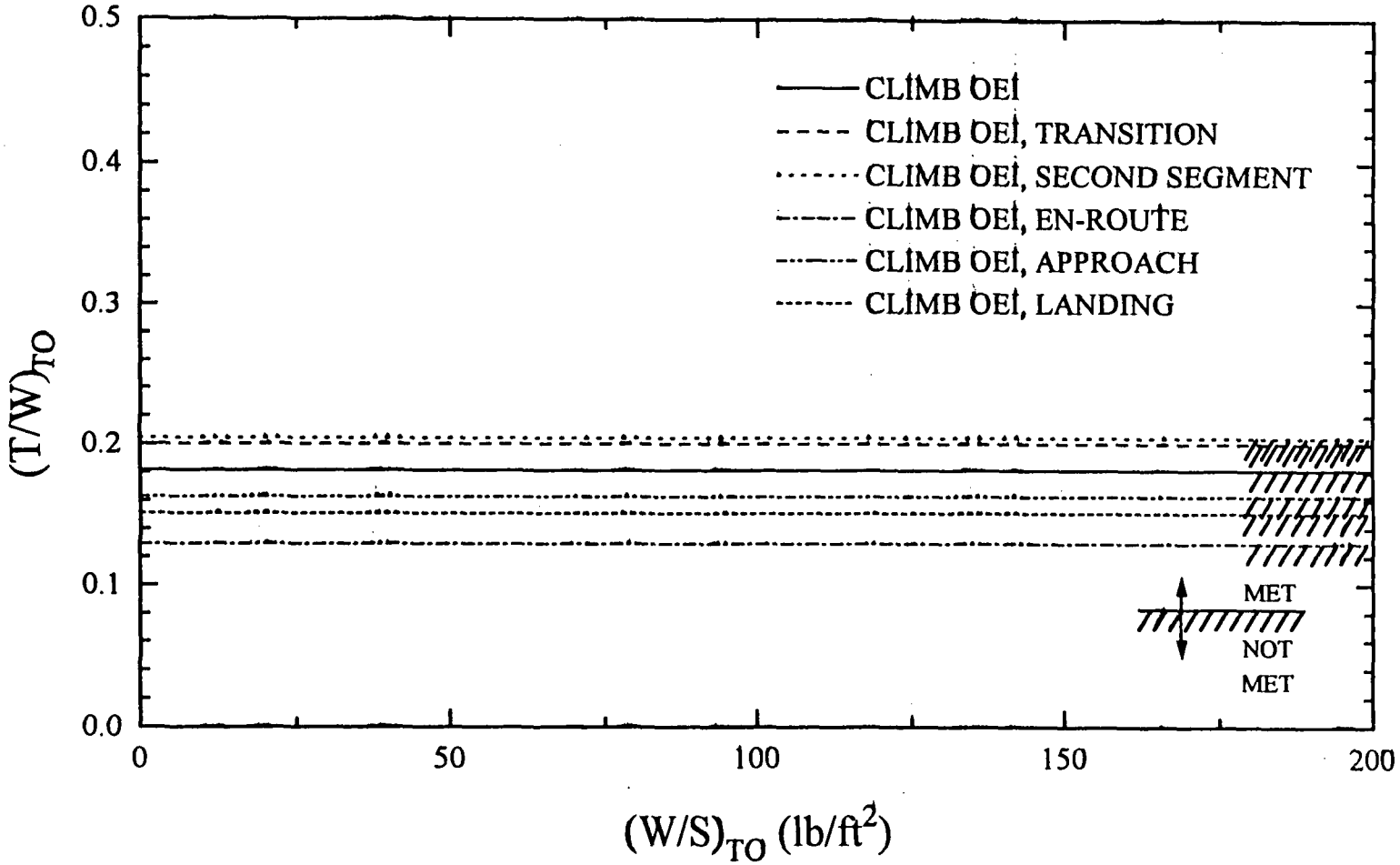

Figure 3.3 Megatransport Performance Sizing, Climb Requirements

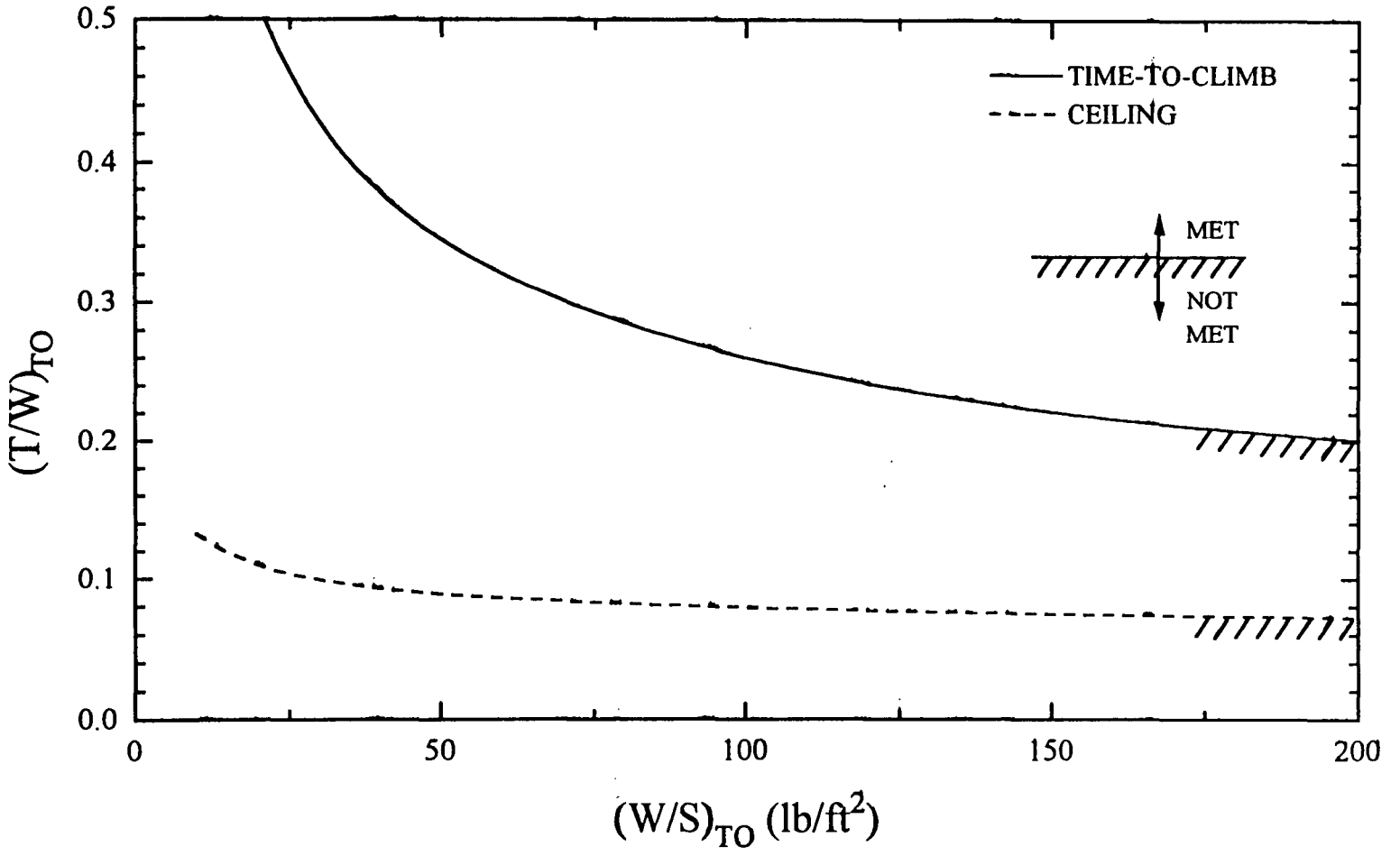

Figure 3.4 Megatransport Performance Sizing, Time-to-Climb and Ceiling Requirements

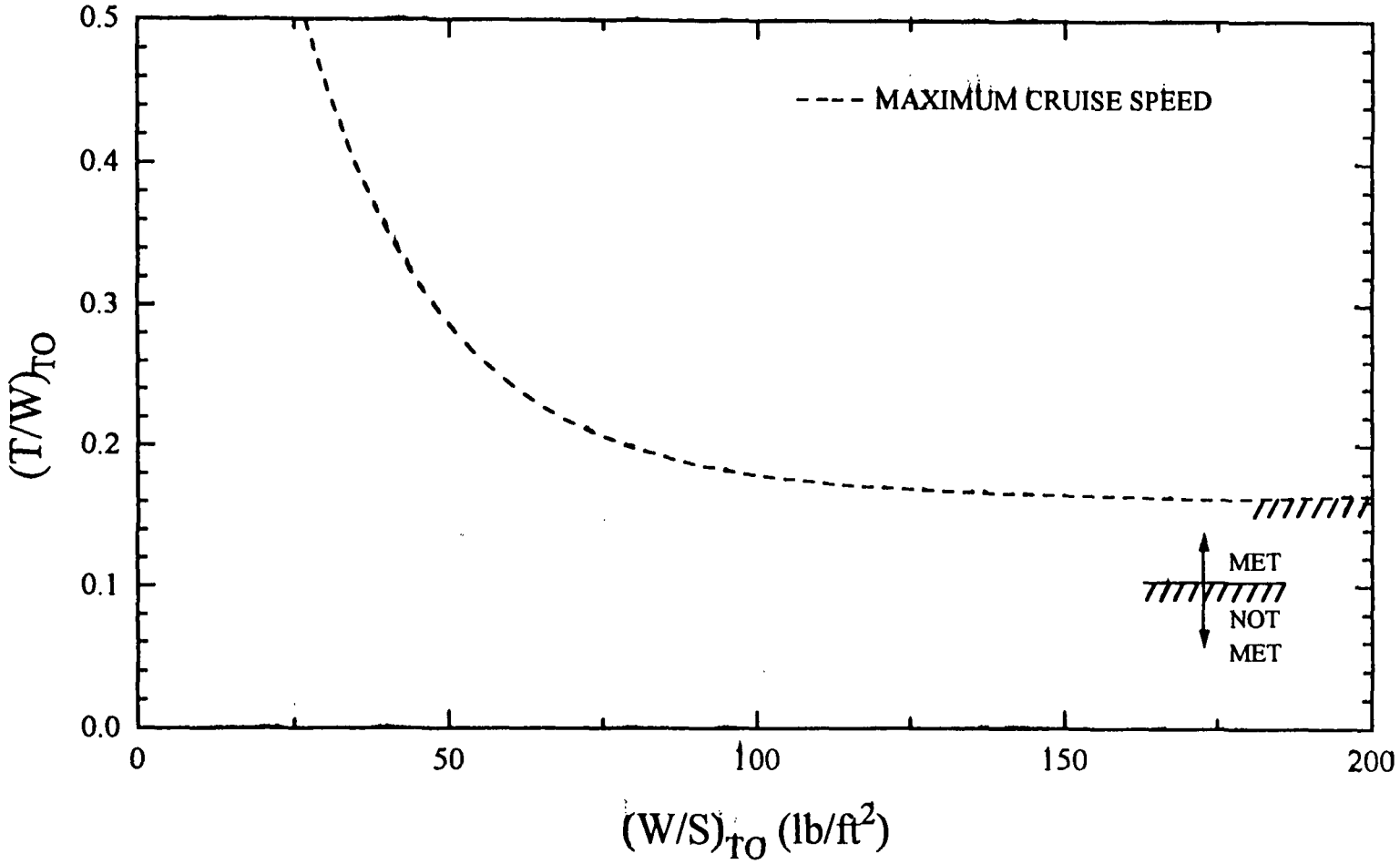

Figure 3.5 Megatransport Performance Sizing, Maximum Cruise Speed Requirements

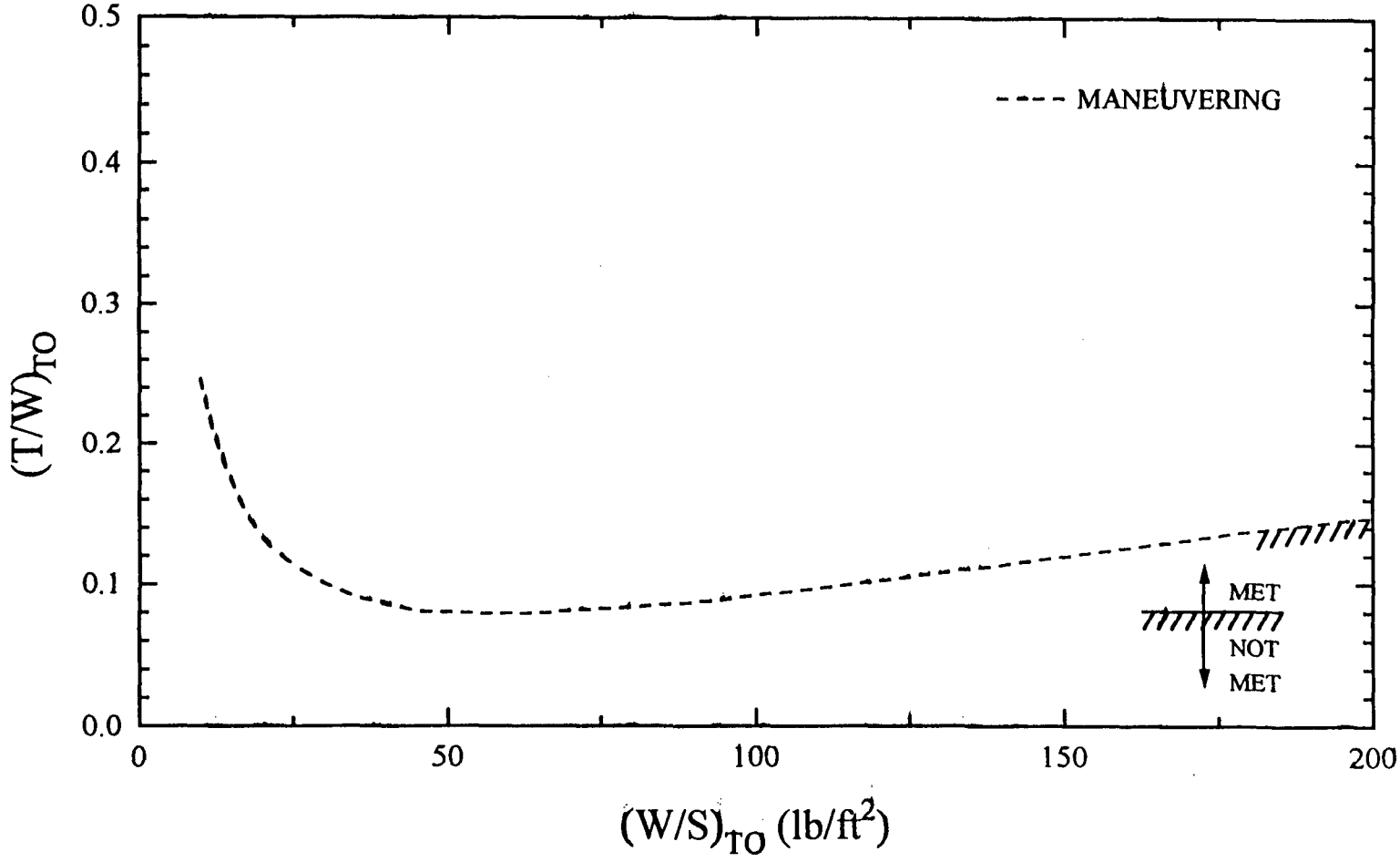

Figure 3.6 Megatransport Performance Sizing, Maneuvering Requirements

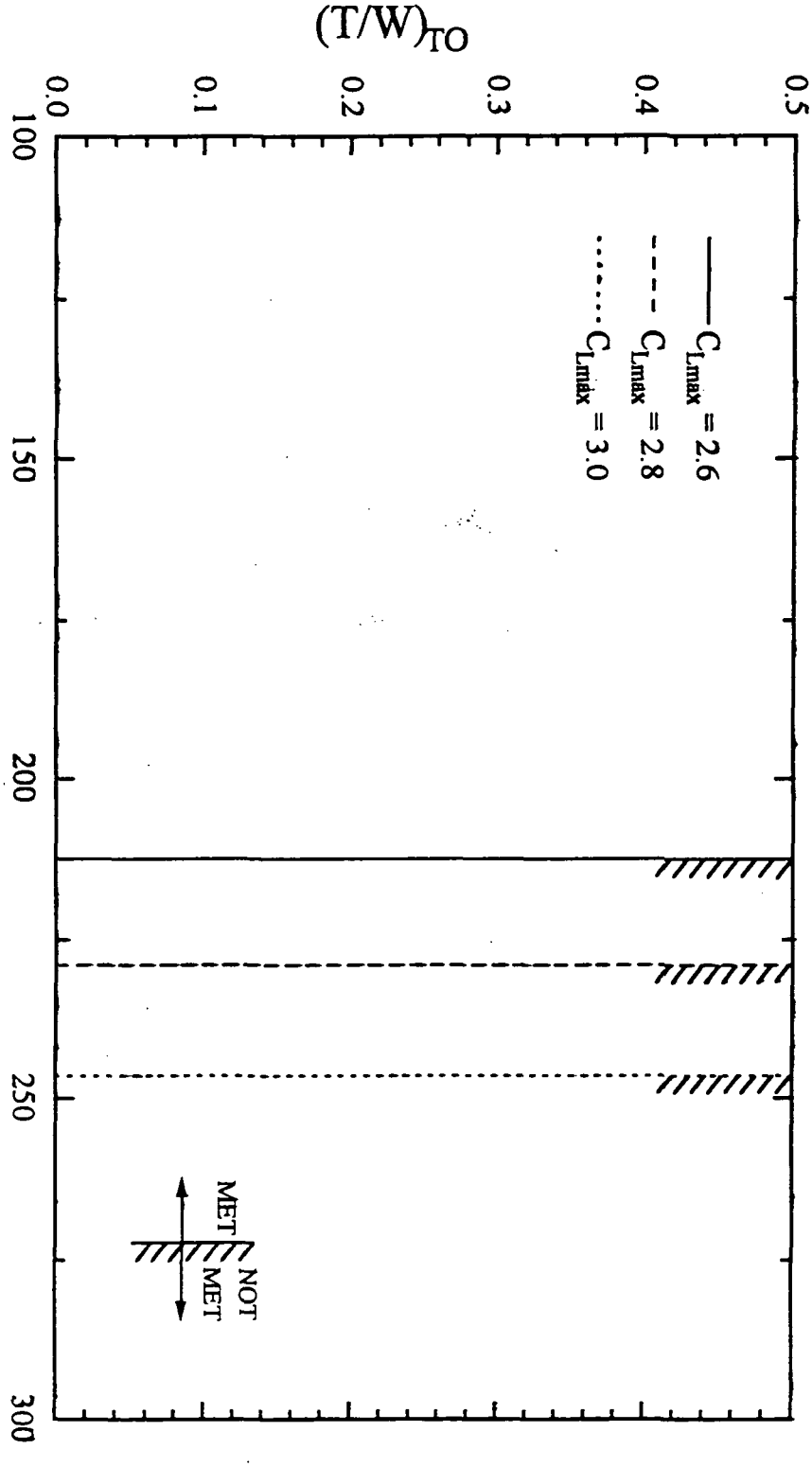

Figure 3.7 Megatransport Performance Sizing, Landing Requirements

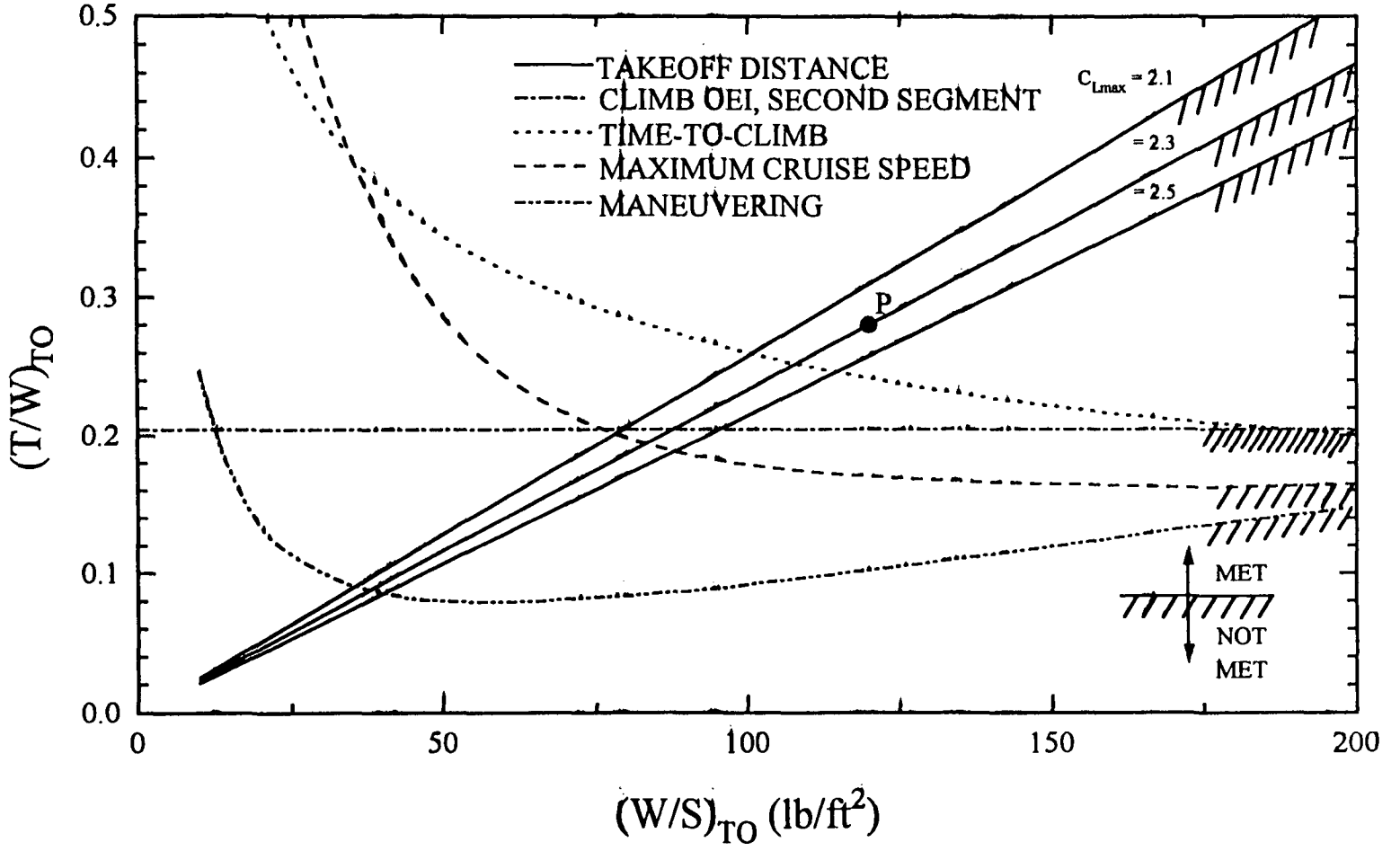

Figure 3.8 Megatransport Performance Sizing Requirements

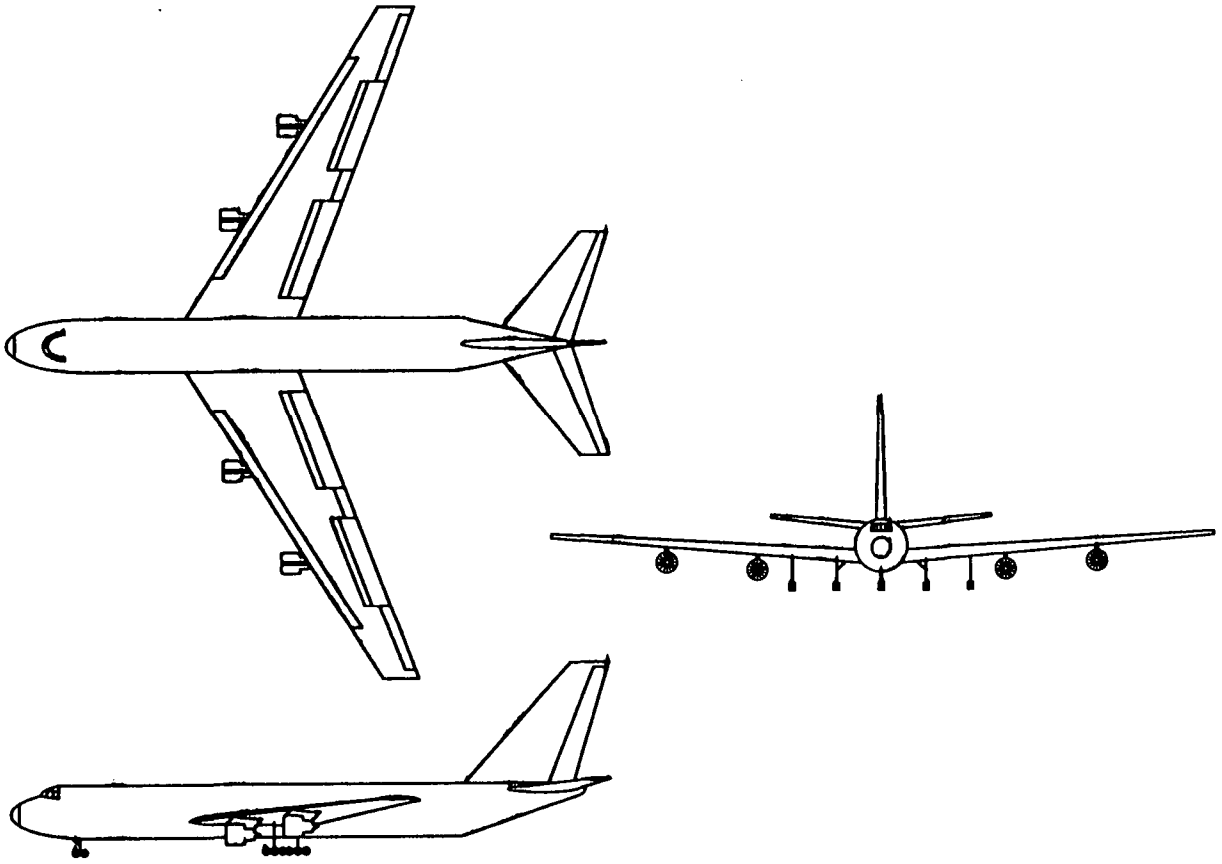

Figure 3.9 Megatransport Three-View

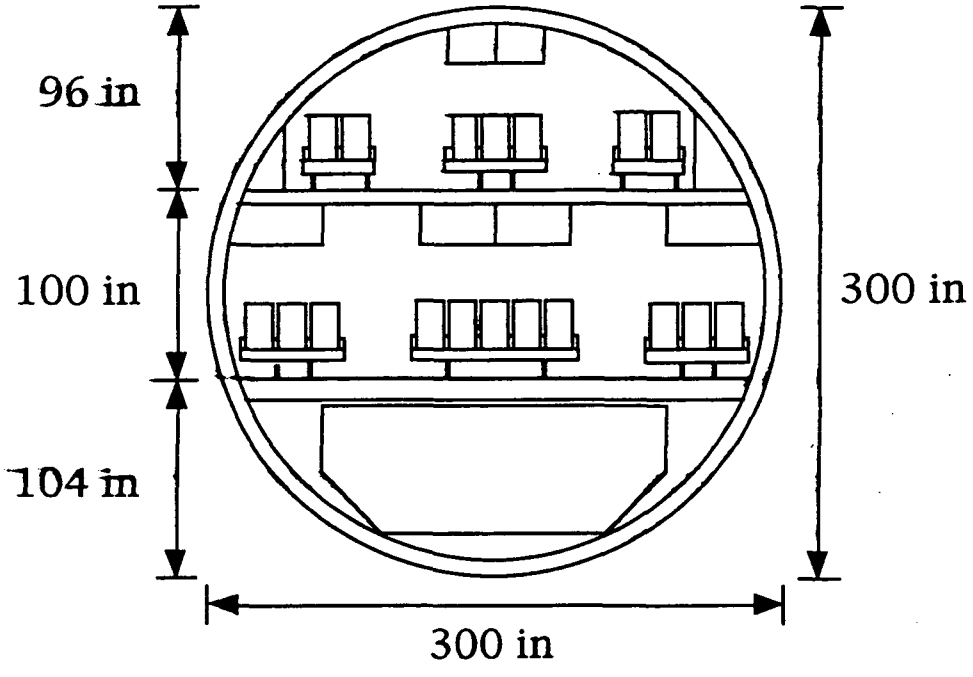

Figure 3.10 Megatransport Fuselage Cross-Section

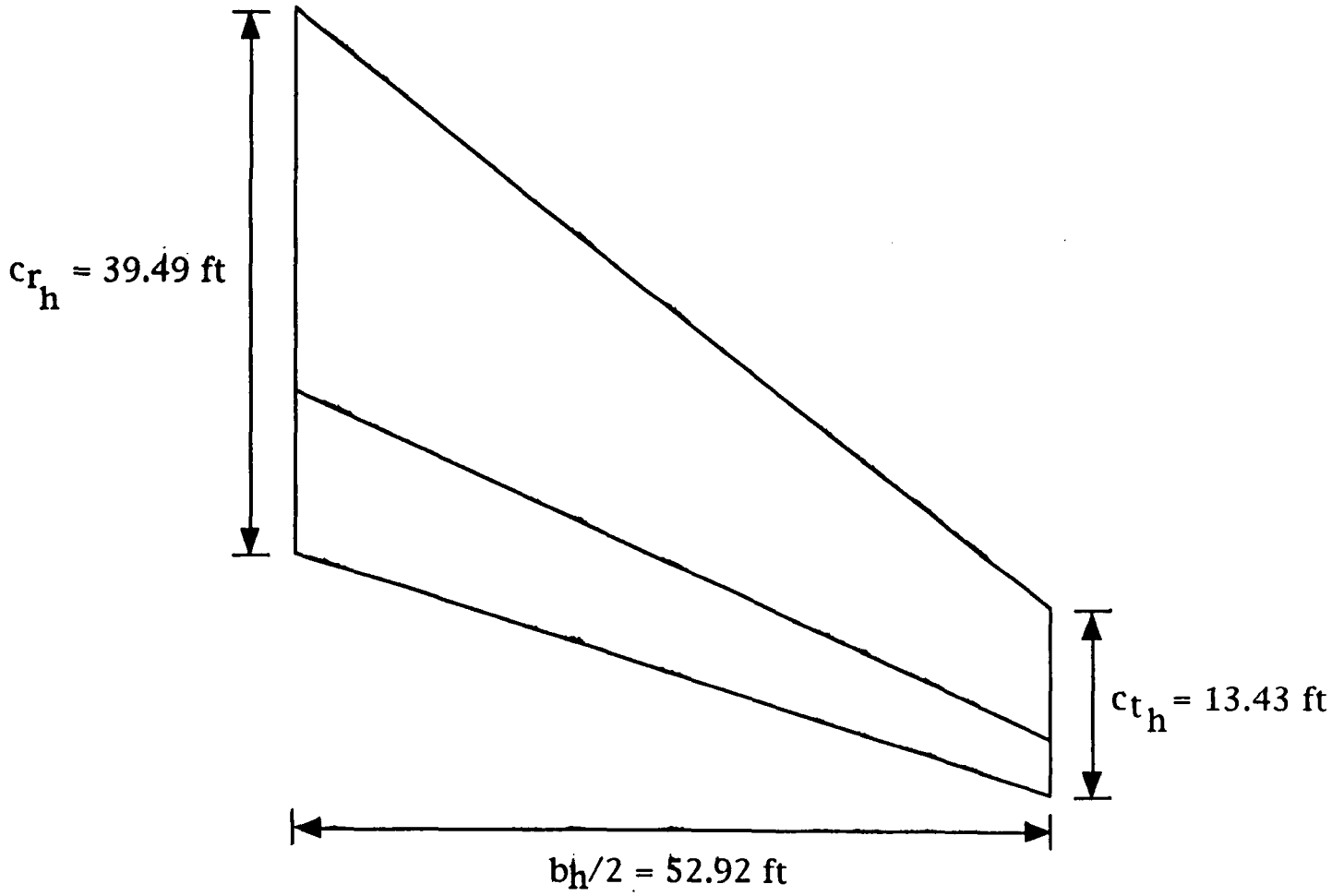

Figure 3.11 Megatransport Horizontal Stabilizer and Elevator

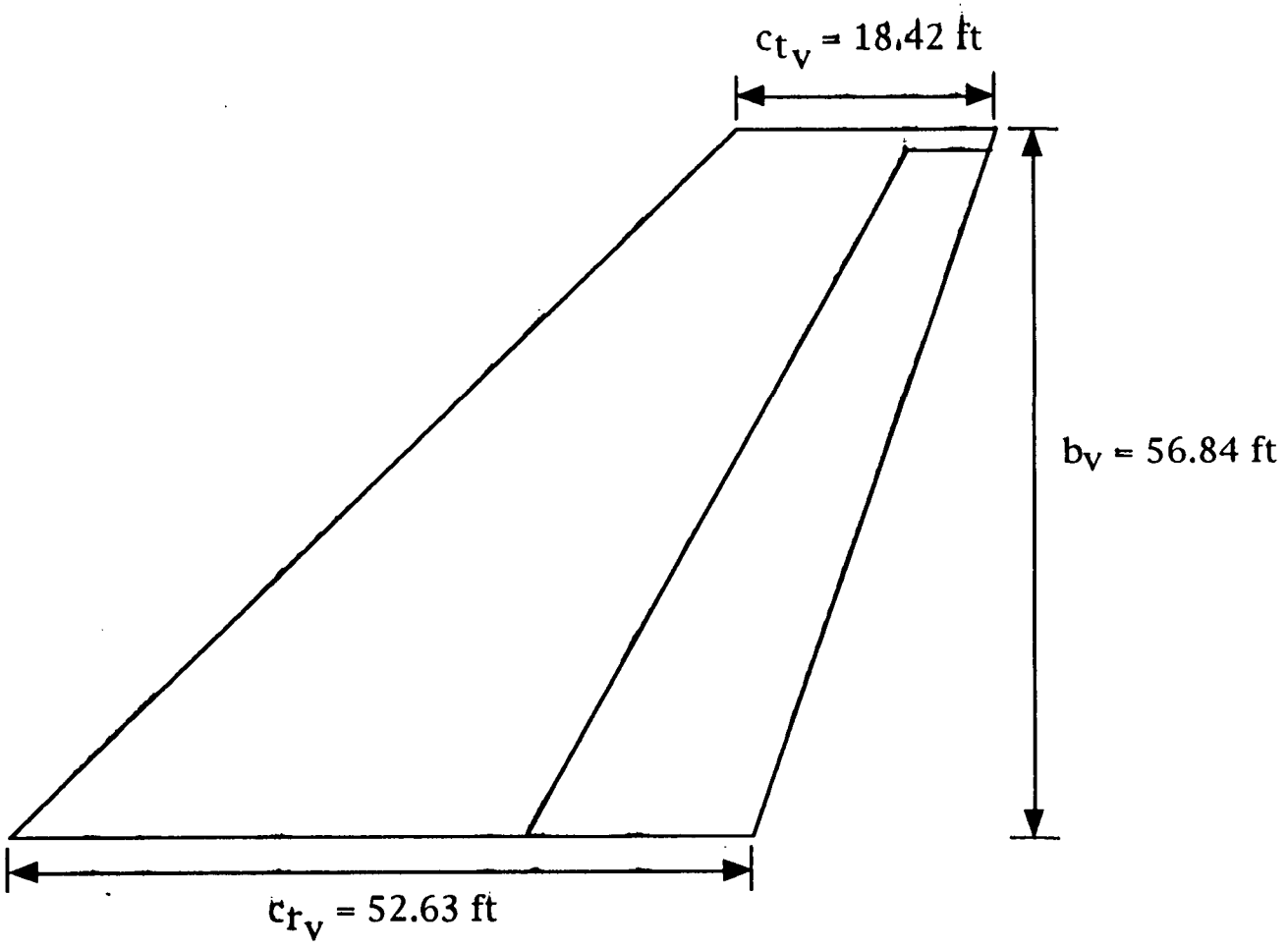

Figure 3.12 Megatransport Vertical Tail and Rudder

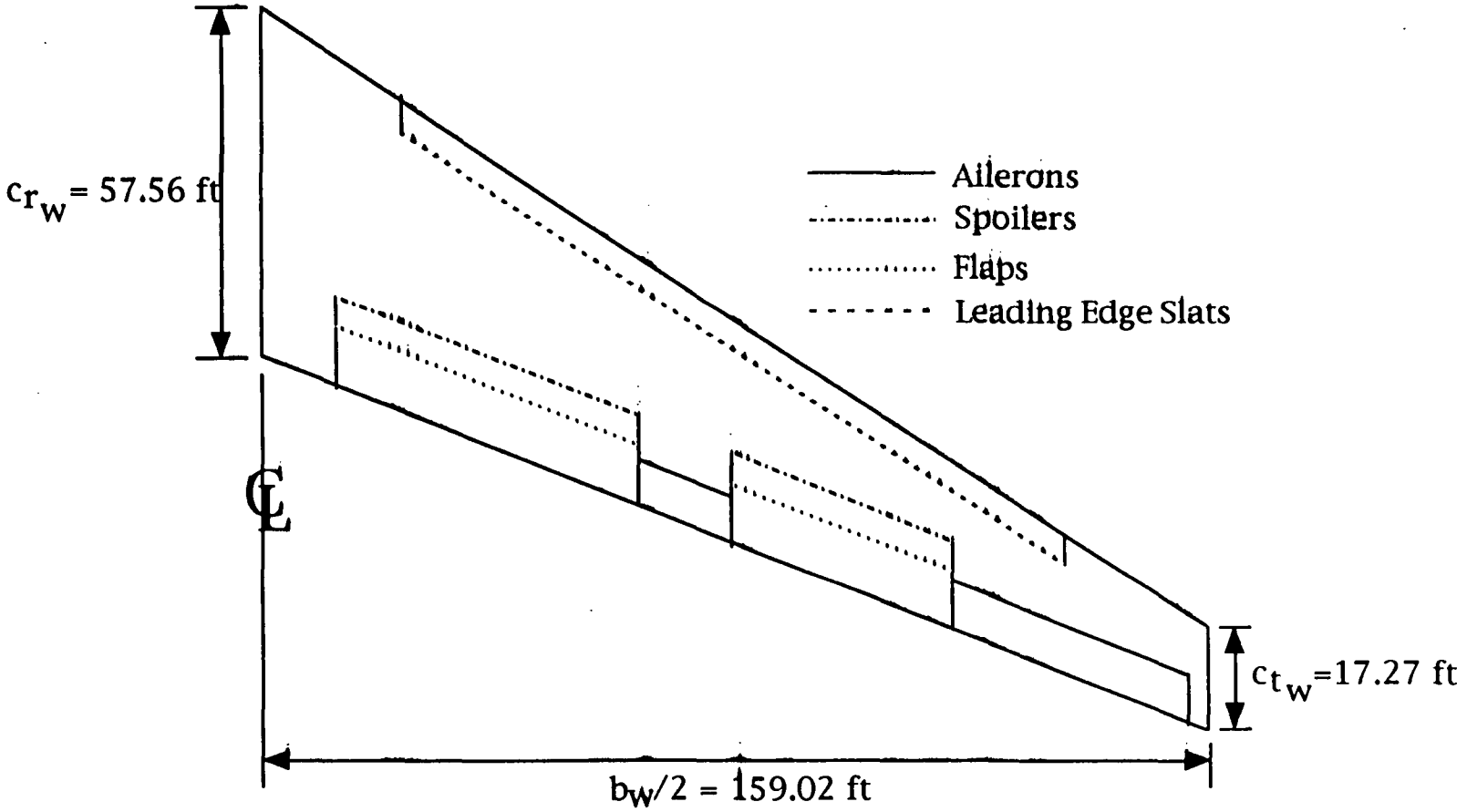

Figure 3.13 Wing and Allerons, Spoilers, Flaps, and Leading Edge Slats of the Megatransport

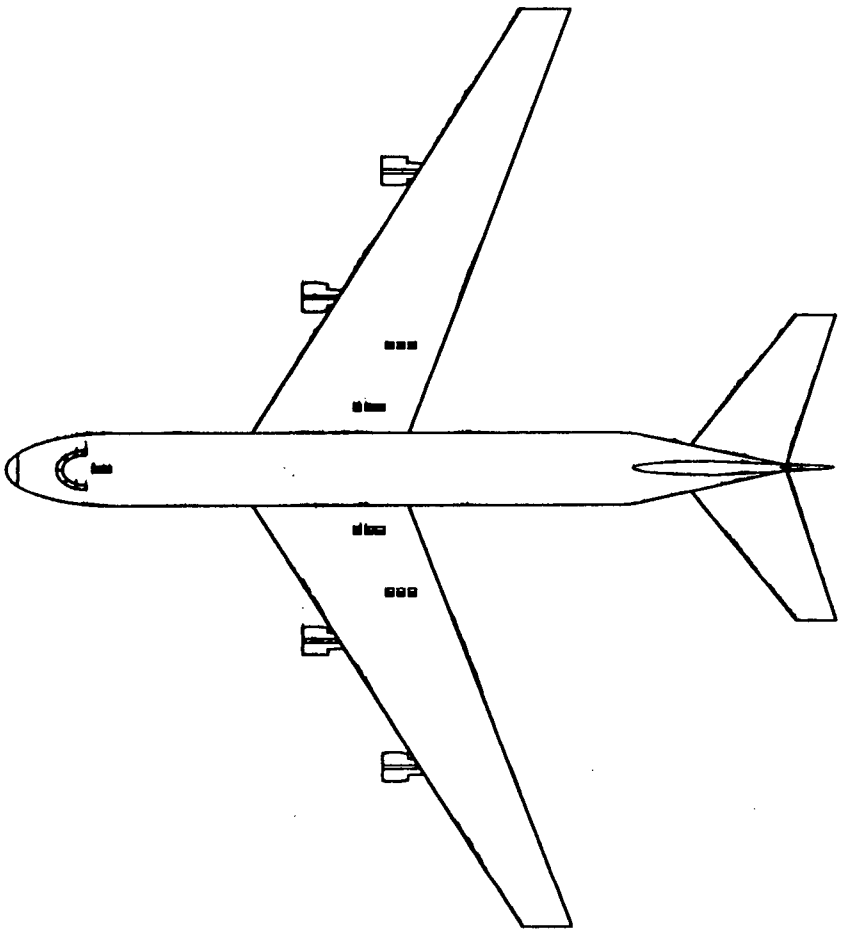

Figure 3.14 Megatransport Landing Gear Layout

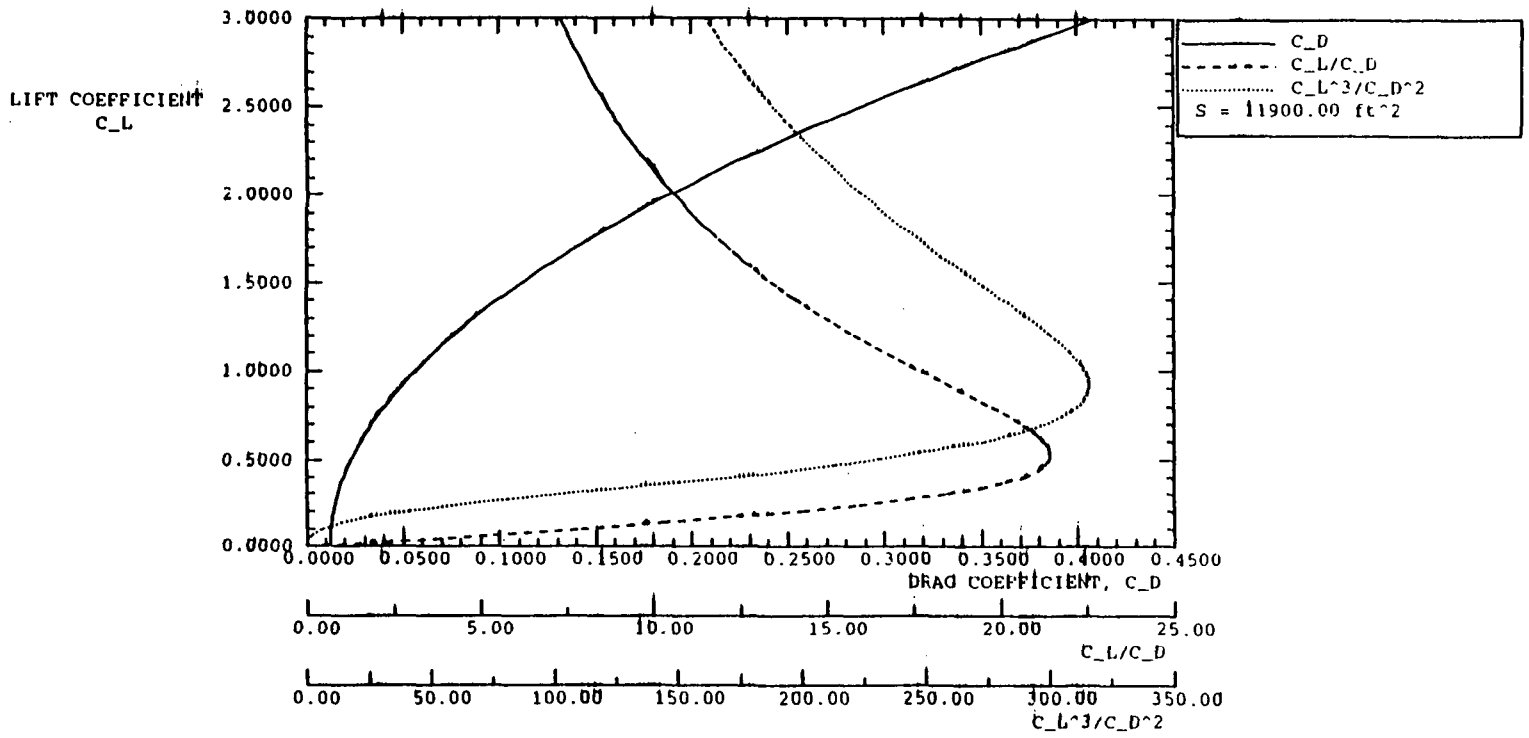

Figure 3.15 Megatransport Drag Polar, Clean Configuration (Ref. 46)

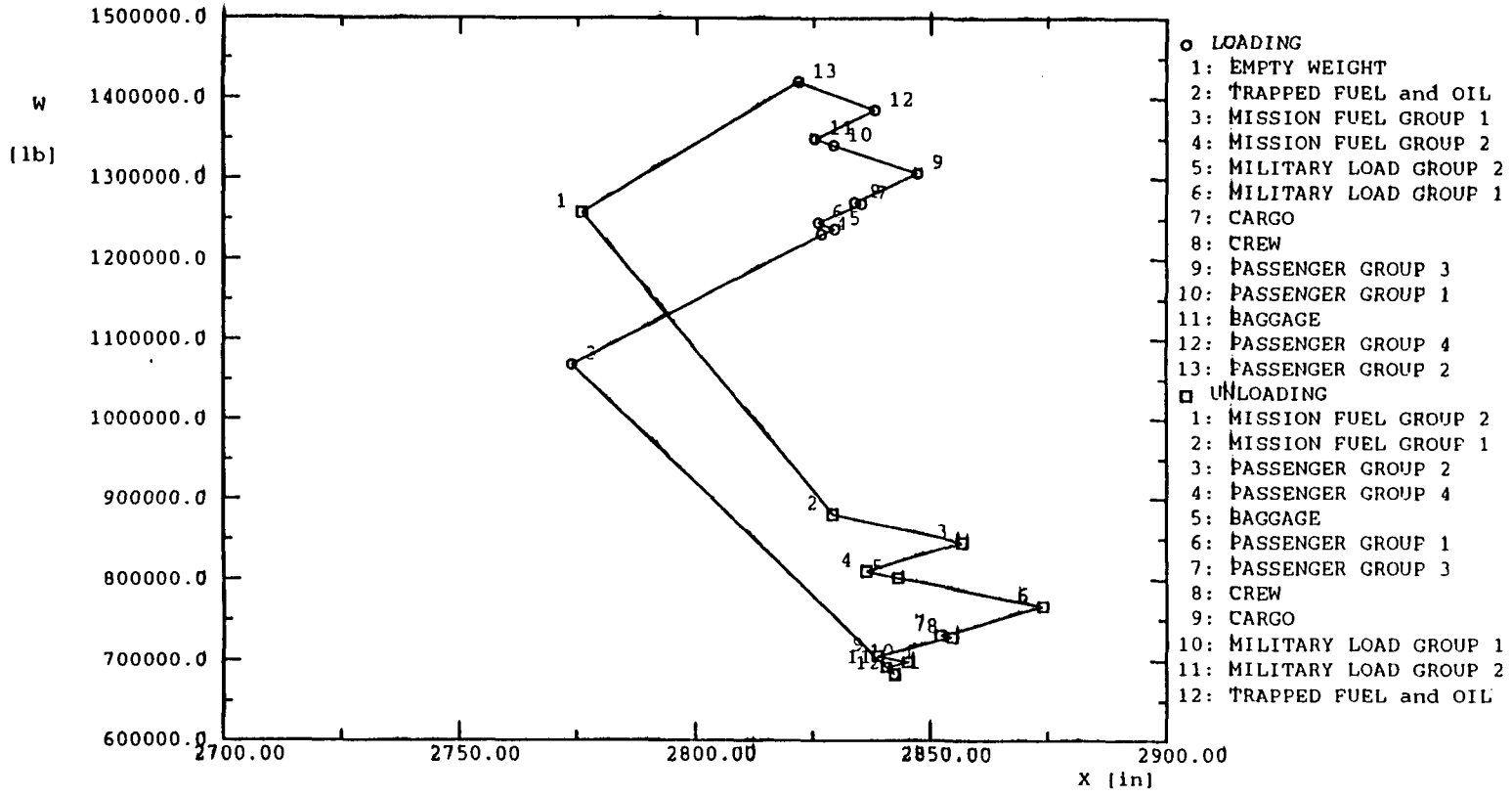

Figure 3.16 Weight - C.G. Excursion for the Megatransport in the X-Direction (Ref. 46)

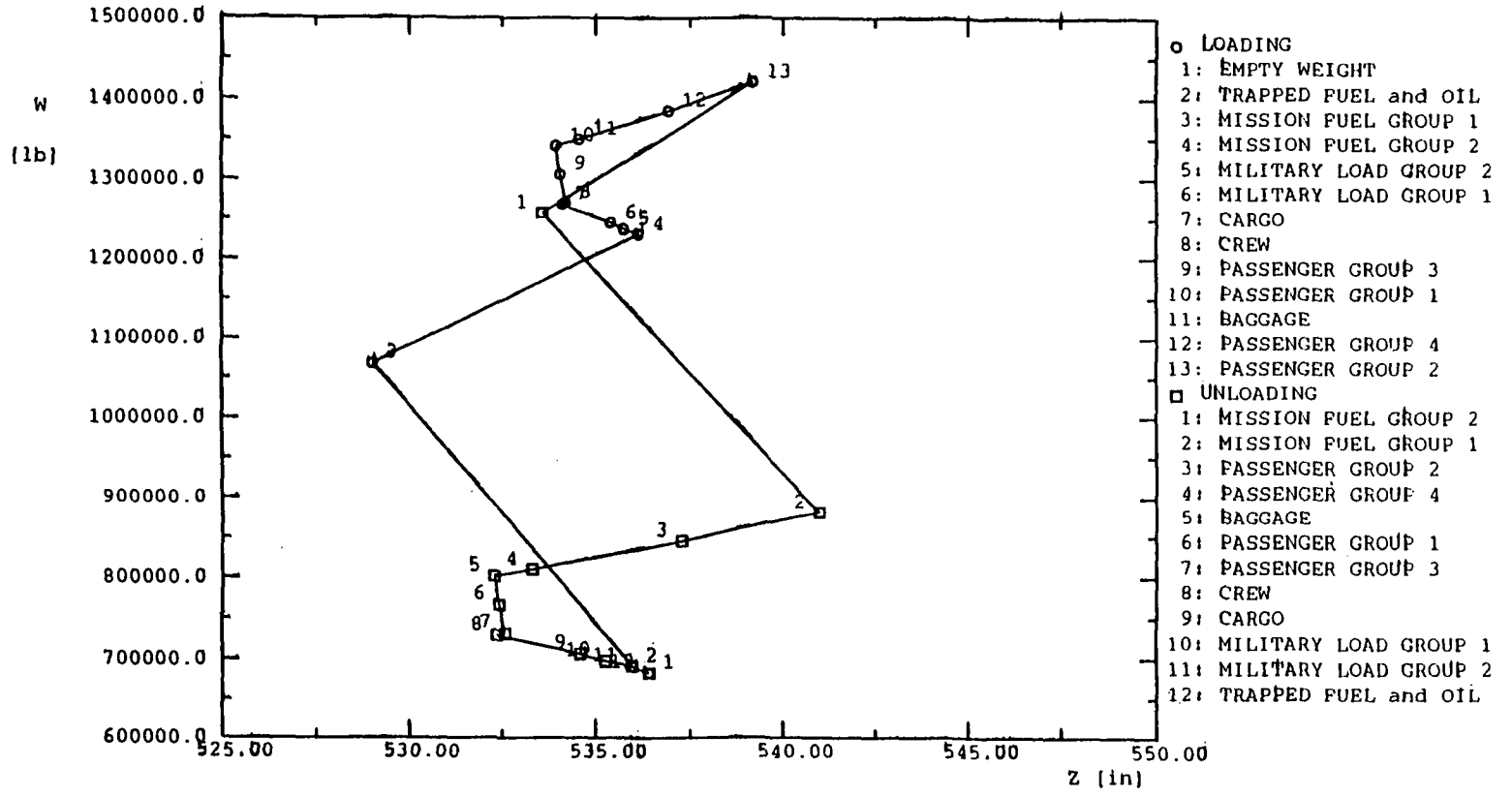

Figure 3.17 Weight - C.G. Excursion for the Megatransport in the Z-Direction (Ref. 46)

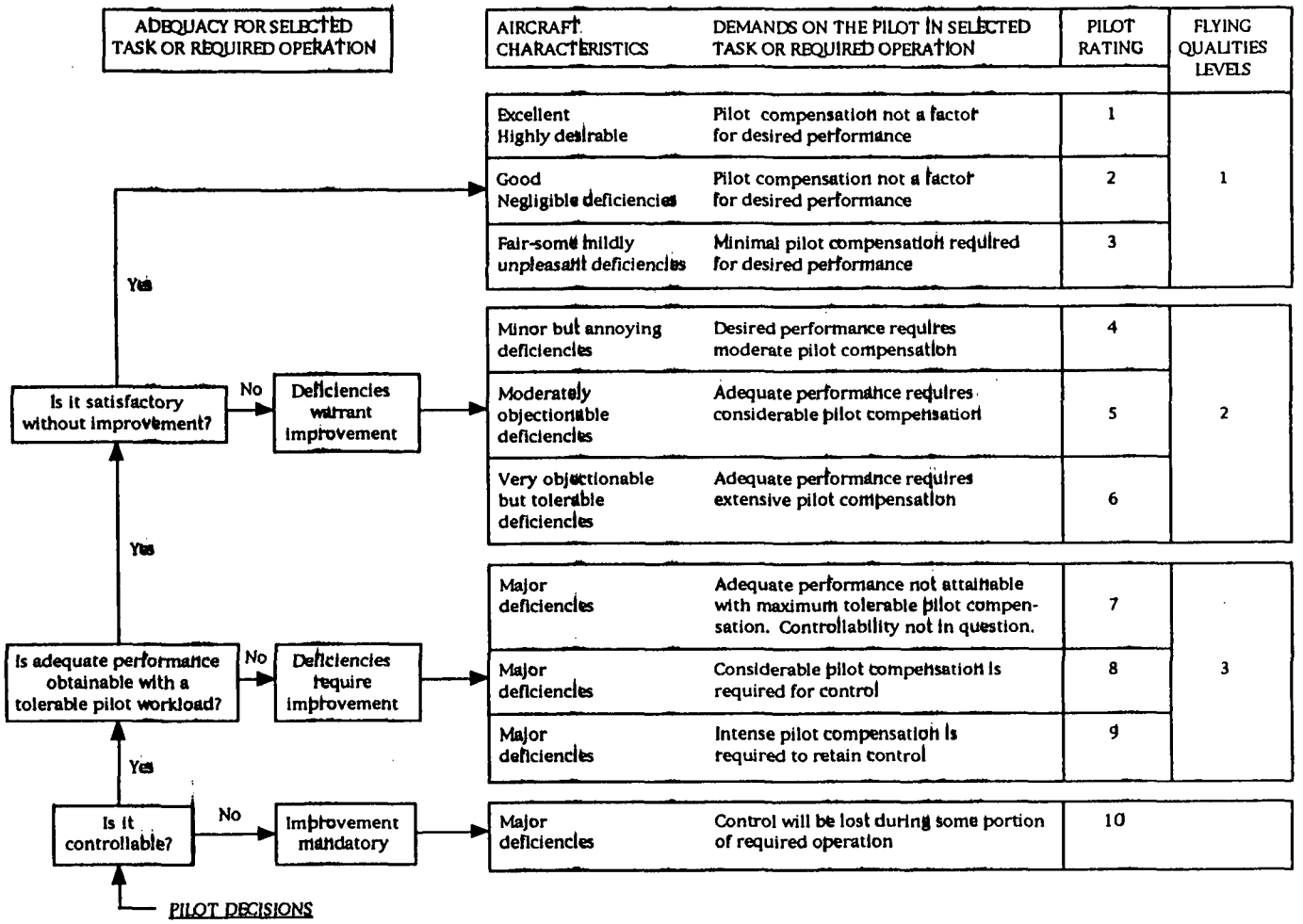

Figure 3.18 Cooper-Harper Pilot Opinion Rating Scale (Ref. 18)

FLIGHT PHASE	PHUGOID LEVEL	LEVEL z_SP	LEVEL w_n_SP
C	STABLE	I	I

Figure 3.19 Flying Quality Levels for Phugoid and Short-Period of the Megatransport (Ref. 46)

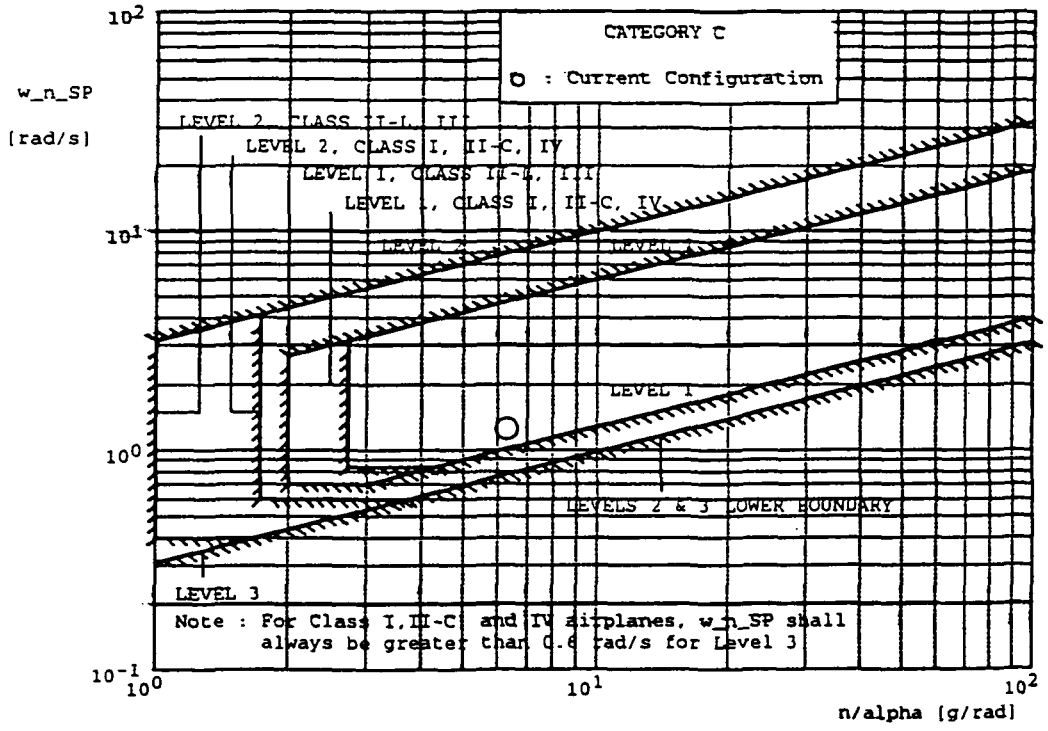

Figure 3.20 Short-Period Frequency Requirements of the Megatransport (Ref. 46)

FLIGHT PHASE	SPIRAL LEVEL	LEVEL w_n_D	LEVEL z_D	LEVEL (z_D*w_n_D)
C	I	I	I	I

Figure 3.21 Flying Quality Levels for Spiral and Dutch Roll Mode of the Megatransport (Ref. 46)

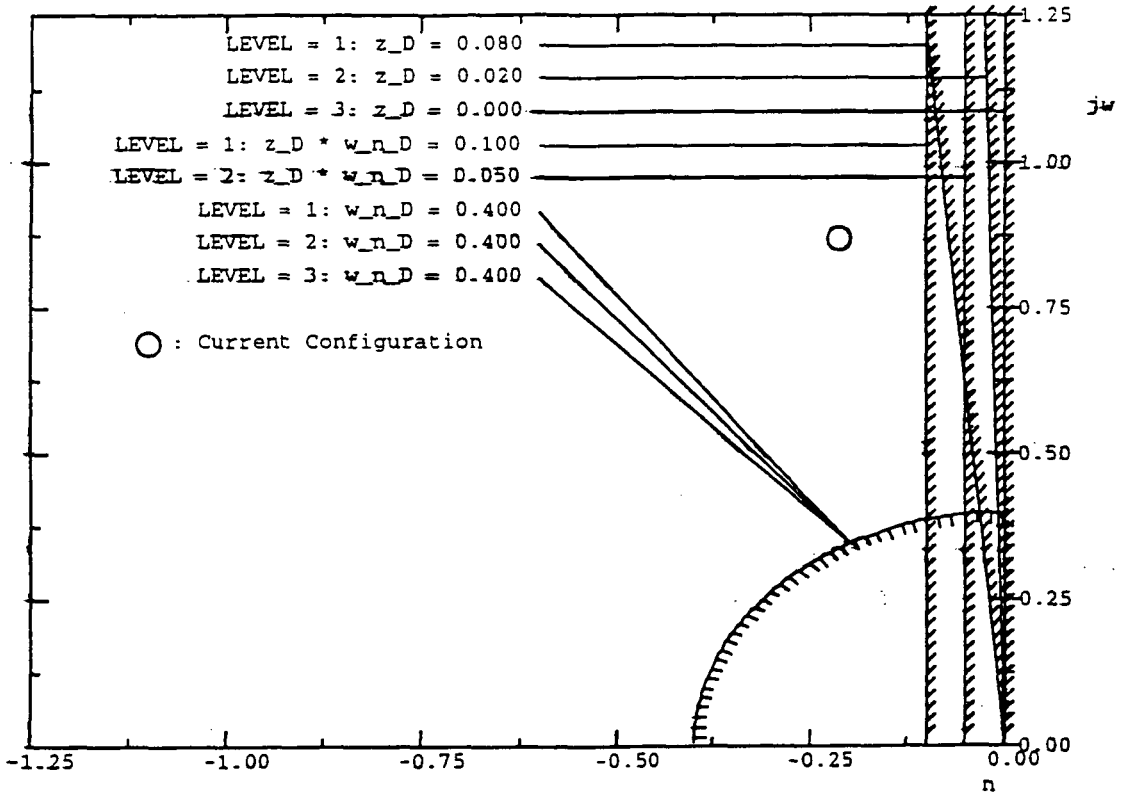

Figure 3.22 Minimum Dutch Roll Frequency and Damping Ratio Requirements of the Megatransport (Ref. 46)

FLIGHT PHASE	ROLL TIME LEVEL	ROLL PERFORMANCE LEVEL
C	I	I

Figure 3.23 Flying Quality Levels for the Roll Mode of the Megatransport (Ref. 46)

CHAPTER 4

MEGATRANSPORT SIMULATION

4.1. INTRODUCTION

A simulation program of the megatransport was developed and implemented in a six-degree-of-freedom, real-time simulator at NASA Dryden Flight Research Center. The following sections will describe the simulator as well as the various aerodynamic, engine, actuator, gear dynamics, ground effects, and control system models which were developed for the megatransport simulation.

4.2. NASA DRYDEN SIMULATOR [Refs. 9,47]

A six-degree-of-freedom, real-time simulator was available for use at NASA Dryden. The simulator was originally used for F-15 flying quality research but has since been used for a variety of smaller projects including the B-720 and, more recently, the megatransport.

This high-fidelity, fixed-base simulation operates by interfacing the models for the aerodynamics, control systems, actuators, gear dynamics, and engines of a particular aircraft to a fixed-base cockpit with user interfaces. The simulator, including the simulator cockpit and computers, can be seen in Figure 4.1.

The cockpit provides the basic flight instruments necessary to operate the aircraft. A photograph of the cockpit layout appears in Figure 4.2. In addition to flight instrumentation, the pilot has control of the simulation through a series of switches that enable him to hold, reset, or operate the simulation, initiate strip chart recording, vary or capture initial conditions, or select automatic trim features. A field of general purpose toggle switches is also provided at the cockpit and is currently used to initiate a control surface failure, initiate an engine failure, enter a propulsion-only control mode, or activate an automatic landing system.

A flight control system failure is simulated by bypassing the actuator model at the activation of a switch, thus locking the surfaces at their last position. In addition to the throttles, the pilot still has control of the flaps and the gear. The flaps are controlled electrically and the gear, while hydraulically controlled, can operate from an electrical backup system if the hydraulics fail.

The simulation has dynamic 'out the window' runway scenes displaying a 160 square nautical mile area of Edwards Air Force Base with its various runways on a 19 inch graphics display unit. In addition to the runway scenes, the graphics unit also shows a heads-up display (HUD) on the graphics screen. The HUD displays flight information such as altitude, rate of climb and descent, heading, airspeed, angle of attack, and flight path angle directly on the screen. This enables the pilot to be aware of pertinent flight information at a glance without having to scan the cockpit flight instruments. The HUD display can be seen in Figure 4.3.

The simulation also includes a Dryden continuous random turbulence model that calculates turbulence velocities and angular rates (u, v, w, p, q,

and *r*). Crosswind components can also be added as a function of altitude. The Dryden turbulence model is described in detail in Appendix D.

4.3. MEGATRANSPORT AERODYNAMIC MODEL

The simulator is programmed with the steady-state equations of motion of the aircraft, which are solved numerically by the simulator computer every 0.02 seconds. Values of the aerodynamic force coefficient equations (lift, drag, and side force) and the aerodynamic moment coefficient equations (pitching, rolling, and yawing moments) as well as information such as the velocity, altitude, angle of attack, geometry, weight, inertias, and thrust of the aircraft are required for calculating the equations of motion.

The aerodynamic force and moment coefficient equations which were developed for the megatransport are as follows:

$$C_L = C_{L_{BASE}} + C_{L_\alpha}\alpha + (1/U_1)\cdot C_{L_u} u + (\bar{c}/2U_1)\cdot\left[C_{L_{\dot\alpha}}\dot\alpha + C_{L_q} q\right] + C_{L_{\delta_H}}\delta H + C_{L_{\delta_E}}\delta E + \Delta C_{L_{HL}} + \Delta C_{L_{SL}} + \Delta C_{L_{SOL}} + \Delta C_{L_{SIL}} + \Delta C_{L_{SIR}} + \Delta C_{L_{SOR}}$$

[Eqn. 4.1]

$$C_D = C_{D_{BASE}} + C_{D_\alpha}\alpha + (1/U1)\cdot C_{D_u} u + C_{D_{\delta H}}\delta H + C_{D_{\delta E}}\delta E + \Delta C_{D_{HL}} + \Delta C_{D_{SL}} + \Delta C_{D_{SOL}} + \Delta C_{D_{SIL}} + \Delta C_{D_{SIR}} + \Delta C_{D_{SOR}} + \Delta C_{D_{GEAR}}\cdot DGEAR$$

[Eqn. 4.2]

$$C_m = \left[C_{m_\alpha} + C_{m_{T_\alpha}}\right]\cdot\alpha + (1/U_1)\cdot\left[C_{m_u} + C_{m_{T_u}}\right]\cdot u$$
$$+(\bar{c}/2U_1)\cdot\left[C_{m_{\dot{\alpha}}}\dot{\alpha} + C_{m_q} q\right] + C_{m_{\delta_H}}\delta_H + C_{m_{\delta_E}}\delta_E \qquad \text{[Eqn. 4.3]}$$
$$+\Delta C_{m_{HL}} + \Delta C_{m_{SL}} + \Delta C_{m_{GEAR}}\cdot DGEAR$$

$$C_\ell = C_{\ell_\beta}\beta + (b/2U_1)\cdot\left[C_{\ell_p} p + C_{\ell_r} r\right] + C_{\ell_{\delta_R}}\delta_R$$
$$+C_{\ell_{\delta_A}}\cdot\left[\delta_{A_O} + \delta_{A_I}\right] + C_{\ell_{\delta_{SOL}}}\delta_{SOL} + C_{\ell_{\delta_{SIL}}}\delta_{SIL} \qquad \text{[Eqn. 4.4]}$$
$$+C_{\ell_{\delta_{SIR}}}\delta_{SIR} + C_{\ell_{\delta_{SOR}}}\delta_{SOR}$$

$$C_n = \left[C_{n_\beta} + C_{n_{T_\beta}}\right]\cdot\beta + (b/2U_1)\cdot\left[C_{n_{\dot{\beta}}}\dot{\beta} + C_{n_p} p + C_{n_r} r\right]$$
$$+C_{n_{\delta_R}}\delta_R + C_{n_{\delta_A}}\cdot\left[\delta_{A_O} + \delta_{A_I}\right] + C_{n_{\delta_{SOL}}}\delta_{SOL} + C_{n_{\delta_{SIL}}}\delta_{SIL}$$
$$+C_{n_{\delta_{SIR}}}\delta_{SIR} + C_{n_{\delta_{SOR}}}\delta_{SOR}$$

[Eqn. 4.5]

$$C_y = C_{y_\beta}\beta + (b/2U1)\cdot\left[C_{y_{\dot{\beta}}}\dot{\beta} + C_{y_p} p + C_{y_r} r\right] + C_{y_{\delta_R}}\delta_R \qquad \text{[Eqn. 4.6]}$$

As can be seen from the equations, each aerodynamic force or moment coefficient equation consists of either nondimensional derivative terms (such as $C_{l_{\delta R}}\delta R$) or coefficient deltas (such as $\Delta C_{m_{HL}}$). The values of these derivatives and coefficients depend on many variables such as the velocity, altitude, or angle of attack of the aircraft.

Because of the dependence of the nondimensional derivatives and coefficient deltas on the current flight condition, values for these derivatives and coefficients cannot be listed in a simple input data file, but must instead be contained in lookup tables. The simulator computer searches the lookup

tables for the value of a particular aerodynamic derivative or coefficient based upon the value of the velocity and angle of attack at which the simulated aircraft is flying. If no exact match can be made with the flight conditions, the computer will calculate a value using linear interpolation methods.

The aerodynamic derivatives and coefficients which make up the aerodynamic lookup tables for the megatransport were calculated using References 18 and 39 and the stability and control module of the Advanced Aircraft Analysis (AAA) design program (Ref. 46). The AAA program, given the geometry and inertia data for the megatransport, calculates the aerodynamic stability and control derivatives for a particular flight condition. In this way, a table of aerodynamic derivatives can be generated for different flight conditions.

Because it would have required an inordinate amount of time and effort to generate aerodynamic data tables for every point in the flight regime, a limited flight envelope was adopted for the purposes of this study. Since the primary purpose of this project was to evaluate the controllability of the megatransport using the throttles-only control system during approach and landing, the altitude limits of the limited flight envelope ranged from zero to 5,000 feet, the velocity limits ranged from zero to 330 knots (corresponding to Mach numbers of approximately zero to 0.5 throughout this altitude range), and the angle of attack varied from –4 to 14 degrees.

Initial conditions of the velocity, altitude, and angle of attack as well as the geometry, weight, and inertias of the megatransport are stored in an initial data file which the computer brings up on the simulator operator's screen each time the simulator is engaged. This enables the operator to make changes to the values in the initial data file real-time before each test run, if desired. For

instance, the operator may want to run a test flight starting at a different velocity or altitude from the previous test flight. If no change is made to the input data file, the values remain at their default setting.

4.4. MEGATRANSPORT ENGINE MODEL [Refs. 20,42,48,49]

In the megatransport performance sizing calculations (see Chapter 3), it was found that the required takeoff thrust was 100,000 pounds of thrust per engine. At present, there is no commercial transport engine that produces this much thrust, although the Pratt & Whitney PW4084 and General Electric GE90 turbofan engines come the closest rated at 84,000 pounds thrust and 87,000 pounds thrust, respectively. Pratt & Whitney is currently working on certifying the 90,000 pounds thrust PW4090 engine in 1996, while General Electric is planning on certifying a 92,000 pound thrust version of the GE90 engine in the near future. An engine capable of producing 100,000 pounds thrust will be realizable just a few years from now.

NASA Dryden was given a static engine deck of the Pratt & Whitney PW4084 turbofan engine by the Pratt & Whitney division of United Technologies Corporation (UTC). With this deck, it was possible to generate a lookup table of engine thrusts for certain flight conditions at specific Mach numbers and altitudes. Since the PW4084 engine thrust is not rated high enough for the thrust levels required for the megatransport engine, the PW4084 thrust data were extrapolated for use in the megatransport simulator. These data are considered proprietary by UTC and will not be published in this study.

Although UTC supplied NASA Dryden with PW4084 data, it was static engine data and contained no information about the engine dynamics. Since engine dynamics and spool up times were an important consideration in this study, it was necessary to have an engine model which included real-life time lags. A dynamic engine model was developed using available data on the Pratt & Whitney JT8D and the General Electric CF6-80 engines.

The megatransport engine thrust response curve is shown in Figure 4.4. The engine time constant value was determined experimentally by running the megatransport simulator with different engine time constants. The results of the engine response were printed out to a strip chart recorder and analyzed. The engine time constant was fine-tuned until the megatransport engine response curve compared favorably with the engine response curves of the JT8D and CF6-80 engines. This dynamic engine model, including engine time lag and time constants, is described in detail in Appendix B.

In addition to developing the megatransport engine model, the simulator code which interfaced the throttle commands to the engine response had to be modified. The NASA Dryden simulator used in the megatransport project uses the cockpit of a modified F-15 fighter. The F-15 has only two throttle levers, one for each of the two F-15 engines. The megatransport, however, has four engines. Therefore, the simulator program was modified so that the inboard and outboard engines on the right wing of the megatransport are both controlled by the right throttle, as the inboard and outboard engines on the left wing are both controlled by the left throttle.

4.5. MEGATRANSPORT ACTUATOR AND GEAR DYNAMICS MODELS

The actuator and gear dynamics models which were used in the B-720 simulation were used in the megatransport simulation as well. Due to time constraints on the project and considering the complexity of the actuator and gear dynamics models, it was decided that these models would be acceptable for use in the megatransport simulator with only minor modifications. The B-720 actuator code in the simulator was programmed to model a general purpose actuator. The actuator routine is based upon a first order actuator system that is both rate limited and position limited and includes hysteresis effects.

The gear dynamics portion of the simulator program calculates not only the forces and moments due to the gear deployment, but also the total braking force available to the aircraft upon landing as well as the forces and moments produced upon the aircraft by runway contact.

The only modifications made to the gear dynamics model were changing the x-, y-, and z-coordinates of the nose gear and the main landing gear of the B-720 for those of the megatransport. Since the main purpose of this project was to evaluate the controllability of the megatransport using the throttles-only control system during the approach and landing phases, once the pilot made contact with the runway the task was considered completed. The rollout characteristics of the megatransport were not considered important to this project, so the B-720 gear dynamics were determined to be adequate for this study.

4.6. GROUND EFFECTS MODEL [Refs. 39,50]

Due to time constraints, ground proximity effects on the megatransport were not implemented in the megatransport simulation. The effects on lift, drag, and pitching moment due to the proximity of the aircraft to the ground generally become measurable at a height above the ground of one wing span (318 feet in the case of the megatransport) and increase in magnitude as the height above the ground decreases. Both theoretical and experimental investigations to date indicate that ground proximity produces an increase in the lift-curve slope, a decrease in drag, and a reduction of nose-up pitching moment for most aircraft planforms.

4.7. MEGATRANSPORT CONTROL SYSTEM MODEL

Once the aerodynamic and engine models of the megatransport had been implemented in the simulator, the B-720 pitch control, roll control, and yaw control systems were modified for use in the megatransport simulation. Control steps, pulses, and doublets were performed on the megatransport either by forward and aft or lateral movement of the control stick. Forward and aft stick pulses generated a megatransport pitch response, while lateral stick pulses generated a megatransport roll response. The pitch and roll responses to these control inputs were observed not only by monitoring a real-time strip chart recording of selected output parameters, but were also evaluated by three volunteer pilots - a propulsion engineer, control systems engineer, and

research test pilot. The output parameters of particular interest, such as pitch rate or roll rate, were evaluated in terms of their amplitude, response time, and settling time to a particular gain. Based upon both the pilot's opinion and the strip chart data, a decision was made whether the gain should continue to be modified or whether the selected value was acceptable.

Using this procedure, the gains in the various feedback loops were systematically modified, one at a time. Not only were the gains in the B-720 control system changed in this way, but some feedback loops were eliminated entirely and others were added as needed.

This process was repeated throughout all the feedback loops in the pitch, roll, and yaw control systems for the B-720 aircraft until a control system was developed for the megatransport which resulted in Level 1 flying qualities. Block diagrams for the megatransport pitch control system, roll control system, and yaw control system are shown in Figures 4.5, 4.6, and 4.7, respectively.

4.8. MEGATRANSPORT PROPULSION CONTROLLED AIRCRAFT (PCA) AUGMENTED CONTROL SYSTEM MODEL [Ref. 9]

Similar to the conventional control system development, the B-720 flight path angle and bank angle control systems were modified for use in the megatransport simulator using the same gain modification technique. Again, not only were the gains in the B-720 control systems changed in this way, but some feedback loops were eliminated entirely and others were added as needed.

This process was repeated throughout all the feedback loops in the flight path angle and bank angle control systems for the B-720 aircraft until a responsive, yet well-damped, control system for the megatransport was obtained. Block diagrams for the megatransport flight path angle control system and bank angle control system are shown in Figures 4.8 and 4.9, respectively. A block diagram relating the PCA commanded thrust output to the overall megatransport dynamics is shown in Figure 4.10.

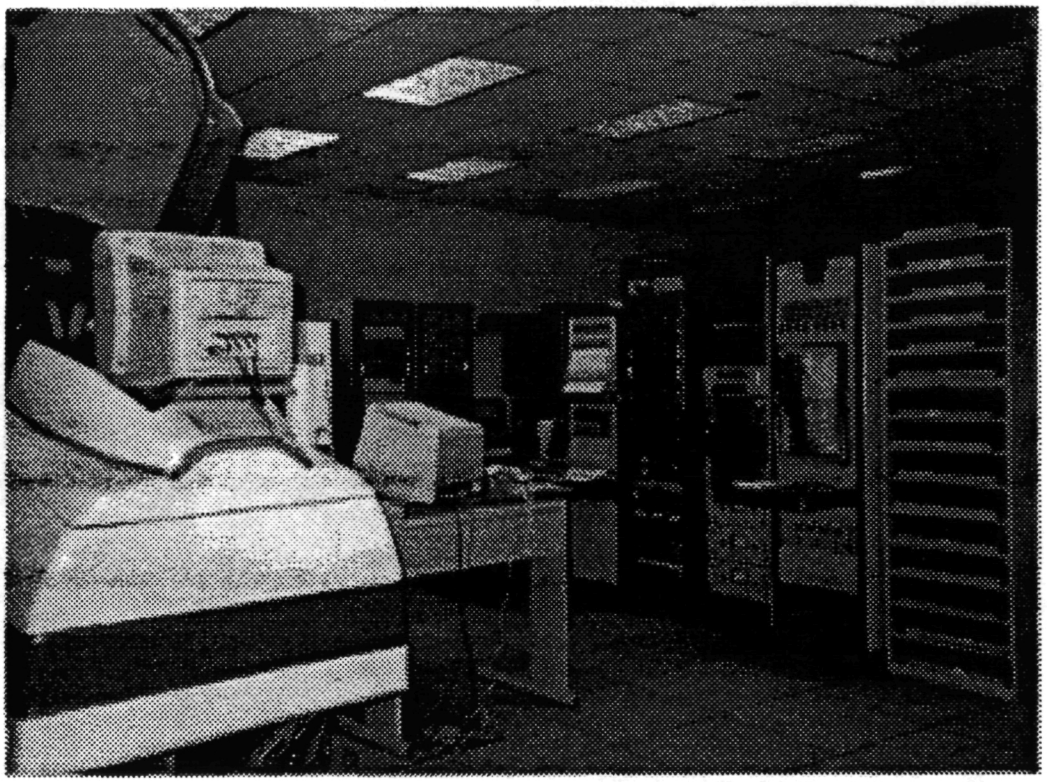

Figure 4.1 NASA Dryden Simulator Cockpit and Computers

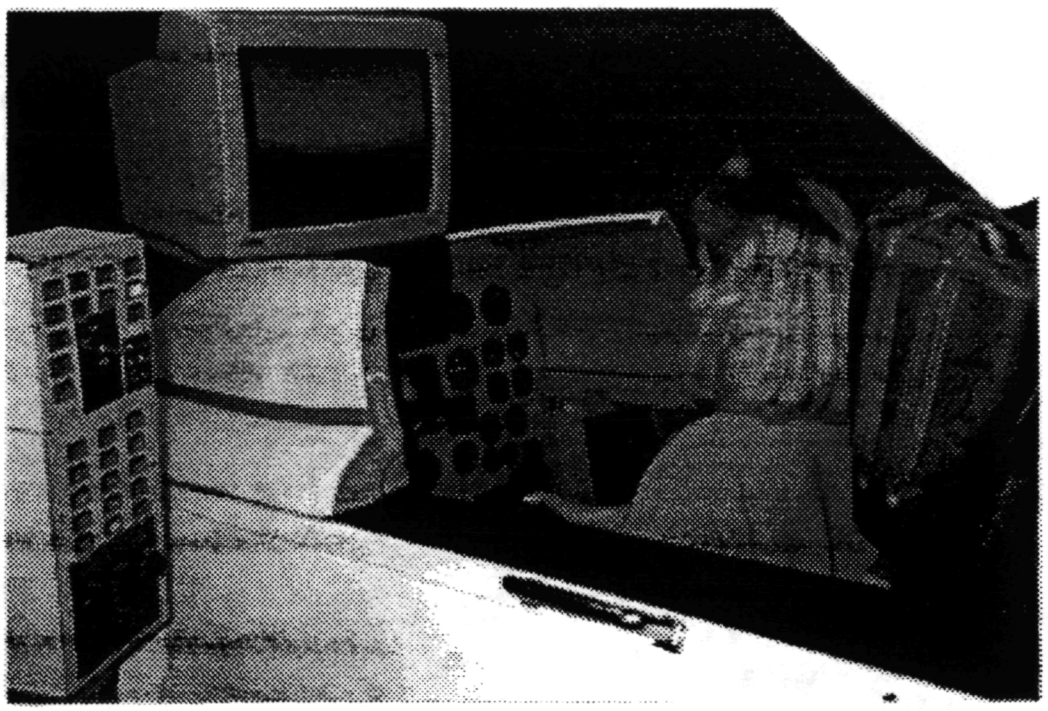

Figure 4.2 NASA Dryden Simulator Cockpit Layout

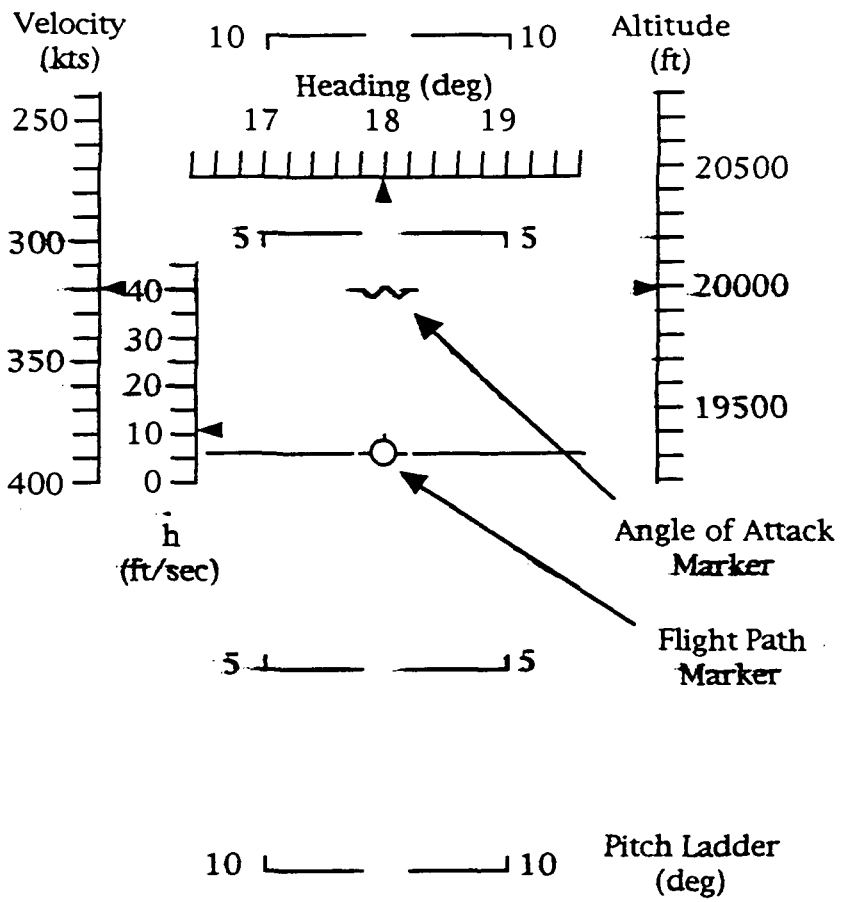

Figure 4.3 NASA Dryden Simulator Heads-Up Display (HUD)

(Ref. 47)

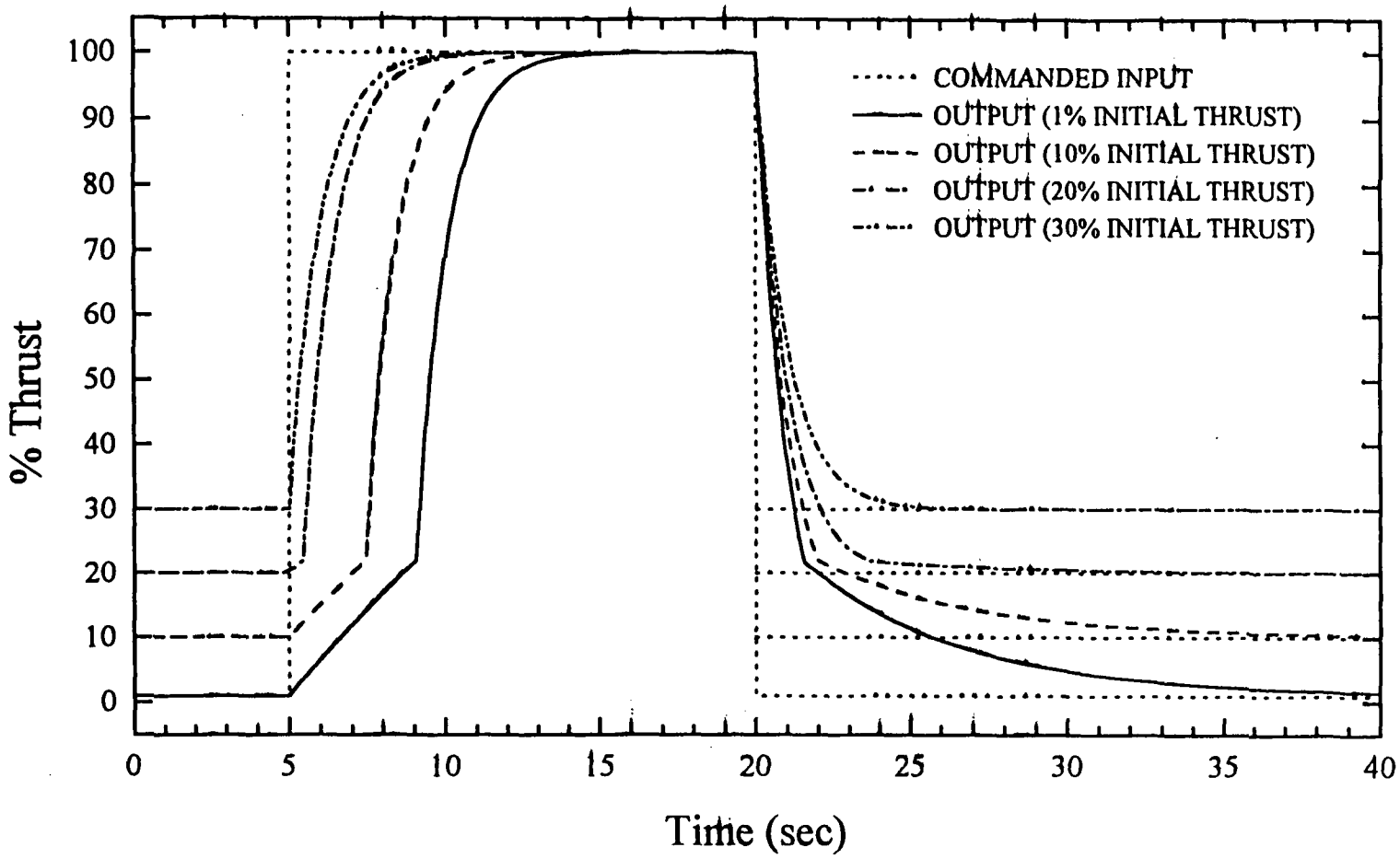

Figure 4.4 Megatransport Engine Model Throttle Step Response

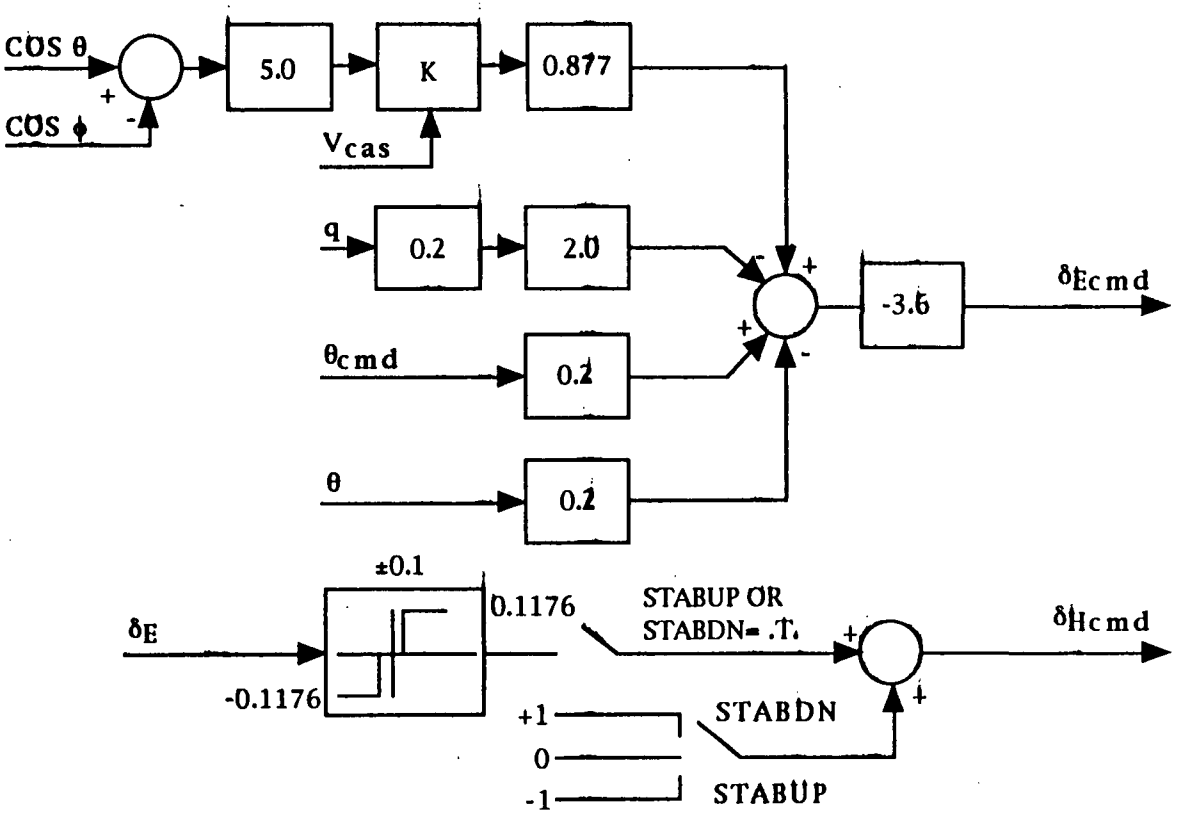

Figure 4.5 Megatransport Pitch Control System

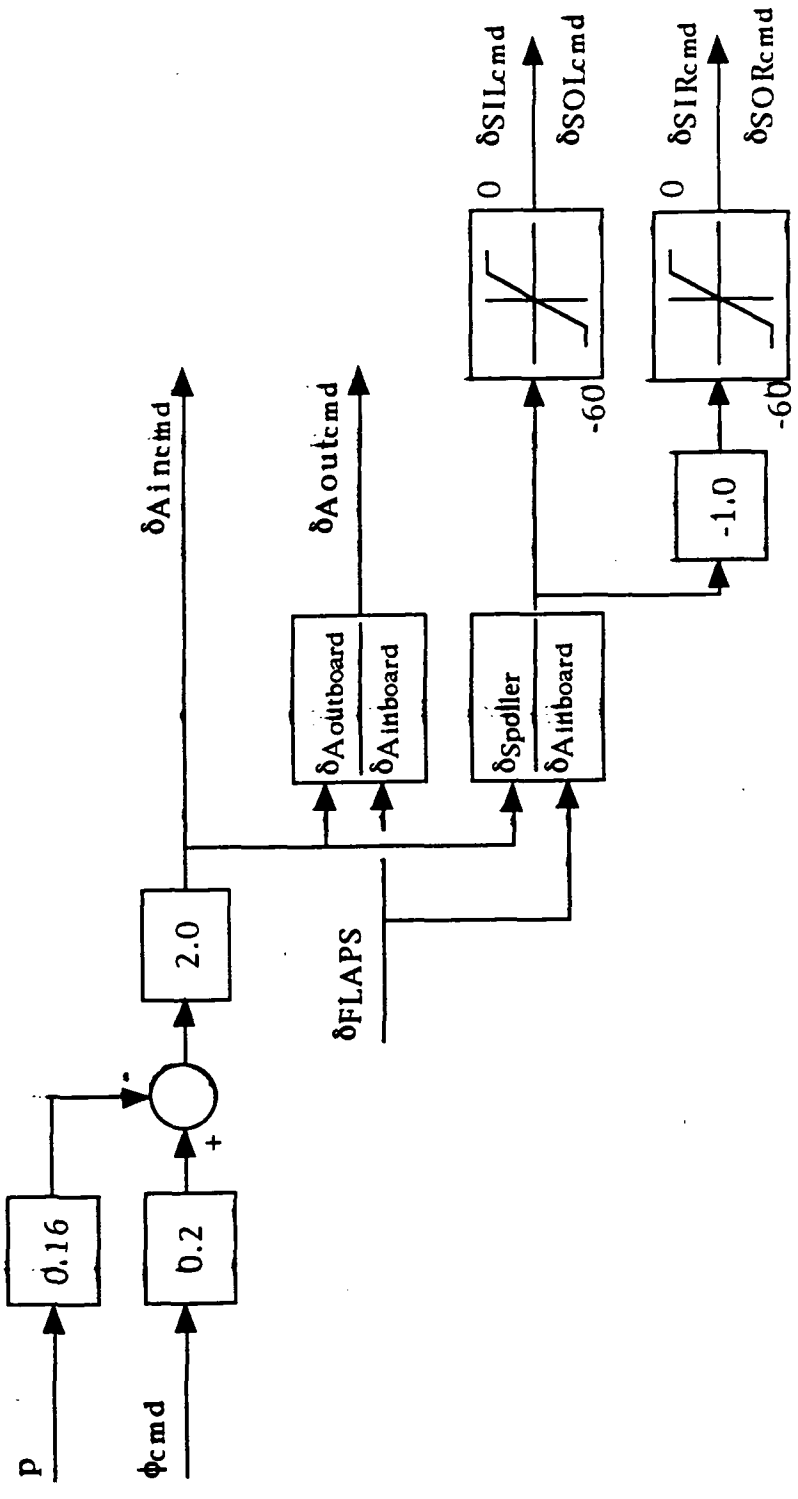

Figure 4.6 Megatransport Roll Control System

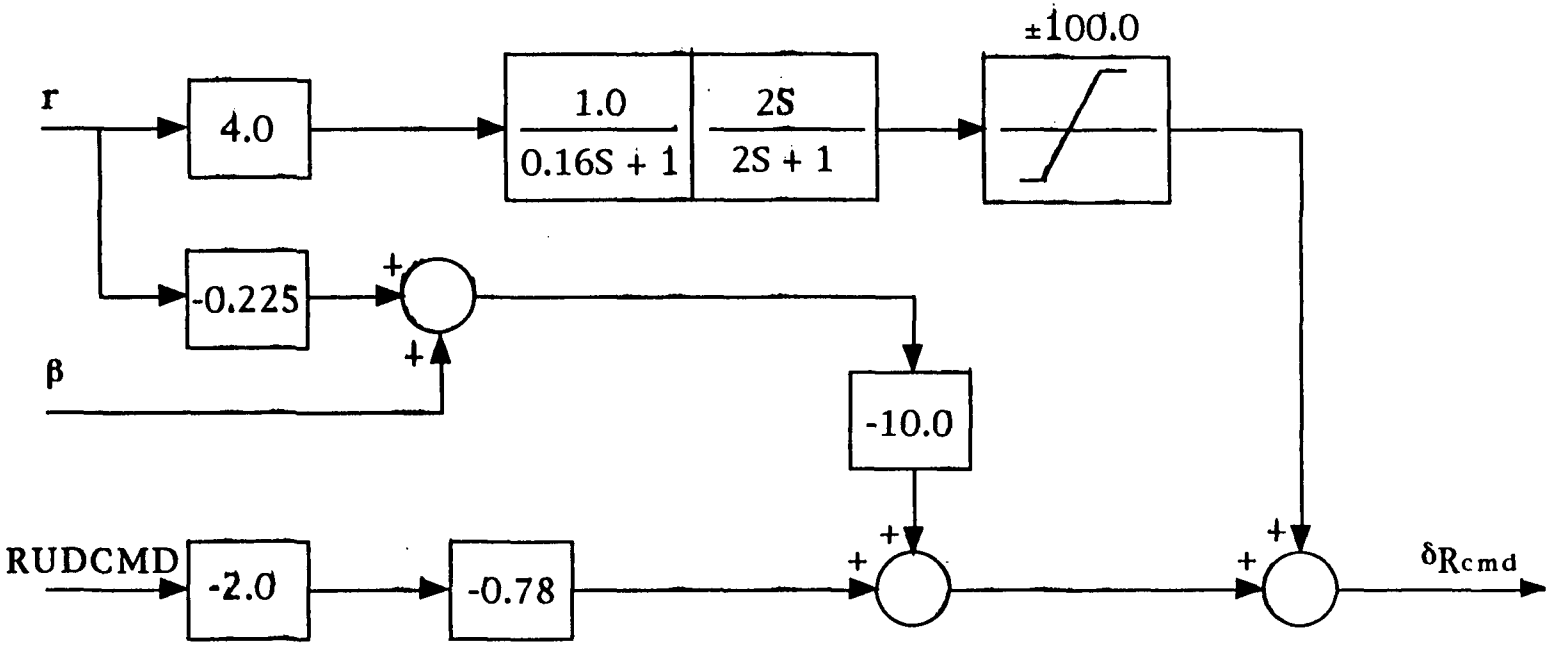

Figure 4.7 Megatransport Yaw Control System

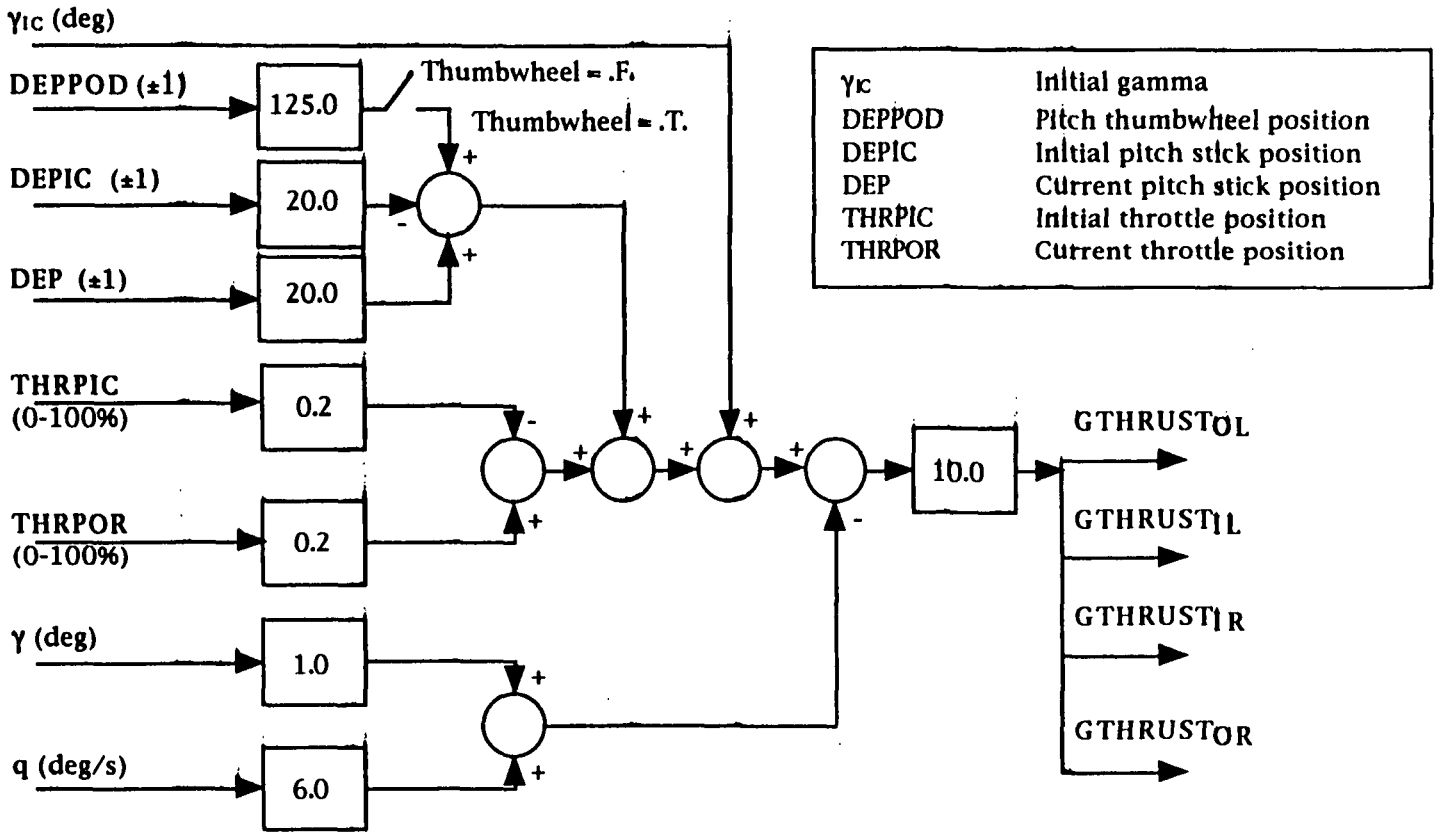

Figure 4.8 Megatransport PCA Flight Path Angle (Gamma) Control System

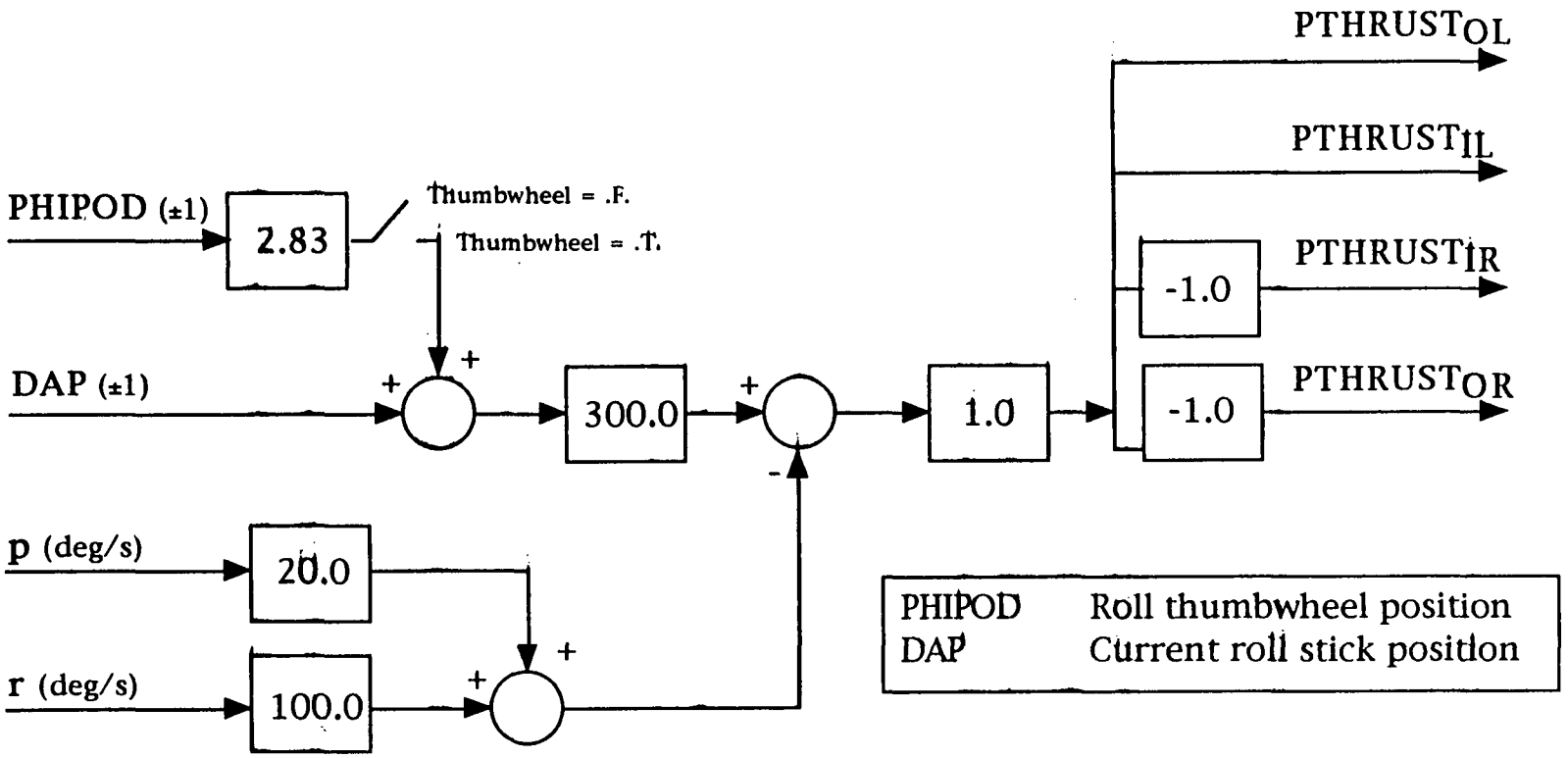

Figure 4.9 Megatransport PCA Bank Angle (Phi) Control System

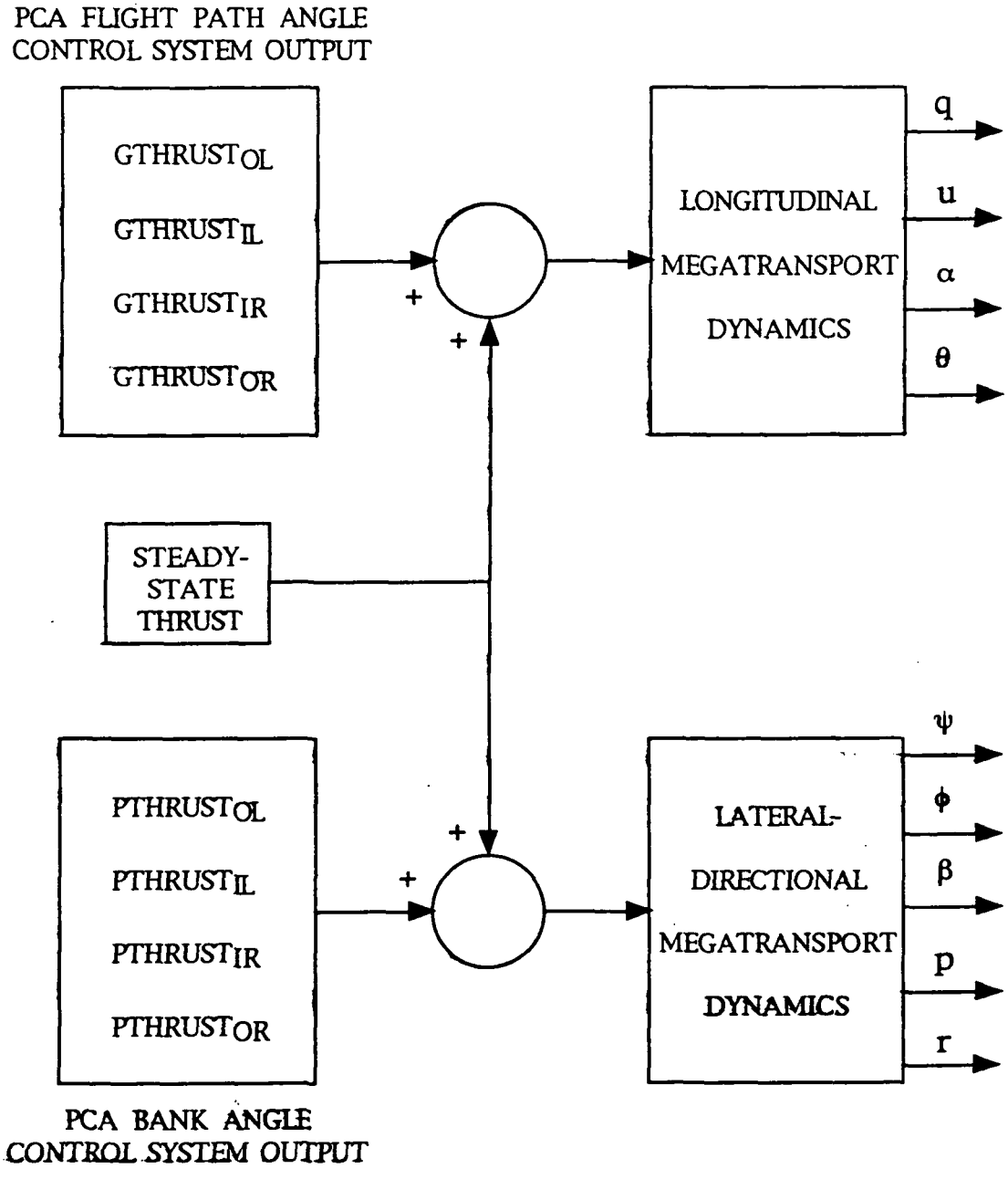

Figure 4.10 Megatransport PCA Control System

CHAPTER 5

TEST DESCRIPTION

5.1. INTRODUCTION

One of the primary objectives of this project was to analyze the thrust-controlled megatransport flying qualities through use of the megatransport simulator. The intent of the simulator sessions was as follows:

- to obtain the test pilot's comments and have the pilots assign Cooper-Harper pilot rating values to the longitudinal, lateral-directional, and overall megatransport flying qualities of each approach and landing test run
- to perform frequency sweeps on the same test configurations which the pilots flew and, using this frequency data, generate Bode plots of the longitudinal transfer function, ($\gamma/\delta T_{sym}$), and the lateral-directional transfer function, ($\phi/\delta T_{asym}$).

The description of the megatransport simulation flight testing, test flight data, frequency sweeps, and Bode plots is covered in this chapter. The analysis of the test data will be discussed in Chapter 6.

5.2. MEGATRANSPORT SIMULATION FLIGHT TESTING [Refs. 18,43,51]

Two NASA Dryden Flight Research Center test pilots participated in this study. Both are extremely experienced pilots, each pilot having thousands of

hours in many different types of aircraft. Appendix E contains more detailed information regarding each pilot's flight experience.

Test pilot A was asked to participate because he had no previous experience flying an aircraft or simulator using a throttles-only control system. Test pilot B, however, was selected because of his very extensive flight experience using the PCA throttles-only system in the MD-11 simulator, the F-15 simulator, and the F-15 test aircraft. It was thought that pilot A's inexperience with the PCA system and pilot B's expertise using the PCA system would provide data from pilots with two very different expectations of the system and experience levels using the system.

Each pilot participated in two simulator sessions which were held over a series of several days. Both pilots received a pre-flight briefing by the author prior to the first simulator session. The pre-flight briefing consisted of informing the pilots of the purpose and objectives of this study as well as acquainting the pilots with the megatransport mission specifications, size, and weight data. In addition, the pilots were briefed on which parameters, such as engine location and engine response time, would be changed over the course of the test runs. The pilots were not, however, told of the order in which the test points would be flown. During the test, they were completely unaware of which test run they were currently flying. The pre-flight briefing handout which was given to the test pilots is found in Appendix F.

Pilots A and B were also given a set of touchdown criteria, including touchdown location and rate of descent at touchdown, which established guidelines for desirable, acceptable, and unacceptable landings. These criteria were established to aid the pilots in assigning Cooper-Harper pilot ratings for the various approach and landing test runs. In this way each pilot

would be judging the landing performance of the aircraft using the same standards. The touchdown criteria used by the pilots are found in Figure 5.1.

Once the test pilot was seated in the megatransport cockpit, the author went over the flight and engine instruments and the aircraft controls with the pilot to acquaint him with the megatransport cockpit. The pilot was also given a thorough check-out with the PCA system pitch attitude and bank angle thumbwheels.

Each pilot requested, and was granted, a few minutes of flight time in the simulator to familiarize himself with the flight characteristics of the megatransport in PCA mode before the actual test runs commenced. After the familiarization flight, a remote microphone was attached to the pilot's lapel and a video recorder was turned on, with the pilot's permission, to record the test session.

The test pilots were to fly the megatransport simulator and assign pilot ratings to the test configurations listed in Table 5.1. Both pilots completed all the flights listed in Table 5.1.

As the test was being conducted, however, some of the test points were randomly repeated by the author to determine how repeatable a Cooper-Harper rating was on the same test point by the same pilot. Also, the pilots themselves occasionally requested to repeat a test point or even to add an additional test point to those in the original test outline. A complete listing of all the test points which were actually flown is given in Table 5.2 A description and analysis of all the test runs flown will be covered in Chapter 6.

The test runs were flown from a starting altitude of 4,100 feet (field elevation is 2,300 feet) with a longitudinal and lateral offset several miles uprange from the runway. All landings were made on Edwards Air Force Base

Runway 22. In all cases, the landing gear was fully extended before the start of the flight. All of the approaches and landings were flown with no flap extension, with the exception of one test run which was flown with full (50 degrees) flaps. The airplane was trimmed for straight and level flight at an approach velocity of 180 knots, an angle of attack of 5 degrees, and each of the four engines was trimmed at approximately 47,000 pounds thrust before each test flight. A flight control system failure was simulated by locking the flight control surfaces at their zero deflection position. All the test runs were flown in light turbulence with the exception of one run which was flown in intermediate turbulence. The turbulence model used is detailed in Appendix D.

Several of the test points involved changing the engine location on the wing. If one of these engine location test points was to be run, the x-, y-, and z-coordinates of the new engine location would be entered into the simulator, along with the new values for the airplane I_{xx}, I_{yy}, I_{zz}, and I_{xz} inertias which had changed due to the new engine location. In addition, the weight of the airplane was also changed and entered into the simulator due to the fact that the location of the engines affect wing weight. The methodology used for calculating the wing weight is found in Appendix C.

After each test flight, the pilot was given a copy of the Cooper-Harper pilot opinion rating scale, shown in Figure 5.2, along with a pilot comment card, shown in Figure 5.3, and was asked to make brief comments on the flight as the author was setting up the simulator for the next approach. After commenting on the specific flying qualities of the flight, the pilot was asked to give a Cooper-Harper pilot opinion rating value for the longitudinal flying qualities, the lateral-directional flying qualities, and for the overall flying

qualities in the landing approach task. Test pilot A followed this procedure and wrote down his comments after each test flight. Pilot B, however, preferred to comment on and evaluate the flying qualities during the flight itself. Either method was acceptable to the author and the pilots were allowed to adopt the procedure with which they were most comfortable. Appendix G contains the pilot's detailed comments and evaluation of each test run.

The pilots were debriefed after the test session. They often made additional comments about the test run after knowing what variable was being changed and examined. It was at this time that they occasionally requested to repeat a run due to their surprise at the flying qualities of a particular point or to add an additional test run to further investigate a trend which seemed to be developing in the data. Their suggestions were taken into account and incorporated into the test plan before their next megatransport simulator session.

5.3. RECORDING THE TEST FLIGHT DATA

During each megatransport simulation test flight, both input commands and output flight variables were recorded on a strip chart recorder or as a data file in the simulator computer. The strip chart recorder is capable of plotting 16 different variables during the test run. The strip chart recorder was used primarily to assist the simulator operator in assessing the test run as it occurred. A computer data file was set up prior to each test run. During the simulator run, the time history of 55 flight variables was recorded. A

complete listing of the flight variables which were recorded is found in Table 5.3.

After the test session was completed, the data were transferred from the simulator computer to a SUN workstation, where the data were compressed and reformatted. The information in each file was then processed using the program XPLOT. XPLOT, which was written by NASA Dryden engineers, was used to plot the time history data found in each of the data files. Data plots of several flight variables from each test run are included with the pilot comments and evaluations in Appendix G.

5.4. FREQUENCY SWEEPS

Although the Cooper-Harper pilot rating is a very successful method used to evaluate the handling qualities of an airplane under certain flight conditions, the evaluation is subject to the pilot's opinion of the ease or difficulty of flying the assigned task. Pilot opinions are likely to vary depending on factors such as pilot training, knowledge, experience, physical condition, and ability to assess the specific task.

Because of the subjective nature of evaluating flying qualities based solely on pilot opinion, it is desirable to quantify these Cooper-Harper rating results by analytically examining the performance of the engine/airframe open loop system.

A very practical and important approach to the analysis of a system is the frequency response method. The frequency response of a system is defined as the steady-state response of the system to a sinusoidal input signal.

For a sinusoidal input signal to a linear system, the resulting steady-state output signal is a sinusoid of the same frequency. The steady-state output signal differs from the input waveform only in amplitude and phase angle. By applying a sinusoidal test signal over various frequencies, the experimental determination of the frequency response of a system is accomplished.

A frequency sweep program was written and installed in the NASA Dryden simulator in which the megatransport engine thrust was modulated by a swept sinusoidal input signal of constant amplitude, 200 seconds duration, and ranging in frequency from 0.001 rad/sec to 6.28 rad/sec. The megatransport simulator was initialized so that all conventional control surfaces (elevator, ailerons, rudder, and spoilers) were locked at their neutral position throughout the frequency sweep.

A longitudinal sweep was obtained by adding the sinusoidal input signal to the trimmed throttle positions of all four engines to generate a change in flight path angle. A lateral-directional sweep was obtained by adding the sinusoidal input signal to the two left trimmed throttle positions and subtracting the sinusoidal input signal from the two right trimmed throttle positions to generate a change in bank angle. A typical frequency sweep run is shown in Figure 5.4.

The PCA system was not engaged during these frequency sweeps, therefore the frequency data obtained was of the open loop system. The intent of this project was not to analyze the PCA system or to design an optimal propulsion control system, but to investigate what the design drivers might be on an aircraft in which the PCA system was integrated into the initial aircraft design as opposed to an 'add-on' to an existing design.

For this purpose, the frequency response of the megatransport to changes in certain design variables such as the placement of the engines and engine response times were analyzed without the PCA system engaged. This allowed the determination of which factors are most important in influencing the flying qualities of a large transport aircraft using engine thrust for emergency flight control.

It was originally intended that two frequency sweeps, one longitudinal and one lateral-directional, were to be run on each of the configurations listed in the original test outline in Table 5.1. Due to the coding of the simulator, however, frequency sweeps could not be performed on the following cases:

- baseline configuration with outboard engine inoperative
- baseline configuration in intermediate turbulence
- baseline configuration with manual throttles-only flight control (Sioux City DC-10 scenario)
- baseline configuration with all control surfaces operational (conventional approach and landing).

A listing of the frequency sweep configurations which were run on the megatransport simulation, along with the corresponding piloted test run numbers, is included in Table 5.4. Again, these sweeps were run on the engine/airframe open loop system - they did not include the PCA system dynamics. The methodology for analyzing the frequency response is discussed in the following section.

5.5. BODE PLOTS [Refs. 52,53]

The unknown transfer function of a system can be obtained from the experimentally determined frequency response of a system. Typical aircraft transfer functions of interest are the response of the aircraft to changes in the elevator deflection for the longitudinal case and to changes in the aileron or rudder deflection for the lateral-directional case. A conventional frequency sweep test will measure the change in flight variables such as speed, angle of attack, attitude angle, heading angle, bank angle, or sideslip angle to pulses of a control surface to determine the longitudinal or lateral-directional response of the aircraft.

Since the main purpose of this project was to evaluate the controllability of the megatransport using the throttles-only PCA control system, however, the transfer functions of interest were the response of the megatransport flight path angle to changes in symmetrical thrust inputs for the longitudinal case and the response of the megatransport bank angle to changes in asymmetrical thrust inputs for the lateral-directional case.

Two frequency sweeps, one longitudinal and one lateral-directional, were run on each of the configurations listed in Table 5.4. The recorded data were then processed using the MATLAB signal processing toolbox programs SPECTRUM and SPECPLOT.

SPECTRUM performs spectral analysis on both the input and output sequences using the method of power spectrum estimation. For the longitudinal sweeps, the input sequence was the total thrust from all four engines and the output sequence was gamma, the flight path angle. For the

lateral-directional sweeps, the input sequence was the differential thrust between the two left and two right engines and the output sequence was phi, the bank angle.

A spectral analysis such as that performed by SPECTRUM may introduce significant anomalies in the estimated spectra, particularly when the data are sinusoidal. To alleviate this problem, it is common to introduce a time window, such as a Hanning window, that tapers the data so as to allow a more gradual entrance to and exit from the time history data to be analyzed. Therefore the frequency sweep input and output data sequences were divided into sections and successive sections were Hanning windowed, transformed with a fast Fourier transform, and accumulated.

SPECTRUM was then used to compute the lateral-directional transfer function, ($\phi/\delta T_{asym}$), and the longitudinal transfer function, ($\gamma/\delta T_{sym}$), for each of the frequency sweep test points listed in Table 5.4, while SPECPLOT was used to plot these transfer functions.

The transfer function representing the sinusoidal steady-state behavior of a system can be represented by magnitude and phase angle plots, called Bode plots. For a Bode diagram, the plot of logarithmic gain in dB versus frequency is normally plotted on one set of axes and the phase angle versus frequency on another set of axes.

Figure 5.5 shows the Bode magnitude and phase angle plots of the lateral-directional transfer function, ($\phi/\delta T_{asym}$), generated for the megatransport baseline configuration. The ($\phi/\delta T_{asym}$) transfer function has been normalized with respect to thrust. ($\phi/\delta T_{asym}$) is defined as the change in bank angle per unit change in thrust, where the unit change in thrust was determined experimentally to be 12,000 pounds thrust. This number is the

average value of the thrust increment used in generating the lateral-directional frequency sweeps.

Figure 5.6 shows the Bode magnitude and phase angle plots of the longitudinal transfer function, ($\gamma/\delta T_{sym}$), generated for the megatransport baseline configuration. Again, the ($\gamma/\delta T_{sym}$) transfer function has been normalized with respect to thrust. ($\gamma/\delta T_{sym}$) is defined as the change in flight path angle per unit change in thrust, where the unit change in thrust was determined experimentally to be 26,000 pounds thrust. This number is the average value of the thrust increment used in generating the longitudinal frequency sweeps.

As will be discussed in Chapter 6, Bode plots provide a significant insight for the analysis of control systems by graphically displaying important system characteristics such as break frequency, crossover frequency, and phase shift.

5.6. BODE PLOT FREQUENCY RANGE CRITERION [Refs. 49,53]

As can be seen from the frequency scale on Figures 5.5 and 5.6, the magnitude and phase angle plots cover the frequencies from 10^{-2} to 10^{2} rad/sec. By examining these plots, however, it becomes apparent that the Bode diagrams are not valid over this entire frequency range, particularly at the higher frequencies. Before using these plots for data analysis, it was necessary to eliminate invalid data by establishing valid lateral-directional and longitudinal frequency ranges. The criteria which were used to establish these frequency ranges were coherence plots.

Much of data analysis centers around determining relationships between two or more sets of data. These relationships are usually expressed in terms of a covariance function in the time domain or a coherence function in the frequency domain. These functions attempt to measure the degree of correlation between the input and output parameters.

For the ideal case, the input and output parameters are perfectly correlated and the coherence function is unity. On the other hand, if the input and output parameters are completely uncorrelated, the coherence function is zero. With actual data, the coherence function is somewhere in between.

The criterion which was used in this analysis was whether the coherence function was larger or smaller than the value of 0.8. In the frequency regions where the coherence function was between 0.8 and unity, the input and output were assumed to be fairly well correlated. A coherence value below 0.8 was assumed to indicate unacceptably low data correlation. These coherence plots were instrumental in determining the frequency regions in which the Bode plots were deemed valid.

Coherence plots for the megatransport baseline configuration transfer functions are shown in Figures 5.7 and 5.8. The coherence plot for the lateral-directional transfer function, ($\phi/\delta T_{asym}$), is shown in Figure 5.7, while the coherence plot for the longitudinal transfer function, ($\gamma/\delta T_{sym}$), is shown in Figure 5.8.

As can be seen from the figures, the valid frequency range is 10^{-1} rad/sec to approximately 4 rad/sec for the lateral-directional case and 10^{-1} rad/sec to approximately 2 rad/sec for the longitudinal case. Although these frequency ranges appear to be fairly limited, they cover a large part of the average operating range of the human pilot. Most pilots cannot easily react to

a system with a frequency either below 0.01 rad/sec or above 5 rad/sec, so data analysis which makes a comparison between Cooper-Harper pilot ratings and the frequency data contained in the Bode plots should share similar frequency ranges.

The Bode plot of the lateral-directional transfer function, ($\phi/\delta T_{asym}$), for the megatransport baseline configuration which was plotted in Figure 5.5 has been replotted in Figure 5.9 within the valid frequency range limits. Similarly, the Bode plot of the longitudinal transfer function, ($\gamma/\delta T_{sym}$), for the megatransport baseline configuration which was plotted in Figure 5.6 has been replotted in Figure 5.10.

5.7. CALCULATED BODE PLOT ANALYSIS [Refs. 18,49]

To corroborate the Bode plots which were generated from megatransport simulator frequency sweeps, both a lateral-directional and a longitudinal Bode plot were generated for the megatransport baseline configuration using the stability derivative data which were programmed into the megatransport simulator.

As was previously mentioned in Section 5.5, the transfer function representing the sinusoidal steady-state behavior of a system can be represented by magnitude and phase angle Bode plots. For an aircraft being controlled by engine thrust instead of a conventional flight control system the transfer functions of interest are the response of the flight path angle to changes in symmetrical thrust inputs for the longitudinal case and the

response of the bank angle to changes in asymmetrical thrust inputs for the lateral-directional case. The megatransport lateral-directional and longitudinal transfer functions, therefore, consist of two parts - the part due to the aircraft dynamics and the part due to the engine dynamics.

For aircraft motions commanded by changes in engine thrust, lateral-directional and longitudinal numerators which contain thrust control derivatives must be developed. The thrust control transfer functions due to the megatransport dynamics are presented in Appendix H.

To obtain the portion of the transfer function due to the engine dynamics, the Laplace transform is performed on the engine time lag equation as described in Reference 49 and the following equation results, where τ is defined as (1/TC) and TC is the engine time constant (see Appendix B):

$$\left(\delta T_{actual}(s)/\delta T_{cmd}(s)\right) = \left(\tau/(s+\tau)\right) = \left(1/(s+1)\right) \qquad \text{[Eqn. 5.1]}$$

Combining the two parts of the megatransport transfer function - the part due to the aircraft dynamics derived in Appendix H and the part due to the engine dynamics in Equation 5.1 above - gives the following equations for the lateral-directional and longitudinal transfer functions, respectively:

$$\left(\phi/\delta T_{asym}\right) = \left(\phi/\delta T_{actual}\right)_{asym} \cdot \left(\delta T_{actual}/\delta T_{cmd}\right) \qquad \text{[Eqn. 5.2]}$$

$$\left(\phi/\delta T_{sym}\right) = \left(1/(s+1)\right) \cdot \left(\frac{0.137s^2 + 3.793s + 9.244}{303.662s^4 + 746.104s^3 + 496.103s^2 + 489.681s - 7.061}\right) \qquad \text{[Eqn. 5.3]}$$

$$\left(\gamma/\delta T_{sym}\right)=\left(\gamma/\delta T_{actual}\right)_{sym}\cdot\left(\delta T_{actual}/\delta T_{cmd}\right) \qquad \text{[Eqn. 5.4]}$$

$$\left(\gamma/\delta T_{sym}\right)=\left(1/(s+1)\right)\cdot\left(\frac{0.045s^3-0.204s^2+0.665s-0.294}{308.516s^4+613.116s^3+505.415s^2+29.798s+8.475}\right) \qquad \text{[Eqn. 5.5]}$$

Equations 5.3 and 5.5 were input into the control module of the AAA program (Ref. 46) and the resultant lateral-directional and longitudinal Bode diagrams were plotted in Figures 5.11 and 5.12, respectively. Like the experimentally generated Bode plots of the lateral-directional transfer function, ($\phi/\delta T_{asym}$), and the longitudinal transfer function, ($\gamma/\delta T_{sym}$), the Bode plots generated from the calculated lateral-directional and longitudinal transfer functions were also normalized with respect to the thrust (see Section 5.5).

Comparing the calculated lateral-directional Bode plot of Figure 5.11 with the experimental lateral-directional Bode plot for the megatransport baseline configuration of Figure 5.9 shows how well the experimental and calculated lateral-directional Bode plots agree.

Starting at a frequency of 0.2 rad/sec, the magnitude plots of both Bode diagrams appear to have a value of approximately 10 dB. Both magnitude plots show a gradual drop off in roll control power until about 0.7 to 0.8 rad/sec. At this frequency, the experimental magnitude plot has a slight resonant peak, while the calculated magnitude plot exhibits a more pronounced resonant peak.

Both experimental and calculated magnitude plots show a similar sharp drop off in roll control power at about 0.9 rad/sec. Both magnitude plots reach values of approximately -40 dB at a frequency of 3 rad/sec.

The experimental and calculated lateral-directional phase angle plots do not compare quite as well as the experimental and calculated magnitude plots. The experimental phase angle starts with a phase lag of -65 degrees at 0.2 rad/sec, while the calculated phase angle is about -105 degrees at that same frequency.

Both experimental and calculated phase lags gradually increase, both phase angle plots passing through an inflection point of -180 degrees at a frequency of 0.7 to 0.9 rad/sec. The experimental and calculated phase angles both reach a value close to -270 degrees at 1.3 rad/sec.

A comparison of the calculated longitudinal Bode plot of Figure 5.12 with the experimental longitudinal Bode plot for the megatransport baseline configuration of Figure 5.10 shows a favorable agreement between the experimental and calculated longitudinal Bode plots.

Starting at a frequency of 0.06 rad/sec, the magnitude plots of both Bode diagrams appear to have values from between 5 to 10 dB. However, the experimental magnitude plot, while showing a slight increase in pitch control power between frequencies of 0.06 to 0.1 rad/sec, does not exhibit the sharp peak shown in the calculated magnitude plot in this same frequency range. Both magnitude plots show a sharp drop off in pitch control power at about 0.15 rad/sec and continue to drop similarly throughout the entire frequency range until reaching approximately -20 dB at 1 rad/sec.

As was found for the lateral-directional phase angle plots, the experimental and calculated phase angle plots do not agree quite as well with

each other, the experimental phase angle having a value of -90 degrees at 0.15 rad/sec and the calculated phase angle having a value of approximately zero degrees at that same frequency location.

The experimental phase lag increases at a constant rate until reaching -124 degrees at 0.3 rad/sec. The phase angle then remains fairly steady until about 0.6 rad/sec, when the phase lag increases sharply and reaches a value of -150 degrees at 1 rad/sec.

The calculated phase angle plot has an inflection at 0.3 rad/sec as does the experimental phase angle plot, but the calculated inflection is very slight. The calculated phase lag does not remain steady, but gradually increases, reaching a value of approximately -200 degrees at 1 rad/sec.

Although the experimental and calculated lateral-directional and longitudinal Bode magnitude and phase angle plots are not an exact match, their overall agreement with each other certainly suggests that the Bode diagrams which were calculated from the megatransport aerodynamic and engine data using the transfer function method tend to validate the Bode diagrams which were generated experimentally using the megatransport simulator input and output data.

Differences between the experimental and calculated Bode diagrams, particularly the phase angle plots, can be attributed to:

- the derivation of the thrust-controlled transfer function numerators (see Appendix H) is based on simple physics concepts - a more complex analysis may lead to more accurate equations
- the engine time lag equation used in the longitudinal and lateral-directional transfer function equations is based on a simple approximation of the engine model, whereas the engine model used in the megatransport

simulator is actually a more complex model which is dependent on the current level of thrust being produced by the engines (see Appendix B)

- equipment and computer time lags involved in the running of the megatransport simulator itself.

Table 5.1 Original Megatransport Simulation Test Matrix

Test Condition[1]	PCA Engaged
Conventional Control Surfaces Operational	No
Manual Throttles	No
Baseline Configuration	Yes
Engines Moved 20 Feet Outboard	Yes
Engines Moved 20 Feet Inboard	Yes
Engines Moved 5 Feet Vertically Downward	Yes
Engines Moved Vertically Upward Into Wing[2]	Yes
Engines Moved Vertically Upward 2.5 Feet Above Wing[3]	Yes
Full (50 Degrees) Flaps	Yes
Outboard Engine Inoperative	Yes
Engine Time Constant Of 0.5 Seconds	Yes
Engine Time Constant Of 3.0 Seconds	Yes
Intermediate Turbulence	Yes

1 All listed test conditions are deviations from the baseline airplane configuration.

2 Inboard engines were below megatransport C.G. and outboard engines were above megatransport C.G.

3 Inboard and outboard engines were above megatransport C.G.

Table 5.2. Actual Megatransport Simulation Test Matrix

Test Condition[1]	PCA Engaged	Test Pilot A	Test Pilot B
		Test Run Number	Test Run Number
Baseline Configuration	Yes	A1/A14	B1/B15
Engines Moved 20 Feet Outboard	Yes	A2/A17	B2
Engines Moved 20 Feet Inboard	Yes	A3	B3
Engines Moved 5 Feet Vertically Downward	Yes	A4	B4
Full (50 Degrees) Flaps	Yes	A5	B5
Outboard Engine Inoperative	Yes	A6/A10	B6
Engine Time Constant Of 3.0 sec	Yes	A7	B7
Engine Time Constant Of 0.5 sec	Yes	A8	B8
Intermediate Turbulence	Yes	A9	B9
Manual Throttles	No	A11/A12	B10/B14
Conventional Control Surfaces Operational	No	A13	B13
Engines Moved Vertically Upward Into Wing[2]	Yes	A15	B16
Engines Moved Vertically Upward 2.5 Feet Above Wing[3]	Yes	A16	B17
Engines Moved 20 Feet Outboard With 10 Knot Crosswind From The Right	Yes	A18	-

Table 5.2. Actual Megatransport Simulation Test Matrix (cont.)

Test Condition[1]	PCA Engaged	Test Pilot A	Test Pilot B
		Test Run Number	Test Run Number
Engines Moved Vertically Upward[4]	Yes	-	B11
Engines Moved Vertically Upward Above Wing[3]	Yes	-	B12
Engines Moved Vertically Upward 2.5 Feet Above Wing[3] - Manual Throttles	No	-	B18

1 All listed test conditions are deviations from the baseline airplane configuration.

2 Inboard engines were below megatransport C.G. and outboard engines were above megatransport C.G.

3 Inboard and outboard engines were above megatransport C.G.

4 Inboard engines were below megatransport C.G. and outboard engines were at megatransport C.G.

Table 5.3 Signals Recorded During Megatransport Simulator Test Runs

VARIABLE	DEFINITION
TIME	Elapsed time
P, PDOT	Roll rate, roll acceleration
Q, QDOT	Pitch rate, pitch acceleration
R, RDOT	Yaw rate, yaw acceleration
V, VDOT	Velocity, acceleration
ALPHA, ALPHADOT	Angle of attack, rate of change of angle of attack
BETA, BETADOT	Sideslip angle, rate of change of sideslip angle
THETA, THETADOT	Pitch attitude angle, rate of change of pitch attitude angle
PSI, PSIDOT	Heading angle, rate of change of heading angle
PHI, PHIDOT, PHIREF	Bank angle, rate of change of bank angle, reference bank angle
H, HDOT	Altitude, rate of change of altitude
XDOT, YDOT	Velocity along x, velocity along y
GAMMA, GAMMAREF	Flight path angle, reference flight path angle
MACH	Mach number
VCAS	Calibrated airspeed
QBAR	Dynamic pressure
DAP	Right/left stick position
DEP	Fore/aft stick position
DRP	Rudder pedal position
DFL	Trailing edge flap deflection
DFLE	Leading edge flap deflection
DH	Horizontal stabilizer position
DE	Elevator position
DR	Rudder position
DAI, DAO	Inboard and outboard aileron position
THRPOL, THRPIL, THRPIR, THRPOR	Throttle position of each engine
THRCOL, THRCIL, THRCIR, THRCOR	Commanded thrust of each engine
THRSOL, THRSIL, THRSIR, THRSOR	Actual thrust of each engine
THRUST	Total thrust
FDWNRG	Forward range
FCRSRG	Crossrange
NRUNS	Test run number

Table 5.4 Megatransport Simulation Frequency Sweep Matrix

Test Condition[1]	Corresponding Piloted Test Run Numbers
Baseline Configuration	A1,A14/B1,B15
Engines Moved 20 Feet Outboard	A2,A17/B2
Engines Moved 40 Feet Outboard	-
Engines Moved 20 Feet Inboard	A3/B3
Outer Engine Moved 20 Feet Outboard; Inner Engine Moved 20 Feet Inboard	-
Outer Engine Moved 20 Feet Inboard; Inner Engine Moved 20 Feet Outboard	-
Engines Moved 5 Feet Vertically Downward	A4/B4
Engines Moved Vertically Upward Into Wing[2]	A15/B16
Engines Moved Vertically Upward 2.5 Feet Above Wing[3]	A16/B17
Full (50 Degrees) Flaps	A5/B5
Gear Down	-
Engine Time Constant Of Zero Seconds (Instantaneous Response)	-
Engine Time Constant Of 0.5 Seconds	A8/B8
Engine Time Constant Of 3.0 Seconds	A7/B7

1 All listed test conditions are deviations from the baseline airplane configuration.

2 Inboard engines were below megatransport C.G. and outboard engines were above megatransport C.G.

3 Inboard and outboard engines were above megatransport C.G.

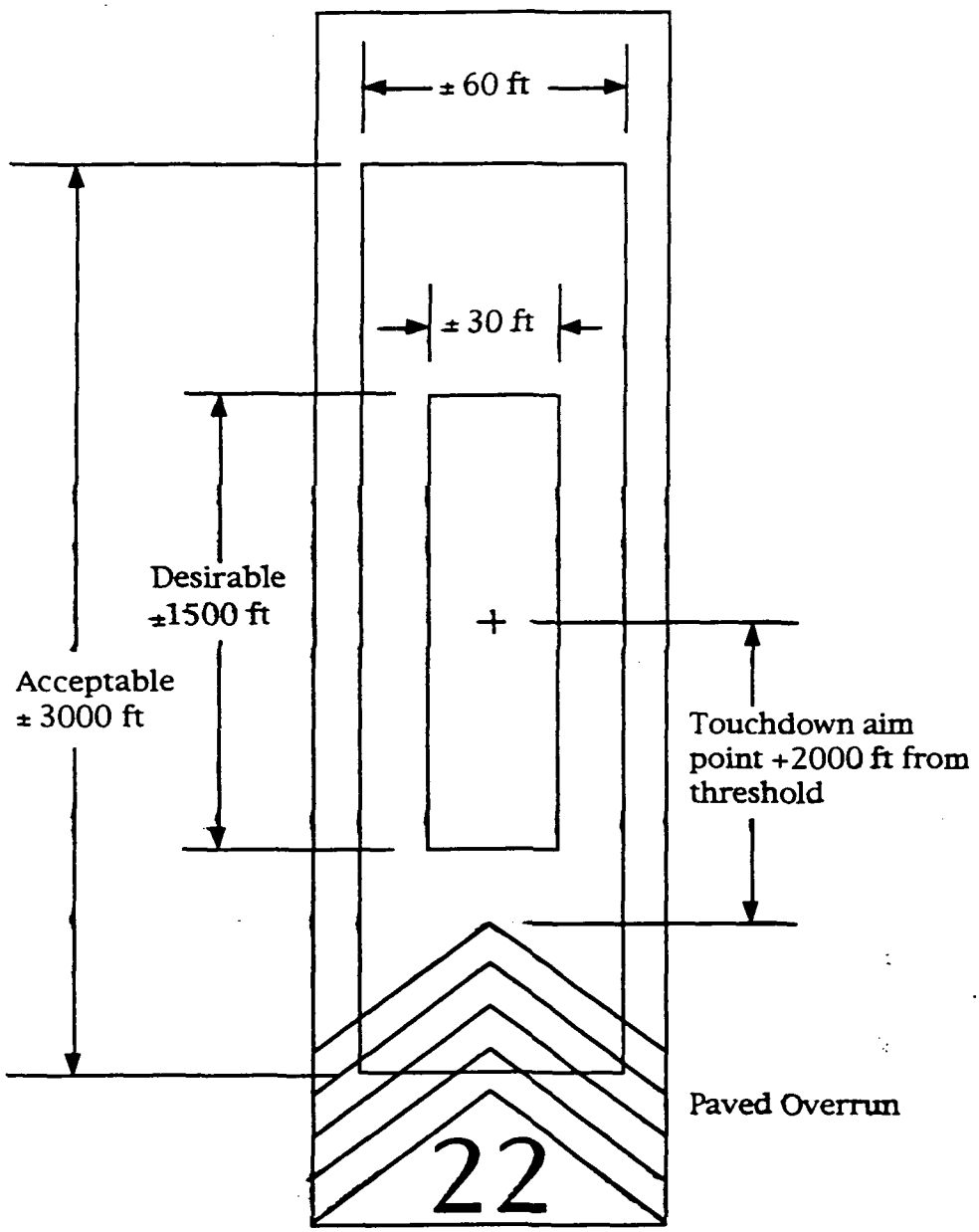

	Desirable	Acceptable
Downrange	± 1500 ft	± 3000 ft
Crossrange	± 30 ft	± 60 ft
Rate of Descent	< 6 fps	< 12 fps
Bank Angle	small	small
Heading Angle	estimate could stay on runway during rollout	

Figure 5.1 Touchdown Criteria Used by Test Pilots

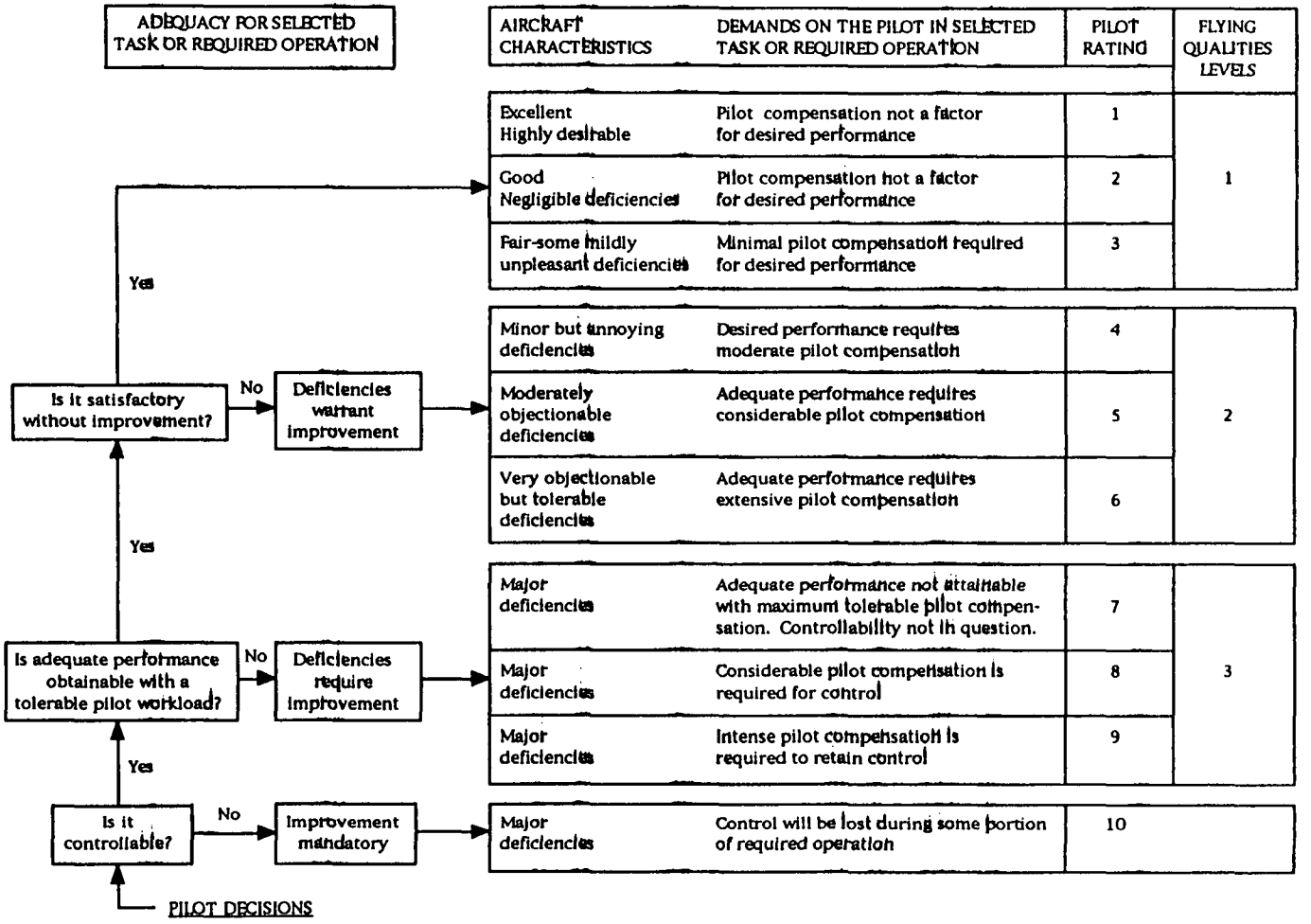

AIRCRAFT CHARACTERISTICS	DEMANDS ON THE PILOT IN SELECTED TASK OR REQUIRED OPERATION	PILOT RATING	FLYING QUALITIES LEVELS
Excellent Highly desirable	Pilot compensation not a factor for desired performance	1	1
Good Negligible deficiencies	Pilot compensation not a factor for desired performance	2	
Fair-some mildly unpleasant deficiencies	Minimal pilot compensation required for desired performance	3	
Minor but annoying deficiencies	Desired performance requires moderate pilot compensation	4	2
Moderately objectionable deficiencies	Adequate performance requires considerable pilot compensation	5	
Very objectionable but tolerable deficiencies	Adequate performance requires extensive pilot compensation	6	
Major deficiencies	Adequate performance not attainable with maximum tolerable pilot compensation. Controllability not in question.	7	3
Major deficiencies	Considerable pilot compensation is required for control	8	
Major deficiencies	Intense pilot compensation is required to retain control	9	
Major deficiencies	Control will be lost during some portion of required operation	10	

Figure 5.2 Cooper-Harper Pilot Opinion Rating Scale (Ref. 18)

PILOT COMMENT CARD

LONGITUDINAL CONFIGURATION

Pitch Attitude Response In General

Predictability Of Final Response

Cooper-Harper Pilot Rating

LATERAL-DIRECTIONAL CONFIGURATION

Roll Response In General

Roll Tendency To Overshoot

Tendency To Maintain Bank Angle

Heading Response In General

Cooper-Harper Pilot Rating

SUMMARY (BRIEF)

Problems

Any Special Control Techniques

Good Features

Overall Cooper-Harper Pilot Rating

Figure 5.3 Pilot Comment Card (Ref. 51)

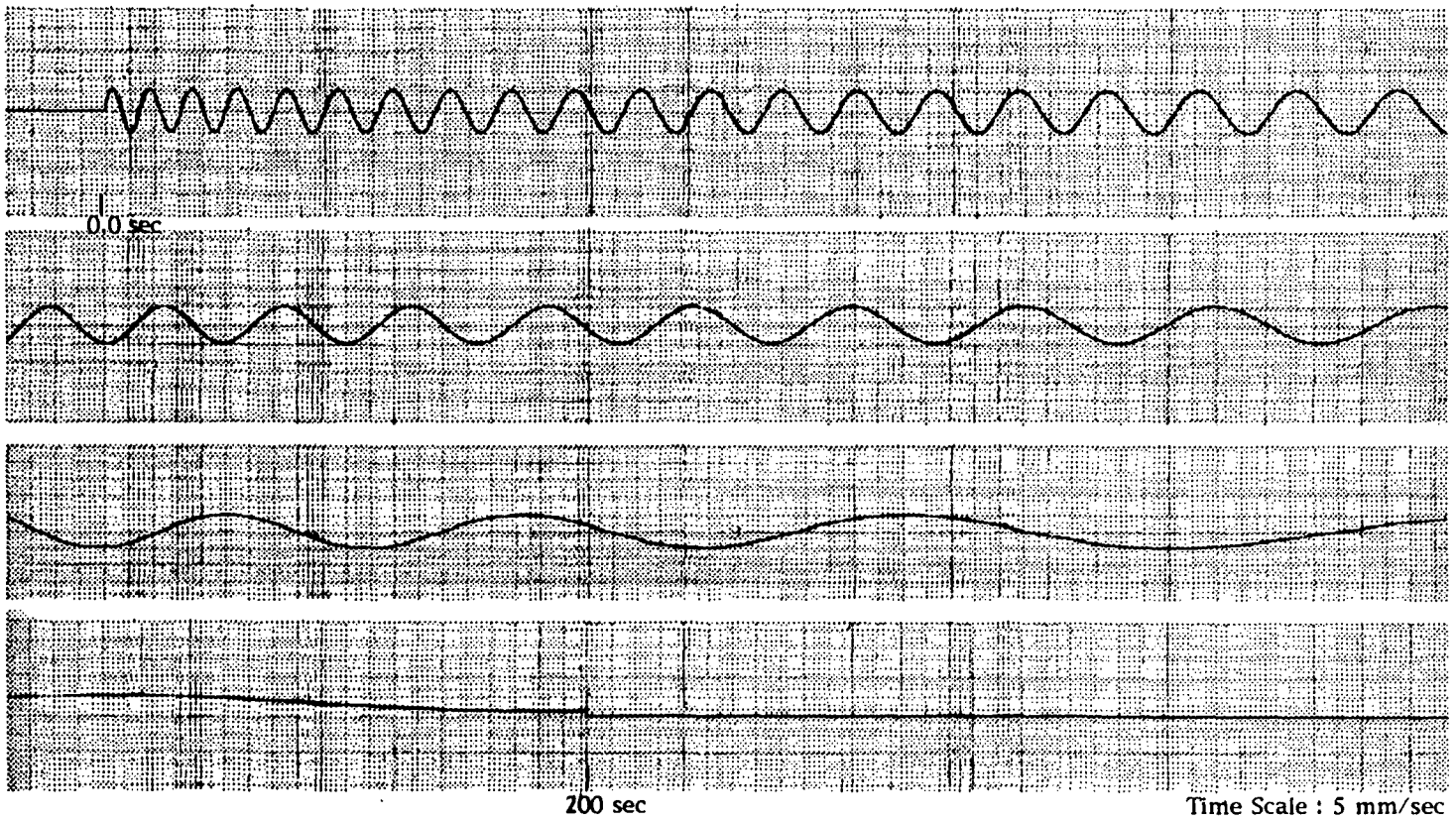

Figure 5.4 Megatransport Simulation Frequency Sweep

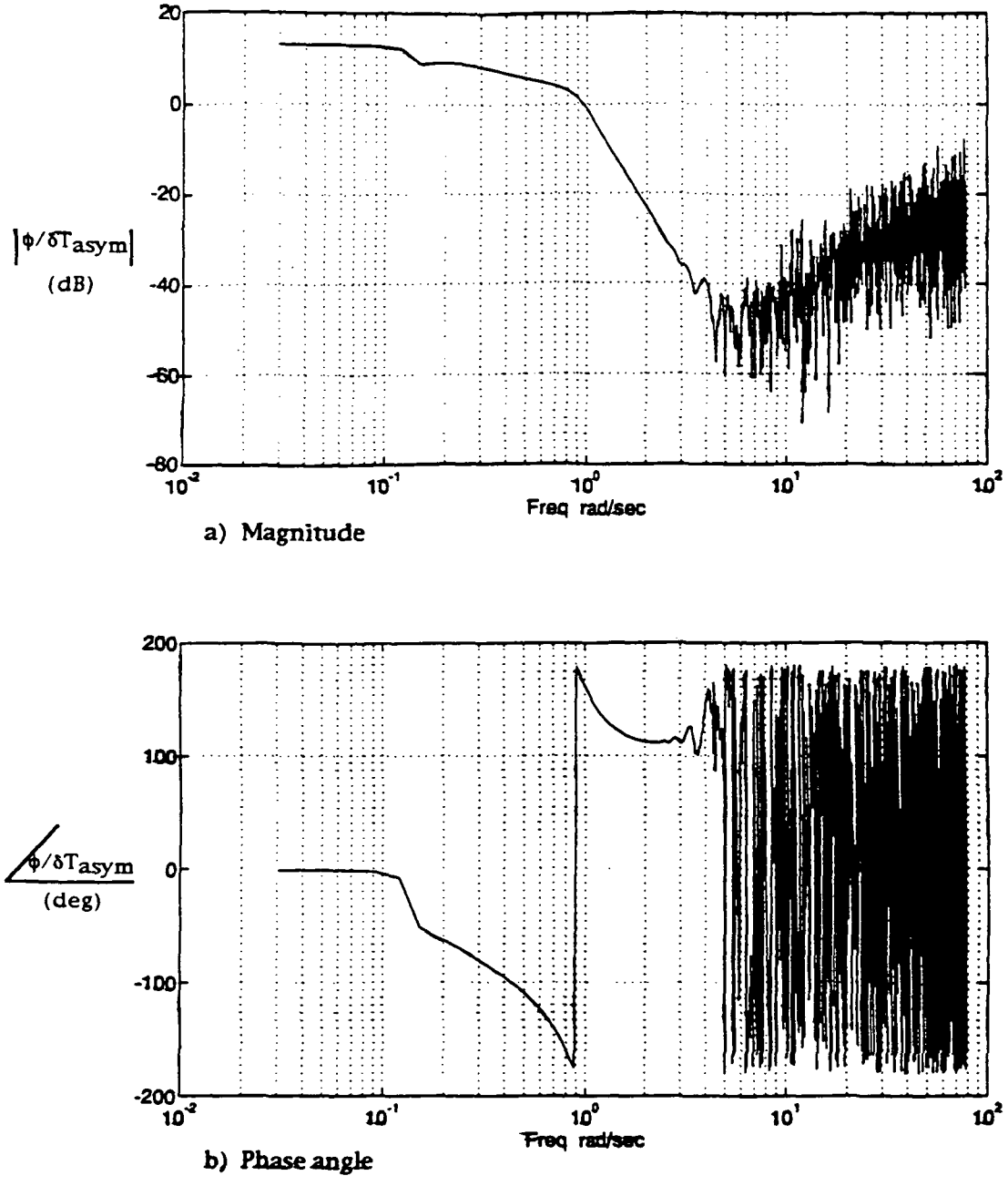

Figure 5.5 Megatransport Lateral-Directional Bank Angle - Asymmetric Thrust Frequency Response: Baseline Configuration

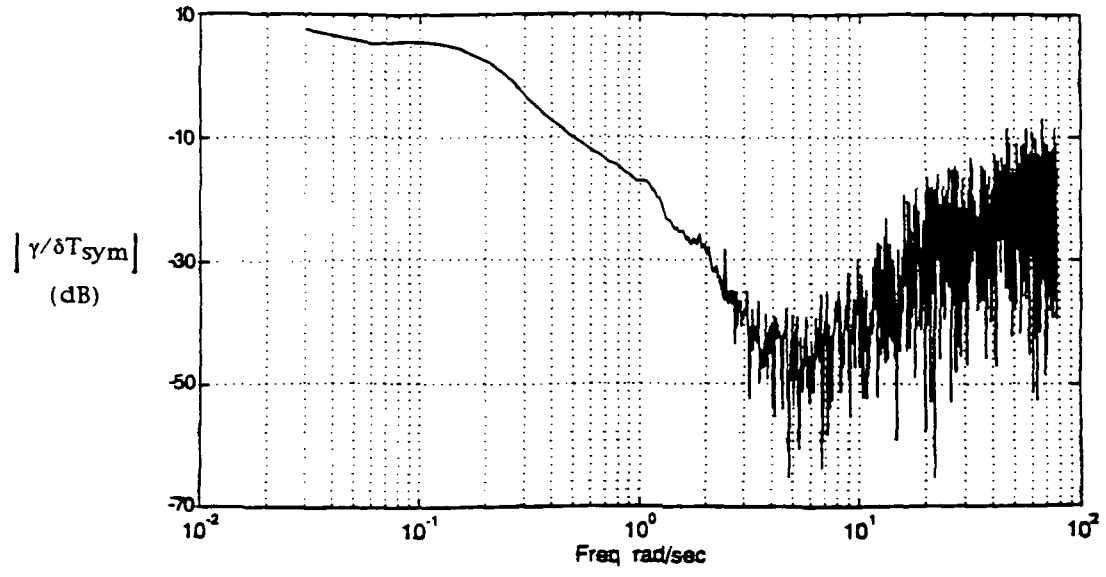

a) Magnitude

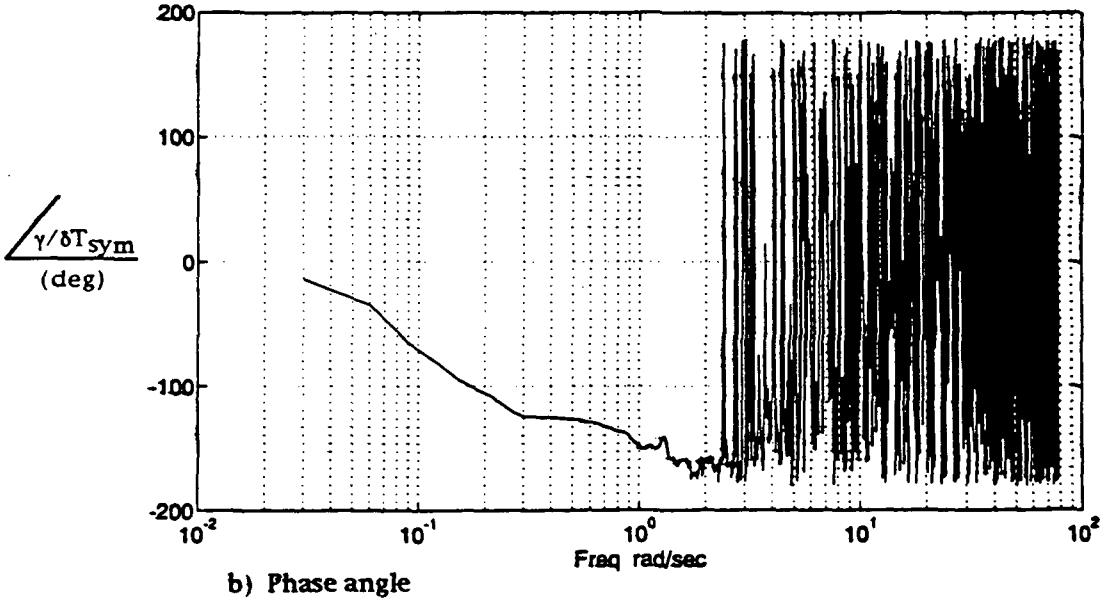

b) Phase angle

Figure 5.6 Megatransport Longitudinal Flight Path Angle - Symmetric Thrust Frequency Response: Baseline Configuration

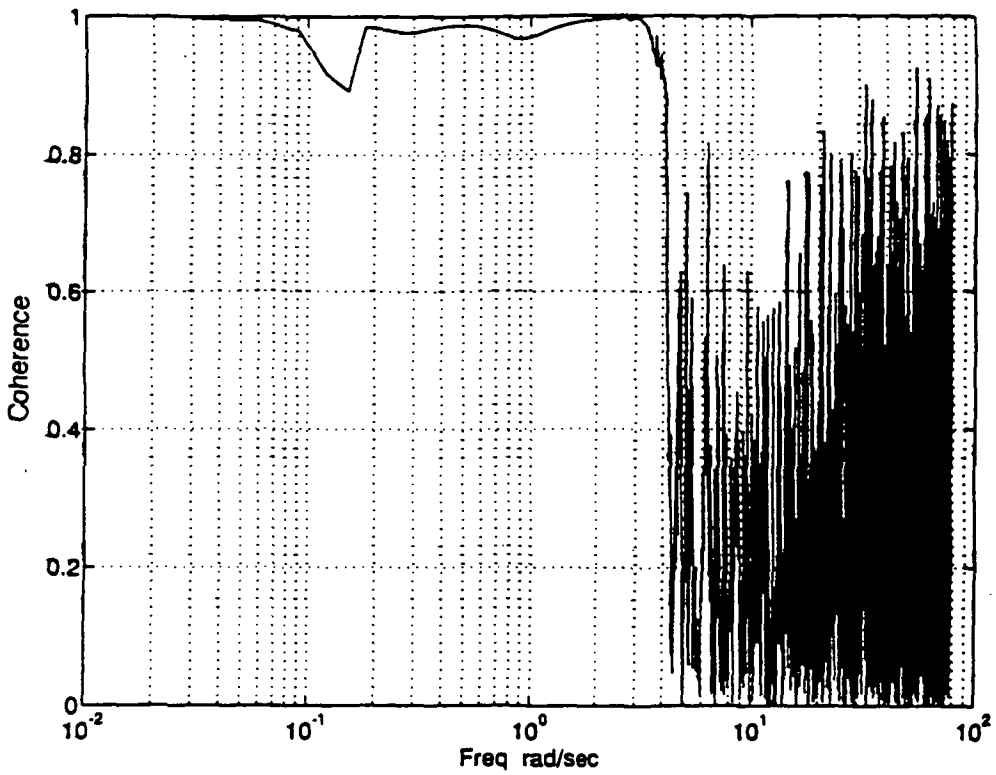

Figure 5.7 Coherence Plot for the Lateral-Directional Transfer Function, ($\phi/\delta T_{asym}$), for the Megatransport Baseline Configuration

C-3.

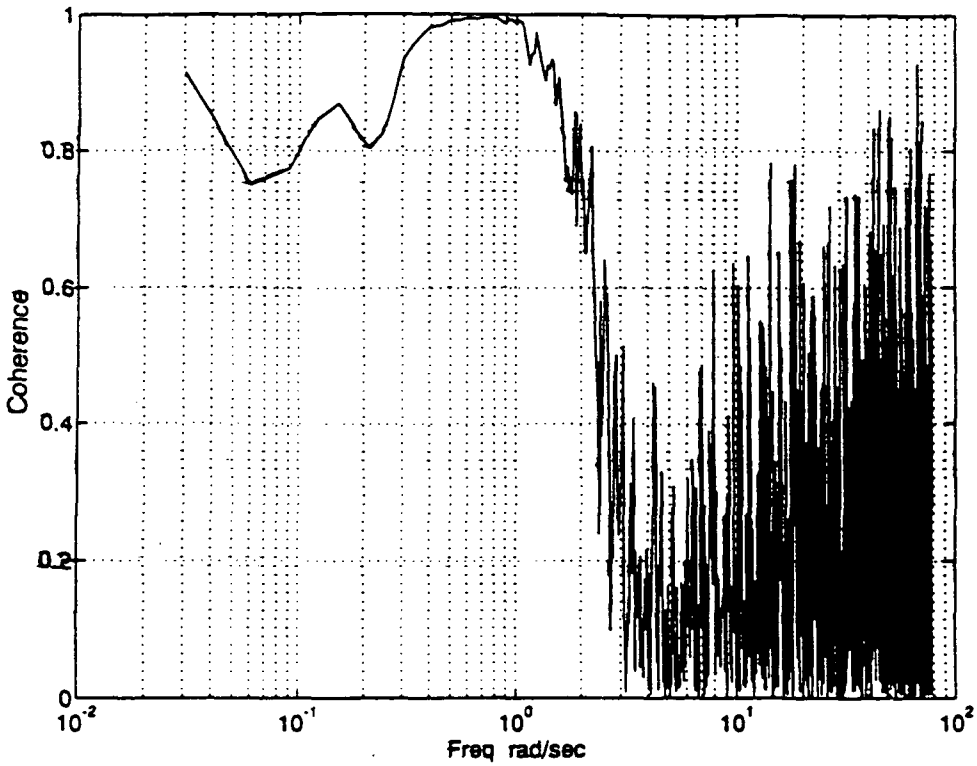

Figure 5.8 Coherence Plot for the Longitudinal Transfer Function, ($\gamma/\delta T_{sym}$), for the Megatransport Baseline Configuration

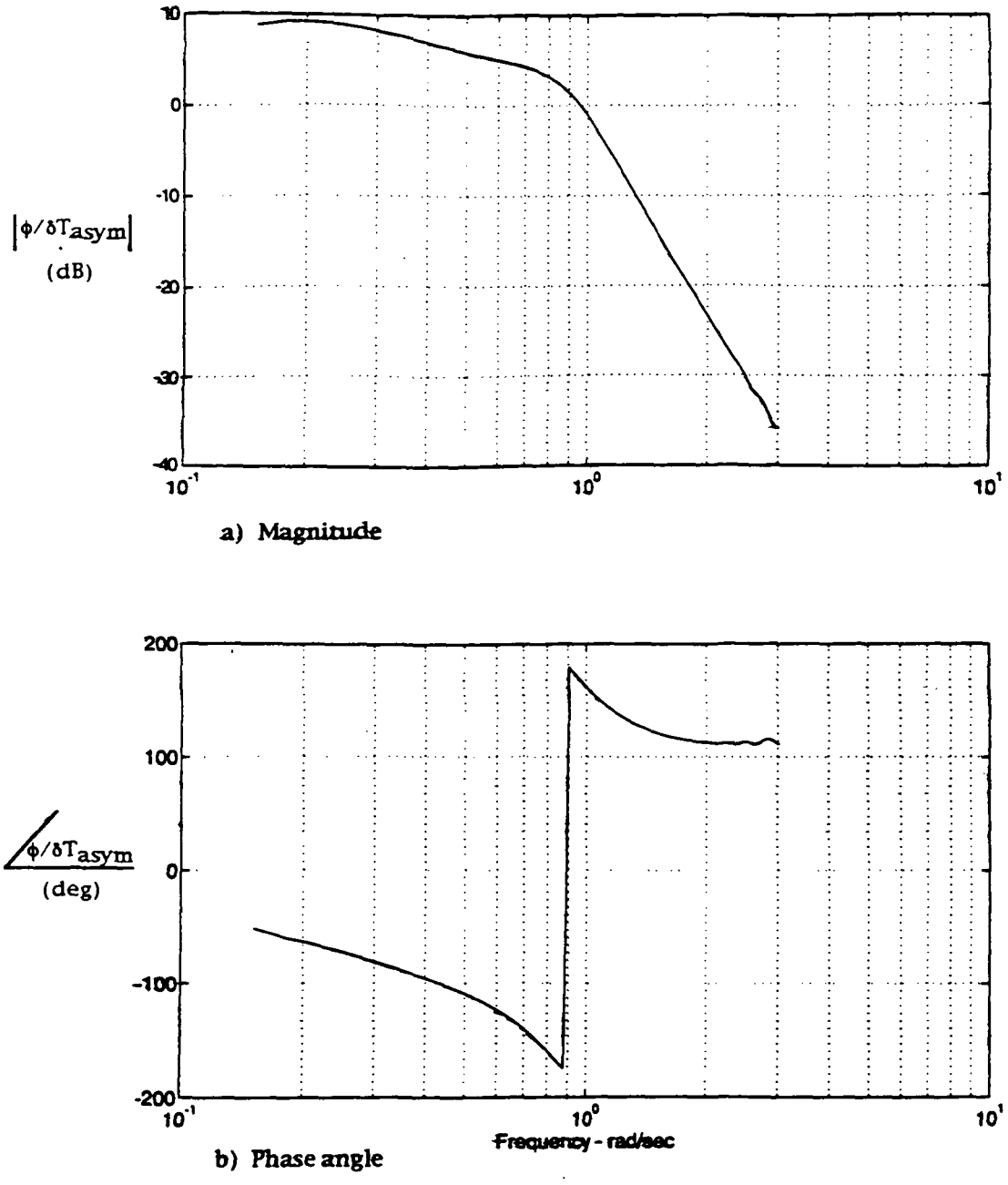

Figure 5.9 Megatransport Lateral-Directional Bank Angle - Asymmetric Thrust Frequency Response of the Baseline Configuration (Reduced Scale)

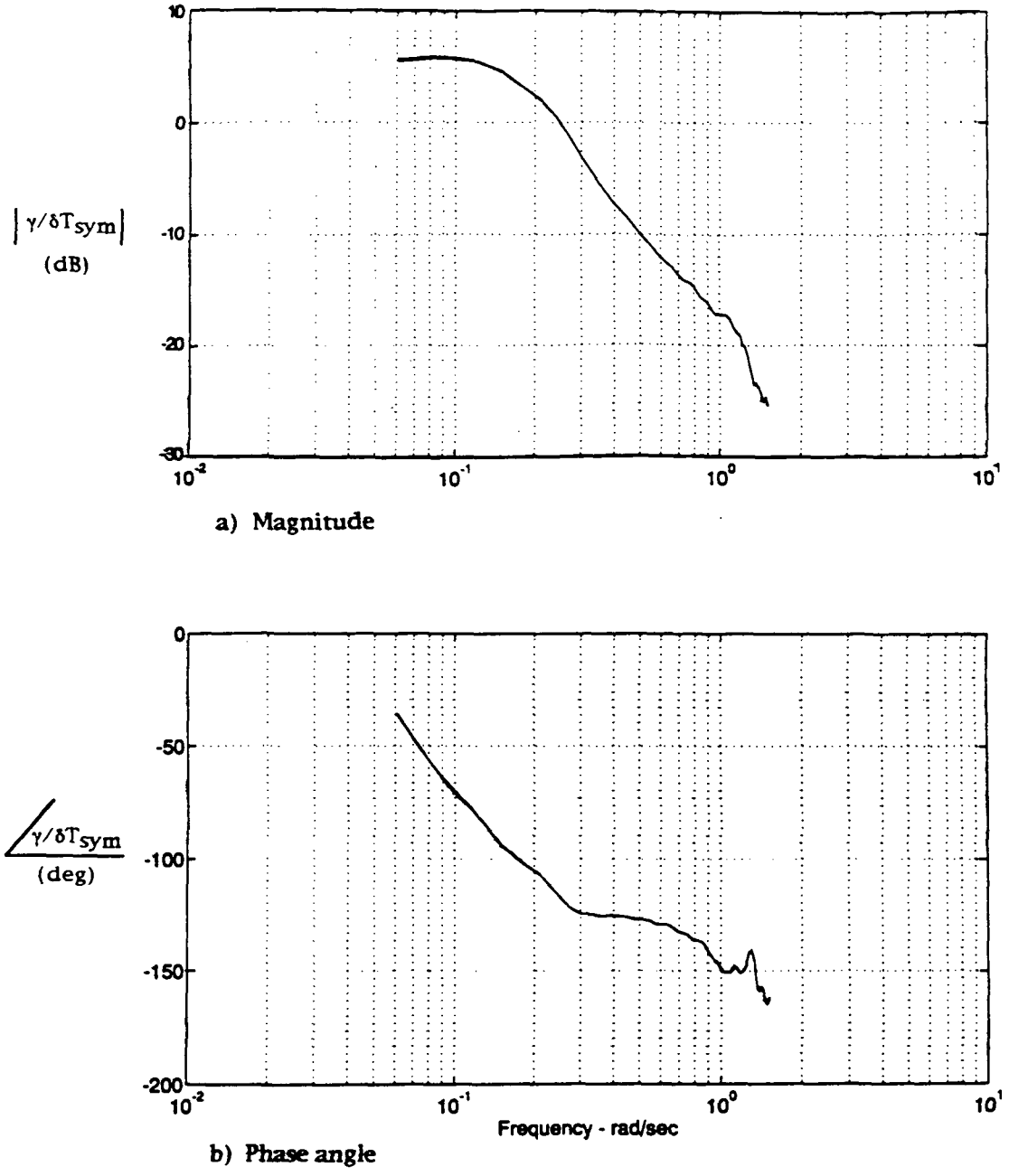

Figure 5.10 Megatransport Longitudinal Flight Path Angle - Symmetric Thrust Frequency Response of the Baseline Configuration (Reduced Scale)

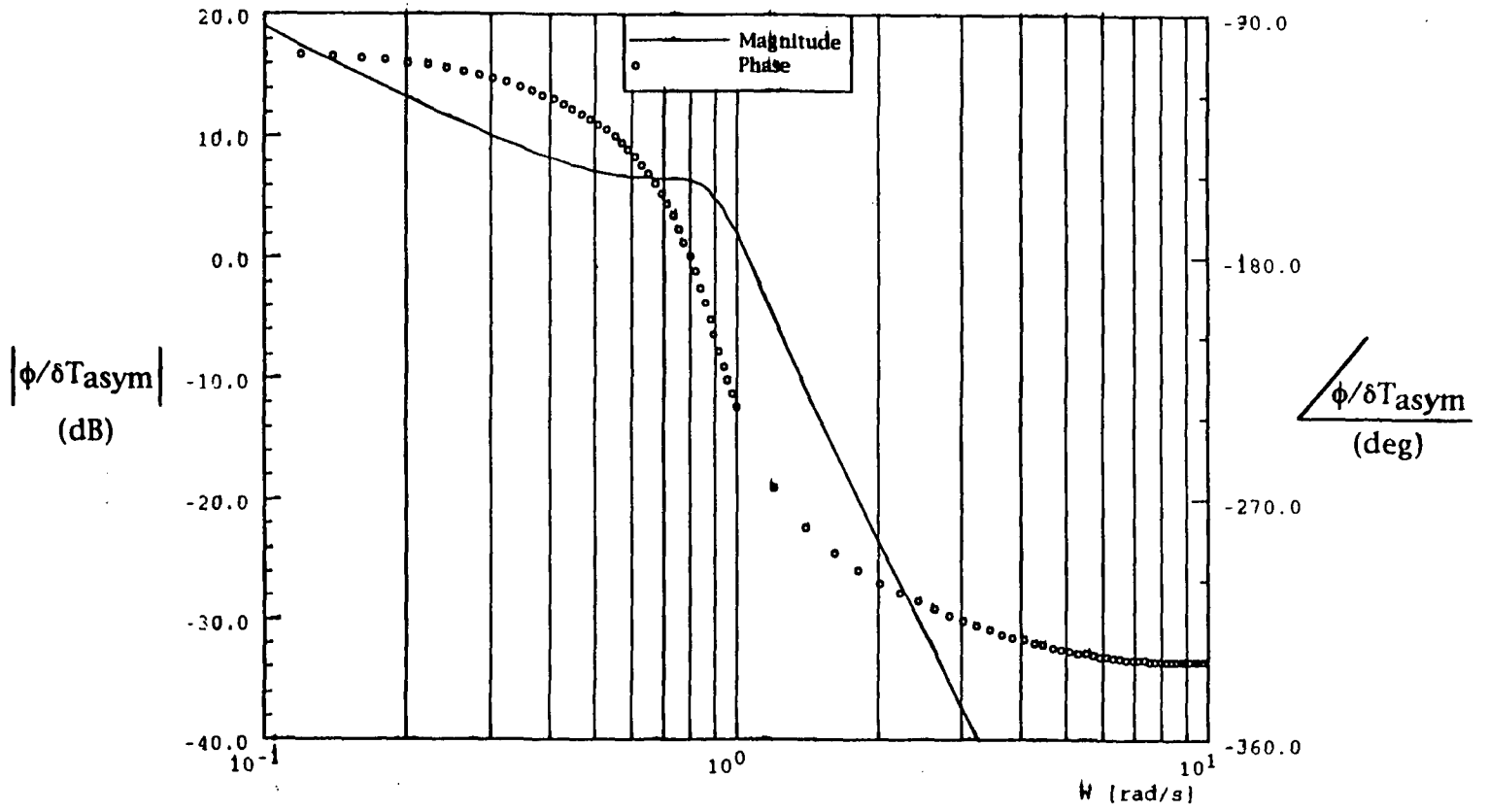

Figure 5.11 Calculated Bode Magnitude and Phase Angle Diagram for the Megatransport Aircraft/Engine Lateral-Directional Transfer Function ($\phi/\delta T_{asym}$) (Ref. 46)

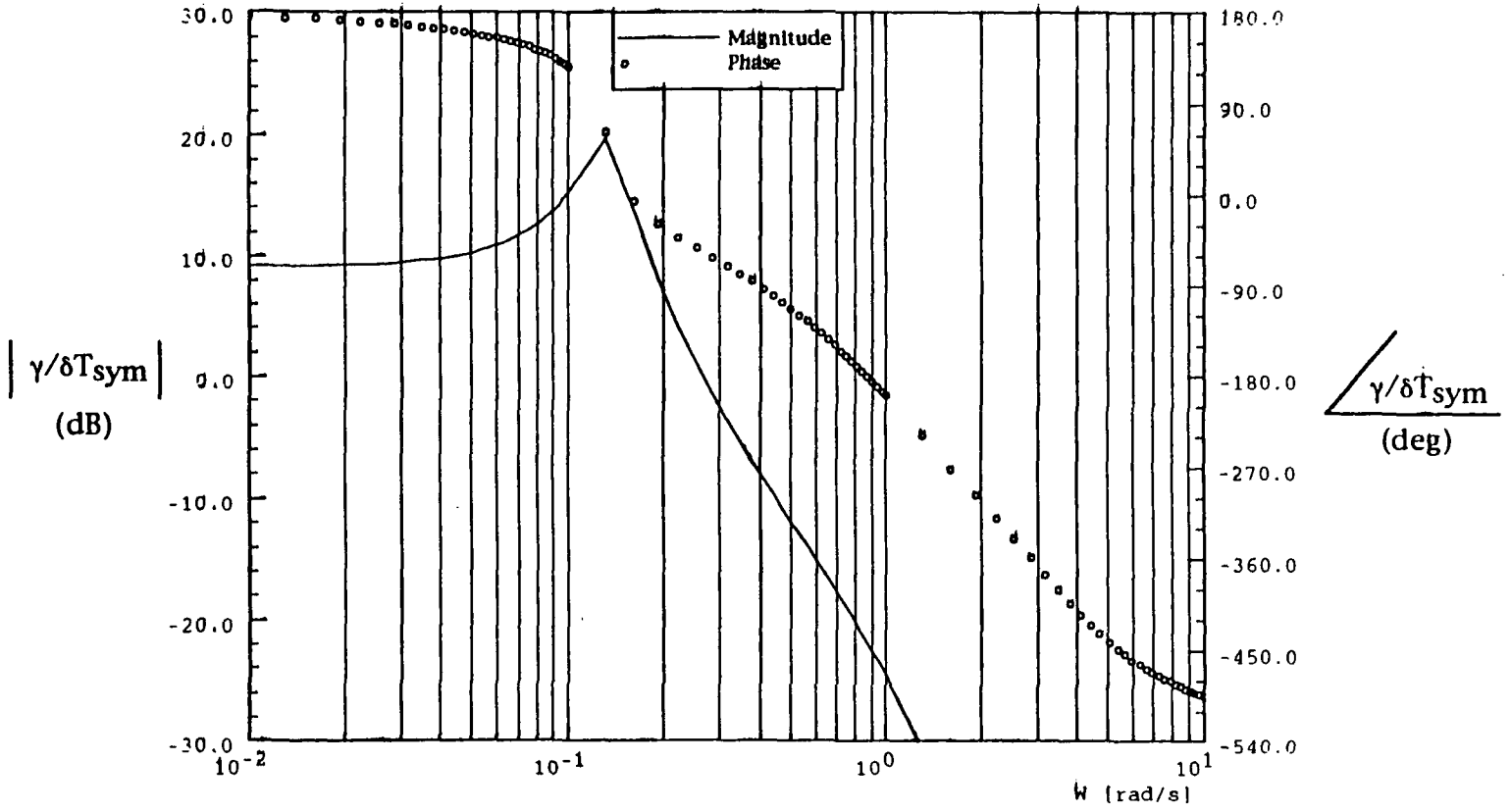

Figure 5.12 Calculated Bode Magnitude and Phase Angle Diagram for the Megatransport Aircraft/Engine Longitudinal Transfer Function ($\gamma/\delta T_{sym}$) (Ref. 46)

CHAPTER 6

DATA ANALYSIS

6.1. INTRODUCTION

The lateral-directional and longitudinal Bode plots which were generated from frequency sweep data (PCA system not engaged) for each individual test configuration listed in Table 5.4 are grouped and analyzed in this chapter according to the following test parameters:

- engine location varied laterally
- engine location varied vertically
- distance between inboard and outboard engines varied
- engine time constant varied
- outboard engine inoperative
- additional test cases.

Section 6.2 presents a comparison between the Bode plots of the various test configurations as grouped above. In addition to the magnitude and phase angle comparisons, the Cooper-Harper pilot ratings corresponding to these test configurations are compared, as well.

Section 6.3 contains root locus plots which were generated to analyze the combined frequency and damping ratio behavior of the megatransport/PCA system. Section 6.4 addresses the flying quality levels of

the megatransport while using engine thrust for flight control and Section 6.5 concludes the chapter with a summary of the data analysis results.

6.2. BODE PLOT ANALYSIS

6.2.1. ENGINE LOCATION VARIED LATERALLY

6.2.1.1. LATERAL-DIRECTIONAL CASE

Figures 6.1a and 6.1b show the experimental Bode magnitude and phase angle plots, respectively, of the lateral-directional transfer function, ($\phi/\delta T_{asym}$), generated for the following four configurations:

- baseline aircraft - engines at original configuration
- inboard and outboard engines all moved 20 feet outboard along wing span from original configuration
- inboard and outboard engines all moved 20 feet inboard along wing span from original configuration
- inboard and outboard engines all moved 40 feet outboard along wing span from original configuration.

Test pilots A and B flew the first three test cases but were unable to fly the fourth case due to time constraints. Their Cooper-Harper pilot ratings are included in Figure 6.1. Figure 6.2 shows the engine positions of these four test configurations.

As the engines are moved outboard, the roll and yaw inertias are greatly increased. As can be seen in Table C1, the roll moment of inertia, I_{XX}, increases from 46,648,096 sl-ft^2 for the test point with the engines located furthest inboard to 90,391,137 sl-ft^2 for the test point with the engines located furthest outboard. Similarly, the yaw moment of inertia, I_{ZZ}, increases from 104,444,836 sl-ft^2 to 147,138,831 sl-ft^2 for the test points with the engines located furthest inboard and outboard, respectively.

As can be seen in the low frequency portion of Figure 6.1a (frequencies less than 1 rad/sec), the further outboard the engines are moved, the higher the magnitude and, hence, the larger the roll control power. The magnitude plot shows a 2 dB increase, or 25% gain, in roll control response between each of the test runs as the engines are moved further outboard.

As the engines are moved outboard, however, a resonant peak begins to appear between 0.6 - 0.7 rad/sec. This indicates that the roll response is becoming less damped, more oscillatory, and exhibits more overshoot in roll near the resonant frequency. While moving the engines outboard increases roll control power at low frequency, it also produces a more oscillatory response near the resonant frequency. Test pilot B noted that as the engines were moved outboard, the bank control appeared to be a "little looser", indicating the pilot noticed that the roll response wasn't as crisp as the baseline case.

As the frequency is increased, all test runs show a sharp drop off in roll control power between 0.7 and 1 rad/sec. The further outboard the engines are located, the faster the roll control power falls off as the frequency increases. While the roll control power may be greater with the engines located further outboard at the lower frequencies, the roll control response is actually slightly better with the engines located further inboard at the higher frequencies.

Although the magnitude plot shows a significant difference at low frequencies in the lateral-directional response of the airplane as the engine location is varied laterally, the difference at frequencies above 1 rad/sec, for the most part, is small.

Figure 6.1b shows that throughout the entire frequency range, the further outboard the engine location, the greater the lateral-directional phase lag. The phase lag between all the engine locations is much the same until about 0.4 rad/sec, then the phase angle responses of the four test runs start to diverge. The difference in phase angle lag between each of the different engine location test runs appears to be 10 degrees with the furthest outboard engine location exhibiting the most phase lag, the inboard engine location exhibiting the least amount of lag. The larger yaw and roll inertias of the furthest outboard engine location increase the response time to yaw and roll and, hence, increase the phase lag. This lag was noted by test pilot A, who commented that there appeared to be more lag in yaw response when the engines were moved outboard. There is no optimal lateral engine location - the roll control power can only be increased at the expense of the lateral-directional phase response.

While the pilots noticed small differences in the airplane response due to moving the engines either inboard or outboard from the baseline configuration, the overall Cooper-Harper pilot ratings didn't change significantly. Test pilot A stated that the test runs "seemed similar" and assigned each run either a 4 or a 5 (Level 2 ratings) on the Cooper-Harper pilot rating scale. Test pilot B commented that "the runs are very, very similar as far as the response goes . . . I don't see much difference." Pilot B rated each

test run either a 3 or an average value of 3 1/2 on the Cooper-Harper scale (Level 1 ratings).

As can be seen by comparing the baseline configuration test runs (Figures G1b, G13b, G18b, and G30b) with the test runs in which the engine location was moved laterally along the wing span (Figures G2b, G16b, G19b, and G20b), there is no significant difference between the lateral-directional flight variables of these simulator test flights.

6.2.1.2. LONGITUDINAL CASE

Figures 6.3a and 6.3b show the experimental Bode magnitude and phase angle plots, respectively, of the longitudinal transfer function, ($\gamma/\delta T_{sym}$), generated for the same four cases which were described in the lateral-directional case. Again, the Cooper-Harper pilot ratings of test pilots A and B are included in the figure.

Figure 6.3a shows that throughout the entire frequency range of the Bode plot, the further inboard the engines are located, the higher the magnitude and, hence, the larger the pitch control power. As can be seen in the figure, the magnitude of the various longitudinal engine location test runs is very similar at low frequencies (frequencies less than 0.3 rad/sec). As the frequency is increased, all test runs show a sharp drop off in pitch control power at about 0.15 rad/sec. Around 0.3 rad/sec, however, the magnitude of the various test runs start to diverge. The further outboard the engines are located, the faster the pitch control power falls off as the frequency increases.

Although the magnitude plot shows small differences at low frequencies (0.5 dB or a 6% difference) in the longitudinal response of the airplane as the engine location is varied laterally, the difference at frequencies above 0.3 rad/sec becomes significant (1 dB or a 12% difference for a 20 foot engine location change and 2 dB or a 25% difference for a 40 foot engine location change).

This difference can be explained by noting that as the engines are moved outboard along the wing span, they also move upward in the -z-direction due to the dihedral of the wing as can be seen in Figure 6.2. This decreases the engine z-axis moment-arm to the airplane center of gravity located above the wing, effectively reducing the pitching moment and decreasing the pitch control power. As can be seen in Table C1, the pitch moment of inertia, I_{yy}, decreases from 61,430,452 sl-ft^2 for the test point with the engines located furthest inboard to 59,759,694 sl-ft^2 for the test point with the engines located furthest outboard.

Figure 6.3b shows that throughout the frequency range, the further outboard the engine location, the greater the longitudinal phase lag. The phase lag between all the engine locations is similar until about 0.15 rad/sec, then the differences between the four phase angle responses become more noticeable. The difference in phase lag between the baseline configuration and moving the engines either inboard or outboard 20 feet is only a degree or two at most, whereas the phase lag is more pronounced for the 40 feet outboard engine location (about 10 degrees more phase lag than baseline). As was seen in Figure 6.3a, the pitch control power becomes so diminished as the engines are moved outboard that the pitch response becomes sluggish, as is reflected in the phase lag plot.

While the longitudinal Bode plots show variations in both the magnitude and phase angle responses of the megatransport due to locating the engines either inboard or outboard from the baseline configuration, the Cooper-Harper pilot ratings show no change. Test pilot A's comments on the pitch attitude response of all three engine location test points flown were "very good . . . remarkable response and stability." As can be seen from Figure 6.3, pilot A rated each test run Level 1 by assigning either a 3 or an average value of 3 1/2 on the Cooper-Harper pilot rating scale. Pilot B stated that the pitch attitude response was "just fine . . . rock solid . . . whatever you want it goes there and stays . . . I really don't see any difference [between the test points]." Pilot B assigned a Cooper-Harper value of either 2 or 3 (Level 1 ratings) for each of these test runs.

Again, comparing the baseline configuration test runs (Figures G1a, G13a, G18a, and G30a) with the test runs in which the engine location was moved laterally along the wing span (Figures G2a, G16a, G19a, and G20a), there is no significant difference between the longitudinal flight variables of these simulator test flights.

These results show that moving the engines inboard or outboard along the wing span will have a greater influence on the lateral-directional flying qualities of the aircraft than the longitudinal flying qualities. This is reflected not only in the Bode plots shown in Figures 6.1 and 6.3, but also the Cooper-Harper pilot ratings.

6.2.2. ENGINE LOCATION VARIED VERTICALLY

6.2.2.1. LATERAL-DIRECTIONAL CASE

Figures 6.4a and 6.4b show the experimental Bode magnitude and phase angle plots, respectively, of the lateral-directional transfer function, ($\phi/\delta T_{asym}$), generated for the following four configurations:

- baseline aircraft - engines at original configuration (inboard and outboard engines below megatransport center of gravity)
- inboard and outboard engines all moved vertically 5 feet downward (+z-direction) from original configuration (inboard and outboard engines below megatransport center of gravity)
- inboard and outboard engines all moved vertically upward (-z-direction) from original configuration into the wing (inboard engines below megatransport center of gravity and outboard engines above megatransport center of gravity)
- inboard and outboard engines all moved vertically upward (-z-direction) from original configuration to 2.5 feet above the wing (inboard and outboard engines above megatransport center of gravity).

Test pilots A and B flew all four test cases. Their Cooper-Harper pilot ratings are included in Figure 6.4. In addition, test pilot B flew three additional test cases at his request with the engines moved vertically from the baseline location. His comments on these additional test flights will be

included with the pilot's comments on the above four test cases. Figure 6.5 shows the engine positions of these four test configurations.

In contrast to the large variation in the roll and yaw inertias which occurred when the engines were moved laterally along the wing, there is relatively little change in the roll and yaw inertias when the engine location is varied vertically. From Table C1, the roll moment of inertia, I_{XX}, only increases from 57,995,453 sl-ft^2 for the test point with the engines located above the wing to 58,434,396 sl-ft^2 for the test point with the engines located below the wing. The yaw moment of inertia, I_{ZZ}, doesn't change at all with vertical engine location.

As can be seen in Figures 6.4a and 6.4b, there is essentially no difference in either the magnitude plot or the phase angle plot between the four vertical engine locations throughout the entire frequency range. All four Bode plots are identical. Since the primary method of producing roll in an aircraft which uses engine thrust for flight control is by producing sideslip, which then induces a change in the bank angle, it is not surprising that configurations with identical yawing moments of inertia produce identical frequency responses.

This is also reflected in the pilot's Cooper-Harper ratings. Test pilots A and B both rated all four conditions nearly the same. With the engines moved down, test pilot B stated that "the bank angle response seems to be exactly as before. Deadbeat . . . I mean, you couldn't ask for more." No improvement over the baseline condition was noted by either pilot.

As the engines were moved upward into the wing, pilot A commented that he "could not see a difference [from the baseline case]" and pilot B stated that the "bank control is fine. I see no change lateral-directionally." As the

engines were moved even further upward 2.5 feet above the wing, pilot A remarked that the lateral-directional characteristics were "unchanged." Test pilot B commented that the "bank response is identical - quick and well damped." Pilot A assigned Cooper-Harper pilot ratings of either 4 or 5 (Level 2 ratings) for these test runs while pilot B rated the test runs either a 3 (Level 1) or 4 (Level 2) on the Cooper-Harper scale.

The similar lateral-directional response between the vertical engine location test runs is also reflected in the comparison of the baseline configuration test runs (Figures G1b, G13b, G18b, and G30b) with the test runs in which the engine location was moved vertically upward or downward (Figures G3b, G14b, G15b, G21b, G27b, G31b, and G32b). There appears to be no significant difference between the lateral-directional flight variables of these simulator test flights.

6.2.2.2. LONGITUDINAL CASE [Refs. 35,39]

Figures 6.6a and 6.6b show the experimental Bode magnitude and phase angle plots, respectively, of the longitudinal transfer function, ($\gamma/\delta T_{sym}$), generated for the same four cases which were described in the lateral-directional case. Again, the Cooper-Harper pilot ratings of test pilots A and B are included in the figure.

The megatransport PCA system was able to function with the engines above the wing, up to a point, because of the downward component of thrust in the z-direction. The megatransport engines are installed on the wing at a cant angle of 2 degrees. This engine cant angle results in a downward component

of engine thrust which creates an upward, or lifting, force on the megatransport. This downward thrust in the z-direction is very small compared to the thrust along the x-axis. For an engine trimmed at 44,000 pounds thrust, the thrust along the x-axis is 43,973 pounds, while the thrust along the z-axis is only 1,536 pounds. Although the thrust in the downward direction is usually negligible for flight using conventional flight control surfaces, when the only moments being used for control are the moments due to engine thrust, normally neglected effects become significant. The megatransport can maintain positive pitching moment until the engines are moved to a point so far above the center of gravity that the pitching moment due to the downward thrust component is no longer able to dominate the negative pitching moment due to the thrust along the x-axis.

Although moving the engines vertically had little effect on the lateral-directional flying qualities of the airplane, Figure 6.6 shows a significant effect on the longitudinal flying qualities. Figure 6.6a shows the magnitude plot of the four configurations. The magnitude plot shows an increase of 2 dB, or 25%, in pitch control between the baseline configuration and the case with engines moved downward. Even more dramatic is the difference between the baseline configuration and the test runs having the engines located either in or above the wing. The magnitude plot shows a decrease of 3 dB, or 41%, in pitch control when the engines are moved upward. These trends become even more pronounced at the higher frequencies (frequencies above 0.3 rad/sec), where the different vertical engine location Bode plots tend to diverge from the baseline case even further. Clearly, moving the engines downward in the +z-direction results in greater pitch control power throughout the entire

frequency range, while moving the engines upward in the -z-direction results in a degradation of pitch control power.

The phase angle response is plotted in Figure 6.6b. There appears to be a 10 degree improvement in the phase response throughout the frequency range for the test run with the engines moved in the downward direction as compared to the baseline configuration. The difference in phase between the baseline configuration and the test runs with the engines moved upward is even more pronounced. The phase lag is increased from the baseline case by 25 degrees at low frequency and as much as 53 degrees at higher frequencies for the test run with the engines in the wing. For the test run with the engines above the wing, the phase lag increased from the baseline case by 30 degrees at low frequencies and as much as 90 degrees at higher frequencies.

Clearly, as the engines are moved further downward, the smaller the phase lag and the quicker the pitch response throughout the entire frequency range. Conversely, as the engines are moved further upward from the baseline condition, the phase lag increases resulting in poorer pitch response.

Pilot comments tend to corroborate this data. Test pilot A did not see a difference in pitch response until the engines were raised vertically to a position above the wings. At that point, pilot A stated that the pitch response was "slow", exhibited "moderate to light damping", and the "response [was] a little harder to anticipate."

As can be seen by comparing Figure G15a with Figures G1a and G13a, pilot A experienced more pitch oscillation with the engines moved vertically above the wings than was experienced in the two baseline configuration test runs. Test pilot A assigned an average Cooper-Harper pilot rating of 3 1/2

(Level 1) to the baseline configuration and a rating of 5 (Level 2) to the configuration with the engines above the wings.

Test pilot B commented that as the engines were raised the airplane was "stable but 'drifty' in pitch . . . I don't see any very quick response . . . [but] it's pretty stable." As the engines were raised further into the wing, pilot B said that he noticed "a bit of an overshoot on the commanded pitch . . . it's not as tight in pitch - it's wandered up a little bit, but still reasonable." Test pilot B stated that although the pitch response was degraded with the engines moved upward, the airplane "certainly responded" and there was "enough control to land the airplane."

As can be seen in Figures G27a, G31a, and G32a, the pitch response did become more oscillatory as the engines were moved vertically upward than for the baseline configuration (Figures G18a and G30a). Test pilot B assigned an average Cooper-Harper pilot rating of 2 1/2 (Level 1) to the baseline configuration, but assigned a rating of 5 (Level 2) to the two test flights with the engines raised.

Pilot B at this point was surprised that the PCA system enabled this configuration (engines located above the wings and above the megatransport center of gravity position) to respond similarly to the baseline configuration. Test pilot B requested an additional flight with the engines located above the wings to be flown with manual throttle manipulation of thrust and the PCA system turned off as a comparison case.

Pilot B commented that by using throttles to manipulate the engine thrust, the megatransport was "a lot tougher to fly manually . . . I'm getting in an airspeed PIO here trying to make it settle down . . . everything you do, you get the wrong thing in the short term. It really requires a lot of

anticipation . . . [performance] clearly degraded. You can really see it manually." Pilot B gave a Cooper-Harper pilot rating of 9 (Level 3) for this manual throttles test flight in which the engines were located above the wing.

The PCA system was again engaged and the engines were moved vertically even further above the wings until the pitch response eventually became unstable. Pilot B observed that "the system is going unstable . . . I think we're in big trouble . . . I think we've hit the limits [of vertical displacement of the engines in PCA mode]." Test pilot B rated this flight a 10 on the Cooper-Harper pilot rating scale. Pilot B's additional test flights demonstrated that although the pitch eventually destabilized, the PCA system is very robust in being able to handle large variations in engine location with only minor effects on the handling qualities.

Since moving the engines laterally along the wing also results in a vertical movement of the engine due to wing dihedral, a comparison was made between moving the engines vertically in Figure 6.6 with moving the engines laterally in Figure 6.3. It can be seen that the results are in agreement with each other.

The plots for the inboard engine location in Figure 6.3 and the downward engine location in Figure 6.6 show similar results - greater pitch control power and quicker pitch response than the baseline condition throughout the entire frequency range. Similarly, the plots for the outboard engine location in Figure 6.3 and the upward engine location in Figure 6.6 show similar results - less pitch control power and slower pitch response than the baseline condition throughout the entire frequency range.

Just looking at Figures 6.3 and 6.6, it might appear that moving the engines vertically or laterally affects the flying qualities of the megatransport

similarly. This may be true for longitudinal flying qualities, but comparing Figures 6.1 and 6.4 shows that while moving the engines vertically has little effect on the lateral-directional flying qualities, moving them along the wing span produces a pronounced lateral-directional effect.

Thus, it is observed that moving the engines vertically only, as by varying the length of the pylon, produces a change in the pitch response of the airplane while not affecting the lateral-directional flying qualities of the aircraft. It would appear that the further downward the engines are located, the better the pitch control power and longitudinal phase response of the aircraft without degrading the aircraft roll response.

However, the vertical location of the engines which are chosen to improve the PCA pitch performance must also take into account other factors such as:

- longer pylons will add additional weight and drag
- the engine nacelles must be high enough from the ground that the engine exhaust nozzle does not scrape the runway during takeoff rotation
- the engines must be high enough on the wing so that there is a 5 degree angle between the outside of the main landing gear and the most outboard engine nacelle to meet lateral ground clearance criterion
- large pitching moments due to thrust, while favorable for PCA performance, may generate unwanted pitching moments for conventional control surface flight when the throttles are advanced or retarded.

6.2.3. DISTANCE BETWEEN INBOARD AND OUTBOARD ENGINES VARIED

6.2.3.1. LATERAL-DIRECTIONAL CASE

The previous test cases described in Section 6.2.1 had the engines moved either all inboard or all outboard from the original configuration. In either case, the original spanwise displacement between the inboard and outboard engines was always preserved. The following test cases were designed to investigate what effect varying the relative distance between the inboard and outboard engines might have on the megatransport flying qualities.

Figures 6.7a and 6.7b show the experimental Bode magnitude and phase angle plots, respectively, of the lateral-directional transfer function, ($\phi/\delta T_{asym}$), generated for the following three configurations:

- baseline aircraft– engines unmoved from original configuration
- inboard engines moved 20 feet further inboard and outboard engines moved 20 feet further outboard along wing span from original configuration
- inboard engines moved 20 feet further outboard and outboard engines moved 20 feet further inboard along wing span from original configuration.

Test pilots A and B did not fly these particular test cases because of time constraints. Figure 6.8 shows the engine positions of these three test configurations.

As can be seen from comparing Figures 6.1 and 6.7, increasing the distance between the engines has the same effect as moving all the engines outboard. The magnitude plot in Figure 6.7a shows that increasing the distance between the inboard and outboard engines slightly increases the roll control power at low frequencies (less than 1 rad/sec). The magnitude falls off faster, however, resulting in a 0.8 dB or 10% decrease in roll control response at higher frequencies. This was the same result that was found by moving all the engines further outboard in Figure 6.1a, although the magnitude of the response is greater if both inboard and outboard engines are moved in the same direction.

Similarly, decreasing the distance between the inboard and outboard engines decreases the roll control power at low frequencies, but slightly improves the roll response at higher frequencies, just as was found by moving all the engines further inboard in Figure 6.1a.

Figure 6.7b shows that increasing the distance between the inboard and outboard engines results in a slightly larger phase lag than that of the baseline case. This was the same result as was found in Figure 6.1b as all engines were moved outboard. Decreasing the spanwise distance between the engines produces slightly less phase lag than that of the baseline case. Again, this is similar to the result shown in Figure 6.1b by moving all engines further inboard and, again, the magnitude of the response is greater if both inboard and outboard engines are moved in the same direction.

These results suggest that the outboard engine location plays the dominant role over the inboard engine in determining the lateral-directional response of the megatransport. Regardless of which way the inboard engines are moved - inboard or outboard - the lateral-directional response of the

airplane is determined by the spanwise location of the outboard engines. The outboard engines, having a larger y-axis moment-arm than the inboard engines, produce greater yaw and roll moments of inertia and, hence, dominate the lateral-directional response.

6.2.3.2. LONGITUDINAL CASE

Figures 6.9a and 6.9b show the experimental Bode magnitude and phase angle plots, respectively, of the longitudinal transfer function, ($\gamma/\delta T_{sym}$), generated for the same three cases which were described in the lateral-directional case. As was discussed previously, these test cases were designed to investigate what effect varying the relative distance between the inboard and outboard engines might have on the megatransport flying qualities. As can be seen from Figure 6.9, there is no difference in either the magnitude plot or the phase angle plot between the three configurations throughout the entire frequency range. All three longitudinal Bode plots are identical.

Figure 6.9 seems to suggest that moving the engines laterally doesn't affect the longitudinal flying qualities of the airplane, contradicting the results found in Figure 6.3. This apparent contradiction can be explained by realizing that as the inboard and outboard engines were all moved either in the inboard or outboard direction together as was seen in Figure 6.3, the total engine mass and center of gravity was relocated, changing the pitching moment-arm, inertia, and pitch response. However, in Figure 6.9 the inboard and outboard engines were moved the same distance in opposite directions, preserving the same total engine center of gravity location as that of the

baseline configuration and, hence, not affecting any change to the pitch inertia or pitch response.

6.2.4. ENGINE TIME CONSTANT VARIED [Refs. 11,20,36,42]

6.2.4.1. LATERAL-DIRECTIONAL AND LONGITUDINAL CASE

In addition to analyzing the effects of various engine locations on the flying qualities of the megatransport, the effect of varying the engine time constant was also evaluated. The megatransport dynamic engine model, including engine time lag and time constants, is described in detail in Appendix B.

Figures 6.10 and 6.11 show the experimental Bode magnitude and phase angle plots of the lateral-directional transfer function, ($\phi/\delta T_{asym}$), and the longitudinal transfer function, ($\gamma/\delta T_{sym}$), respectively, generated for the following four configurations:

- baseline aircraft - engine time constant equal to 1 second
- engine time constant equal to zero seconds (instantaneous response)
- engine time constant equal to 0.5 seconds
- engine time constant equal to 3 seconds.

Test pilots A and B flew the above test cases with the exception of the instantaneous engine response case. Their Cooper-Harper pilot ratings are included in the figures. Figures 6.10a and 6.10b show the experimental Bode magnitude and phase angle plots, respectively, of the lateral-directional

transfer function, ($\phi/\delta T_{asym}$), of the various engine time constant test runs. As can be seen in both the magnitude plot and phase angle plot, there is no difference in the lateral-directional response of the megatransport between any of the different engine time constant cases.

As can be seen by the identical Cooper-Harper pilot ratings assigned by test pilots A and B to the various engine time constant test flights, they could detect little difference. Test pilot B commented that he found that the "bank response is instantaneous" for the 0.5 second time constant run. Pilot B thought that the airplane responded "laterally - just fine" for the 3 second time constant case. He found it "very similar" to the baseline condition. Test pilot A thought that the 0.5 second time constant test run flew "similar to baseline", but stated that for the 3 second time constant case, "roll response seemed somewhat looser than baseline."

Comparisons of the nominal 1 second engine time constant test runs given in Figures G1b, G13b, G18b, and G30b with the 0.5 second and 3 second engine time constant test runs shown in Figures G6b, G7b, G24b, and G25b show that no significant differences exist between the lateral-directional flight variables of the various engine time constant test runs.

Figures 6.11a and 6.11b show the experimental Bode magnitude and phase angle plots, respectively, of the longitudinal transfer function, ($\gamma/\delta T_{sym}$), of the various engine time constant test runs. Neither Figure 6.11a nor Figure 6.11b show any appreciable difference between the various test runs from about 0.15 rad/sec to 1 rad/sec, the upper limit of the frequency response. However, at frequencies lower than 0.15 rad/sec, there appears to be slight differences between the various engine time constant test runs.

As might be anticipated, the pitch control power in Figure 6.11a is greatest for the instantaneous engine response and least for the 3 second engine response time. At low frequencies (frequencies less than 0.1 rad/sec), the instantaneous engine response shows a 0.7 dB or 8% increase in pitch control power from the baseline, or 1 second engine time constant, case. There is a more pronounced effect for the 3 second time constant test run, which shows a 2 dB or 25% decrease in pitch control power from the baseline case at low frequencies.

The phase angle plot of Figure 6.11b shows the greatest amount of phase lag for the 3 second constant case and the least amount of phase lag for the instantaneous engine response case. The phase angle for the instantaneous response test run leads that of the baseline case only by approximately 3 degrees at frequencies less than 0.09 rad/sec. The phase angle for the 3 second engine time constant case lags that of the baseline by about 7 degrees at frequencies less than 0.11 rad/sec.

These results are corroborated by the Cooper-Harper pilot ratings, both pilots rating the 3 second time constant run worse with a Level 2 Cooper-Harper rating than the 1 second engine time constant baseline case rated Level 1 by both pilots. Pilot A rated the pitch response of the 3 second constant run "somewhat looser than baseline." Pilot B responded that the "pitch is a little 'wandery' . . . The pitch response is just slower . . . degraded . . . a little looser, a little more correction's required a little more often."

As can be seen by comparing Figures G6a, G7a, G24a, and G25a with Figures G1a, G13a, G18a, and G30a, both pilots A and B experienced more pitch oscillation with the 3 second engine time constant than was experienced in the 0.5 second or 1 second engine time constant case.

Interestingly, the pilots rated the 0.5 second time constant equal to or worse than the baseline case. Pilot A rated it "similar to baseline", and pilot B stated that "the pitch is fine." Surprisingly, although the Bode plots showed differences between the different engine time constant runs, the differences were slight. The pilot ratings were at an acceptable Level 2 even with an engine time constant of 3 seconds.

It appears from these data that the engine response time may not have a significant effect on large transport flying qualities. However, if one considers the engine dynamics as described in Appendix B, it can be seen that the response time of the engine is dependent not only on the engine time constant, but also on the current level of thrust.

If the pilot is flying at a thrust level greater than 25 percent of the total thrust, the engine and PCA system responses are relatively fast, even with a time constant as large as 3 seconds. If, however, the engine thrust is below 25 percent total thrust, the engines take much longer to respond to pilot commands. The author flew the megatransport simulator in the PCA mode with the thrust below the 25 percent level and found the flying qualities very unsatisfactory.

This thrust limitation is not expected to be a problem, however, since the power for level flight in the approach/landing phase for most turbine powered airplanes is typically 25 to 35 percent of thrust. This is the flight phase which requires the fastest aircraft reaction time, not only for lining up on the runway, but also in the event of a forced go-around or in avoiding aircraft traffic.

One instance in which the engine thrust level may be a concern is in the case of an engine failure. For example, if an engine should fail on the left side

of the megatransport, the megatransport PCA system is programmed so that the one remaining engine on the left side produces exactly enough thrust to balance that produced by the two engines on the right side of the aircraft.

This is not a problem unless each of the two engines on the right side are running at more than 50 percent thrust. This would require the one engine on the left side to produce more than 100 percent thrust. In this case, a procedure must be used or PCA software developed to throttle down the two right engines so that a balance between the two sides can be achieved and the aircraft can be retrimmed, accordingly.

It should also be noted that the value of excess thrust decreases very rapidly with increasing airspeed. When excess thrust is zero, thrust control power is zero. If the flight control system should fail at a high speed flight condition, the airspeed will need to be reduced so the aircraft will have enough thrust for flight control.

6.2.5. OUTBOARD ENGINE INOPERATIVE

Due to the coding of the simulator, frequency sweeps could not be performed on the megatransport with one engine inoperative. Therefore, Bode plots of the aircraft response during this test run could not be generated. However, pilot ratings can still provide valuable information about the flying qualities of the megatransport for this test case.

One of the important questions addressed in this study is whether flight path control satisfying Level 1 or Level 2 handling quality requirements is still possible with one engine inoperative (OEI) using the PCA system. Test

pilots A and B flew the megatransport using the PCA system with the left outboard engine failed. An outboard engine was selected for failure because the results obtained and previously discussed in this study indicate that the outboard engine is the critical engine in determining the response of the megatransport.

Pilot A commented that there was "much poorer pitch response and stability. I think it could be satisfactory with a little practice." Pilot A gave the OEI test flight a Cooper-Harper rating of 3 for the lateral-directional response and 6 for the longitudinal response with an overall Level 2 Cooper-Harper rating. At pilot A's request, a repeat was made of this test run. Pilot A again commented that the aircraft exhibited a "slow pitch response" and a "slightly slow roll response." Pilot A gave the second OEI test flight a Cooper-Harper rating of 5 for the lateral-directional response and 6 for the longitudinal response, both Level 2 ratings. As can be seen in Figures G5a and G9a, the pitch response for the OEI test flights is noticeably more oscillatory than for the baseline configuration (with all engines operating) shown in Figures G1a and G13a. Figures G5b and G9b show that a slight oscillation also exists in the roll response for the OEI case as compared with the baseline test runs shown in Figures G1b and G13b.

Test pilot B commented that "it's having a lot more trouble with the pitch now . . . it's drifting up and down from the commanded . . . a definite degradation in pitch attitude response - slower, looser . . . there's a lot more worry about keeping the nose where you want it. Lateral-directionally - maybe a little looser than before . . . [the performance is] still adequate, if you work at it." Pilot B gave the OEI test flight a Cooper-Harper rating of 4 for the lateral-directional response and 5 for the longitudinal response with an overall

Cooper-Harper rating of Level 2. Figures G23a and G23b show noticeable pitch and roll oscillations for pilot B's OEI test run as compared with the baseline configuration (with all engines operating) shown in Figures G18a, G18b, G30a and G30b. These oscillations may account for the looseness noticed by test pilot B in the aircraft response.

It should be noted that even with one of the critical outboard engines inoperative, both test pilots rated the flying qualities of the megatransport within Level 2 limits.

6.2.6. ADDITIONAL TEST CASES

In addition to the data already presented in Sections 6.2.1 through 6.2.5, test pilots A and B also flew several additional test points in the megatransport simulator. Additional test points were flown for the following five cases:

- baseline configuration with full (50 degrees) flaps (test run numbers A5 and B5)
- baseline configuration in intermediate turbulence (test run numbers A9 and B9)
- baseline configuration with a crosswind (test run number A18)
- baseline configuration with manual throttles-only flight control - Sioux City DC-10 scenario (test run numbers A11, A12, B10, and B14)
- baseline configuration with all control surfaces operational - conventional approach and landing (test run numbers A13 and B13).

Although frequency sweeps were not performed on the five cases listed above, the pilot's comments on these additional test cases, as well as plots of selected longitudinal and lateral-directional flight variables, can be found in Appendix G.

Time limitations prevented an in-depth investigation into the effects of flaps, turbulence, and crosswinds on the flying qualities of the megatransport/PCA system. However, preliminary results indicate that:

- the use of flaps, while not affecting the flying qualities of the megatransport, does enable the pilot to land at a reduced airspeed, making a safe, controllable landing even more likely
- turbulence and crosswinds do have an adverse effect on the flying qualities of the megatransport/PCA system.

The test points flown with manual throttles-only flight control and those flown with the conventional flight control surfaces operational were run primarily as control cases to enable the pilots to have a comparison between flying the megatransport using manual throttle control, conventional flight controls, and the PCA system.

6.2.7. CROSSOVER FREQUENCY AND PHASE ANGLE ANALYSIS [Ref. 49]

Crossover frequencies and phase lag are important criteria by which to judge the relative performance of a system. The system crossover frequency is that frequency where the Bode magnitude plot crosses the zero dB axis. It is the frequency at which the system output equals the input and is the limit at

which the system can perform before attenuation occurs. The higher the crossover frequency, the larger the useful frequency range of the system.

Phase lag is a measure of the time required for the system to respond to a commanded input. Aircraft lag and pilot rating are related by the fact that pilots, while not expecting an instantaneous aircraft response to a command input, find a long time interval for the aircraft to respond undesirable. If a long enough time interval elapses between pilot input and aircraft response, the pilot is actually forced to anticipate the reaction of, or lead, the aircraft. The larger the phase lag, the more difficult it becomes for the pilot to fly the aircraft.

The crossover frequencies of each of the lateral-directional and longitudinal Bode magnitude plots and the phase relationship between the various test configurations of the lateral-directional and longitudinal Bode phase angle plots are listed in Tables 6.1 and 6.2. Included with this frequency and phase information for each of the Bode plots are the Cooper-Harper pilot ratings for the corresponding megatransport simulator test flights.

As can be seen from Tables 6.1 and 6.2, when the engine location was varied laterally, both pilots rated all three test cases that were flown the same level, both longitudinally and lateral-directionally, in spite of the large variations in crossover frequencies and phase angle. There does not appear to be a specific crossover frequency or phase lag at which the flying qualities are perceived as either improved or degraded.

Interestingly, for certain cases in which there was no change in either the crossover frequency or the phase angle (the lateral-directional case when the engine location was varied vertically and both the lateral-directional and

longitudinal case when the engine time constant was varied), the pilots gave the test points different ratings.

In the case of the vertical engine location, the lateral-directional pilot ratings may have been influenced by the longitudinal flying qualities. For the lateral-directional and longitudinal test runs in which the engine time constant was varied, there were differences in the low frequency response which may have affected the pilot ratings.

It is apparent that factors other than crossover frequency and phase lag, such as low or high frequency response, affect the perceived flying qualities of the aircraft. However, even different frequency response does not always elicit different pilot rating levels as can be seen in the lateral engine location test runs, where all the test runs were rated the same level.

Even the pilots themselves were not always in agreement with each other on whether a particular configuration was an improvement over the baseline configuration or not. In some instances a change in the engine location was perceived as improving the baseline flying qualities by one pilot, while the same change was considered to degrade the baseline flying qualities by the other pilot.

From looking at Tables 6.1 and 6.2, there does not appear to be a trend between the pilot ratings and the crossover frequencies or phase lag of either the lateral-directional transfer function, ($\phi/\delta T_{asym}$), Bode plot or the longitudinal transfer function, ($\gamma/\delta T_{sym}$), Bode plot.

6.3. ROOT LOCUS PLOT ANALYSIS [Refs. 18]

As was discussed in Section 6.2.7, for both the lateral-directional and longitudinal test points which were run with different engine time constants, there were no differences in the crossover frequencies or phase angle at the baseline break frequency between any of the cases.

Additionally, it was found in Section 6.2.4.1 that there were no differences at all in the lateral-directional response of the megatransport between any of the different engine time constant cases. Regarding the longitudinal response of the megatransport to the various engine time constant test runs, there were no appreciable differences between the test runs except at frequencies lower than 0.15 rad/sec, where slight differences in both the magnitude and phase plots exist.

Yet in spite of the fact that the Bode diagrams seem to indicate very little difference in the frequency response of the megatransport between the various engine time constant test runs, the pilots did perceive slight differences in the flying qualities. As was suggested in Section 6.2.7, this appears to indicate that factors other than frequency response are important in determining Cooper-Harper pilot ratings.

The engine time constant, along with the initial level of thrust, determine the time required for the engine to produce the commanded level of thrust as can be seen in Figures B3 and B4. The megatransport engine with the nominal one second engine time constant can produce 100 percent of thrust from an initial minimum idle thrust setting in 10 seconds. This same engine with a 3 second engine time constant requires 30 seconds to achieve

the same level of thrust, while the engine with a 0.5 second engine time constant can reach the desired thrust in only 5 seconds.

Along with observing the frequency response of the megatransport to the various engine time constant cases, the time response of the megatransport to the various engine time constant cases should be analyzed, as well. The frequency response of the megatransport has been analyzed using Bode plots - the time response of the megatransport can be inferred using root locus plots.

The same longitudinal transfer function equation which was used to generate the calculated longitudinal Bode plots, Equation 5.5, is now used to generate a series of root locus plots, shown in Figures 6.12 through 6.14. Each figure shows a root locus plot of the megatransport/engine longitudinal transfer function, ($\gamma/\delta T_{sym}$), the only difference being the value of the engine time constant. Figures 6.12, 6.13, and 6.14 show plots of the root locus for the engine time constant of 1, 3, and 0.5 seconds, respectively. In each figure, a gain of 0.04 is represented on the root locus by a small diamond.

As can be see in Figure 6.12, for the one second engine time constant case, the phugoid becomes unstable when the gain equals 0.04. Figure 6.13 shows that for the slower 3 second engine time constant case, the phugoid is actually unstable at a gain equal to 0.04, the point of instability being reached when the gain is equal to 0.015. For the faster 0.5 second engine time constant case as seen in Figure 6.14, the phugoid is still stable at a gain of 0.04, remaining stable until a gain of 0.085 is reached. These longitudinal root locus plots show that faster engine response improves phugoid stability, thus improving thrust-controlled aircraft performance.

Similarly, the same lateral-directional transfer function equation which was used to generate the calculated lateral-directional Bode plots, Equation 5.3, is now used to generate a series of root locus plots, shown in Figures 6.15 through 6.18. Figure 6.15 shows the root locus plot of the megatransport/engine lateral-directional transfer function, ($\phi/\delta T_{asym}$), with an engine time constant of one second. The same root locus plot can be seen in Figure 6.16 except that the scales have been changed to give a magnified view of the origin - the furthest zero is not shown on this scale. Figures 6.17 and 6.18 show plots of the root locus for an engine time constant of 3 and 0.5 seconds, respectively. Again, these figures are plotted to give a magnified view of the origin. In each figure, a gain of 0.0017 is represented on the root locus by a small diamond.

As can be see in Figure 6.16, for the one second engine time constant case, the dutch roll becomes unstable when the gain equals 0.0017. Figure 6.17 shows that for the slower 3 second engine time constant case, the dutch roll is actually unstable at a gain equal to 0.0017, the point of instability being reached when the gain is equal to 0.001. For the faster 0.5 second engine time constant case as seen in Figure 6.18, the dutch roll is still stable at a gain of 0.0017, remaining stable until a gain of 0.0027 is reached.

Interestingly, the root locus plots show that the spiral mode and engine lag poles combine to form an oscillatory pair for the one second and three second engine time constant cases, while the roll mode and engine lag poles combine to form an oscillatory pair for the 0.5 second engine time constant case. It is interesting to note that a smaller engine time constant, while resulting in a faster engine response, may also alter the basic dynamic response of the aircraft/engine combination.

6.4. THRUST-CONTROLLED MEGATRANSPORT FLYING QUALITY ANALYSIS

[Refs. 41,55,56,57,58,59,60,61,62,63]

Most large transport aircraft have certain well-defined lateral-directional modes (dutch roll, spiral, and roll modes) and longitudinal modes (short-period and phugoid modes). The USAF Military Specification - Flying Qualities of Piloted Airplanes (MIL-Specs) document has established criteria which defines the various levels of flying qualities, many of which are based on the values of the frequency, damping ratio, or time constants of these various modes.

The longitudinal and lateral-directional modes of the megatransport in the Category C approach and landing flight phase were covered in detail in Sections 3.9.2 and 3.9.3, respectively. According to the MIL-Specs, the megatransport phugoid damping ratio, as well as the short-period frequency and damping ratio, all satisfy Level 1 longitudinal requirements (there is no phugoid frequency requirement). The megatransport spiral time constant, roll time constant, dutch roll frequency and damping ratio, and roll performance all satisfy Level 1 lateral-directional requirements.

One of the principal objectives of this study was to determine whether Level 1 flying qualities could be obtained using engine thrust to control the flight path of the megatransport in the event that the primary flight control system was inoperable. The longitudinal and lateral-directional modes which have been discussed so far are dependent only on the dynamics of the megatransport as determined by the mass, geometry, velocity, inertias, and stability derivatives of a particular configuration and flight condition. These

modes are independent of whether the aircraft is controlled by conventional control surfaces or engine thrust, so the megatransport will satisfy Level 1 requirements in these areas regardless of the control method.

There are, however, two important flying quality criteria which deal not with frequency or damping ratio requirements, but with time - the time required for the aircraft to achieve a 30 degree bank angle and the time for the aircraft to respond to a control input. It is likely that the time for the megatransport to bank or to respond to a control input will depend on whether the input is a control surface command or an engine thrust command.

The time for the megatransport to achieve a 30 degree bank angle using conventional lateral-directional control surfaces was found in Chapter 3 to be 2.4 seconds, falling within the Level 1 flying qualities requirements. These data were obtained by making measurements from actual megatransport simulator strip chart recordings. Similarly, it was found that the time for the megatransport to achieve a 30 degree bank angle using asymmetric engine thrust for lateral-directional control was found to be 3.0 seconds, falling outside Level 1 but within Level 2 flying qualities requirements.

The megatransport strip chart recordings were again utilized to measure the time interval between an asymmetric thrust input and the resultant bank angle response while using engine thrust for lateral-directional control. The time interval before the megatransport responded to the thrust input was 0.4 seconds, falling below the Level 3 flying qualities requirement.

For MIL-Spec criteria which specified time requirements, the megatransport did not achieve Level 1 flying qualities when using thrust to control the flight path of the aircraft. If the time response of the

megatransport engines could be improved, it is possible that the flying quality levels of the megatransport would improve, as well.

The engine time constant, which is a measure of the time it takes the engine to produce the commanded thrust, is primarily a function of the spool up time from the current thrust level to the commanded thrust level. The spool up time depends on many variables such as gas temperature, pressure levels, engine materials, radial and axial clearances, variable stator vane position, rotor balance, aerodynamic matching of components, inlet flow conditions, and age of the engine, but the most important factors in determining the engine spool up time are the rotor moment of inertia and the torque required for acceleration or deceleration of the rotor.

The change in angular velocity of the rotor is dependent on the rotor blade incidence angle, a larger angle producing greater lift on the blades and, therefore, increasing the angular velocity of the rotor. One method which could be used to increase the rotor angular velocity, and hence decrease the spool up time, is to have variable incidence blades and/or variable inlet vanes in the engine. Another option is to have engines with thrust vectoring capabilities.

Thrust vectoring engines require a variable geometry nozzle or a flap or paddle nozzle to direct the engine thrust in the desired direction. These types of engines, while not currently available for commercial transports, are being developed for military aircraft and studied for possible commercial development by both General Electric and Pratt & Whitney. Besides the improved engine response time which thrust vectoring would provide, thrust vectoring could also be used to produce moments which could be used in

trimming the aircraft, a function particularly useful in the absence of operational flight controls.

While it may be possible to improve the engine response time with the aid of vectored thrust, the time for the aircraft to respond to the engine thrust is a function of the aircraft weight and inertias. Because transport aircraft have increased in size and complexity over the last several years, there is an increased awareness in the aviation community that existing flying quality requirements may be outdated.

Although research is currently being done at NASA Langley Research Center in an effort to study the situation, no clearly defined requirements or criteria have been established for very large transports thus far. Perhaps the requirements for large transport aircraft will have to be changed before the thrust controlled megatransport is able to satisfy all flying quality requirements within Level 1 specifications.

6.5. SUMMARY [Ref. 41]

Many different analysis methods were used to evaluate the flying qualities of the megatransport, including:

- Bode and root locus plot analysis to evaluate the frequency and damping ratio response of the megatransport
- analysis of actual simulator strip chart recordings to evaluate the time history response of the megatransport
- analysis of Cooper-Harper pilot ratings by two NASA test pilots.

Analysis of these data showed that engine location did not appear to be a critical parameter in the performance of the megatransport/PCA system. Most of the pilot ratings and comments indicate that the pilots really couldn't perceive much difference in the flying qualities of the megatransport between various spanwise and vertical engine locations even though there were large variations in the crossover frequencies and phase lags of the various test points. There does not appear to be a specific crossover frequency or phase lag at which the flying qualities are perceived as either improved or degraded.

Interestingly, for certain cases in which there was no change in either the crossover frequency or the phase angle, the pilots gave the test points different ratings. It is apparent that factors other than crossover frequency and phase lag, such as the response time, affected the perceived flying qualities of the aircraft.

The frequency response of the megatransport did not seem as important to the pilots as the time response. Indeed, in looking at the MIL-Spec flying qualities requirements for large transport aircraft, the megatransport/PCA system actually satisfied the Level 1 flying quality requirements based upon the frequencies, damping ratios, and time constants of the longitudinal and lateral-directional modes. The megatransport/PCA system fell short of satisfying Level 1 requirements, however, in two areas:

- the time required for the aircraft to achieve a 30 degree bank angle (Level 2 requirements were satisfied)
- the time for the aircraft to respond to a control input (Level 3 requirements were not met).

Except for the time requirement for the megatransport/PCA system to respond to a control input, all megatransport/PCA flying qualities satisfied at

least Level 2, and in many cases, Level 1 MIL-Spec requirements. In addition, the two NASA test pilots consistently rated the megatransport/PCA system either Level 1 (test pilot B) or Level 2 (test pilot A) on the Cooper-Harper pilot rating scale.

Table 6.1 Lateral-Directional Crossover Frequency And Phase Angle Analysis

Test Condition[1]	Corresponding Test Run Numbers Pilot A/Pilot B	Cooper-Harper Pilot Rating Pilot A/Pilot B	Flying Qualities Level Pilot A/Pilot B	Crossover Frequency (rad/sec)	Phase Angle At Baseline Configuration Break Frequency	Phase Relation To Baseline Configuration Break Frequency
Baseline Configuration	A1,A14/B1,B15	4,4/3,4	2/1	0.93	-180°	same
Engines Moved 20 Feet Outboard	A2,A17/B2	5,4/3	2/1	1.00	-193°	13° lag
Engines Moved 40 Feet Outboard	-	-/-	-/-	1.00	-215°	35° lag
Engines Moved 20 Feet Inboard	A3/B3	5/3	2/1	0.81	-163°	17° lead
Outer Engine Moved 20 Feet Outboard; Inner Engine Moved 20 Feet Inboard	-	-/-	-/-	0.93	-185°	5° lag
Outer Engine Moved 20 Feet Inboard; Inner Engine Moved 20 Feet Outboard	-	-/-	-/-	0.93	-172°	8° lead
Engines Moved 5 Feet Vertically Downward	A4/B4	5/3	2/1	0.93	-180°	same
Engines Moved Vertically Upward Into Wing[2]	A15/B16	4/4	2/2	0.93	-180°	same
Engines Moved Vertically Upward 2.5 Feet Above Wing[3]	A16/B17	4/4	2/2	0.93	-180°	same
Full (50 Degrees) Flaps	A5/B5	5/3	2/1	0.92	-187°	7° lag
Gear Down	-	-/-	-/-	0.93	-180°	same

Table 6.1 Lateral-Directional Crossover Frequency And Phase Angle Analysis (cont.)

Test Condition[1]	Corresponding Test Run Numbers Pilot A/Pilot B	Cooper-Harper Pilot Rating Pilot A/Pilot B	Flying Qualities Level Pilot A/Pilot B	Crossover Frequency (rad/sec)	Phase Angle At Baseline Configuration Break Frequency	Phase Relation To Baseline Configuration Break Frequency
Engine Time Constant of Zero Seconds (Instantaneous Response)	-	-/-	-/-	0.93	-180°	same
Engine Time Constant of 0.5 Seconds	A8/B8	4/4	2/2	0.93	-180°	same
Engine Time Constant of 3.0 Seconds	A7/B7	4/4	2/2	0.93	-180°	same

1 All listed test conditions are deviations from the baseline airplane configuration.

2 Inboard engines were below megatransport C.G. and outboard engines were above megatransport C.G.

3 Inboard and outboard engines were above megatransport C.G.

Table 6.2 Longitudinal Crossover Frequency And Phase Angle Analysis

Test Condition[1]	Corresponding Test Run Numbers Pilot A/Pilot B	Cooper-Harper Pilot Rating Pilot A/Pilot B	Flying Qualities Level Pilot A/Pilot B	Crossover Frequency (rad/sec)	Phase Angle At Baseline Configuration Break Frequency	Phase Relation To Baseline Configuration Break Frequency
Baseline Configuration	A1,A14/B1,B15	4,3/2,3	1/1	0.23	-124°	same
Engines Moved 20 Feet Outboard	A2,A17/B2	3,3/2	1/1	0.22	-128°	4° lag
Engines Moved 40 Feet Outboard	-	-/-	-/-	0.21	-136°	12° lag
Engines Moved 20 Feet Inboard	A3/B3	3/2	1/1	0.24	-121°	3° lead
Outer Engine Moved 20 Feet Outboard; Inner Engine Moved 20 Feet Inboard	-	-/-	-/-	0.23	-124°	same
Outer Engine Moved 20 Feet Inboard; Inner Engine Moved 20 Feet Outboard	-	-/-	-/-	0.23	-124°	same
Engines Moved 5 Feet Vertically Downward	A4/B4	5/2	2/1	0.28	-113°	11° lead
Engines Moved Vertically Upward Into Wing[2]	A15/B16	3/5	1/2	0.18	-171°	47° lag
Engines Moved Vertically Upward 2.5 Feet Above Wing[3]	A16/B17	5/5	2/2	0.18	-190°	66° lag
Full (50 Degrees) Flaps	A5/B5	3/2	1/1	0.30	-123°	1° lead
Gear Down	-	-/-	-/-	0.23	-125°	1° lag

Table 6.2 Longitudinal Crossover Frequency And Phase Angle Analysis (cont.)

Test Condition[1]	Corresponding Test Run Numbers Pilot A/Pilot B	Cooper-Harper Pilot Rating Pilot A/Pilot B	Flying Qualities Level Pilot A/Pilot B	Crossover Frequency (rad/sec)	Phase Angle At Baseline Configuration Break Frequency	Phase Relation To Baseline Configuration Break Frequency
Engine Time Constant of Zero Seconds (Instantaneous Response)	-	-/-	-/-	0.23	-124°	same
Engine Time Constant of 0.5 Seconds	A8/B8	4/4	2/2	0.24	-124°	same
Engine Time Constant of 3.0 Seconds	A7/B7	5/5	2/2	0.24	-124°	same

1 All listed test conditions are deviations from the baseline airplane configuration.

2 Inboard engines were below megatransport C.G. and outboard engines were above megatransport C.G.

3 Inboard and outboard engines were above megatransport C.G.

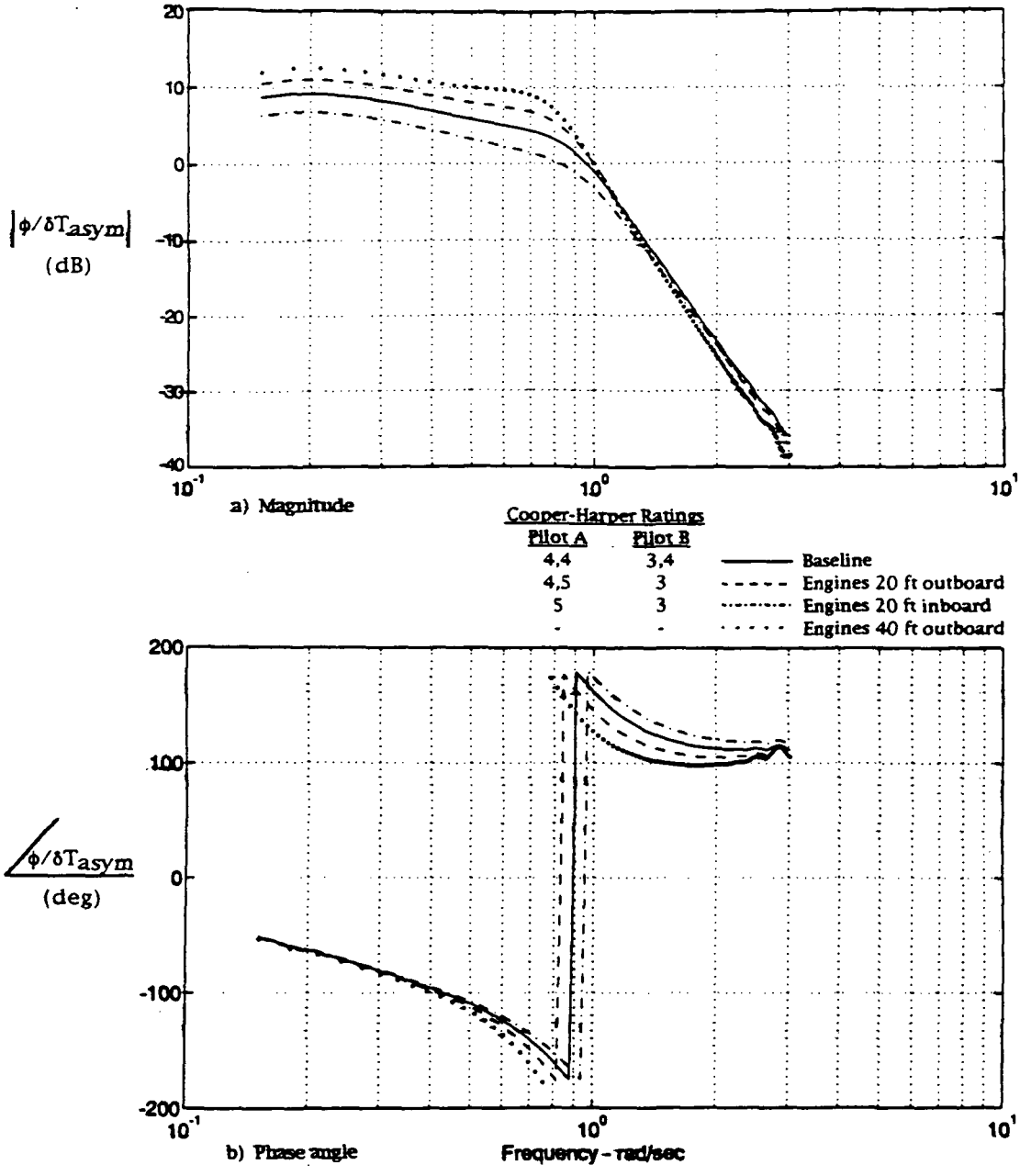

Figure 6.1 Megatransport Lateral-Directional Bank Angle - Asymmetric Thrust Frequency Response: Engine Location Varied Laterally

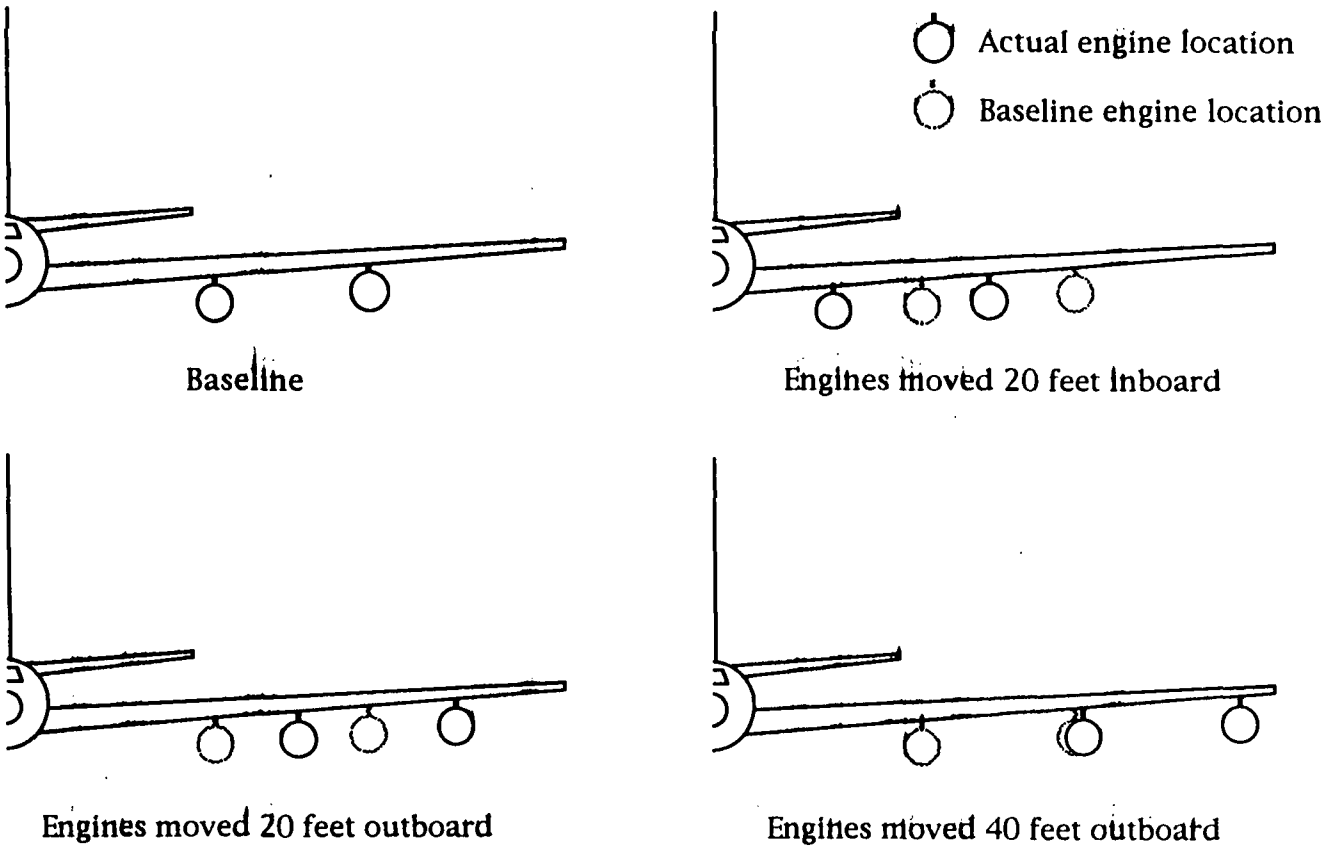

Figure 6.2 Megatransport Engines Moved Laterally Along Wing Span

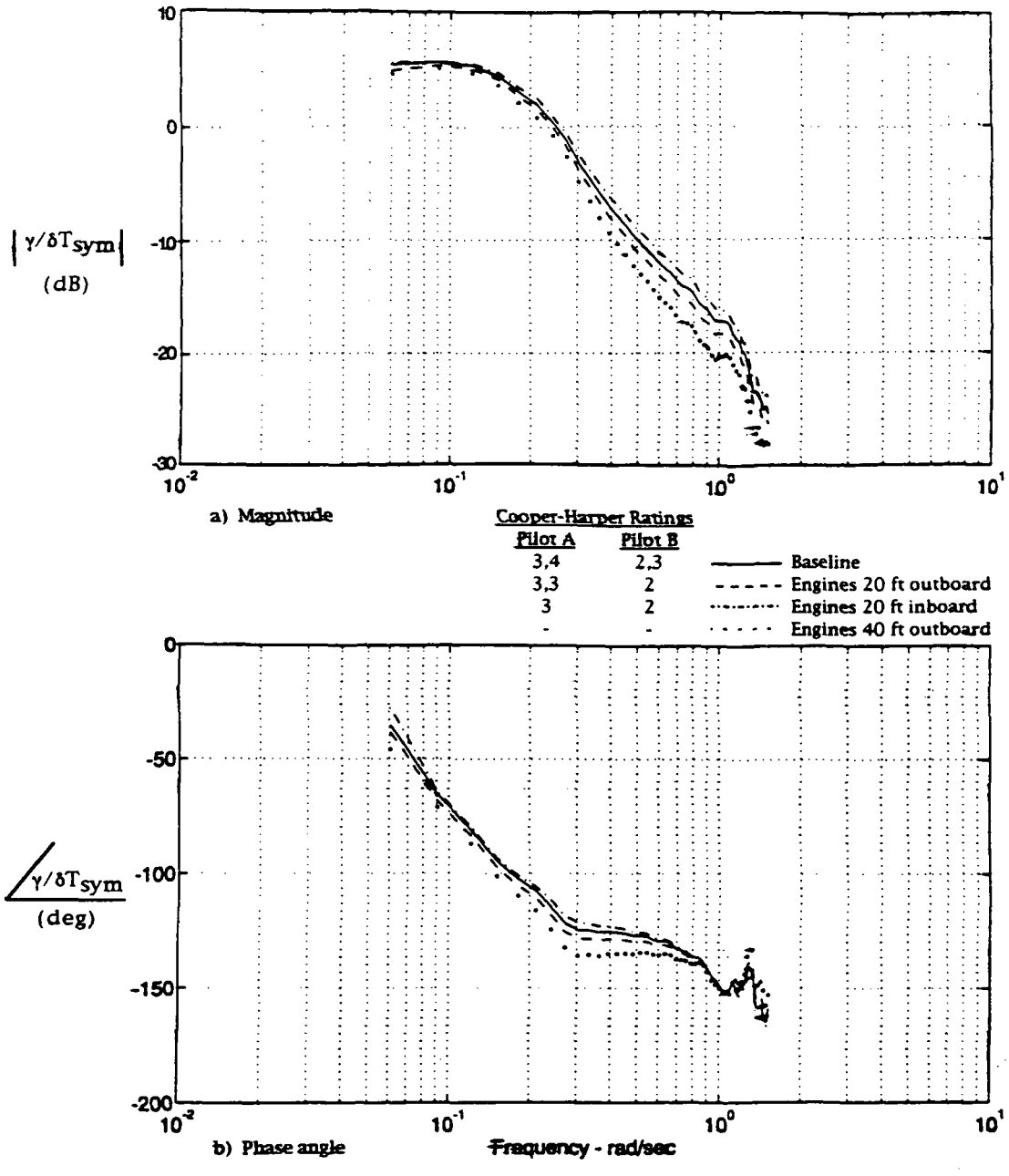

Figure 6.3 Megatransport Longitudinal Flight Path Angle - Symmetric Thrust Frequency Response: Engine Location Varied Laterally

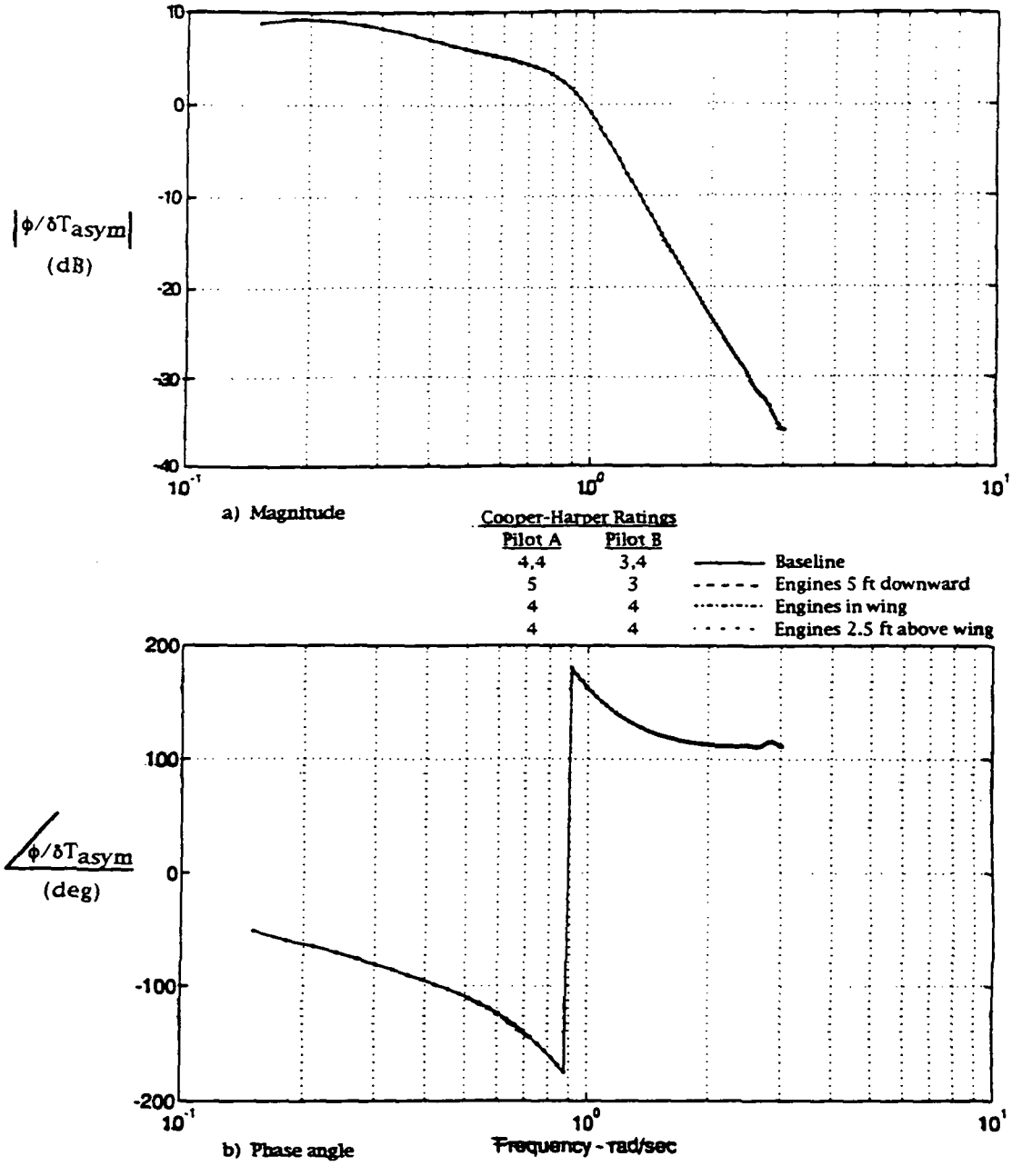

Figure 6.4 Megatransport Lateral-Directional Bank Angle - Asymmetric Thrust Frequency Response: Engine Location Varied Vertically

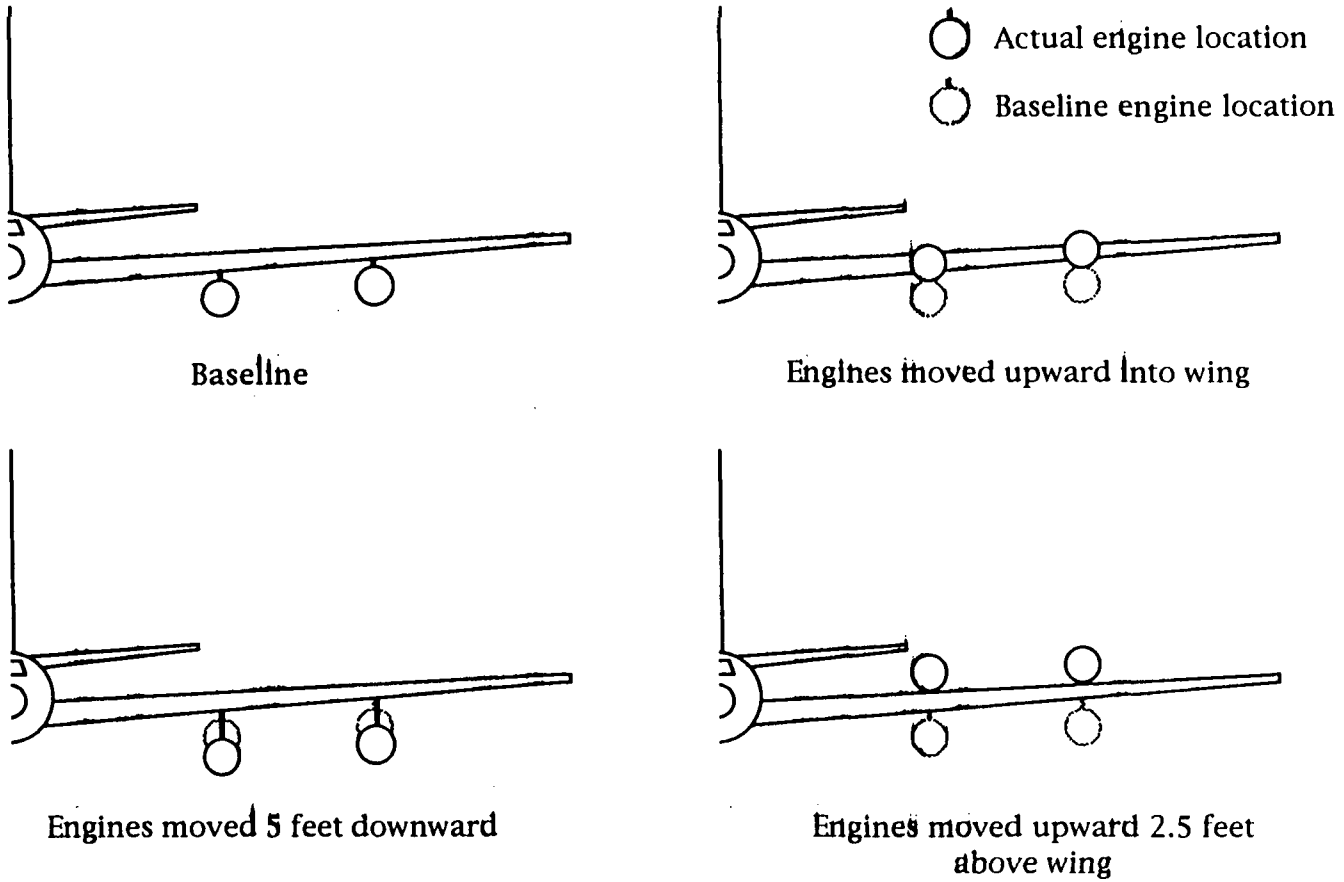

Figure 6.5 Megatransport Engines Moved Vertically

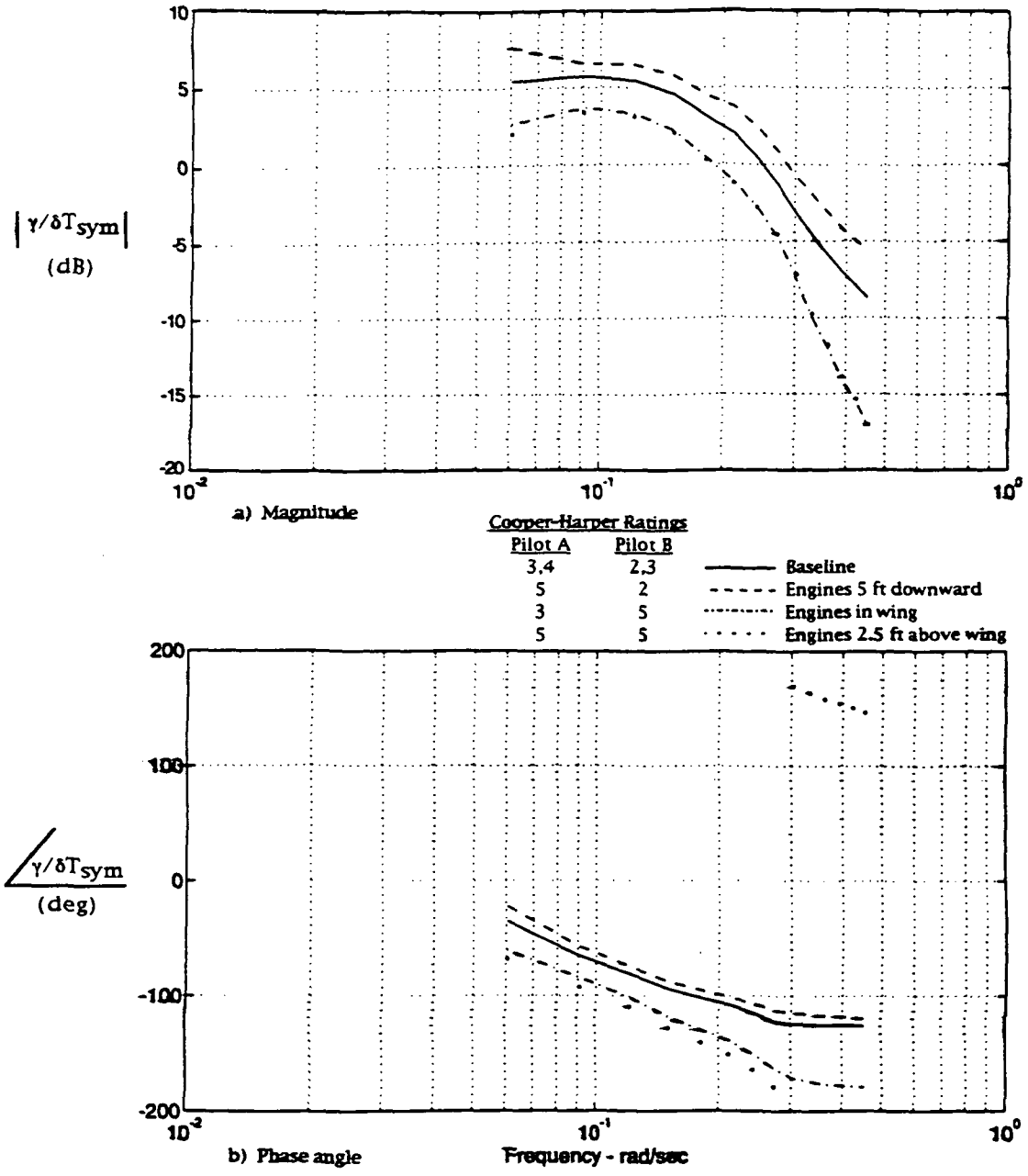

Figure 6.6 Megatransport Longitudinal Flight Path Angle - Symmetric Thrust Frequency Response: Engine Location Varied Vertically

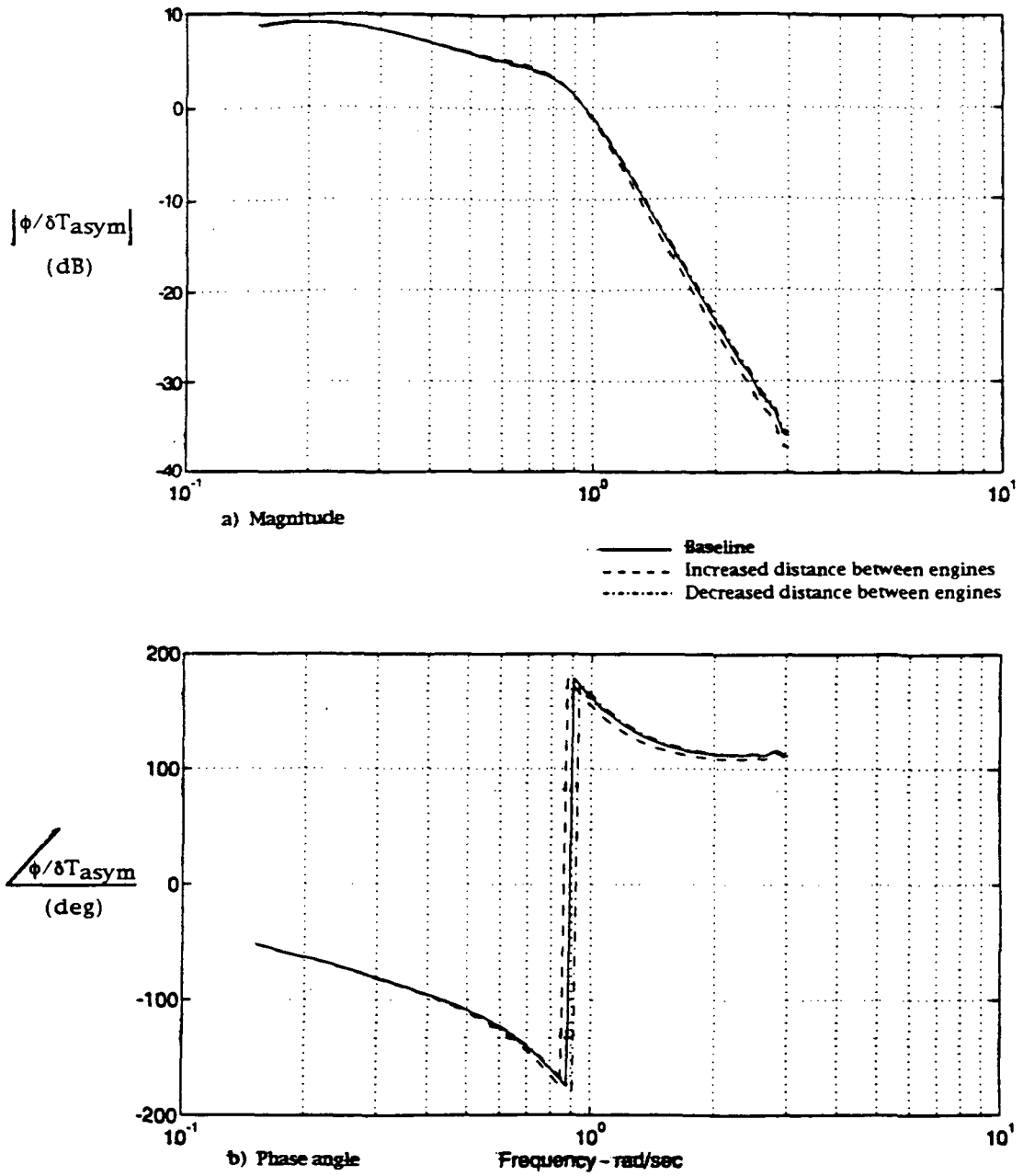

Figure 6.7 Megatransport Lateral-Directional Bank Angle - Asymmetric Thrust Frequency Response: Distance Between Inboard and Outboard Engines Varied

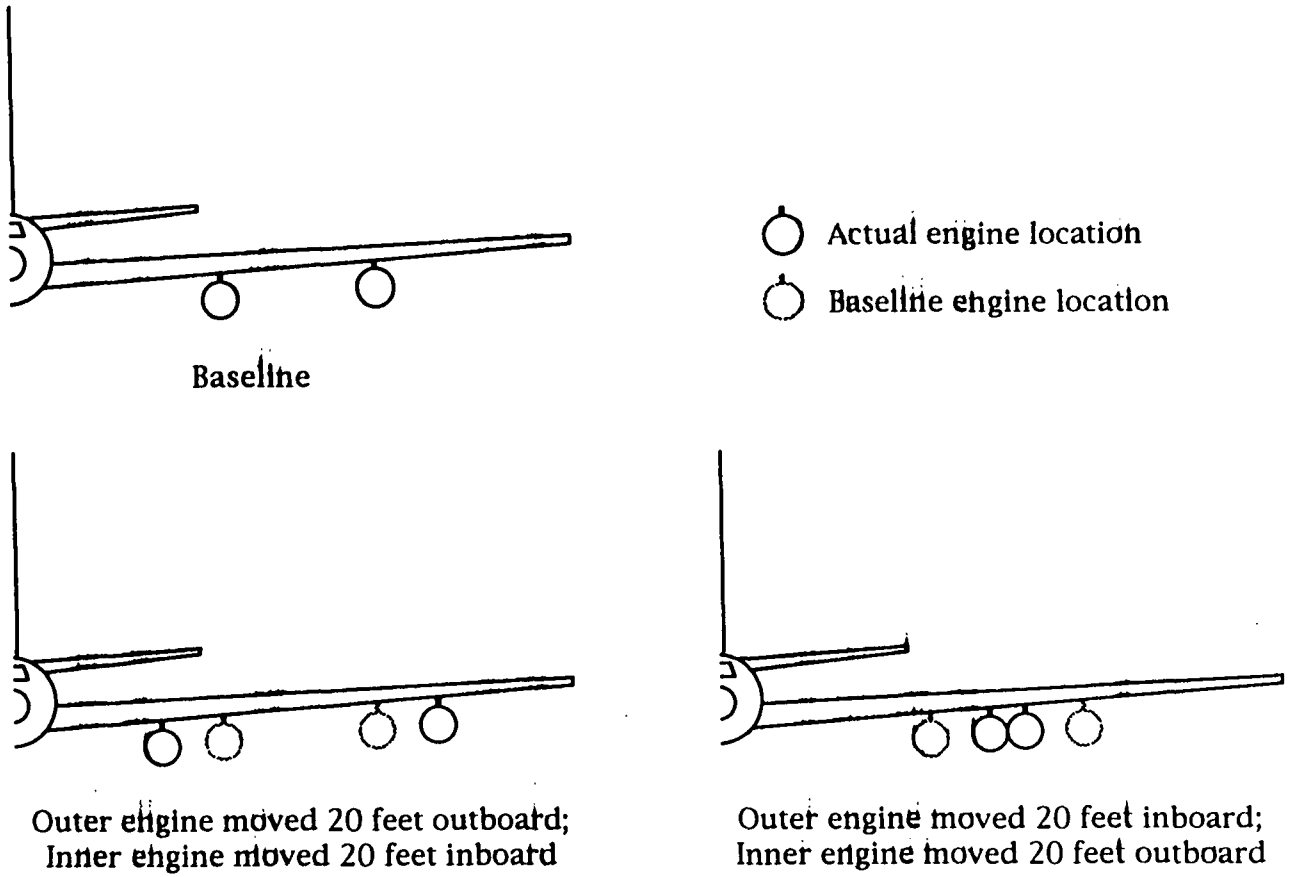

Figure 6.8 Distance Varied Between the Inboard and Outboard Engines of the Megatransport

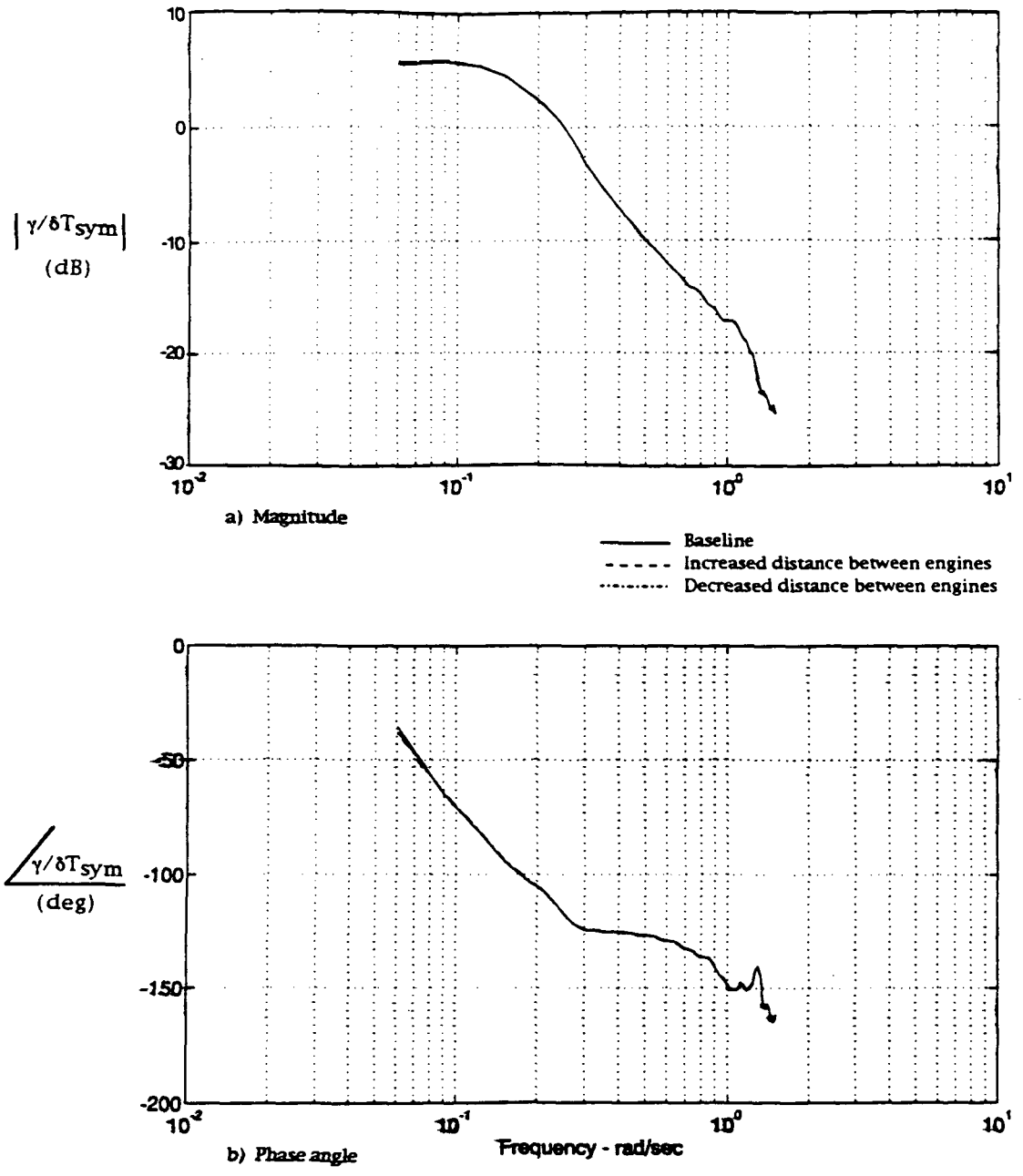

Figure 6.9 Megatransport Longitudinal Flight Path Angle - Symmetric Thrust Frequency Response: Distance Between Inboard and Outboard Engines Varied

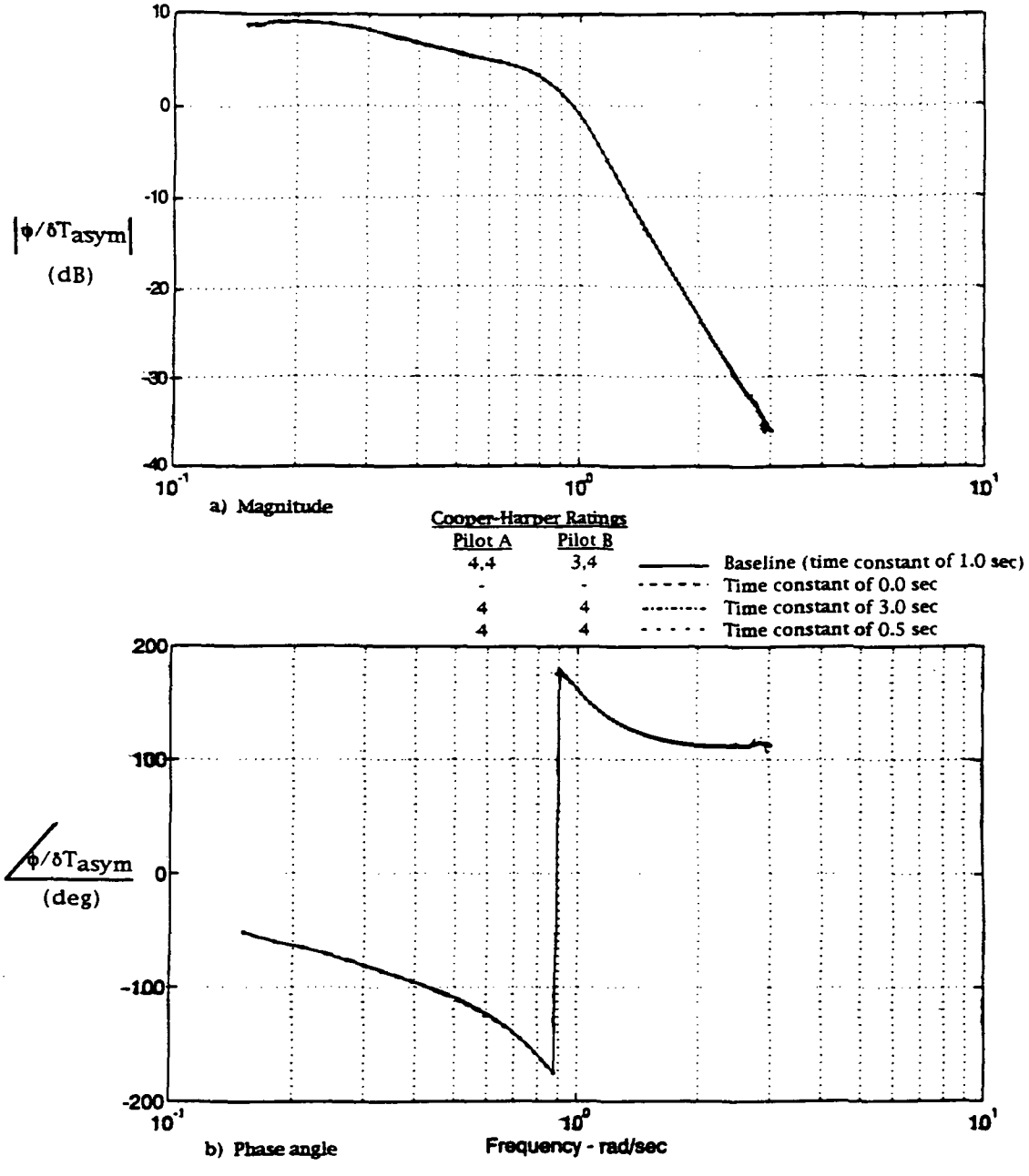

Figure 6.10 Megatransport Lateral-Directional Bank Angle - Asymmetric Thrust Frequency Response: Engine Time Constant Varied

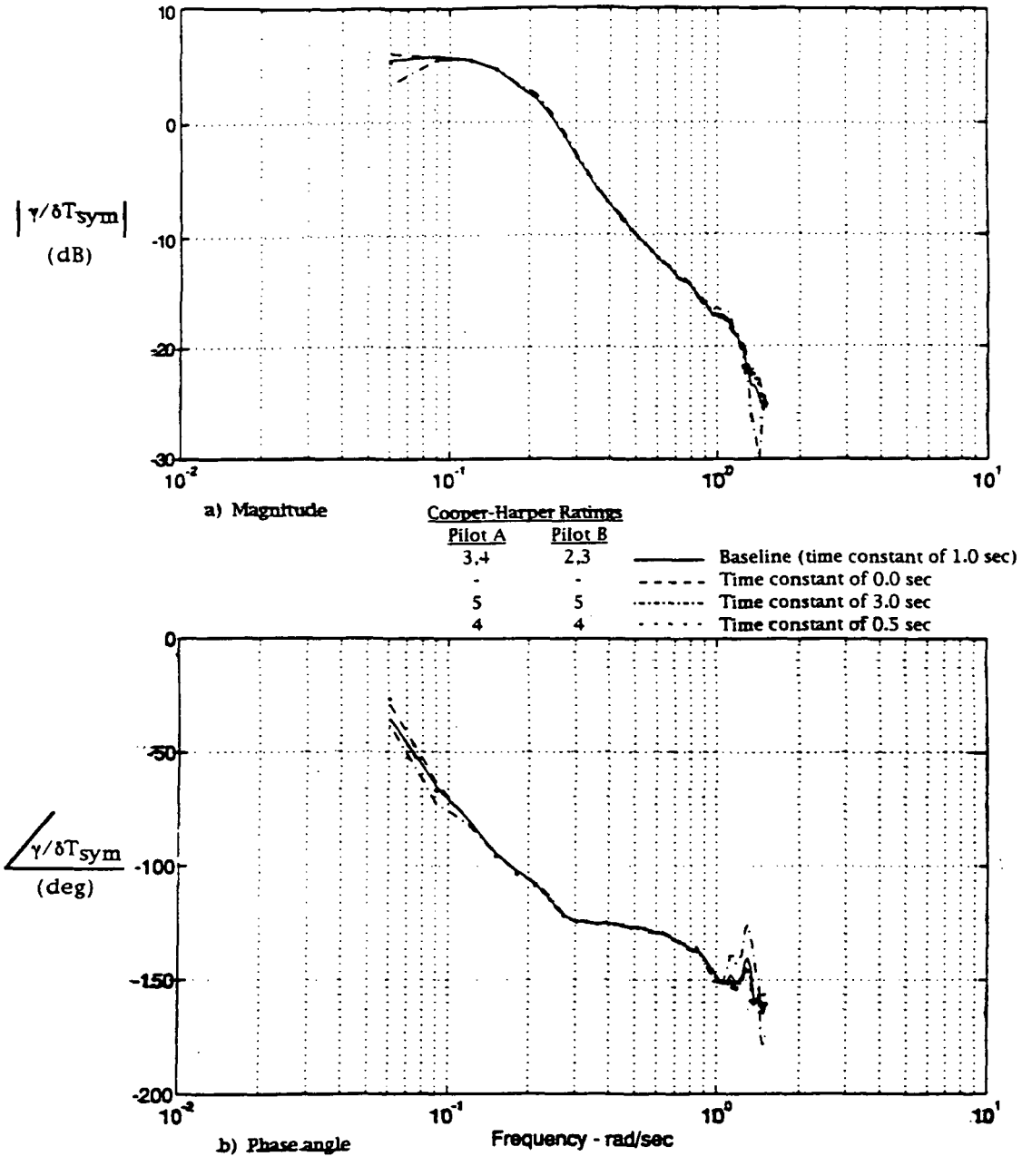

Figure 6.11 Megatransport Longitudinal Flight Path Angle - Symmetric Thrust Frequency Response: Engine Time Constant Varied

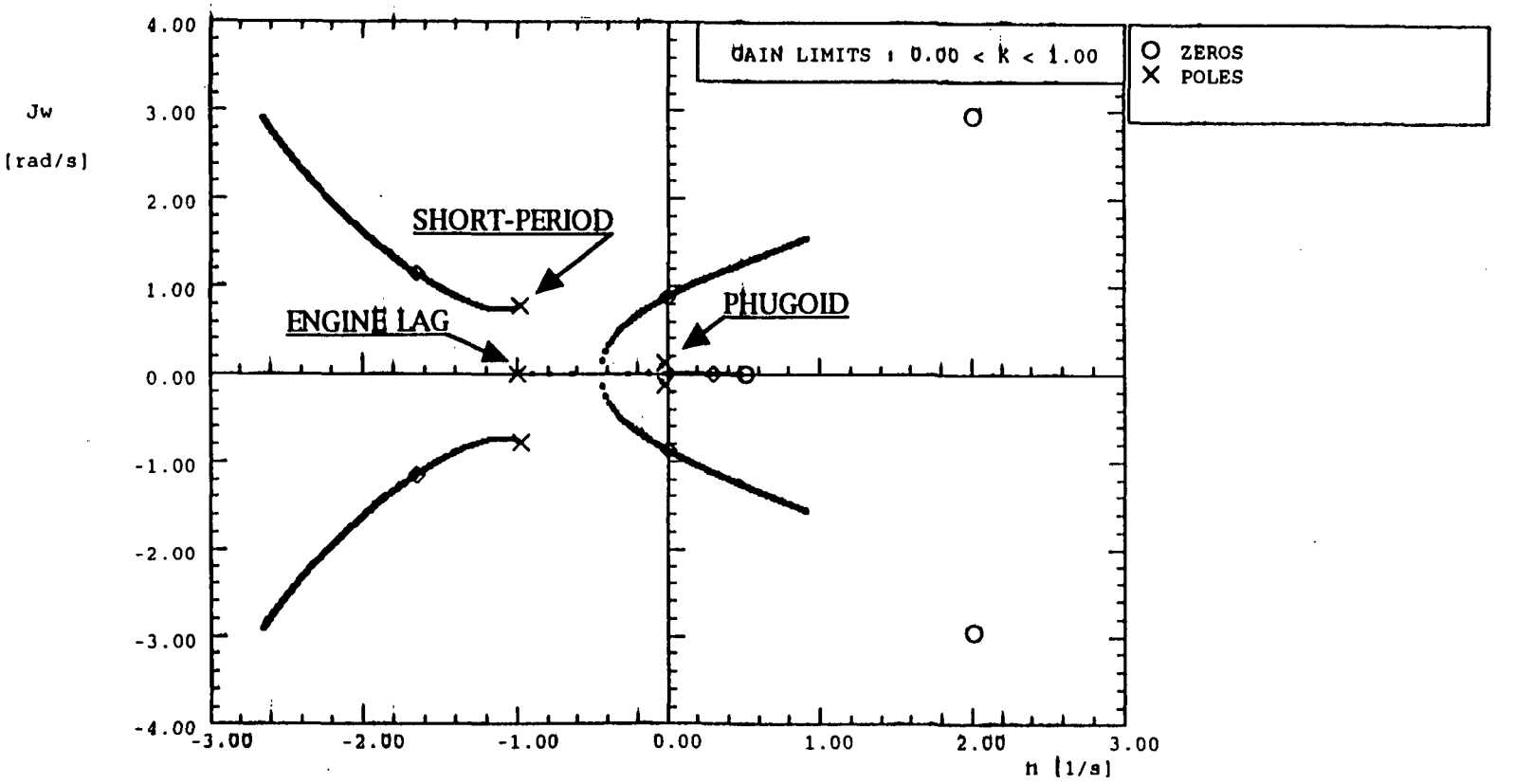

Figure 6.12 Root Locus Plot for the Megatransport Aircraft/Engine Longitudinal Transfer Function ($\gamma/\delta T_{sym}$) for an Engine Time Constant of 1.0 Second (Ref. 46)

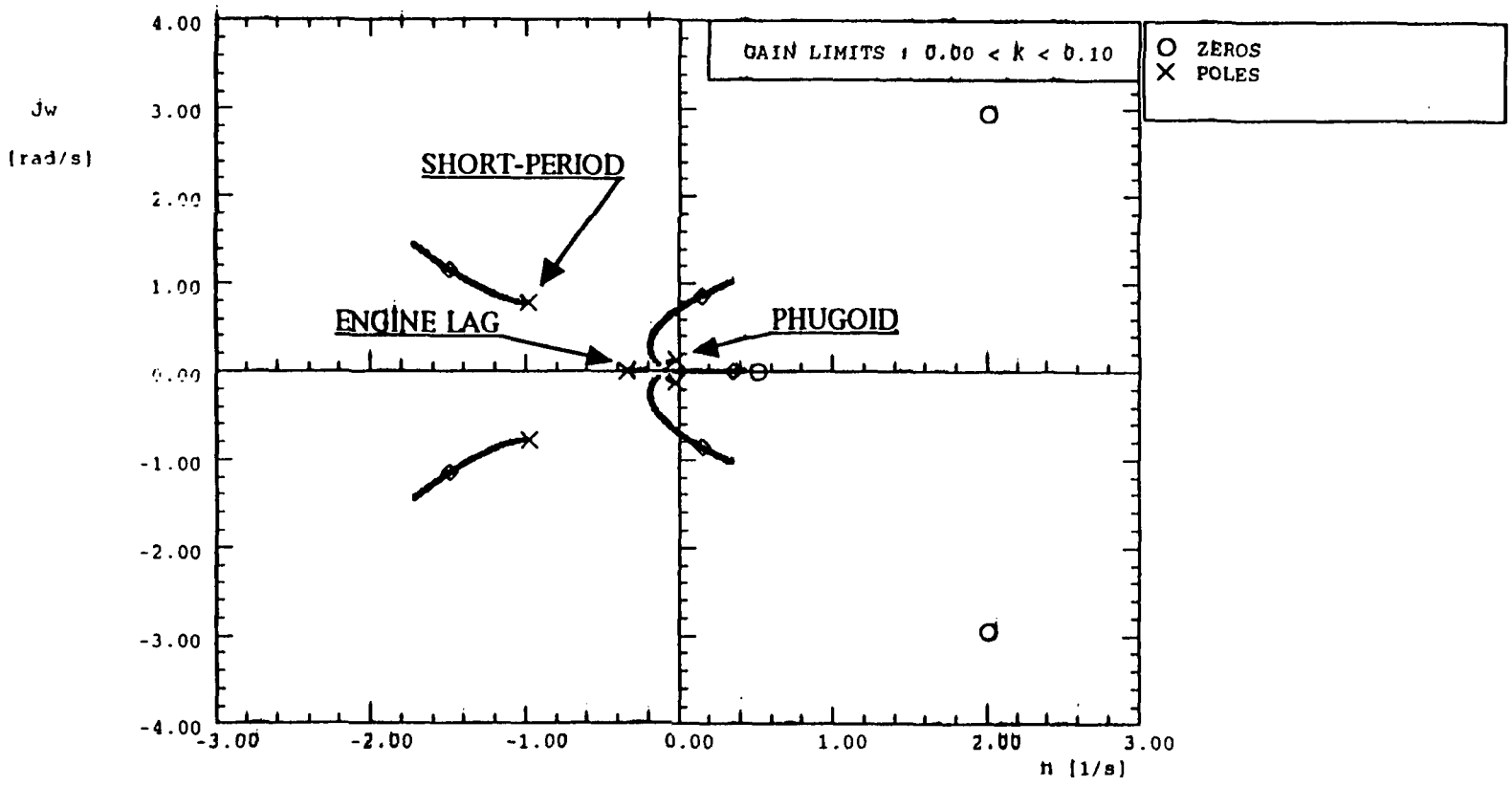

Figure 6.13 Root Locus Plot for the Megatransport Aircraft/Engine Longitudinal Transfer Function ($\gamma/\delta T_{sym}$) for an Engine Time Constant of 3.0 Seconds (Ref. 46)

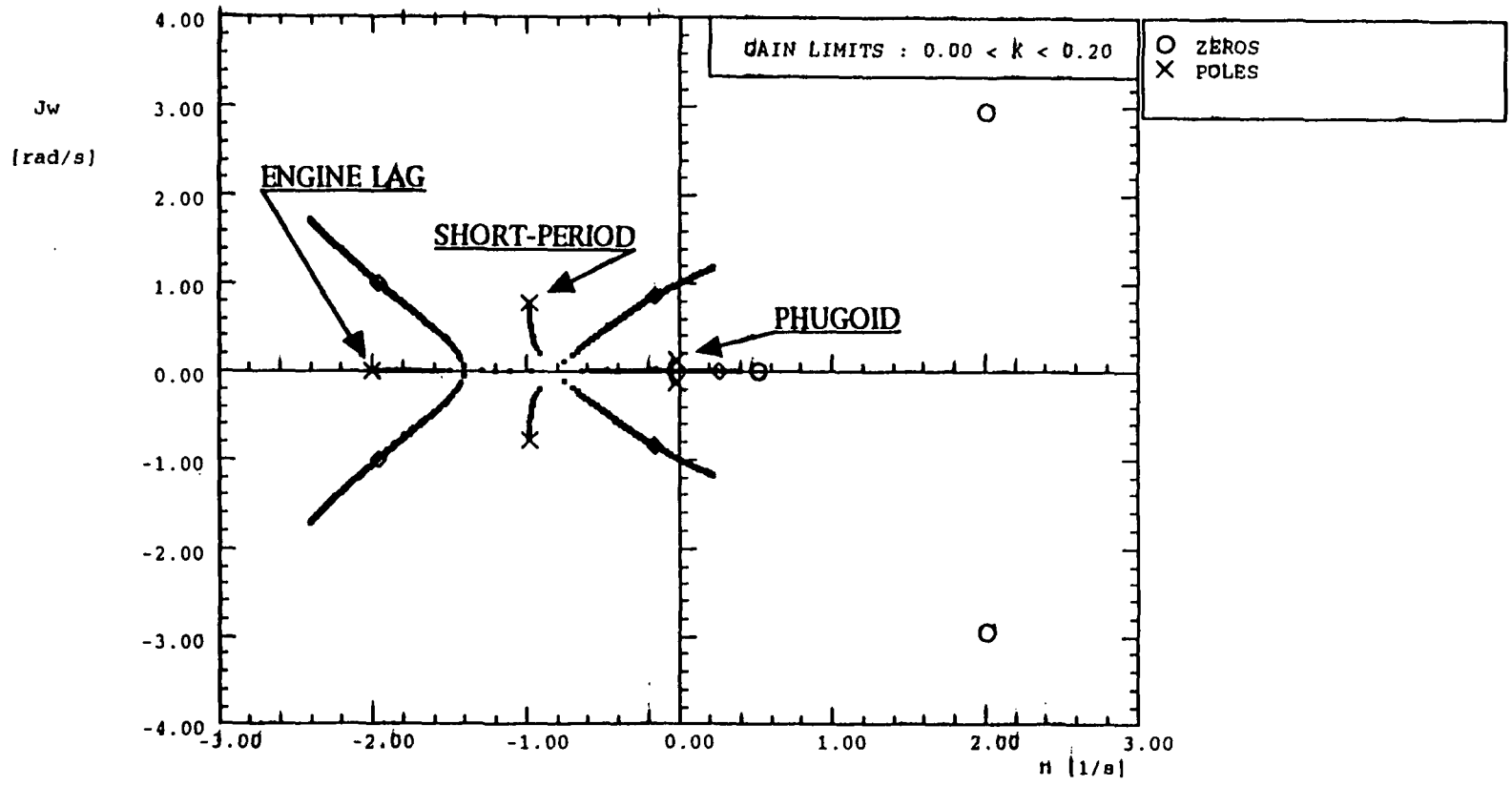

Figure 6.14 Root Locus Plot for the Megatransport Aircraft/Engine Longitudinal Transfer Function ($\gamma/\delta T_{sym}$) for an Engine Time Constant of 0.5 Seconds (Ref. 46)

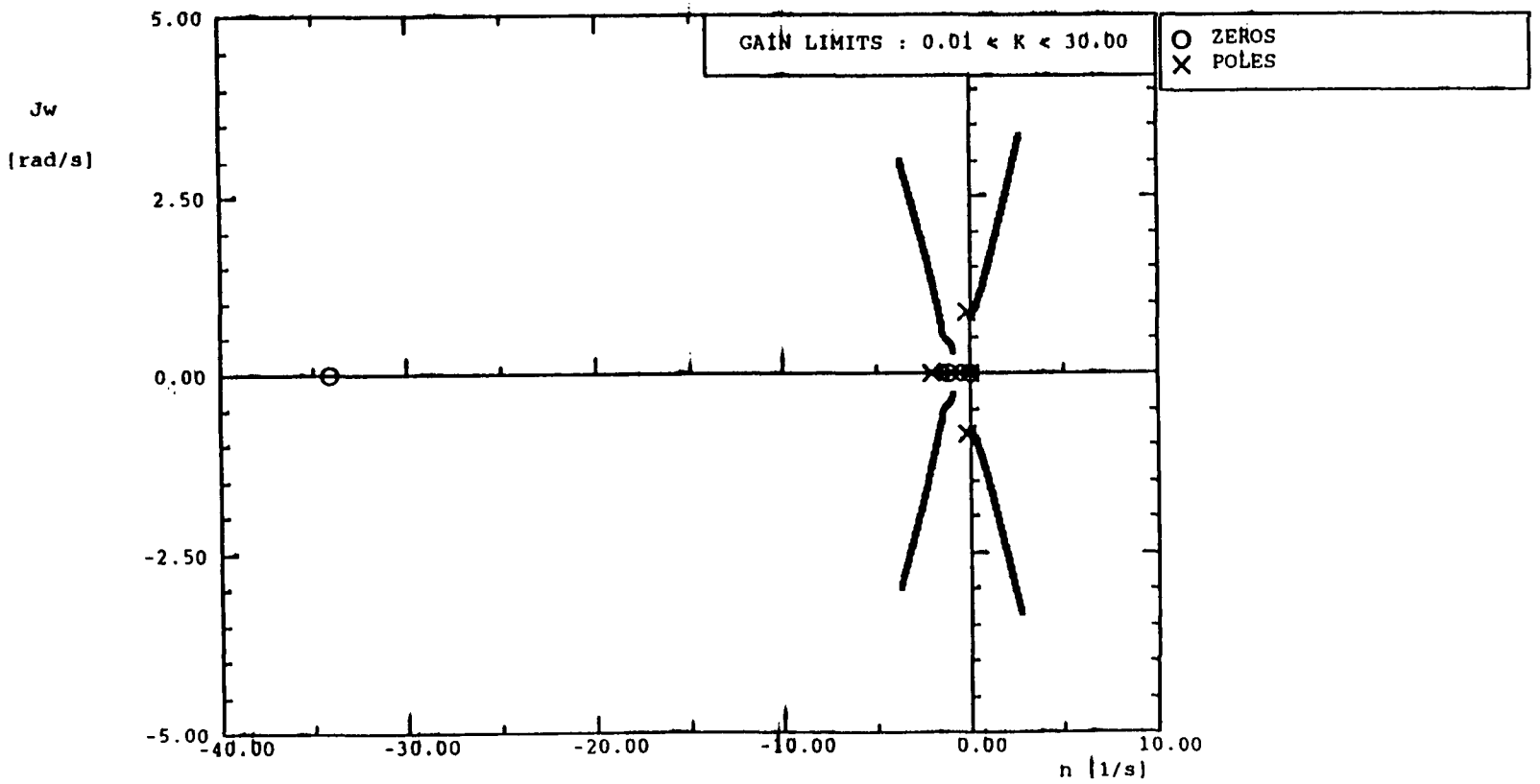

Figure 6.15 Root Locus Plot for the Megatransport Aircraft/Engine Lateral-Directional Transfer Function ($\phi/\delta T_{asym}$) for an Engine Time Constant of 1.0 Second (Ref. 46)

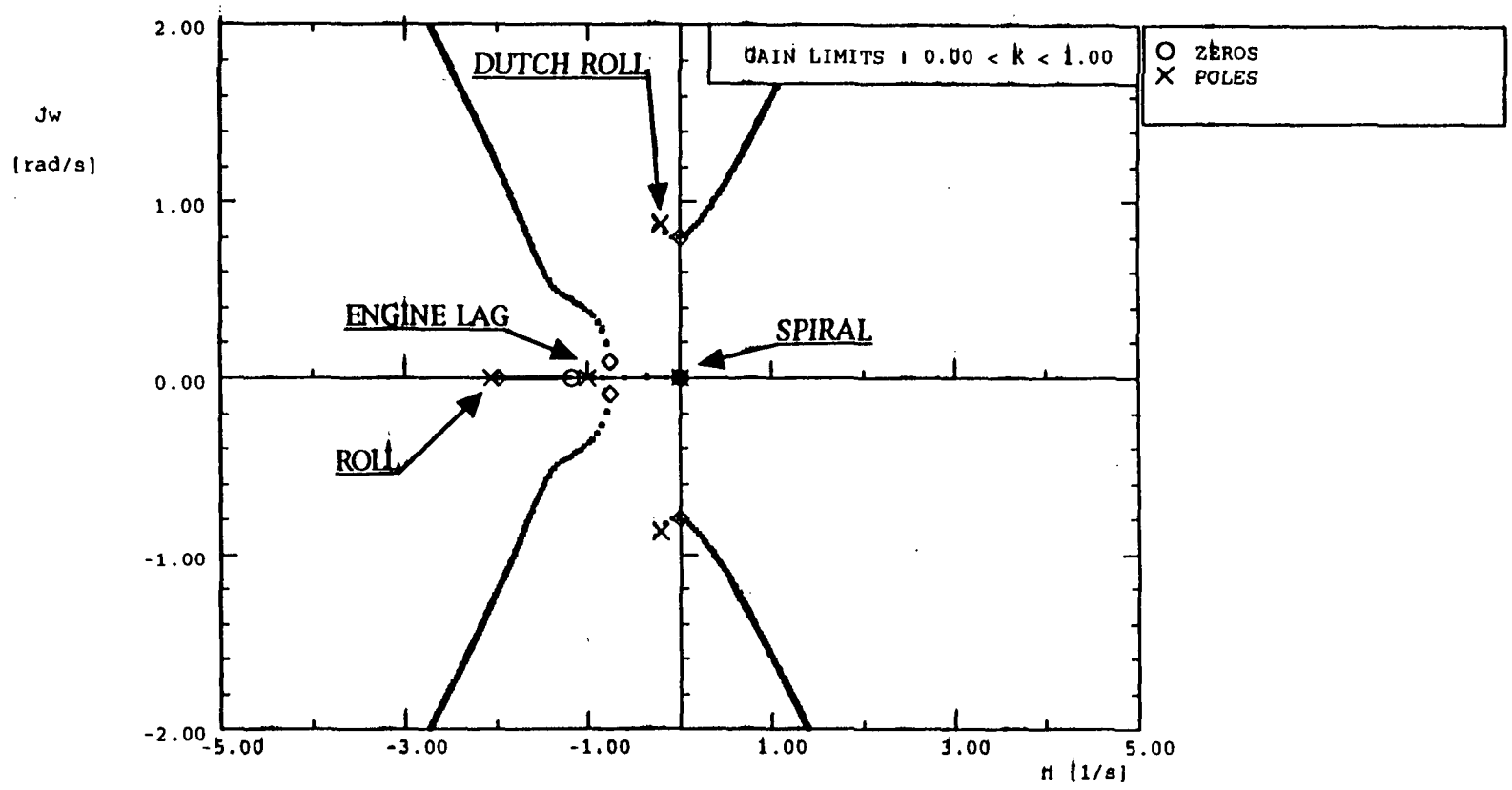

Figure 6.16 Root Locus Plot for the Megatransport Aircraft/Engine Lateral-Directional Transfer Function ($\phi/\delta T_{asym}$) for an Engine Time Constant of 1.0 Second (Reduced Scale) (Ref. 46)

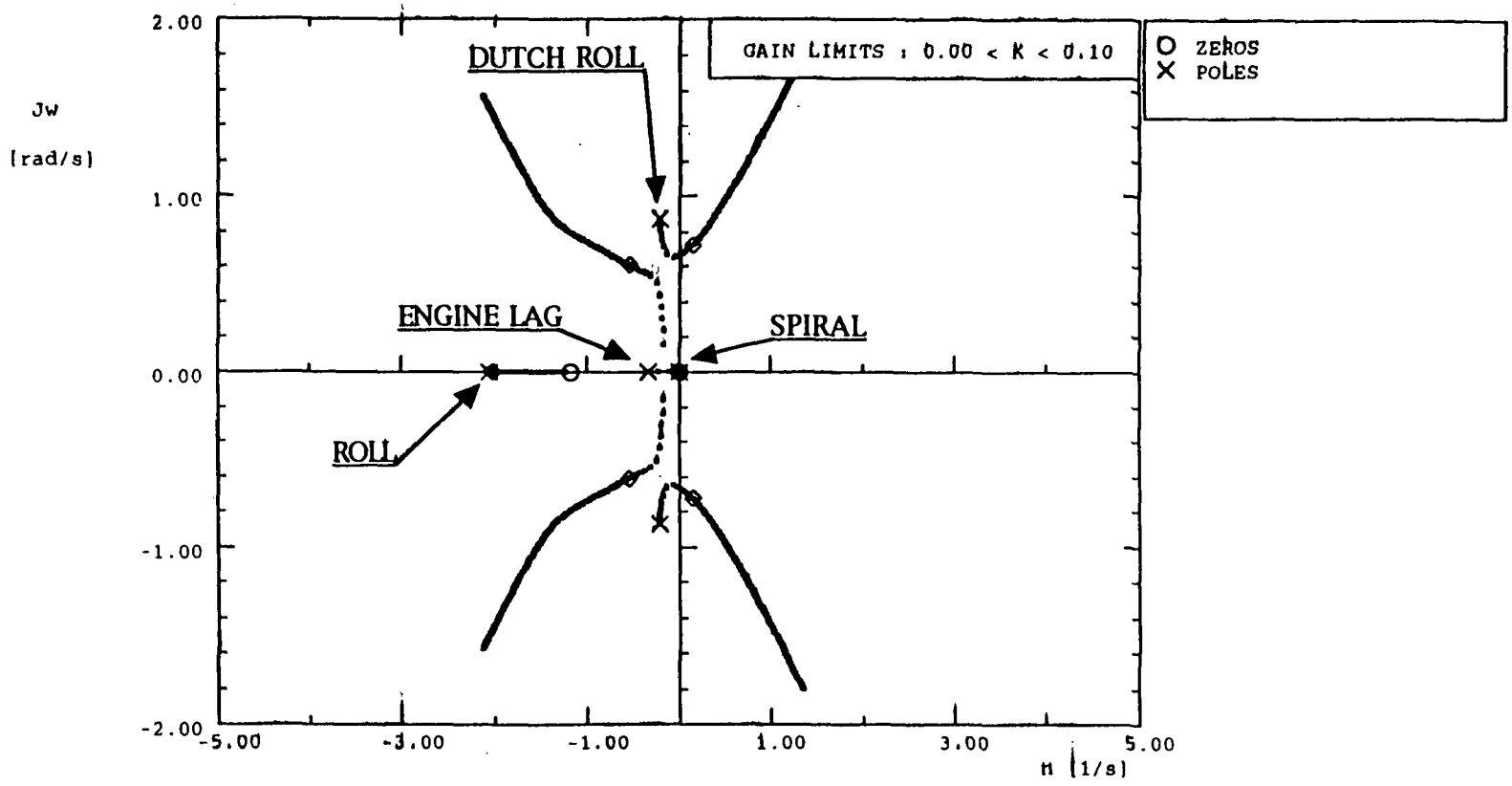

Figure 6.17 Root Locus Plot for the Megatransport Aircraft/Engine Lateral-Directional Transfer Function ($\phi/\delta T_{asym}$) for an Engine Time Constant of 3.0 Seconds (Reduced Scale) (Ref. 46)

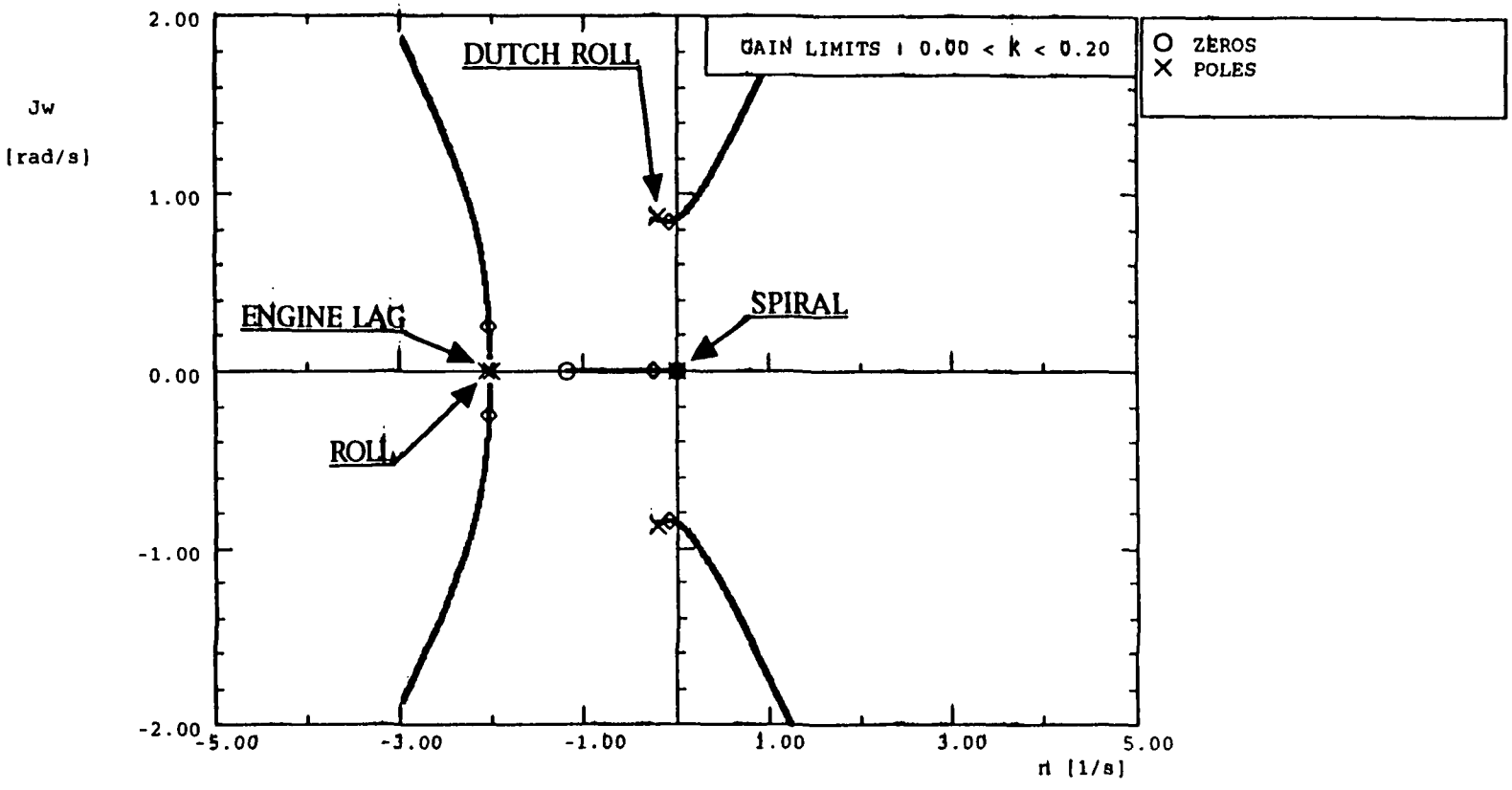

Figure 6.18 Root Locus Plot for the Megatransport Aircraft/Engine Lateral-Directional Transfer Function ($\phi/\delta T_{asym}$) for an Engine Time Constant of 0.5 Seconds (Reduced Scale) (Ref. 46)

CHAPTER 7

CONCLUSIONS AND RECOMMENDATIONS

7.1. CONCLUSIONS

This study has demonstrated that a PCA system is a viable emergency backup control system for a large transport aircraft. Based upon dynamic analysis and piloted simulation, it is concluded that:

- the megatransport/PCA system satisfied the Level 1 flying quality requirements based upon the frequencies, damping ratios, and time constants of the longitudinal and lateral-directional modes. The megatransport/PCA system fell short of satisfying Level 1 requirements, however, for the time required for the aircraft to achieve a 30 degree bank angle (Level 2 requirements were satisfied) and the time for the aircraft to respond to a control input (Level 3 requirements were not met).

- engine location did not appear to be a critical parameter in the performance of the megatransport/PCA system. Most of the pilot ratings and comments indicate that the pilots really couldn't perceive much difference in the flying qualities of the megatransport between various spanwise and vertical engine locations even though there were large variations in the crossover frequencies and phase lags of the various test points.

- there appears to be little correlation between the system crossover frequency and the pilot ratings. It is apparent that factors other than

crossover frequency and phase lag, such as the response time, affected the perceived flying qualities of the aircraft.

• the engine response time was a critical parameter in the performance of the megatransport/PCA system as was demonstrated by both root locus plot analysis and pilot ratings.

• although the flying qualities of the megatransport/PCA system were degraded for the engine-out test case, the system was still rated Level 2 on the Cooper-Harper pilot rating scale by both test pilots.

7.2. RECOMMENDATIONS

Before installation of a PCA system on a large commercial transport is considered or a level of control system redundancy is eliminated, a more complete evaluation of the PCA system should be investigated. Some items which require further study are:

• installation requirements of the PCA system such as the addition of PCA pitch and roll thumbwheels in the cockpit. The pilot's heads-up display, or HUD, will require changes such as a signal, or message, notifying the pilot that the PCA system is engaged. Also, a PCA targeting symbol would assist the pilot in adjusting the pitch and roll thumbwheels to attain the desired flight path. Finally, there will be the PCA program itself which will need to be installed in the flight computer along with software interfacing the HUD, pitch and roll thumbwheels, flight computer, and engine controls.

• the reliability of the PCA system, including possible failure modes of the PCA system. Scenarios which should be considered include whether PCA

can be engaged unintentionally, whether PCA can be used in the event of a partial flight control system failure where only some of the flight control surfaces are rendered inoperative, the effects of asymmetric or floating control surfaces on the PCA system since it is unlikely that all control surfaces will fail with zero deflection, and whether PCA should automatically engage in the event of a flight control system failure or whether the pilot should have the option of engaging the system.

• impact of the PCA system on aircraft certification, flight crew training requirements, aircraft inspection and maintenance, and airline operating costs and affordability.

• megatransport/PCA response within the entire flight envelope should be examined, including trimmability from a high speed flight condition to a lower speed approach condition. Methods of trimmability which should be studied include variable stabilizer control, lowering the flaps, extending the landing gear, moving the center of gravity aft by fuel transfer or payload movement, and differential thrust.

• the aeroelastic effects on the stability and control derivatives and the pitching moments as a function of engine location.

• the effects of the variation of engine thrust during use of the PCA system on the aircraft structure, particularly regarding the resonant frequency of the aircraft.

• the effects of thrust vectoring and variable pitch fans or inlet guide vanes on the engine response time and flying quality levels.

• the effects of the level of thrust on the megatransport/PCA flying qualities. Initial studies showed that PCA flight at thrust levels less than 25

percent total thrust resulted in unsatisfactory flying qualities due to large engine spool up times.

- the development of flying quality requirements specifically for large ultra-high capacity transport aircraft.

- additional research regarding the effects of ground effects, turbulence, and crosswinds on the flying qualities of the megatransport/PCA system.

Although the PCA system has been demonstrated to be a viable backup system for primary flight control system failure, it will require further study to determine whether the PCA system is feasible or not. Aircraft manufacturers and airlines, while concerned with the relative costs of the PCA system, should not lose sight of the primary benefit of the augmented throttles-only control system - saving human lives. The level of passenger and flight crew safety could be improved as the complete loss of the flight control system would no longer render an aircraft uncontrollable.

APPENDIX A

AIRCRAFT INCIDENTS WITH SIGNIFICANT FLIGHT CONTROL FAILURES

The DC-10 accident in Sioux City, Iowa, was not an isolated incident regarding the loss of the flight control system. Significant flight control failures have been documented in at least five other recent incidents. These incidents are described in detail in the following subsections.

A.1. DOUGLAS DC-10 AMERICAN AIRLINES INCIDENT [Ref. 64]

On June 12, 1972, American Airlines Flight 96 took off for Buffalo from Detroit with 57 passengers and 10 crew members on board. Approximately 10 minutes into the flight, the aft left cargo door separated from the aircraft, causing cargo compartment decompression.

When the door separated, a section of the aft coach lounge floor 6 - 8 feet square on the left side of the cabin broke loose from the support frames and dropped part way into the cargo bay. Part of the right side floor buckled to a lesser degree. There were no passengers seated there.

The only sign of an abnormal condition initially was a swirl of dust and debris in the cockpit and in the cabin, the pilot reported. Then the aircraft entered a slight right yaw as a result of the severing of several control cables when the aft cabin floor buckled. The control cables which were severed were the rudder control cables, except for those controlling the rudder trim system,

the left elevator control and stabilizer trim, and the power control and fuel shutoff cables for the tail-mounted engine.

Both sections of the rudder and the left elevator went into trail position and the tail engine went to idle power. The pilot reported no unusual attitude changes except for a slight right yaw. There were no significant difficulties in controlling the aircraft during flight. Ailerons alone appeared to provide enough heading control.

Controlling the aircraft after touchdown was more difficult. The flight crew used spoilers and differential reverse thrust on the two wing-mounted engines to steer and stop the aircraft. Minor injuries were suffered by nine passengers in the escape chute evacuation of the aircraft on the ground, but none were hospitalized.

A.2. DOUGLAS DC-10 TURKISH AIRLINES ACCIDENT [Refs. 65,66]

A Turkish Airlines DC-10 took off from Paris to London with 335 passengers and 11 crew members aboard on March 3, 1974. Approximately 9 minutes after takeoff, the aft left cargo door separated while the aircraft was at 12,000 feet and cruising at 300 knots. Cabin depressurization followed separation of the door.

The aircraft went into a pronounced nose-down attitude, power was reduced, and a roll to the left began. Accident investigators determined that the DC-10 hit the ground at 420 knots and with the left wing down. A swath more than 3,000 feet long had been cut through the forest where the aircraft

struck. The aircraft literally disintegrated as it plowed through the trees, killing all on board.

It was assumed that when the cabin depressurized, the cabin floor buckled, severing the hydraulic lines and control cables in a manner similar to that of the American Airlines incident in 1972. When the hydraulic lines were severed, the hydraulic-powered flight control systems were rendered inoperative.

A.3. LOCKHEED C-5A USAF ACCIDENT [Refs. 67,68]

April 4, 1975, a USAF/C-5A took off from an airfield in Viet Nam with 178 persons, mostly Vietnamese orphans, aboard. The aircraft was passing through 23,000 feet and was about 5 miles offshore en route to Clark air base in the Philippines when the rear pressure bulkhead, which is part of the cargo-loading ramp, failed. This failure caused the complete loss of the primary and secondary hydraulic systems, loss of cabin pressurization, and secondary damage to the aft fuselage.

Loss of both the hydraulic systems caused the crew to lose rudder, elevator, and flap control. The aircraft remained roughly in trim and was maneuvered using ailerons and throttle controls. The crew commented on the difficulty in achieving precise control due to the slow response of the engines. They practiced using this control mode for 30 minutes, made a practice landing at 10,000 feet, then tried an approach to the runway.

About 7 miles from the airport at 5,000 feet and aligned with the runway, the crew lowered the landing gear and at about the same time the

aircraft's rate of descent increased excessively. The aircraft hit very hard about 1.5 miles short of the runway, broke up, and was destroyed by fire. There were no survivors.

A.4. LOCKHEED L-1011 DELTA AIRLINES INCIDENT [Ref. 69]

Near midnight, April 12, 1977, Delta Airlines Flight 1080 prepared to depart San Diego for a flight to Los Angeles. During taxi out, a flight control check of the stabilizer, ailerons, and spoilers was made. The proper response was verified by the surface position indicators and by the normal 'feel' of the wheel.

During takeoff acceleration, the L-1011 lifted off with little or no control input and a zero stick force. Immediately after liftoff, an abrupt nose-high excursion in pitch and a roll to the left was experienced that was controllable, although the pilot did hit the full forward limit of the control column during the abrupt pitch-up.

At an altitude of approximately 400 feet and an airspeed of 170 knots, the pitch attitude exceeded 18 degrees. The aircraft was trimmed with full nose-down stabilizer trim, but no change in the pitch attitude was observed. The aircraft continued to pitch up and climb as the airspeed decayed. In addition, the pilot continually fought a tendency of the aircraft to maintain a left-bank attitude.

Pitch attitude exceeded 22 degrees and the airspeed fell to 138 knots when the pilot felt that loss of the aircraft due to stall was eminent. If pitch

could be reduced, airspeed would be regained and some degree of controllability might be obtained.

The pilot abruptly reduced thrust on all three engines and recognized a change in control 'feel'. The airspeed increased as the pitch angle dropped. Increased thrust on the left engine was implemented to compensate for the left-roll tendency. One inch of control stick movement was now available to the pilot.

The L-1011 was controlled during flight by using the throttles as the primary flight control system. The approach was set up and a successful landing was made. Upon touchdown, the pilot found that the nose did not come down even with the control column full-forward. It was necessary to apply main-wheel braking to force the nose wheel down.

Upon examination of the aircraft, the malfunction was determined to be the left elevator jammed in a 19 degree nose-up attitude. Presumably the left elevator aft drive quadrant and drive cable failed during the flight control check prior to takeoff. There is no cockpit indication for this type of failure on the L-1011.

A.5. BOEING 747 JAPAN AIRLINES ACCIDENT [Refs. 70,71,72,73,74,75]

August 12, 1985, Japan Airlines Flight 123 took off from Tokyo's Haneda Airport bound for Osaka. At an altitude of 24,000 feet, an explosion occurred which raised the nose of the 747 aircraft. Immediately after the explosion, hydraulic pressure dropped and rudders, ailerons, elevators, and yaw dampers became inoperative. Significant altitude and speed changes and

roll oscillations occurred. The aircraft rolled +/-40 degrees and altitude and speed changed by +/-1,500 feet and +/-25 knots, respectively.

The flight crew attempted to fly the aircraft using only throttle controls for approximately 30 minutes. The pilot radioed that he was unable to control the aircraft immediately before the aircraft crashed into a mountainside 51 miles from Tokyo. The 747 had 520 passengers aboard. There were only 4 survivors.

Upon examination of the wreckage, it was believed that explosive decompression occurred due to a ruptured aft bulkhead. When the bulkhead ruptured, the rudders, part of the vertical stabilizer, and most of the tail cone separated from the fuselage while the aircraft was in flight. All four hydraulic lines, which run into the tail cone, were severed when the tail cone separated, rendering all control surfaces inoperable.

APPENDIX B

MEGATRANSPORT DYNAMIC ENGINE MODEL

[Refs. 20,42,49,76]

A dynamic engine model was developed for the megatransport using available data on the Pratt & Whitney JT8D and the General Electric CF6-80 engines. Figures B1 and B2 show the engine response to throttle step commands for these two engines, respectively. The thrust and throttle setting scales have been nondimensionalized for proprietary reasons.

Figure B1 shows the thrust response to various initial thrust levels for the NASA Langley Research Center JT8D real-time engine model. The JT8D, which entered commercial service in 1964, is the most widely used commercial jet engine flying today. This turbofan powers the Boeing 727 and 737 aircraft along with the McDonnell Douglas DC-9 airplane. As can be seen from the figure, the time to achieve maximum thrust depends upon the initial thrust setting.

From an initial setting of 67% thrust, it takes the engine only about 1 second to spool up to 100% thrust. From an initial minimum idle setting, however, it takes the engine nearly 6.5 seconds to spool up to the maximum thrust level.

Comparing the engine response curves in Figure B1, the response for all cases is fairly rapid above the 25% thrust level. Below this level, however, it takes the engine approximately 3.5 seconds, or more than half of the total engine response time, just to spool up from idle to 25% thrust.

Figure B2 shows the thrust response to various power level angles (PLA), or throttle settings, over a period of one minute for the CF6-80 engine. The CF6-80 turbofan engine, which entered commercial service in 1985, powers the Airbus A300, A310, and A330 aircraft, along with the Boeing 747, 767 and McDonnell Douglas MD-11 aircraft. Again, it can be seen that the time to achieve maximum thrust depends upon the initial thrust setting.

For the first throttle step input at 6 seconds, it takes the engine about 2 seconds to spool up from a setting of approximately 35% thrust to 100% thrust. For the throttle step input at 38 seconds, it takes the engine nearly 6 seconds to spool up from minimum to maximum thrust. Most of this time lag occurs in spooling up the engine from idle to 30% thrust.

Based on the data in Figures B1 and B2, the response of the megatransport engine was modeled by an exponential function of time, commanded thrust$*(1 - e^{-t/TC})$, where TC is defined as the engine time constant. Initially, only one value of the engine time constant was used throughout the entire engine model.

A single value time constant model, however, was inadequate when compared to actual engine dynamics, particularly in the low thrust regime. As can be seen from Figures B1 and B2, the time to change the engine thrust takes much longer if the engine is operating at thrust levels below approximately 25% maximum thrust.

In creating a dynamic engine model for the megatransport, it was important to incorporate not only a time delay factor, but to incorporate a time delay factor depending on the initial thrust setting. Consequently, the megatransport engine model actually incorporates three different engine time constants in an effort to more accurately reflect actual engine dynamics.

A time constant simply equal to the value of TC was used in the region where the engine thrust was greater than 20% of the maximum thrust. When the engine thrust was less than 20% of the maximum thrust, one of two different time constants was used depending on whether the thrust was increasing or decreasing. If the thrust was increasing, the time constant was equal to a value of TC*17. If the thrust was decreasing, the time constant was equal to a value of TC*5.

These values were determined experimentally by running the megatransport simulator with different multipliers of the engine time constant. The results of the engine response were printed out to a strip chart recorder and analyzed. The values which were selected (5 and 17) were those that gave an engine response curve which most closely resembled the responses shown in Figures B1 and B2.

Figure B3 shows the thrust response to various initial thrust levels for the megatransport dynamic engine model. As can be seen from the figure, the engine response model incorporates different time delay factors depending on the initial thrust.

Since the value of the engine time constant itself was to be a test parameter in this project, the megatransport simulator was programmed such that the value of the variable TC was entered by the user prior to starting the simulator, allowing the engine time constant to be changed easily real-time.

Figure B4 shows the response of the megatransport engine model to values of the engine time constant equal to 0.5, 1, and 3 seconds. The megatransport engine with the one second engine time constant can produce 100 percent of thrust from an initial minimum idle thrust setting in 10 seconds. This same engine with a 3 second engine time constant requires 30

seconds to achieve the same level of thrust, while the engine with a 0.5 second engine time constant can reach the desired thrust in only 5 seconds.

One second was selected as the nominal value for the megatransport engine time constant based primarily on a comparison of the megatransport engine response with that of the General Electric CF6-80 turbofan engine. An actual strip chart recording of the megatransport engine model throttle step response from minimum idle to maximum thrust is shown in Figure B5.

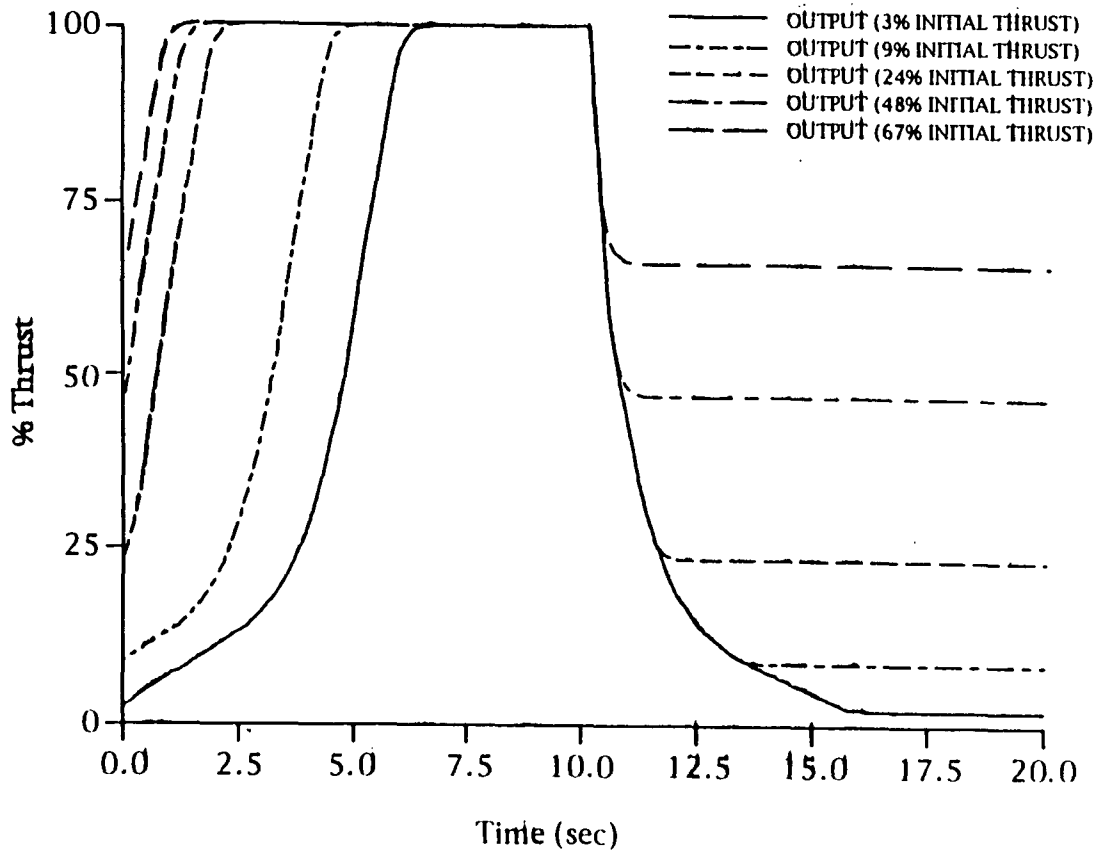

Figure B1 Langley JT8D Real-Time Engine Model Throttle Step Response: M = 0.2, H = 3,000 ft (Ref. 76)

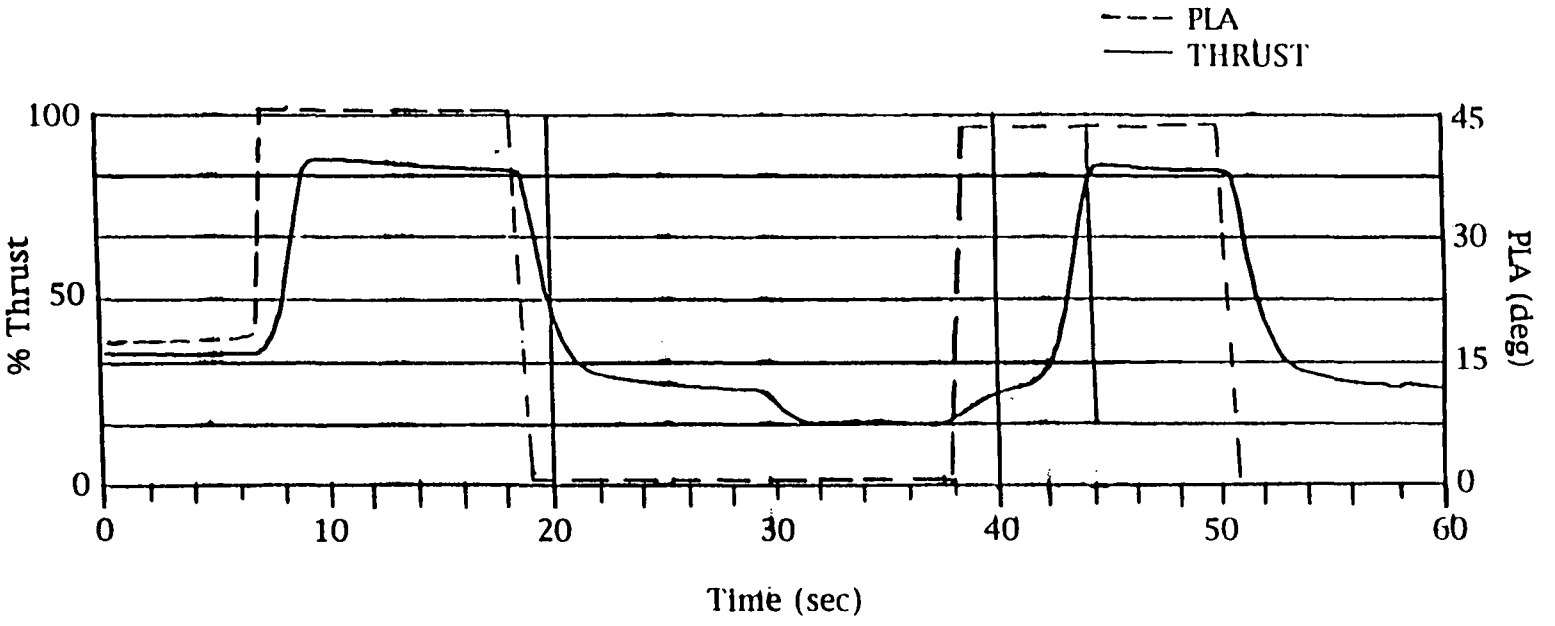

Figure B2 CF6-80 Engine Throttle Step Response: M = 0.3, H = 2,000 ft (Ref. 76)

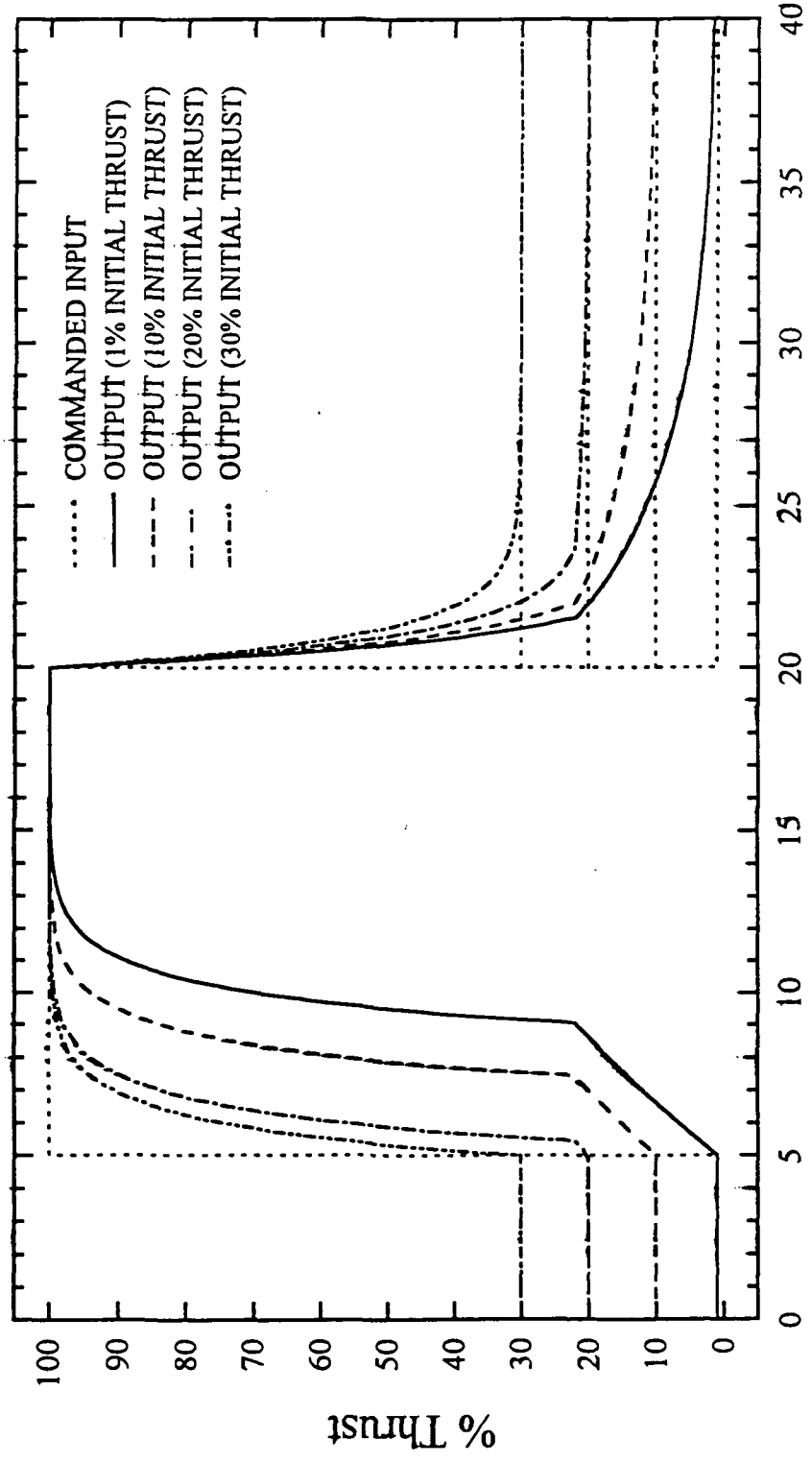

Figure B3 Megatransport Engine Model Throttle Step Response at Different Initial Thrust Levels

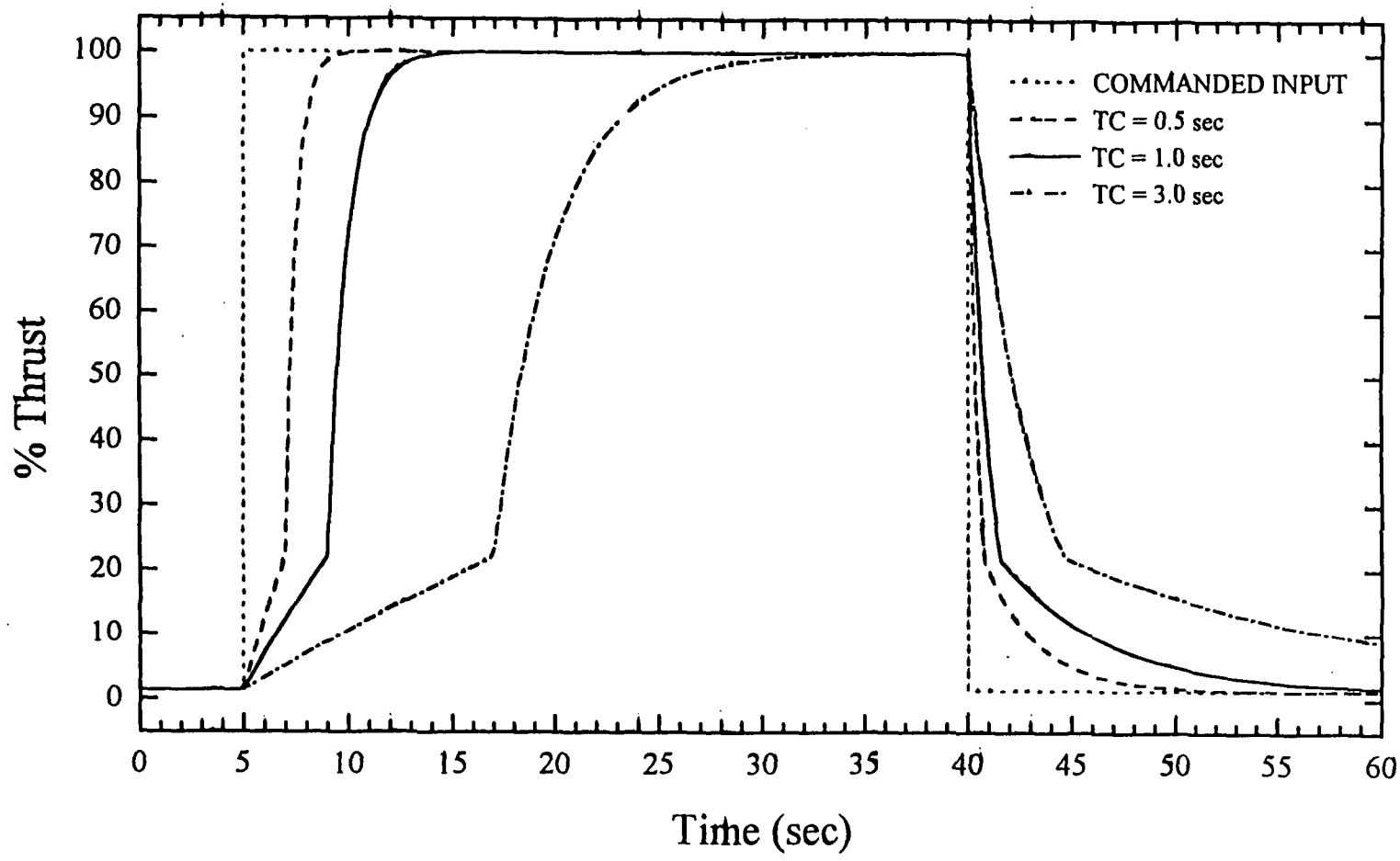

Figure B4 Megatransport Engine Model Throttle Step Response for Different Values of the Engine Time Constant, TC

238

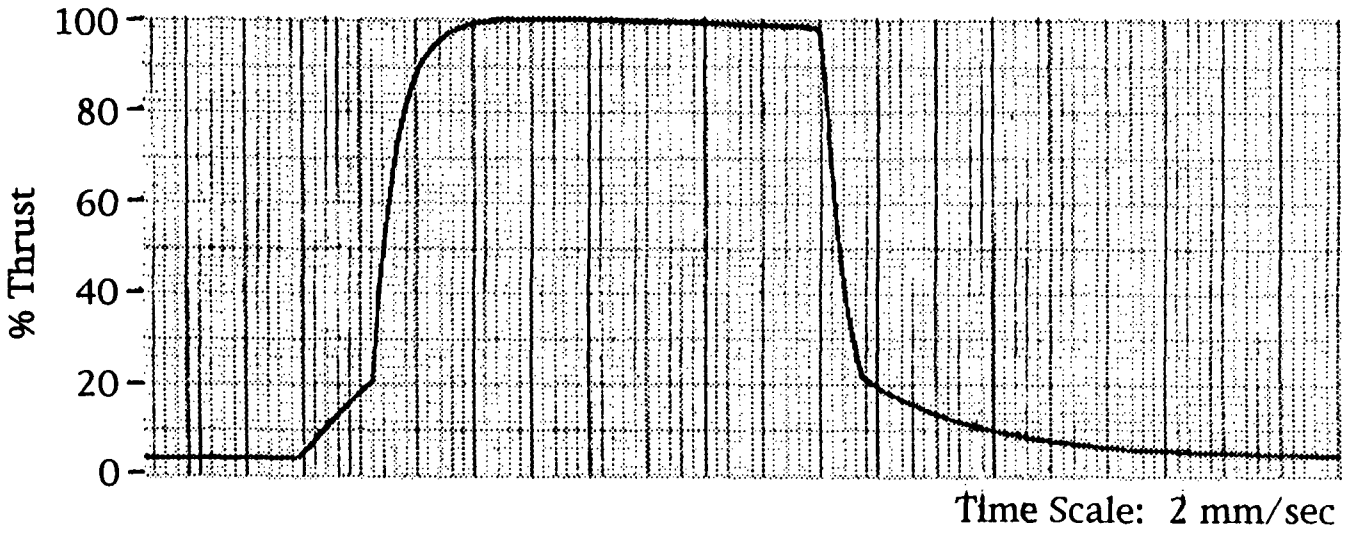

Figure B5 Actual Megatransport Engine Model Throttle Step Response (Time Constant of 1.0 Second)

239

APPENDIX C

MEGATRANSPORT WING WEIGHT PREDICTION METHOD

[Ref. 43]

The wing weight is a function of many factors such as shear forces, bending moments, stress levels, and material properties. These, in turn, depend upon the placement of the engines. Torenbeek, at Delft University of Technology, has developed a design-sensitive weight prediction method for wing structures which can be used to modify the wing weight, and therefore the total airplane weight, according to the engine location on the wing.

Torenbeek breaks the wing weight, W_W, into primary and secondary structural weight as follows:

$$W_W = W_{PRIM} + W_{SEC} \qquad \text{[Eqn. C1]}$$

where W_{PRIM}, the primary structural weight, is defined as:

$$W_{PRIM} = W_{BASIC} + \Sigma \Delta W_{NO} + \Delta W_{ST} \qquad \text{[Eqn. C2]}$$

and:

- W_{BASIC} is the minimum weight of the primary structure required to resist bending and shear loads
- $\Sigma \Delta W_{NO}$ is the non-optimum weight penalty for sheet taper and joints, cutouts, mounting and connections, and torsion loads

- ΔW_{ST} is the stiffness requirements weight penalty.

W_{SEC} is the secondary structural weight consisting of:

- leading and trailing edge structure
- high lift devices at leading and/or trailing edges
- control surfaces.

When moving the engine location, the only significant structural weight change will be to W_{BASIC}, the structure required to resist bending and shear loads, and that portion of $\sum \Delta W_{NO}$ required to resist torsional loads. Since Torenbeek estimates the entire non-optimal weight penalty term, $\sum \Delta W_{NO}$, to be less than 10% of the total wing weight, the torsional effects on the weight change due to engine location position were considered to be negligible.

Torenbeek defines W_{BASIC} by the following equation:

$$W_{BASIC} = (1/3)\cdot(\rho g/\bar{\sigma}_r)\cdot rnWbm_{cp}\cdot\left[(1.08/\eta_t)\cdot R_C + 1.50\cdot(\bar{\sigma}_r/\bar{\tau})\right] + k_r \rho g S\cdot\left[t_{ref} + ((t_r + t_t)/2)\right]$$

[Eqn. C3]

The author redefines Equation C3 as follows:

$$W_{BASIC} = K_1 r + K_2$$

[Eqn. C4]

where:

- $K_1 = (1/3)\cdot(\rho g/\bar{\sigma}_r)\cdot nWbm_{cp}\cdot\left[(1.08/\eta_t)\cdot R_C + 1.50\cdot(\bar{\sigma}_r/\bar{\tau})\right]$ [Eqn. C5]
- $K_2 = k_r \rho g S\cdot\left[t_{ref} + ((t_r + t_t)/2)\right]$ [Eqn. C6]

- $r = 1 + \Sigma(\Delta W_{B+S}/W_{B+S})$ [Eqn. C7]

r, the weight relief factor, is a function of engine location as will be seen later. K_1 and K_2 are independent of the location of the engine. Solving first for K_2, Torenbeek suggests the following values for k_r, t_{ref}, and ρg:

- $k_r = 0.5 \times 10^{-3}$
- $t_{ref} = 1$ m $= 3.281$ ft
- $\rho g = 28 \times 10^3$ N/m^3 $= 178.21$ lb/ft^3 for an aluminum alloy

where:

- $g = 32.17$ ft/sec^2

Values for the wing area, wing root thickness, and wing tip thickness of the megatransport are:

- $S = 11{,}900$ ft^2
- $t_r = 6.3316$ ft
- $t_t = 1.5543$ ft

Substituting these values into Equation C6:

$$K_2 = \left(0.5 \times 10^{-3}\right) \cdot (178.21) \cdot (11{,}900) \cdot \left[3.281 + \left(\frac{(6.3316 + 1.5543)}{2}\right)\right] \text{lb}$$

[Eqn. C8]

- $K_2 = 7{,}660.28$ lb

r, the weight relief factor defined in Equation C7, is calculated next. Equation C7 can be rewritten as follows:

$$r = 1 + \left(\Delta W_{B+S}/W_{B+S}\right)_F + \left(\Delta W_{B+S}/W_{B+S}\right)_W + \left(\Delta W_{B+S}/W_{B+S}\right)_P$$

[Eqn. C9]

where:

- $\left(\Delta W_{B+S}/W_{B+S}\right)_F$ is the fuel mass bending relief factor
- $\left(\Delta W_{B+S}/W_{B+S}\right)_W$ is the wing weight relief factor
- $\left(\Delta W_{B+S}/W_{B+S}\right)_P$ is the relief factor for the powerplant.

According to Torenbeek, $(\Delta W_{B+S}/W_{B+S})_F$, the fuel mass bending relief factor, is only used in the case where the maneuver load is critical. For that reason, it is not used here. $(\Delta W_{B+S}/W_{B+S})_W$ and $(\Delta W_{B+S}/W_{B+S})_P$ are defined as:

$$\left(\Delta W_{B+S}/W_{B+S}\right)_W = -0.80\left(W_w/W_{TO}\right) \qquad \text{[Eqn. C10]}$$

$$\left(\Delta W_{B+S}/W_{B+S}\right)_P = -1.50 \sum_{1}^{N_e} \left(\frac{2}{\eta_p}/\eta_{cp}\right) \cdot \left[\left(W_p/N_e\right)/\left(W_{TO}/2\right)\right]$$

[Eqn. C11]

where:

- W_w is the wing weight
- W_{TO} is the takeoff weight

- η_p is the nondimensional lateral coordinate of a wing-mounted engine
- η_{cp} is the nondimensional lateral coordinate of the center of pressure of the half-wing
- N_e is the number of engines
- (W_p/N_e) is the weight per engine of the powerplant, nacelle, and pylon combination.

The values for W_w, W_{TO}, N_e, and (W_p/N_e) for the megatransport were calculated in Chapter 3. First calculating $(\Delta W_{B+S}/W_{B+S})_W$:

$$\left(\Delta W_{B+S}/W_{B+S}\right)_W = -0.80(162{,}585/1{,}421{,}900) = -0.0915 \qquad \text{[Eqn. C12]}$$

Next calculating $(\Delta W_{B+S}/W_{B+S})_P$:

$$\left(\Delta W_{B+S}/W_{B+S}\right)_P = -1.50\sum_{1}^{4}\left(\eta_p^2/\eta_{cp}\right)\cdot\left[(129{,}210/4)/(1{,}421{,}900/2)\right] = -0.0682\sum_{1}^{4}\left(\eta_p^2/\eta_{cp}\right) \qquad \text{[Eqn. C13]}$$

η_{cp} is defined as:

$$\eta_{cp} = \left[(1+2\lambda)/3(1+\lambda)\right] \qquad \text{[Eqn. C14]}$$

where λ is the taper ratio. Substituting in a value of 0.3 for λ:

- $\eta_{cp} = 0.4103$

$(\Delta W_{B+S}/W_{B+S})_P$ then becomes:

$$\left(\Delta W_{B+S}/W_{B+S}\right)_P = -0.166\sum_{1}^{4}\left(\eta_p\right)^2 \qquad \text{[Eqn. C15]}$$

The megatransport has 4 engines - 2 inboard and 2 outboard along the wing span. Breaking the engine location parameter, η_p, into inboard and outboard components:

$$\left(\Delta W_{B+S}/W_{B+S}\right)_P = -0.166\left[\sum_{1}^{2}\left(\eta p_{in}\right)^2 + \sum_{1}^{2}\left(\eta p_{out}\right)^2\right] \qquad \text{[Eqn. C16]}$$

For the baseline engine location configuration:

$$\eta p_{in} = \left[y_{in}/(b/2)\right] = \left[59.625/(318/2)\right] \qquad \text{[Eqn. C17]}$$
$$= 0.375$$

$$\eta p_{out} = \left[y_{out}/(b/2)\right] = \left[103.35/(318/2)\right] \qquad \text{[Eqn. C18]}$$
$$= 0.65$$

$(\Delta W_{B+S}/W_{B+S})_P$ now becomes:

$$\left(\Delta W_{B+S}/W_{B+S}\right)_P = -0.166\left[2(0.375)^2 + 2(0.65)^2\right] \qquad \text{[Eqn. C19]}$$
$$= -0.1869$$

Substituting into Equation C9:

$$r = 1 - 0.0915 - 0.1869 = 0.7216 \qquad \text{[Eqn. C20]}$$

Substituting this value of r, along with the value of K_2 calculated in Equation C8, into Equation C4 for W_{BASIC} gives:

$$W_{BASIC} = K_1(0.7216) + 7{,}660.28 \text{ lb} \qquad \text{[Eqn. C21]}$$

Now substituting in the basic wing weight which has been previously calculated in Chapter 3:

$$162{,}585 = K_1(0.7216) + 7{,}660.28 \text{ lb} \qquad \text{[Eqn. C22]}$$

Solving for K_1:

- $K_1 = 214{,}696.12$ lb

Assuming that the only significant structural weight change due to moving the engine location will be to W_{BASIC}, the equation for changing the wing weight as a function of the engine location becomes:

$$W_{BASIC} = (214{,}696.12) \cdot r + 7{,}660.28 \text{ lb} \qquad \text{[Eqn. C23]}$$

where:

$$r = 1 - \left[0.0915 + \left(\Delta W_{B+S}/W_{B+S}\right)_P\right] \qquad \text{[Eqn. C24]}$$

and:

$$\left(\Delta W_{B+S}/W_{B+S}\right)_P = -0.166\left[\sum_1^2\left(\eta p_{in}\right)^2 + \sum_1^2\left(\eta p_{out}\right)^2\right] \qquad \text{[Eqn. C25]}$$

Table C1 contains a listing of all the test conditions which were either test flown in the megatransport flight simulator by the NASA flight test pilots and/or the configurations upon which frequency sweeps were performed. This table includes values for the wing weight, the total airplane weight, and the I_{XX}, I_{YY}, I_{ZZ}, and I_{XZ} body-axis inertias of the megatransport which were programmed into the simulator for each configuration.

Table C1 Megatransport Wing Weight, Total Airplane Weight, and Body-Axis Inertias Calculated for the Various Test Conditions (Ref. 43)

Test Condition[1]	Wing Weight (lb)	Total Airplane Weight (lb)	I_{xx} (sl-ft^2)	I_{yy} (sl-ft^2)	I_{zz} (sl-ft^2)	I_{xz} (sl-ft^2)
Baseline Configuration	162,585	948,650	57,995,453	59,538,365	114,154,212	3,154,588
Conventional Control Surfaces Operational	162,585	948,650	57,995,453	59,538,365	114,154,212	3,154,588
Manual Throttles	162,585	948,650	57,995,453	59,538,365	114,154,212	3,154,588
Engines Moved 20 Feet Outboard	141,937	928,002	72,576,832	58,989,219	128,392,879	2,734,967
Engines Moved 20 Feet Outboard With 10 Knot Crosswind From The Right	141,937	928,002	72,576,832	58,989,219	128,392,879	2,734,967
Engines Moved 40 Feet Outboard	116,792	902,857	90,391,137	59,759,694	147,138,831	2,512,673
Engines Moved 20 Feet Inboard	178,697	964,762	46,648,096	61,430,452	104,444,836	3,749,887
Outer Engine Moved 20 Feet Outboard; Inner Engine Moved 20 Feet Inboard	155,385	941,451	63,147,005	61,675,925	121,368,676	3,433,669
Outer Engine Moved 20 Feet Inboard; Inner Engine Moved 20 Feet Outboard	165,248	951,313	56,078,011	58,743,418	111,468,624	3,051,265

Table C1 Megatransport Wing Weight, Total Airplane Weight, and Body-Axis Inertias Calculated for the Various Test Conditions (cont.)

Test Condition[1]	Wing Weight (lb)	Total Airplane Weight (lb)	I_{xx} (sl-ft^2)	I_{yy} (sl-ft^2)	I_{zz} (sl-ft^2)	I_{xz} (sl-ft^2)
Engines Moved 5 Feet Vertically Downward	162,585	948,650	58,434,396	59,977,308	114,154,212	3,370,201
Engines Moved Vertically Upward[2]	162,585	948,650	57,995,453	59,538,365	114,154,212	3,154,588
Engines Moved Vertically Upward Into Wing[3]	162,585	948,650	57,708,921	59,251,834	114,154,212	2,731,278
Engines Moved Vertically Upward 2.5 Feet Above Wing[4]	162,585	948,650	57,753,024	59,295,937	114,154,212	2,623,446
Engines Moved Vertically Upward 2.5 Feet Above Wing[4] - Manual Throttles	162,585	948,650	57,753,024	59,295,937	114,154,212	2,623,446
Engines Moved Vertically Upward Above Wing[4]	162,585	948,650	57,995,453	59,538,365	114,154,212	3,154,588
Full (50 Degrees) Flaps	162,585	948,650	57,995,453	59,538,365	114,154,212	3,154,588
Gear Down	162,585	948,650	57,995,453	59,538,365	114,154,212	3,154,588
Outboard Engine Inoperative	162,585	948,650	57,995,453	59,538,365	114,154,212	3,154,588

Table C1 Megatransport Wing Weight, Total Airplane Weight, and Body-Axis Inertias Calculated for the Various Test Conditions (cont.)

Test Condition[1]	Wing Weight (lb)	Total Airplane Weight (lb)	I_{xx} (sl-ft^2)	I_{yy} (sl-ft^2)	I_{zz} (sl-ft^2)	I_{xz} (sl-ft^2)
Engine Time Constant Of Zero Seconds (Instantaneous Response)	162,585	948,650	57,995,453	59,538,365	114,154,212	3,154,588
Engine Time Constant Of 0.5 Seconds	162,585	948,650	57,995,453	59,538,365	114,154,212	3,154,588
Engine Time Constant Of 3.0 Seconds	162,585	948,650	57,995,453	59,538,365	114,154,212	3,154,588
Intermediate Turbulence	162,585	948,650	57,995,453	59,538,365	114,154,212	3,154,588

1 All listed test conditions are deviations from the baseline airplane configuration.

2 Inboard engines were below megatransport C.G. and outboard engines were at megatransport C.G.

3 Inboard engines were below megatransport C.G. and outboard engines were above megatransport C.G.

4 Inboard and outboard engines were above megatransport C.G.

APPENDIX D

MEGATRANSPORT TURBULENCE MODEL

[Refs. 41,49,54]

The megatransport simulation includes a Dryden continuous random turbulence model that calculates turbulence velocities and angular rates (u, v, w, p, q, and r). Crosswind components can also be added as a function of altitude.

The Dryden form was used in the megatransport simulator because it is simpler to implement than the von Karman form. Although the von Karman form is generally accepted as fitting available turbulence data somewhat better, the complexity that the von Karman form requires to simulate real-world atmospheric disturbances is often a drawback.

Modeling items such as boundary layer effects, patchiness, correlation of turbulence with steady wind velocity and terrain, and detailed wind shear characteristics can require an extraordinary effort. To alleviate this problem, the simpler Dryden disturbance model was used. This model retains all the essential features found to be useful in many piloted simulator handling quality investigations using complex disturbance models.

The standard random wind component consists of the basic Dryden spectral form for each of the translational and rotary components. The translational spectral forms are:

$$\Phi_{u_g}(\Omega) = \sigma_u^2 \frac{2L_u}{\pi} \frac{1}{1+(L_u\Omega)^2} \qquad \text{[Eqn. D1]}$$

$$\Phi_{v_g}(\Omega) = \sigma_v^2 \frac{L_v}{\pi} \frac{1+3(L_v\Omega)^2}{\left[1+(L_v\Omega)^2\right]^2} \qquad \text{[Eqn.D2]}$$

$$\Phi_{w_g}(\Omega) = \sigma_w^2 \frac{L_w}{\pi} \frac{1+3(L_w\Omega)^2}{\left[1+(L_w\Omega)^2\right]^2} \qquad \text{[Eqn. D3]}$$

where $\Omega = (\omega/V_{ref})$ and b is the wing span. u_g, v_g, and w_g are the gust velocities in the x-, y-, and z-directions, respectively. L_u, L_v, and L_w are the corresponding scales of turbulence and σ_u, σ_v, and σ_w the corresponding gust intensities.

The angular velocities due to turbulence are defined as follows:

$$-\dot{\alpha}_g = q_g = \left(\partial w_g / \partial x\right) \qquad \text{[Eqn. D4]}$$

$$p_g = -\left(\partial w_g / \partial y\right) \qquad \text{[Eqn. D5]}$$

$$r_g = -\left(\partial v_g / \partial x\right) \qquad \text{[Eqn. D6]}$$

The spectra of the angular velocity disturbances due to turbulence are then given by:

$$\Phi_{p_g}(\Omega) = \frac{\sigma_w^2}{L_w} \frac{0.8(\pi L_w/4b)^{1/3}}{1+\left[(4b/\pi)\Omega\right]^2} \qquad \text{[Eqn. D7]}$$

$$\Phi_{q_g}(\Omega) = \frac{\Omega^2}{1 + \left[(4b/\pi)\Omega\right]^2} \Phi_{w_g}(\Omega) \qquad \text{[Eqn. D8]}$$

$$\Phi_{r_g}(\Omega) = \frac{\Omega^2}{1 + \left[(3b/\pi)\Omega\right]^2} \Phi_{v_g}(\Omega) \qquad \text{[Eqn. D9]}$$

The mean-square turbulence velocity is found by integrating the power spectrum over all positive spatial frequencies:

$$\sigma_i^2 = \int_0^\infty \Phi_i(\Omega) d\Omega; \qquad i = u, v, \text{ or } w \qquad \text{[Eqn. D10]}$$

The root-mean-square velocity, or standard deviation, σ_i, is the square root of the integral in Equation D10.

The megatransport simulator is programmed such that the user can input any desired values of the variables σ_u, σ_v, σ_w, L_u, L_v, L_w, and V_{ref} or can choose instead to use the preprogrammed levels of turbulence by selecting 'light', 'intermediate', 'moderate', or 'heavy' turbulence. The values of the turbulence variables for the various levels are as follows:

- L_u = 1,750 ft
- L_v = 1,750 ft
- L_w = 500 ft
- V_{ref} = 200 kts

for all levels.

Light Turbulence

- $\sigma_u = 1.0$
- $\sigma_v = 1.0$
- $\sigma_w = 0.5$

Intermediate Turbulence

- $\sigma_u = 3.0$
- $\sigma_v = 3.0$
- $\sigma_w = 1.5$

Moderate Turbulence

- $\sigma_u = 5.0$
- $\sigma_v = 5.0$
- $\sigma_w = 2.5$

Heavy Turbulence

- $\sigma_u = 10.0$
- $\sigma_v = 10.0$
- $\sigma_w = 5.0$

In addition, a crosswind component can be added to the turbulence model. The crosswind component, or wind shear, is represented by wind speed and direction at different altitudes as follows:

$$u_g = V_{wind} \cos\psi \qquad \text{[Eqn. D11]}$$

$$v_g = V_{wind} \sin\psi \qquad \text{[Eqn. D12]}$$

where V_{wind} is the wind speed and ψ the wind direction angle. A different wind speed and direction can be specified for up to eleven different altitudes.

All of the test runs, with the exception of one, were flown in light turbulence, and one test point was flown with both light turbulence and a crosswind. Light turbulence was considered fairly representative of the weather conditions most usually encountered during flight.

The one test run not flown in light turbulence was flown in intermediate turbulence. This point was flown to examine how the megatransport PCA system responded to more severe atmospheric disturbances. Intermediate turbulence was selected as being representative of fairly strong gusts and thermals. According to test pilot A, intermediate turbulence is about as severe as a pilot would normally encounter. Pilot A stated that intermediate turbulence was "like a hot summer day out here [NASA Dryden] with big thermals . . . Heavy [turbulence] is something you seldom see. Maybe once in my life I've seen heavy turbulence."

APPENDIX E

TEST PILOT BIOGRAPHICAL DATA

EINAR ENEVOLDSON

Einar Enevoldson is a flight test consultant and test pilot for E-Systems and an X-31 senior flight control engineer for PRC, Inc. at NASA's Dryden Flight Research Center. He is also involved as a test pilot for various contractors in testing and evaluating new sailplane designs.

Enevoldson, a former Air Force pilot, was a NASA research pilot at NASA Dryden from 1968 until his retirement in 1988. Some of the projects he has participated in include principal pilot for general aviation advanced control systems development, fighter handling qualities relating to gun tracking, evaluation of the fighter supercritical wing TACT using an F-111 testbed, F-14 stall/spin prevention system, flight testing of a special control system algorithm to reduce pilot induced oscillations on the Space Shuttle, and F-111 mission adaptive continuously variable camber wing.

In addition, he was project pilot on the F-111 integrated propulsion control aircraft development and evaluation, F-18 stall/spin research program, and a participating pilot in the X-24B lifting body project, YF-12A high speed aircraft, and the F-8 fly-by-wire and oblique wing programs.

Enevoldson has piloted over 75 different types of aircraft, including the T-6, T-28, T-33, T-37, T-38, F-86, F-104, F-111, F-14, F-15, B-57, F-18, Jet Provost, Meteor, Hunter, Javelin, Lightning, Sabreliner, DC-3, KC-135, JetStar, Viscount, F-8, and B-52, as well as approximately 35 different sailplanes.

Enevoldson attended the USAF Graduate School and the University of Wyoming, where he earned Master of Science degrees in Mechanical Engineering.

Among the awards and honors Enevoldson has received are the FAI time-to-climb record in an F-104, winner of the USAF fighter weapons competition ('William Tell'), and NASA Ames Associate Fellow.

C. GORDON FULLERTON [Ref. 77]

C. Gordon Fullerton is a NASA research pilot at NASA's Dryden Flight Research Center. His assignments include a variety of flight research and support activities including piloting NASA's 747 Shuttle Carrier Aircraft, the B-52 launch aircraft, and other multi-engine and high performance aircraft.

Fullerton, who logged more than 380 hours in space flight, was a NASA astronaut from September, 1969, until November, 1986, when he joined the research pilot office at NASA Dryden.

As project pilot on the B-52 launch aircraft, Fullerton was involved in developing a new F-111 crew module recovery system and also in the development and test of the Pegasus space launch vehicle. Fullerton also serves as project pilot on the NASA Convair 990 aircraft which has being modified as a landing systems research aircraft.

In addition to these activities, Fullerton has been project pilot on a number of other research programs at NASA Dryden. Among them were the C-140 JetStar laminar flow control, F-111 mission adaptive wing, F-14 variable sweep flow transition, space shuttle orbiter drag chute tests with the B-52, and the F-15 propulsion controlled aircraft (PCA) flights using engine thrust alone to control the flight path of the aircraft.

With over 13,000 hours of flying time, Fullerton has piloted 112 different types of aircraft. Approximately half of Fullerton's flight time has been in large transport aircraft (KC-135, C-140, B-47, B-52, Convair 990, DC-8, MD-11, Boeing 747, and Space Shuttle), the other half in high

performance aircraft (T-33, T-34, T-37, T-38, T-39, F-86, F-101, F-104, F-106, F-111, F-14, F-15, F-18, and X-29).

Fullerton received Bachelor of Science and Master of Science degrees in Mechanical Engineering from the California Institute of Technology, Pasadena, California. Fullerton, inducted into the International Space Hall of Fame in 1982, is a Fellow of the Society of Experimental Test Pilots and the American Astronautical Society.

Among the special awards and honors Fullerton has received are the Iven C. Kincheloe Award from the Society of Experimental Test Pilots, Department of Defense Distinguished Service and Superior Service medals, Air Force Distinguished Flying Cross, NASA Distinguished and Exceptional Service medals, NASA Space Flight Medals, General Thomas D. White Space Trophy, Haley Space Flight Award from the American Institute of Aeronautics and Astronautics, and the Certificate of Achievement Award from the Soaring Society of America.

APPENDIX F

MEGATRANSPORT PRE-FLIGHT BRIEFING HANDOUT

DESIGN, ANALYSIS, AND CONTROL OF A LARGE TRANSPORT AIRCRAFT UTILIZING SELECTIVE ENGINE THRUST AS A BACKUP SYSTEM FOR THE PRIMARY FLIGHT CONTROLS

BY

DONNA S. GERREN
UNIVERSITY OF KANSAS
NASA DRYDEN FLIGHT RESEARCH CENTER
NASA GRANT NAG 2-789

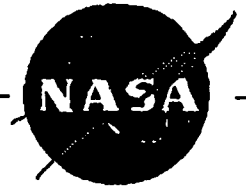

PURPOSE AND OBJECTIVES

- IS IT POSSIBLE TO ARRANGE THE ENGINES IN A LARGE PASSENGER TRANSPORT IN SUCH A WAY THAT FLIGHT PATH CONTROL USING ONLY THE ENGINES IS NOT ONLY POSSIBLE, BUT MEETS LEVEL 1 OR LEVEL 2 FLYING QUALITY REQUIREMENTS?

- SINCE TOTAL FAILURE OF THE PRIMARY FLIGHT CONTROL SYSTEM CAN BE CAUSED BY THE FAILURE OF AN ENGINE, CAN THE NUMBER OF ENGINES AND THEIR ARRANGEMENT BE SELECTED SUCH THAT FLIGHT PATH CONTROL WITH ONE ENGINE INOPERATIVE IS STILL POSSIBLE WITH LEVEL 1 OR LEVEL 2 FLYING QUALITY REQUIREMENTS?

- CAN ONE OR MORE LEVELS OF PRIMARY FLIGHT CONTROL SYSTEM REDUNDANCY BE ELIMINATED IN AN AIRPLANE EQUIPPED WITH A LEVEL 1 OR LEVEL 2 ENGINE CONTROL SYSTEM, ALLOWING THE ENGINE THRUST TO BE USED AS A BACKUP FLIGHT CONTROL SYSTEM?

Megatransport Mission Specifications

- Role
  - 800 passenger capacity commercial jet transport aircraft
- Crew
  - 2 flight crews - each flight crew consisting of 1 pilot and 1 co-pilot
  - 16 flight attendants
- Payload
  - Each crewmember is allowed 30 lb of baggage
  - Each passenger is allowed 40 lb of baggage
- Performance
  - Range: 5,000 nautical miles
  - Cruise Speed: M = 0.85 at 35,000 ft
  - Cruise Altitude: 35,000 ft
  - Service Ceiling: 40,000 ft
  - Field Length: 10,000 ft @ 5,000 ft field elevation, 95°F day
  - Climb: Direct climb to cruise altitude
- Powerplant
  - 4 turbofan engines
- Certification
  - FAR 25
- Fuel Reserves
  - Must meet FAR 121.645 fuel supply requirements for turbine-engine-powered flag carrier operations

Summary of Geometry and Weight Data for the Megatransport

GEOMETRY

Wing

- S_W, wing area ..... 11,900 ft^2
- b_W, wing span ..... 318.0 ft
- AR_W, wing aspect ratio 8.5
- λ_W, wing taper ratio 0.30
- $\Lambda_{WC/4}$, wing quarter-chord sweep ..... 30 deg
- C_W, wing mean geometric chord ..... 41.0 ft
- C_{rW}, wing root chord ..... 57.6 ft
- C_{tW}, wing tip chord ..... 17.3 ft

Horizontal Tail

- S_h, horizontal tail area ..... 2,800 ft^2
- b_h, horizontal tail span ..... 105.8 ft

Vertical Tail

- S_V, vertical tail area ..... 2,019 ft^2
- b_V, vertical tail span ..... 56.8 ft

Fuselage

- L_{fus}, fuselage length ..... 277 ft
- D_{fus}, average fuselage diameter ..... 25 ft

WEIGHT

- W_{PL}, payload weight ..... 186,500 lb
- W_E, empty weight ..... 683,400 lb
- W_F, fuel weight ..... 541,400 lb
- W_{TO}, gross takeoff weight ..... 1,421,900 lb

EVALUATE MEGATRANSPORT SIMULATION FLYING QUALITIES

- VARY PARAMETERS WHICH COULD AFFECT FLYING QUALITIES OF THE MEGATRANSPORT
  - PLACEMENT OF ENGINES (VERTICAL AND LATERAL)
  - ENGINE OUT
  - ENGINE TIME CONSTANTS
  - FLAPS/SLATS
- ASSIGN THE FLYING QUALITIES A RATING ON THE COOPER-HARPER SCALE
- DETERMINE UNDER WHAT CONDITIONS LEVEL 1 OR LEVEL 2 FLYING QUALITIES ARE OBTAINABLE WITH TOTAL PRIMARY FLIGHT CONTROL SYSTEM FAILURE

APPENDIX G

PILOT'S COMMENTS,

COOPER-HARPER PILOT RATINGS,

AND

FLIGHT VARIABLE PLOTS

OF THE

TEST POINTS FLOWN IN THE

MEGATRANSPORT SIMULATOR

Table G1 Megatransport Simulator Flight Test Matrix with Cooper-Harper Pilot Ratings

Test Condition[1]	PCA Engaged	Test Pilot A				Test Pilot B			
			Cooper-Harper Pilot Ratings				Cooper-Harper Pilot Ratings		
		Test Run Number	Long.	Lat.-Dir.	Overall	Test Run Number	Long.	Lat.-Dir.	Overall
Baseline Configuration	Yes	A1/A14	4/3	4/4	5/-	B1/B15	2/3	3/4	3/-
Engines Moved 20 Feet Outboard	Yes	A2/A17	3/3	5/4	5/-	B2	2	3	3
Engines Moved 20 Feet Inboard	Yes	A3	3	5	5	B3	2	3	3
Engines Moved 5 Feet Vertically Downward	Yes	A4	3	5	5	B4	2	3	3
Full (50 Degrees) Flaps	Yes	A5	3	5	5	B5	2	3	3
Outboard Engine Inoperative	Yes	A6/A10	6/6	3/5	6/7	B6	5	4	5
Engine Time Constant of 3.0 sec	Yes	A7	3	4	6	B7	5	4	5
Engine Time Constant of 0.5 sec	Yes	A8	4	4	5	B8	4	4	4
Intermediate Turbulence	Yes	A9	4	4	5	B9	6	6	6
Manual Throttles	No	A11/A12	-/7	-/7	-/7	B10/B14	5/5	5/6	5/-
Conventional Control Surfaces Operational	No	A13	3	5	-	B13	2	2	2

Table G1 Megatransport Simulator Flight Test Matrix with Cooper-Harper Pilot Ratings (cont.)

Test Condition[1]	PCA Engaged	Test Pilot A				Test Pilot B			
			Cooper-Harper Pilot Ratings				Cooper-Harper Pilot Ratings		
		Test Run Number	Long.	Lat.-Dir.	Overall	Test Run Number	Long.	Lat.-Dir.	Overall
Engines Moved Vertically Upward Into Wing[2]	Yes	A15	3	4	-	B16	5	4	-
Engines Moved Vertically Upward 2.5 Feet Above Wing[3]	Yes	A16	5	4	-	B17	5	4	-
Engines Moved 20 Feet Outboard With 10 Knot Crosswind From The Right	Yes	A18	3	4	-				
Engines Moved Vertically Upward[4]	Yes					B11	4	4	4
Engines Moved Vertically Upward Above Wing[3]	Yes					B12	10	10	10
Engines Moved Vertically Upward 2.5 Feet Above Wing[3] - Manual Throttles	No					B18	9	9	9

1 All listed test conditions are deviations from the baseline airplane configuration.

2 Inboard engines were below megatransport C.G. and outboard engines were above megatransport C.G.

3 Inboard and outboard engines were above megatransport C.G.

4 Inboard engines were below megatransport C.G. and outboard engines were at megatransport C.G.

TEST PILOT A

TEST POINTS A1 - A18

Megatransport/PCA System Pre-Test

Check-Out Flight And Landing By Test Pilot A

Comments During Flight

Test Pilot A: Wow, a sharp response here. 14 feet per second (touchdown rate) - that's about your gear limit so you've got to flare a little given the initial trim conditions. It's pretty amazing how well this thing flies.

Test Point A1

Baseline Configuration With PCA

Comments During Flight

none

Post-Flight Comments

Test Pilot A (TPA): It really flies amazingly well. I think it flies extremely well.

Author (DG): That PCA system's amazing.

TPA: It really is - I'm impressed.

DG: You can hardly believe you're flying using the engines.

TPA: Yeah, that's right. Even with the lags and everything in there, it really does work impressively well.

Pilot Comment Card

I. Longitudinal Configuration

Pitch attitude response in general - very good

Predictability of final response - very good

Cooper-Harper pilot rating - 4

II. Lateral-Directional Configuration

Roll response in general - very good

Roll tendency to overshoot - very good

Tendency to maintain bank angle - very good

Heading response in general - good

Cooper-Harper pilot rating - 4

III. Summary (Brief)

Problems - hard to find bank knob position for zero change in heading angle quickly

Any special control techniques -

a) watch HUD (heads up display) like hawk

b) open loop flare one notch up (of the pitch thumbwheel) at approximately 50 feet AGL

Good features - remarkable response and stability

Suggestions -

a) might like crisper detent on bank knob

b) would like 50 foot AGL radar altimeter light

Overall Cooper-Harper pilot rating - 5

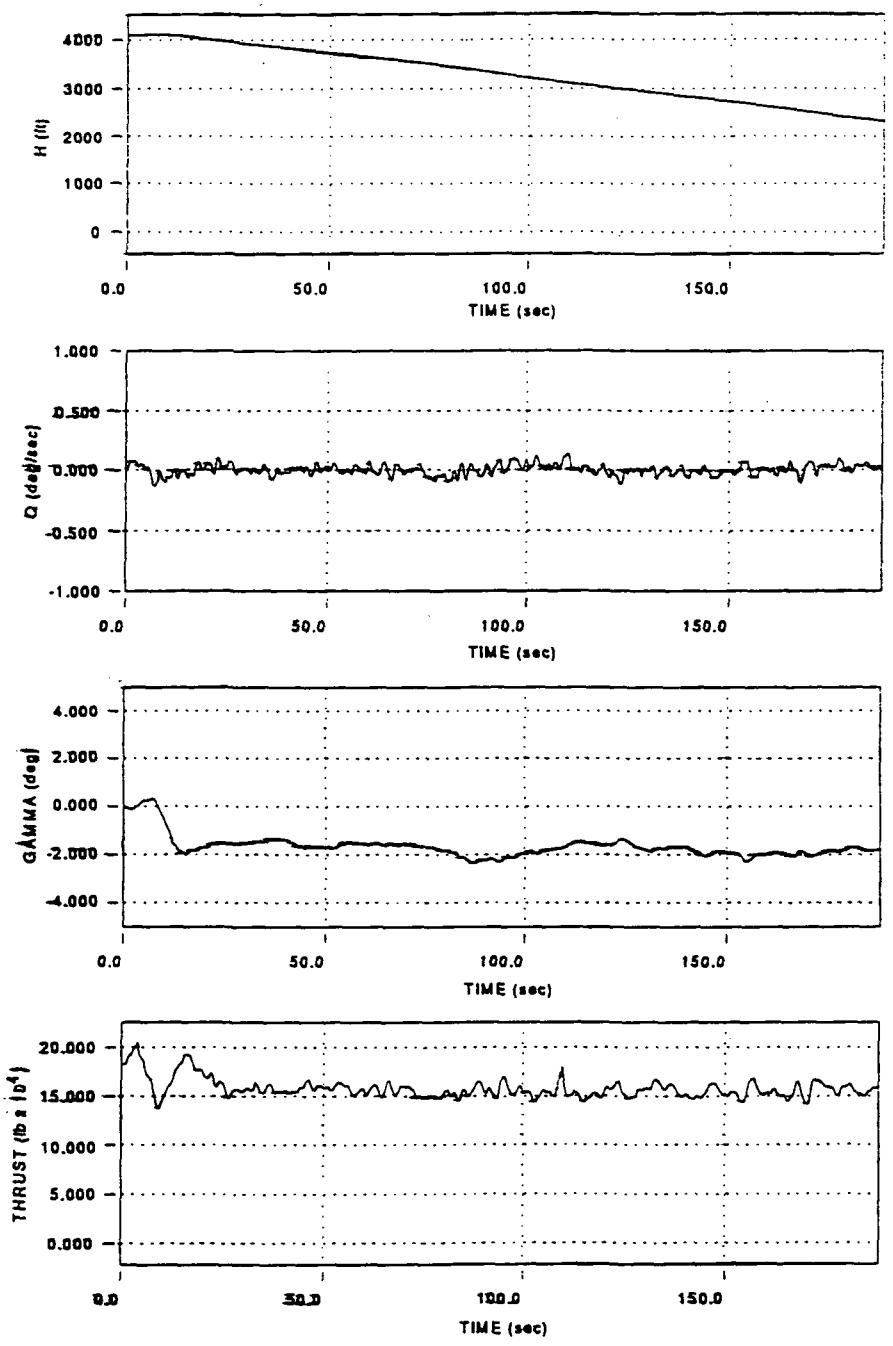

Figure G1(a) Longitudinal Flight Variables for Test Flight A1: Baseline Configuration with PCA

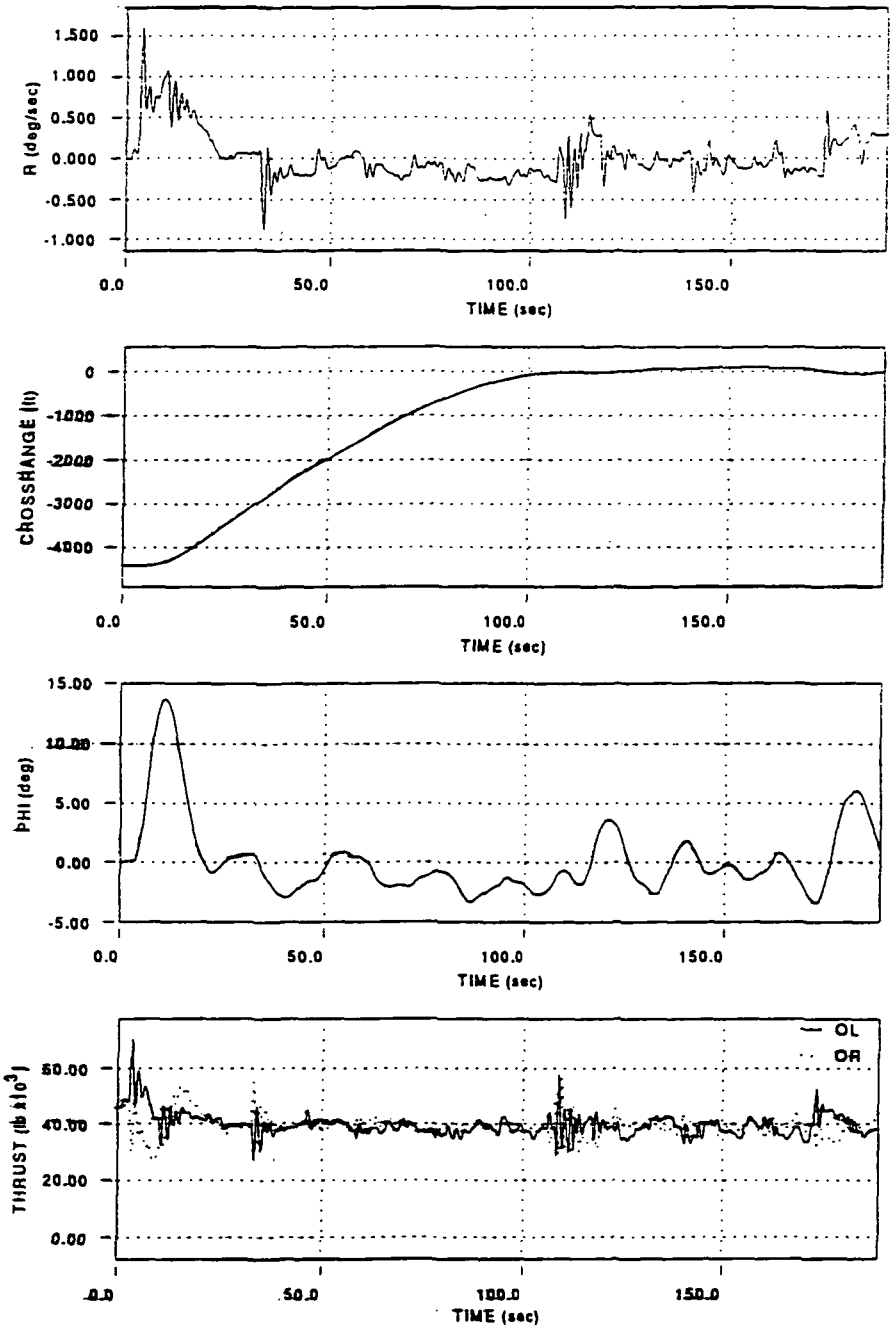

Figure G1(b) Lateral-Directional Flight Variables for Test Flight A1: Baseline Configuration with PCA

Test Point A2

Engines Moved 20 Feet Outboard With PCA

Comments During Flight

none

Post-Flight Comments

Test Pilot A: I gave roll worse (Cooper-Harper pilot rating) but, you know, plus or minus one, I wouldn't worry too much about it. Unless you really flew a couple of them and were really able to analyze it, it's basically about the same as far as I can tell. I couldn't tell any difference.

Pilot Comment Card

I. Longitudinal Configuration

Cooper-Harper pilot rating - 3

II. Lateral-Directional Configuration

Cooper-Harper pilot rating - 5

III. Summary (Brief)

Comments -

a) like test point 1, but harder to control heading angle - appeared to have more response lag in heading

b) noticed slight increase in rate of sink when rolling into turn. Not a problem for landing because only small bank used near ground.

Overall Cooper-Harper pilot rating - 5

Test Point A3

Engines Moved 20 Feet Inboard With PCA

Comments During Flight

Test Pilot A: It's (the landing's) kind of a little bit short that time, but not bad.

Post-Flight Comments

none

Pilot Comment Card

I. Longitudinal Configuration

Cooper-Harper pilot rating - 3

II. Lateral-Directional Configuration

Cooper-Harper pilot rating - 5

III. Summary (Brief)

Comments -

a) seemed similar to test point 2

b) some learning helps improve heading control

Overall Cooper-Harper pilot rating- 5

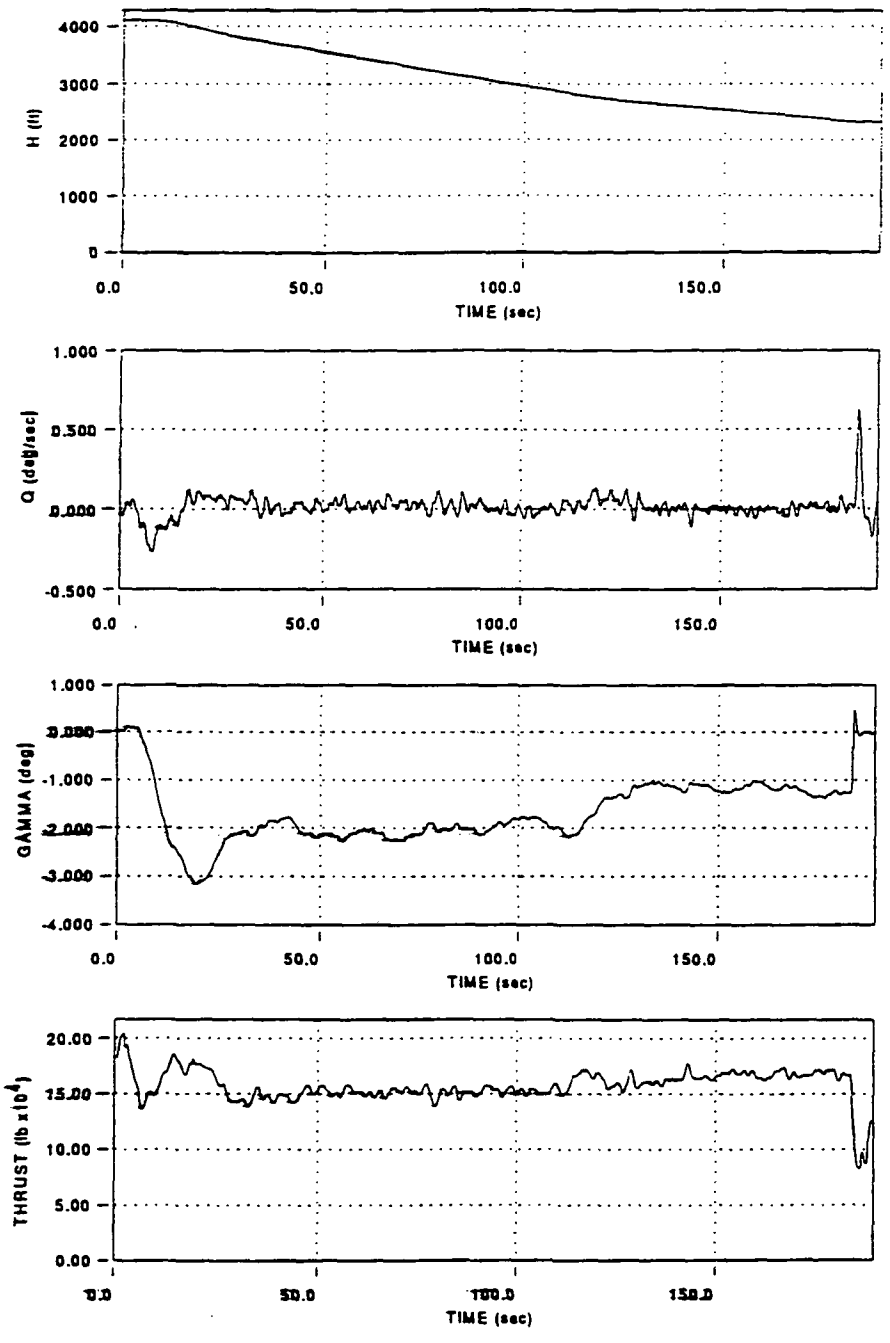

Figure G2(a) Longitudinal Flight Variables for Test Flight A3: Engines Moved 20 Feet Inboard with PCA

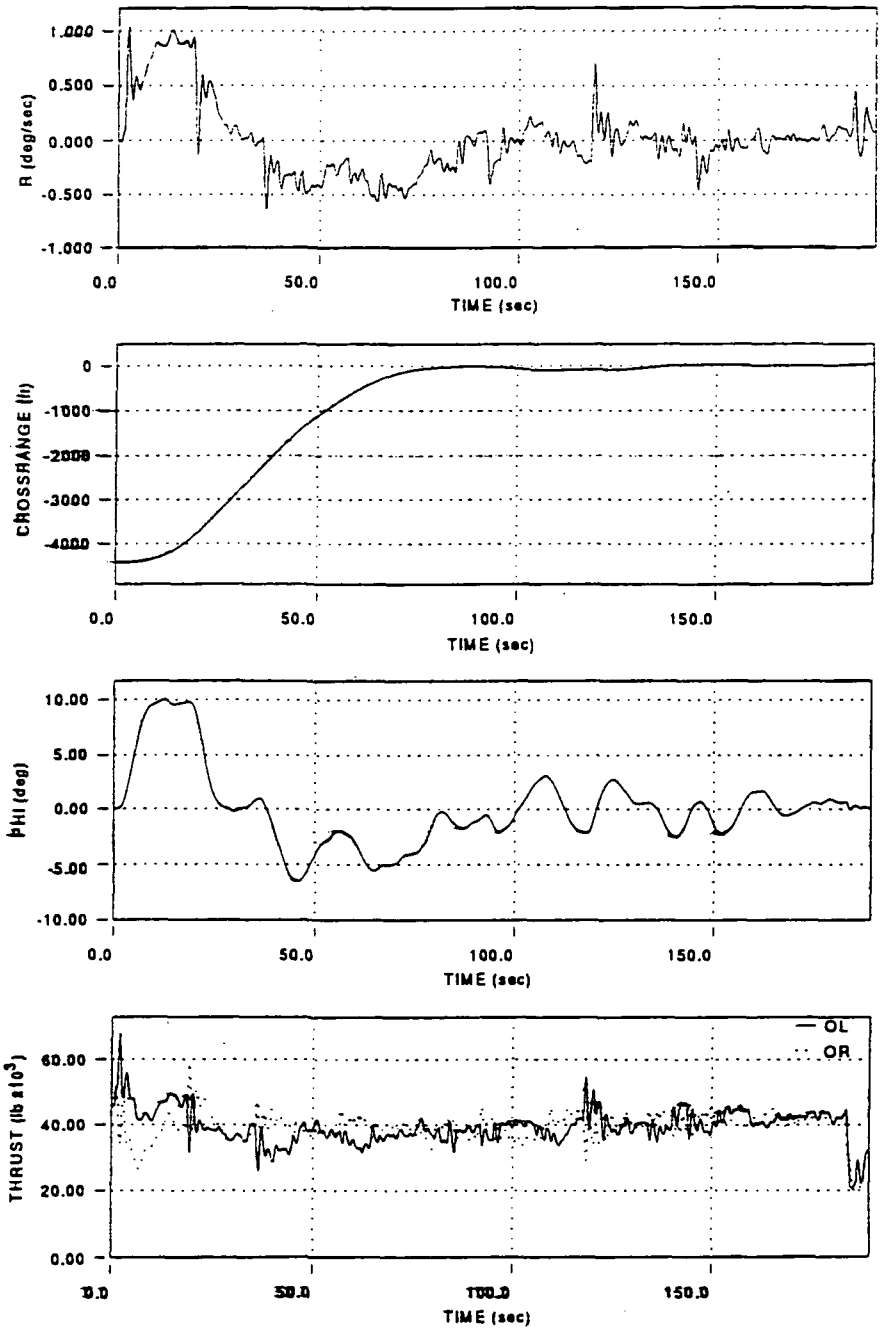

Figure G2(b) Lateral-Directional Flight Variables for Test Flight A3: Engines Moved 20 Feet Inboard with PCA

Test Point A4

Engines Moved 5 Feet Vertically Downward With PCA

Comments During Flight

Test Pilot A (TPA): Hmm, what's going on here?

Author (DG): Do you find there's a learning curve?

TPA: Oh yeah.

DG: Is there?

TPA: There's a lot, yeah.

Post-Flight Comments

TPA: That's interesting (engines moved downward). I actually said I had . . . I had it degraded, slower. Well, I think that's a real effect. I noticed that, definitely noticed that. I would have guessed you'd get better response with them down, but for whatever reason, it was worse. You've got more authority there. I think that was a fairly small effect here - it wasn't a major effect.

Pilot Comment Card

I. Longitudinal Configuration

Cooper-Harper pilot rating - 5

II. Lateral-Directional Configuration

Cooper-Harper pilot rating - 5

III. Summary (Brief)

Comments - pitch response seemed degraded - slower. Okay after adjusted piloting technique.

Overall Cooper-Harper pilot rating - 5

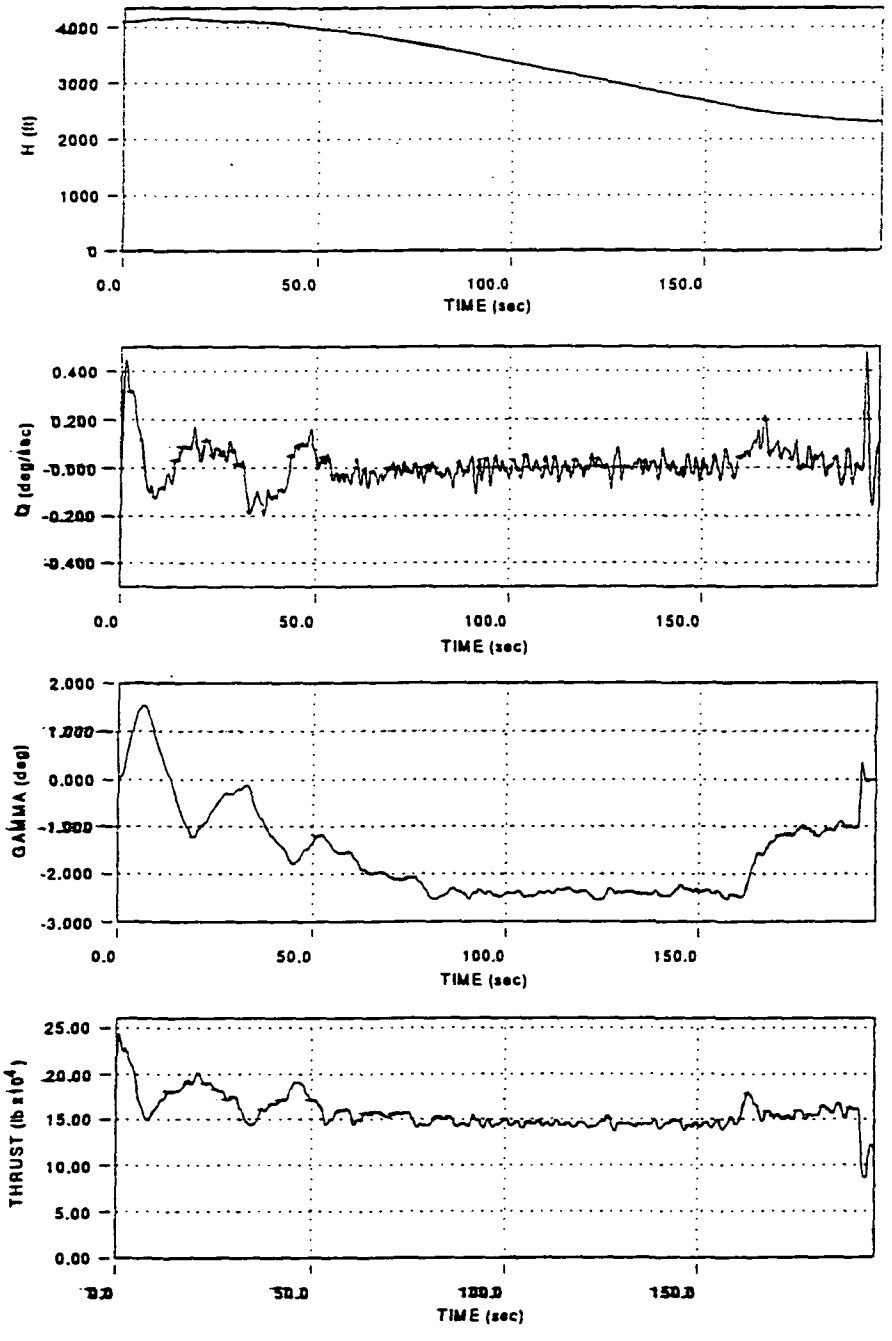

Figure G3(a) Longitudinal Flight Variables for Test Flight A4: Engines Moved 5 Feet Vertically Downward with PCA

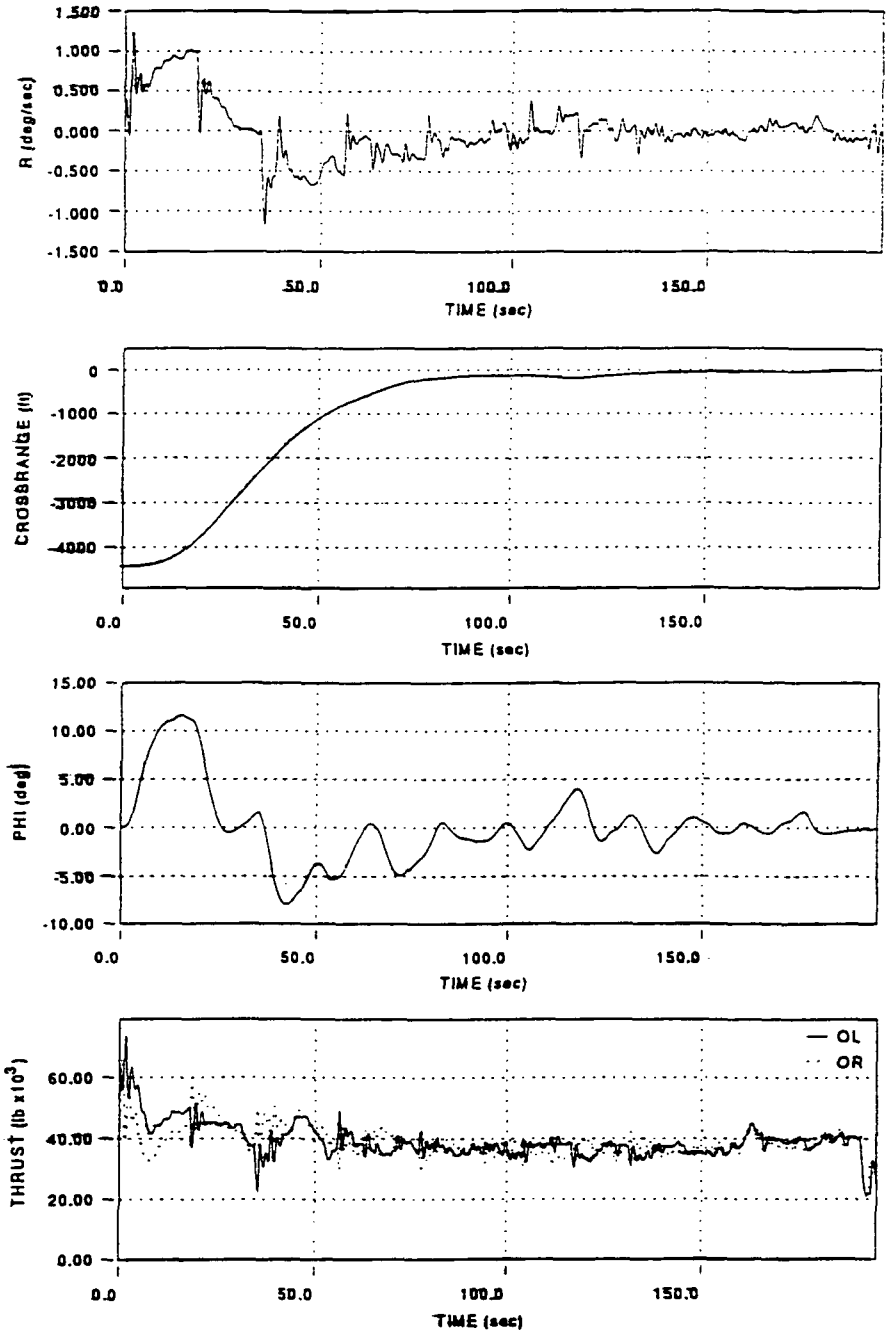

Figure G3(b) Lateral-Directional Flight Variables for Test Flight A4: Engines Moved 5 Feet Vertically Downward with PCA

Test Point A5

Full (50 Degrees) Flaps With PCA

Comments During Flight

Test Pilot A (TPA): Okay, were sitting here at 180 (knots). Boy, your control system is really handling it well, so far. Boy, it really worked well.

Author: Is it easier to land with flaps, you think?

TPA: No, I don't think that it's any easier, but it's 40 knots slower which is nice.

Post-Flight Comments

TPA: It worked great - it worked very nicely. I thought it might have felt a little more 'Dutch-rolly' or maybe a little more adverse yaw, maybe, a kind of an effective adverse yaw. I think I mentioned more difficulty maintaining centerline.

Pilot Comment Card

I. Longitudinal Configuration

Cooper-Harper pilot rating - 3

II. Lateral-Directional Configuration

Cooper-Harper pilot rating - 5

III. Summary (Brief)

Comments - very good in general - slightly more difficult to maintain centerline near touchdown

Overall Cooper-Harper pilot rating - 5

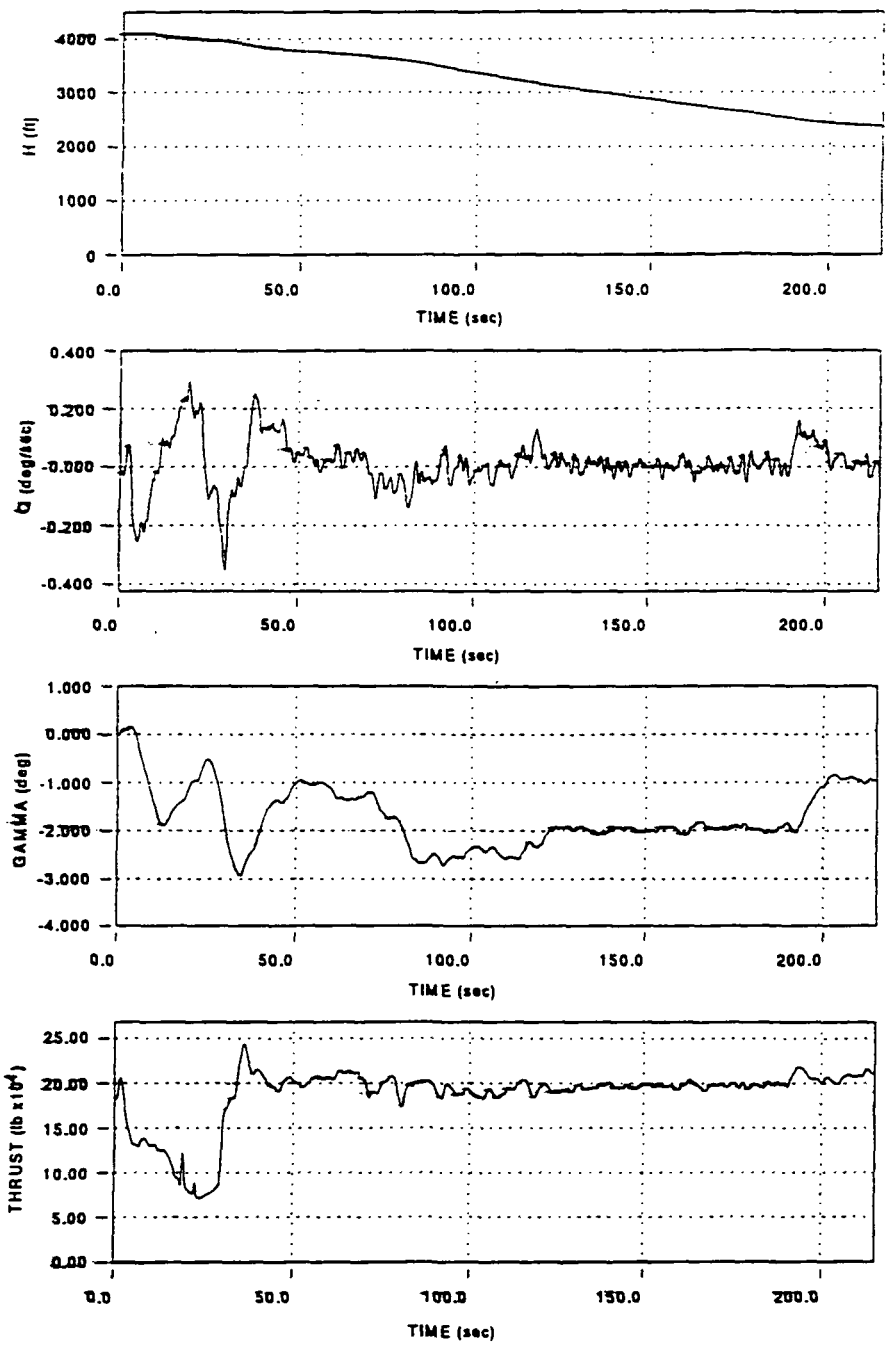

Figure G4(a) Longitudinal Flight Variables for Test Flight A5: Full (50 Degrees) Flaps with PCA

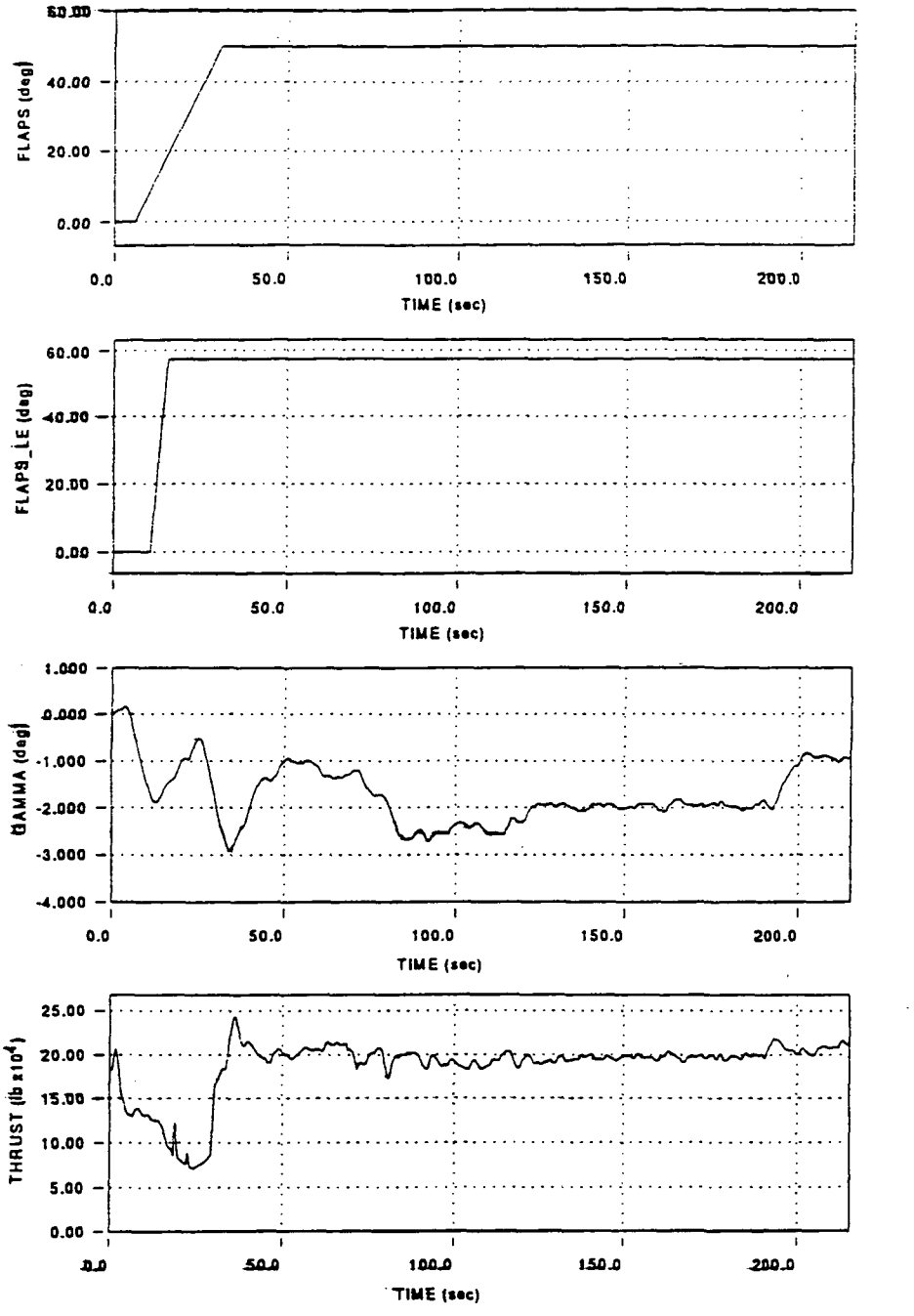

Figure G4(a) Longitudinal Flight Variables for Test Flight A5: Full (50 Degrees) Flaps with PCA (cont.)

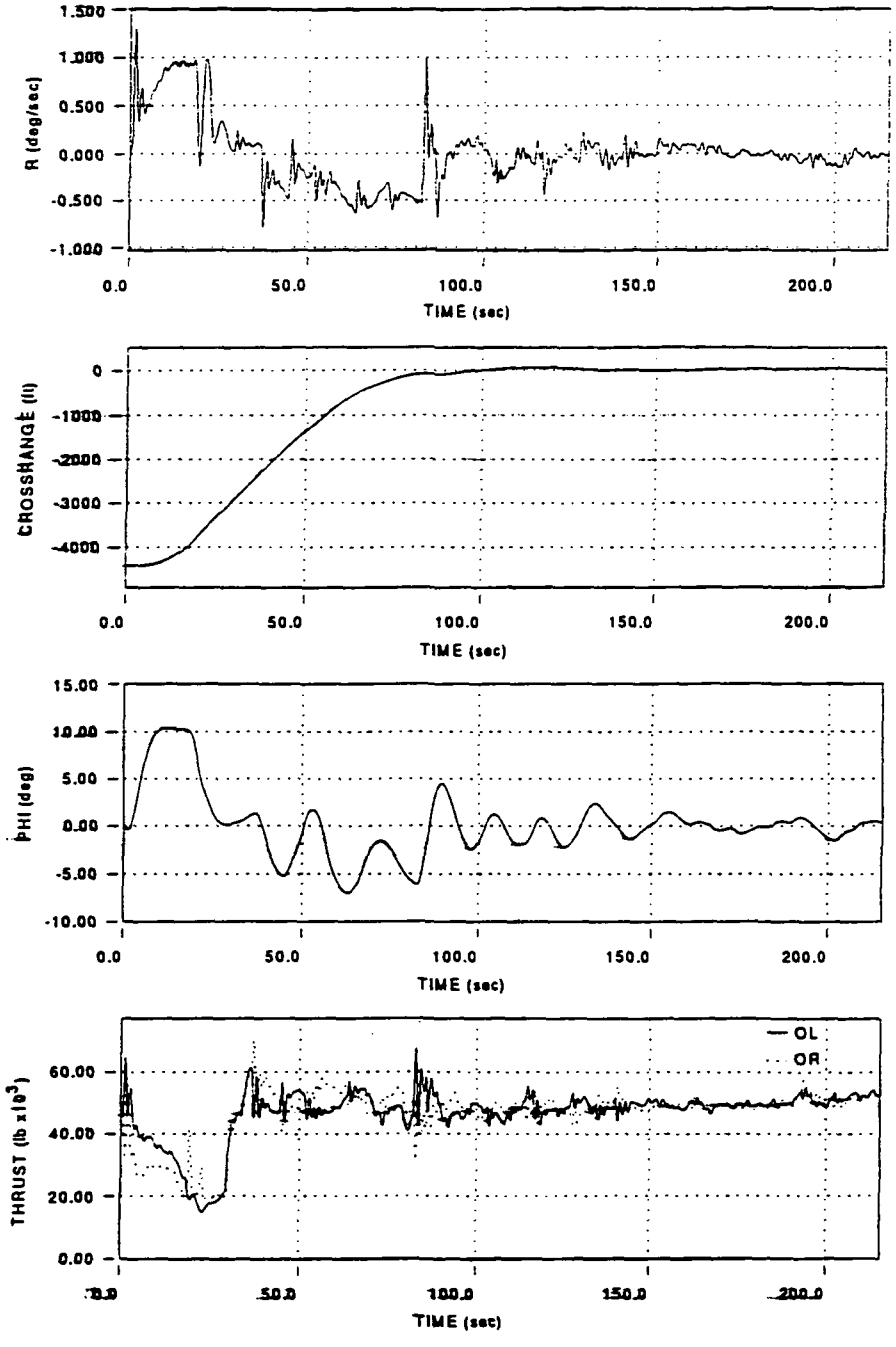

Figure G4(b) Lateral-Directional Flight Variables for Test Flight A5: Full (50 Degrees) Flaps with PCA

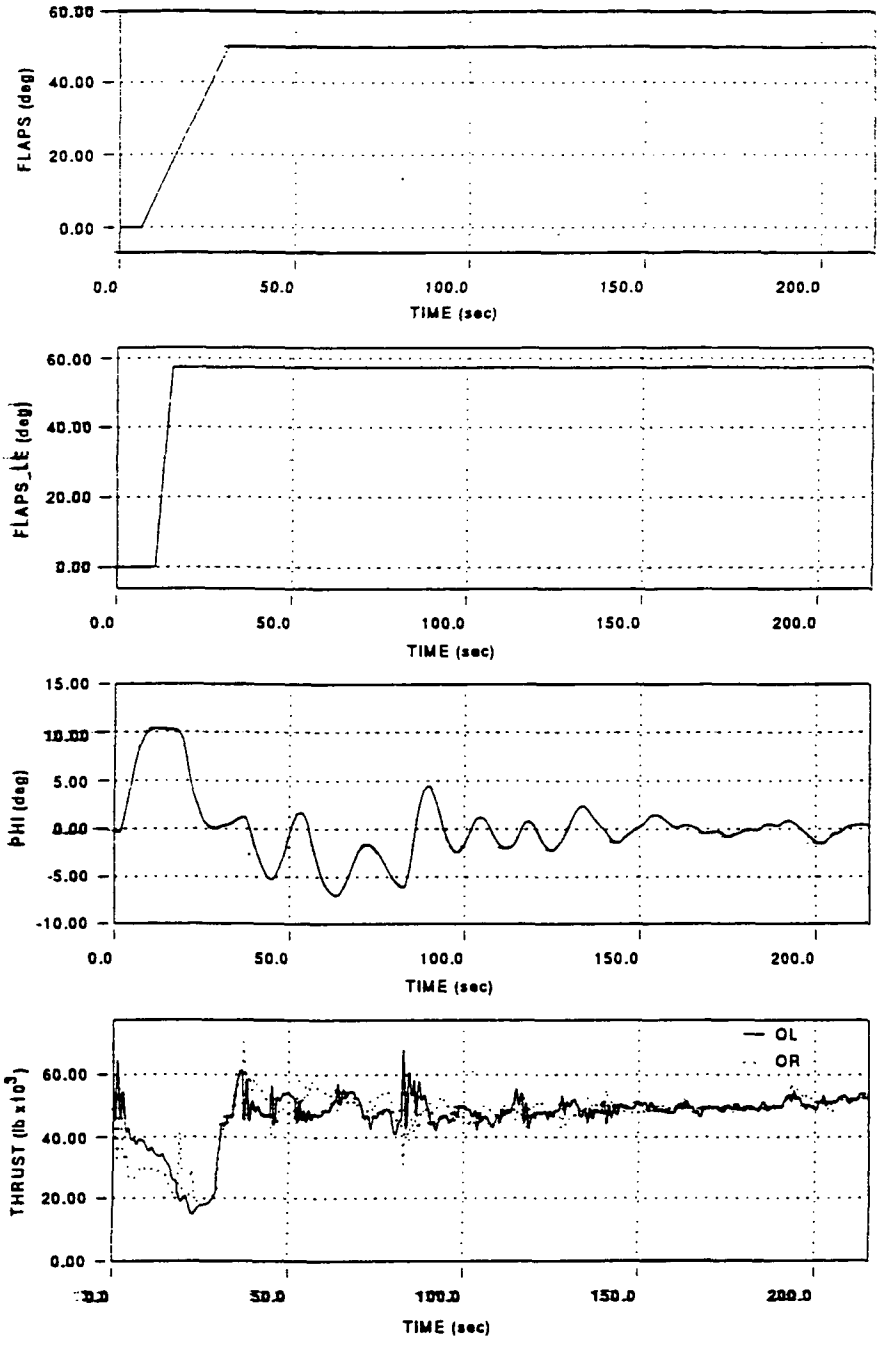

Figure G4(b) Lateral-Directional Flight Variables for Test Flight A5: Full (50 Degrees) Flaps with PCA (cont.)

Test Point A6

Outboard Engine Inoperative With PCA

Comments During Flight

Test Pilot A (TPA): Well, not too good. I don't know if the overrun counts or not, but . . . actually, I think honestly you could fly that a lot better. If that's what you were expecting, then you could get pretty good results with that even though I didn't get very good results. Potentially, the ratings are not as bad as I gave them on that one. If you want, do another one just to see what you can do when you expect it to behave that way. I know you did something to make the pitch response very weak and, like I say, potentially it's not as bad as the Cooper-Harper rating I'm giving it. We can do a repeat on that.

Post-Flight Comments

TPA: Well, it still flies acceptably, but it was definitely more difficult. Well, the first time it caught me off guard because it got into a big dive there when I went into the turn. No, I pitched over and it pitched over normally, but it just kept pitching and I lost a bunch of altitude. So, I thought if I did it again I'd be a little more careful not to lose so much altitude initially there. It was still more difficult in close, but it's amazing how well it did. Where you really notice it is in pitch. The roll is a little slower but you really notice a long delay in pitch. You can certainly handle it - it's not that bad.

Pilot Comment Card

I. Longitudinal Configuration

Cooper-Harper pilot rating - 6

II. Lateral-Directional Configuration

Cooper-Harper pilot rating - 3

III. Summary (Brief)

Comments - much poorer pitch response and stability. I think it could be satisfactory with a little practice.

Overall Cooper-Harper pilot rating - 6

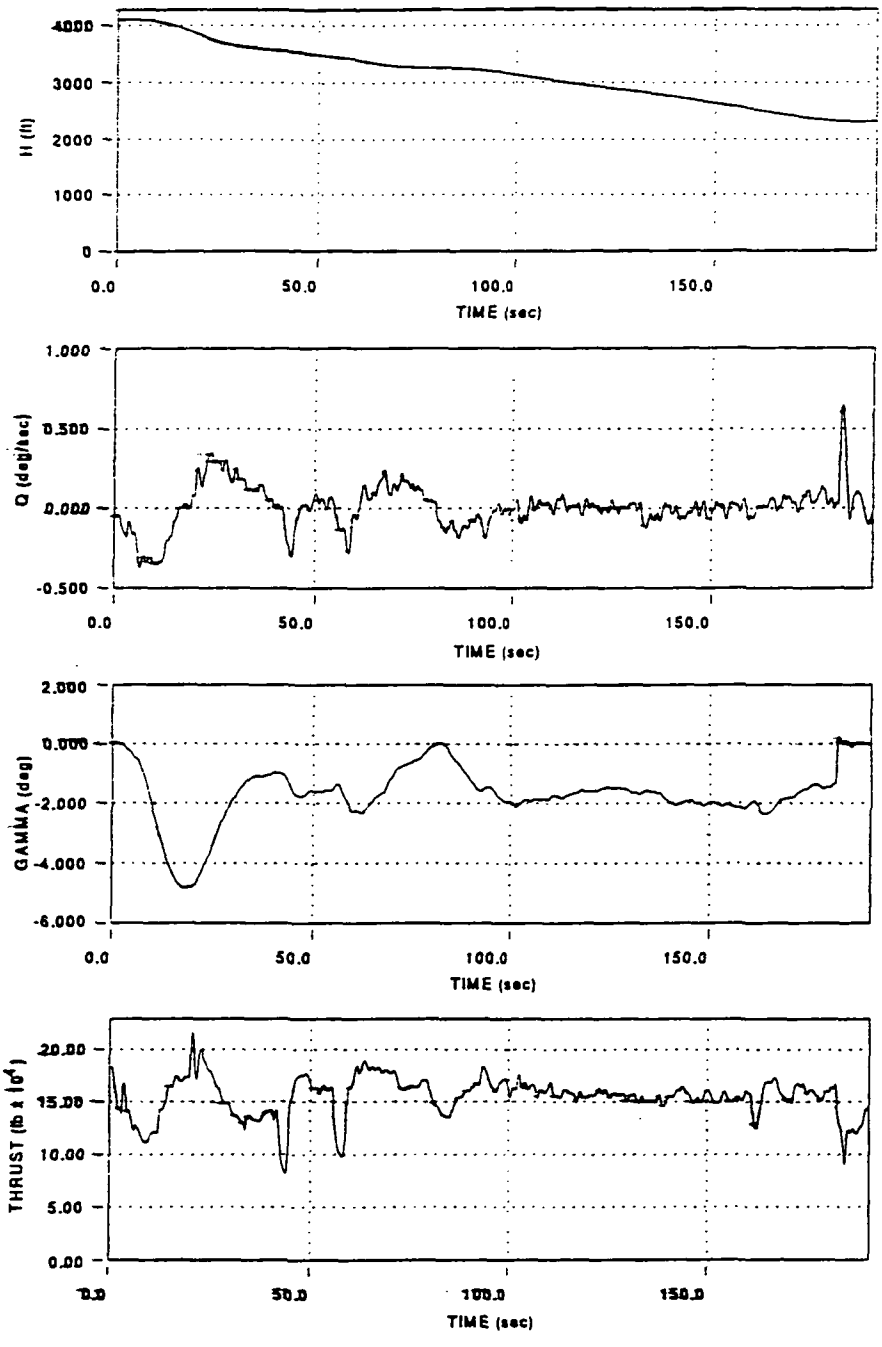

Figure G5(a) Longitudinal Flight Variables for Test Flight A6: Outboard Engine Inoperative with PCA

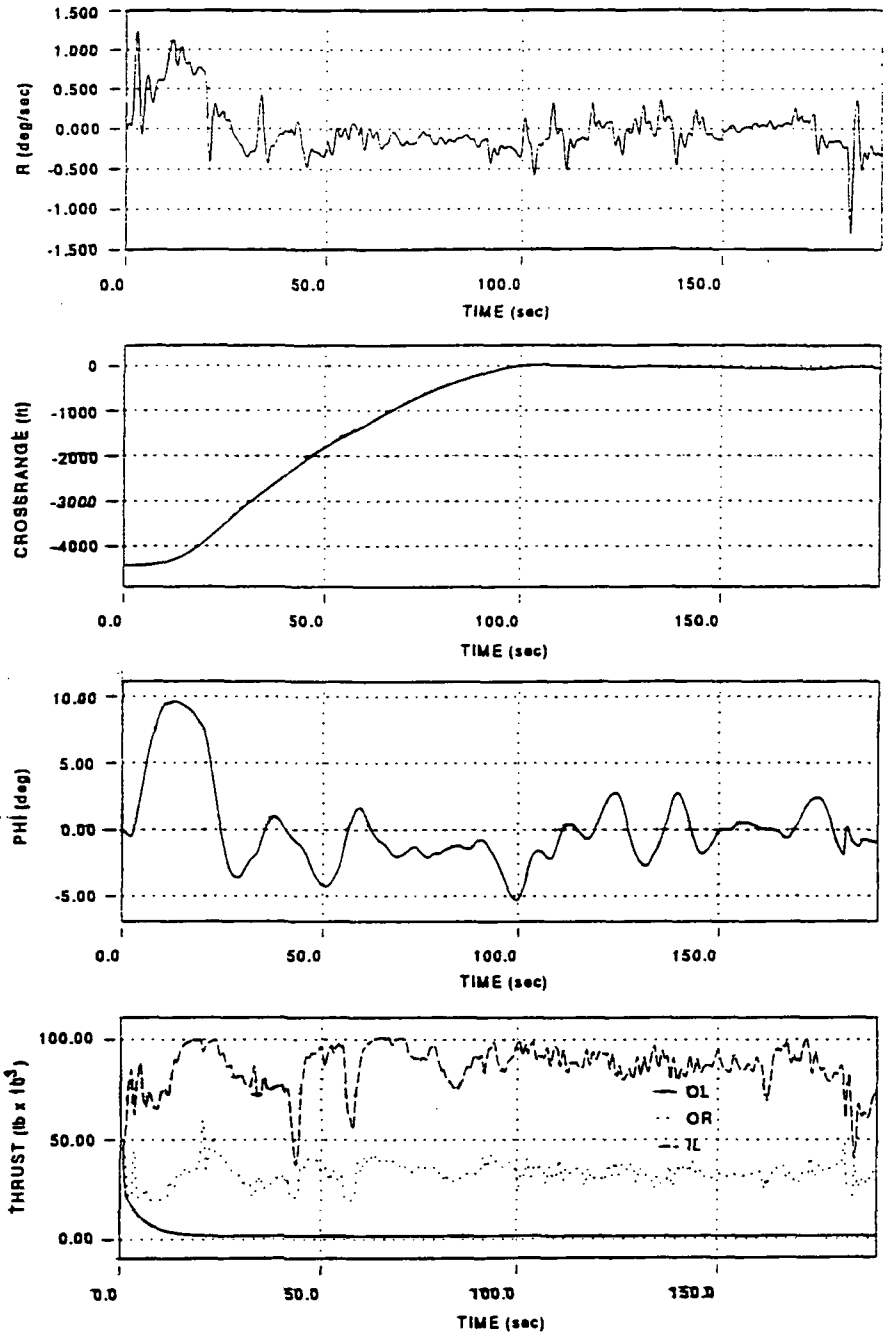

Figure G5(b) Lateral-Directional Flight Variables for Test Flight A6: Outboard Engine Inoperative with PCA

Test Point A7

Engine Time Constant Of Three Seconds With PCA

Comments During Flight

none

Post-Flight Comments

none

Pilot Comment Card

I. Longitudinal Configuration

Cooper-Harper pilot rating - 5

II. Lateral-Directional Configuration

Cooper-Harper pilot rating - 4

III. Summary (Brief)

Comments - pitch and roll response seemed somewhat looser than baseline

Overall Cooper-Harper pilot rating - 6

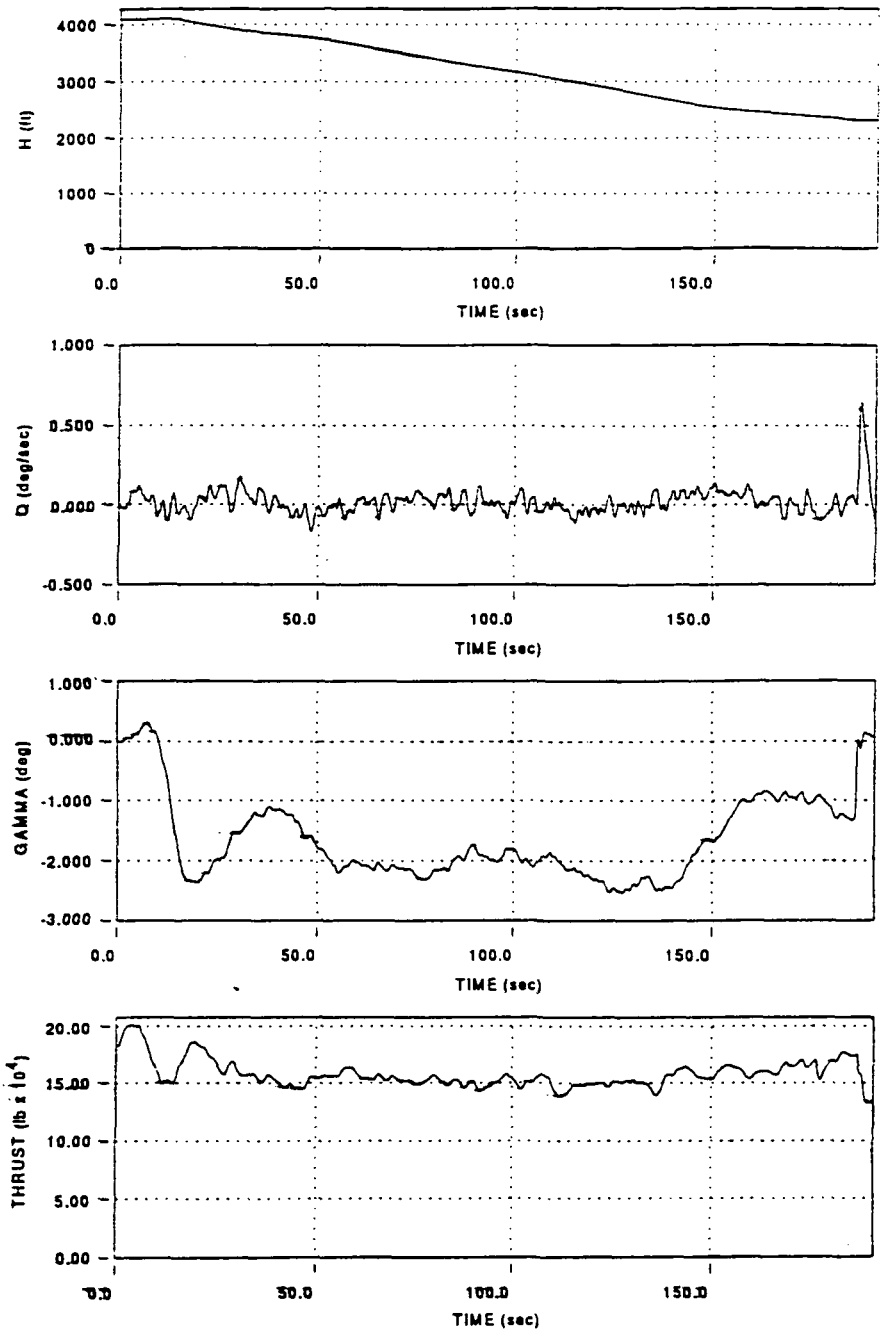

Figure G6(a) Longitudinal Flight Variables for Test Flight A7: Engine Time Constant of 3.0 Seconds with PCA

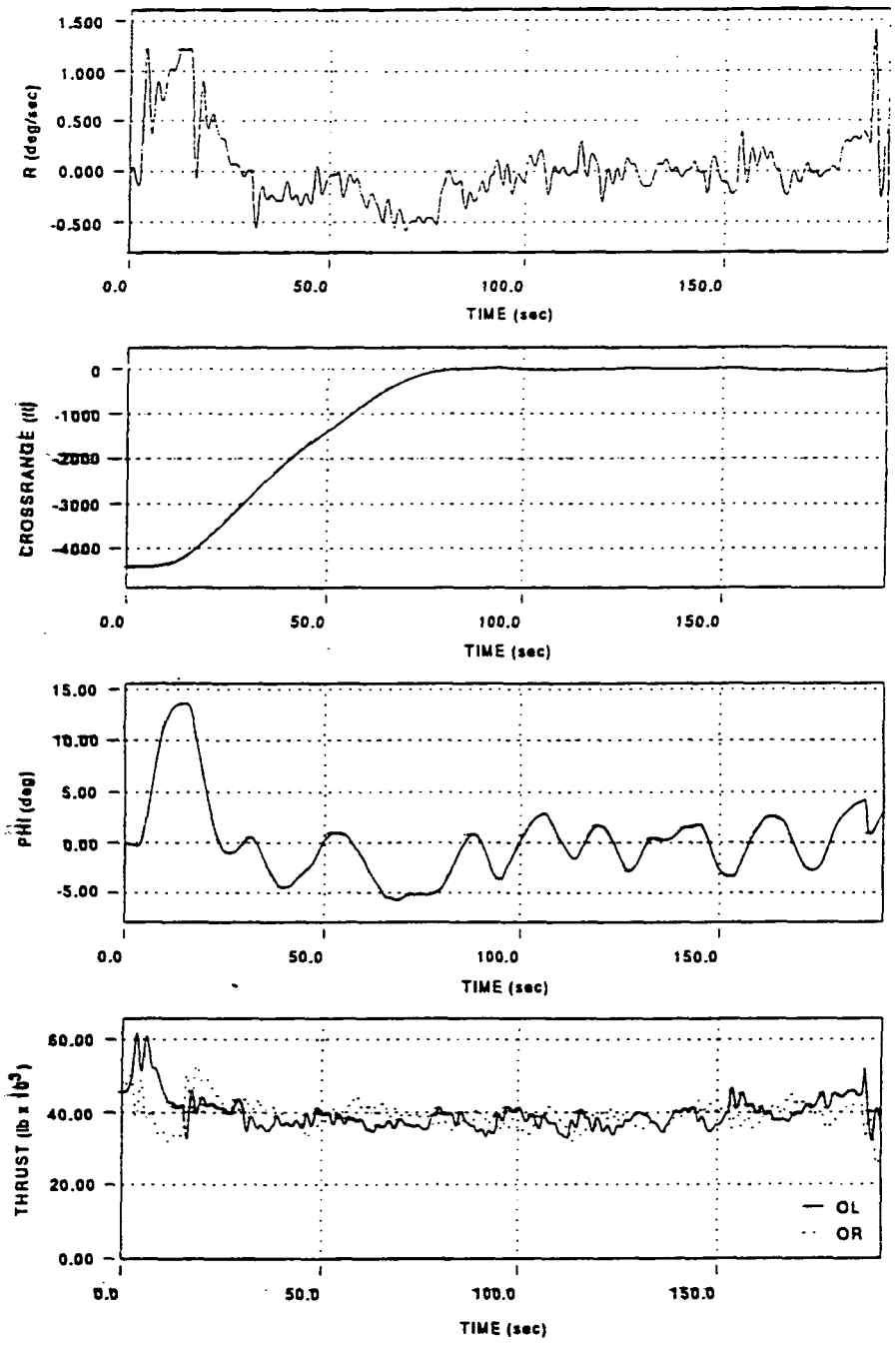

Figure G6(b) Lateral-Directional Flight Variables for Test Flight A7: Engine Time Constant of 3.0 Seconds with PCA

Test Point A8

Engine Time Constant Of One-Half Second With PCA

Comments During Flight

none

Post-Flight Comments

none

Pilot Comment Card

I. Longitudinal Configuration

Cooper-Harper pilot rating - 4

II. Lateral-Directional Configuration

Cooper-Harper pilot rating - 4

III. Summary (Brief)

Comments - similar to baseline

Overall Cooper-Harper pilot rating - 5

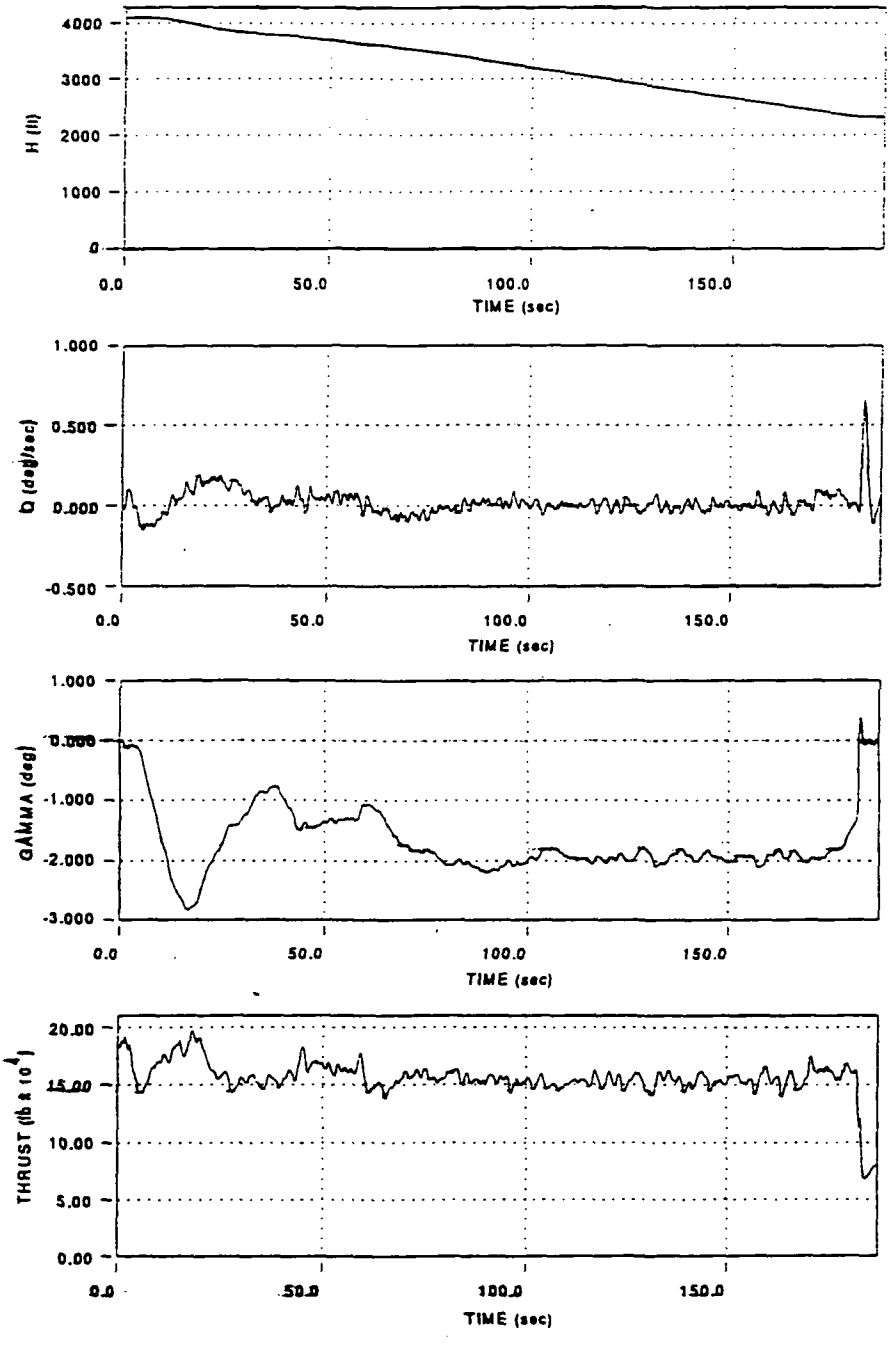

Figure G7(a) Longitudinal Flight Variables for Test Flight A8: Engine Time Constant of 0.5 Seconds with PCA

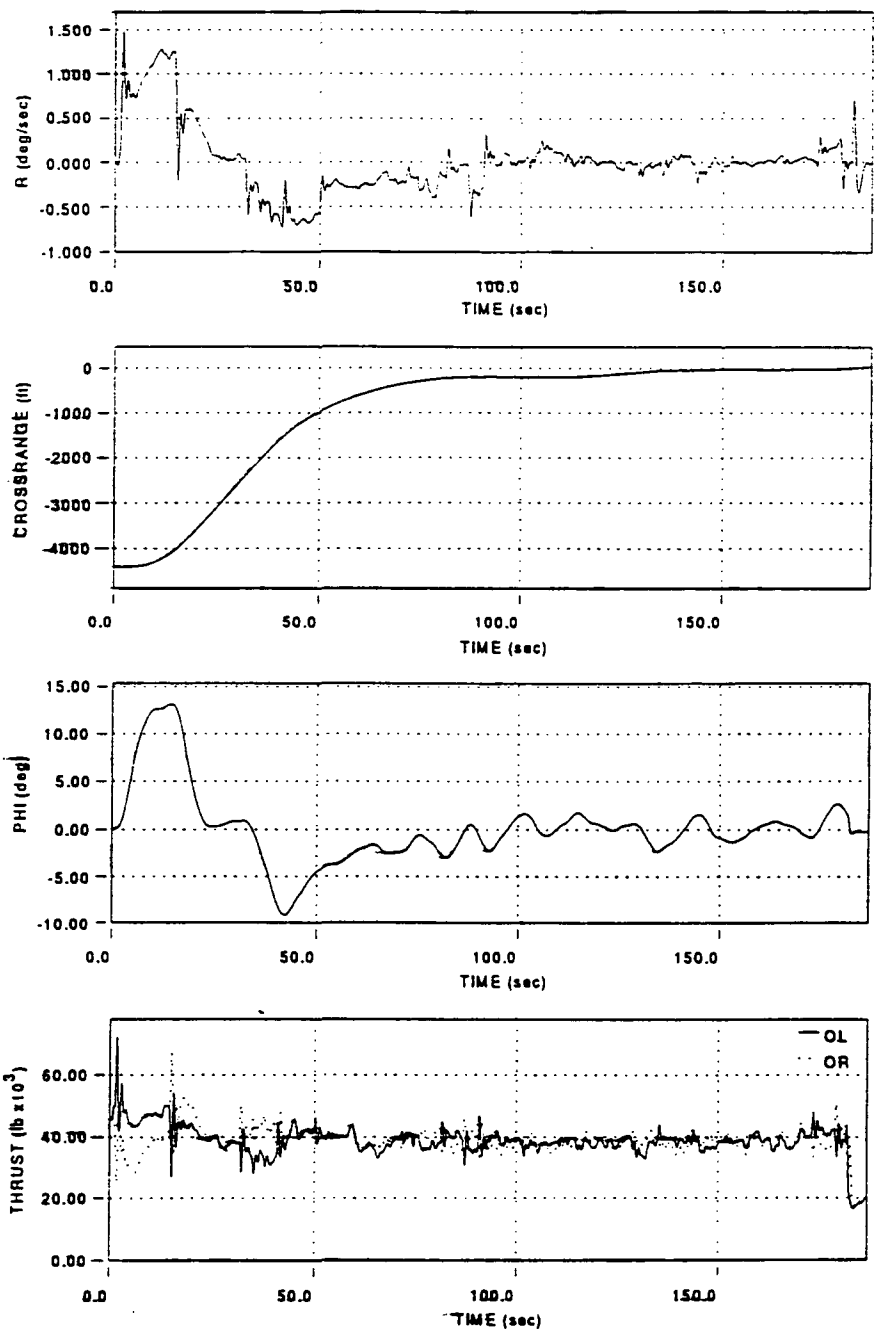

Figure G7(b) Lateral-Directional Flight Variables for Test Flight A8: Engine Time Constant of 0.5 Seconds with PCA

Test Point A9

Intermediate Turbulence With PCA

Comments During Flight

Author (DG): You had a little bit of a bumpy ride on that one.

Test Pilot A (TPA): Yeah, yeah. It handled it pretty well.

Post-Flight Comments

TPA: That's a lot of turbulence - intermediate is a lot of turbulence.

DG: Some of the people that I've had in have said that they think that intermediate is about as bad as you could expect.

TPA: That's right - that's absolutely right. Heavy (turbulence) is something you seldom see. Maybe once in my life I've seen heavy turbulence. If you look at the criteria, that (the turbulence level flown in test point 9) is what is called moderate, but you very seldom see moderate. So, it handled it well. That's like a hot summer day out here with big thermals and stuff.

Pilot Comment Card

I. Longitudinal Configuration

Cooper-Harper pilot rating - 4

II. Lateral-Directional Configuration

Cooper-Harper pilot rating - 4

III. Summary (Brief)

Comments - system handled turbulence well

Overall Cooper-Harper pilot rating - 5

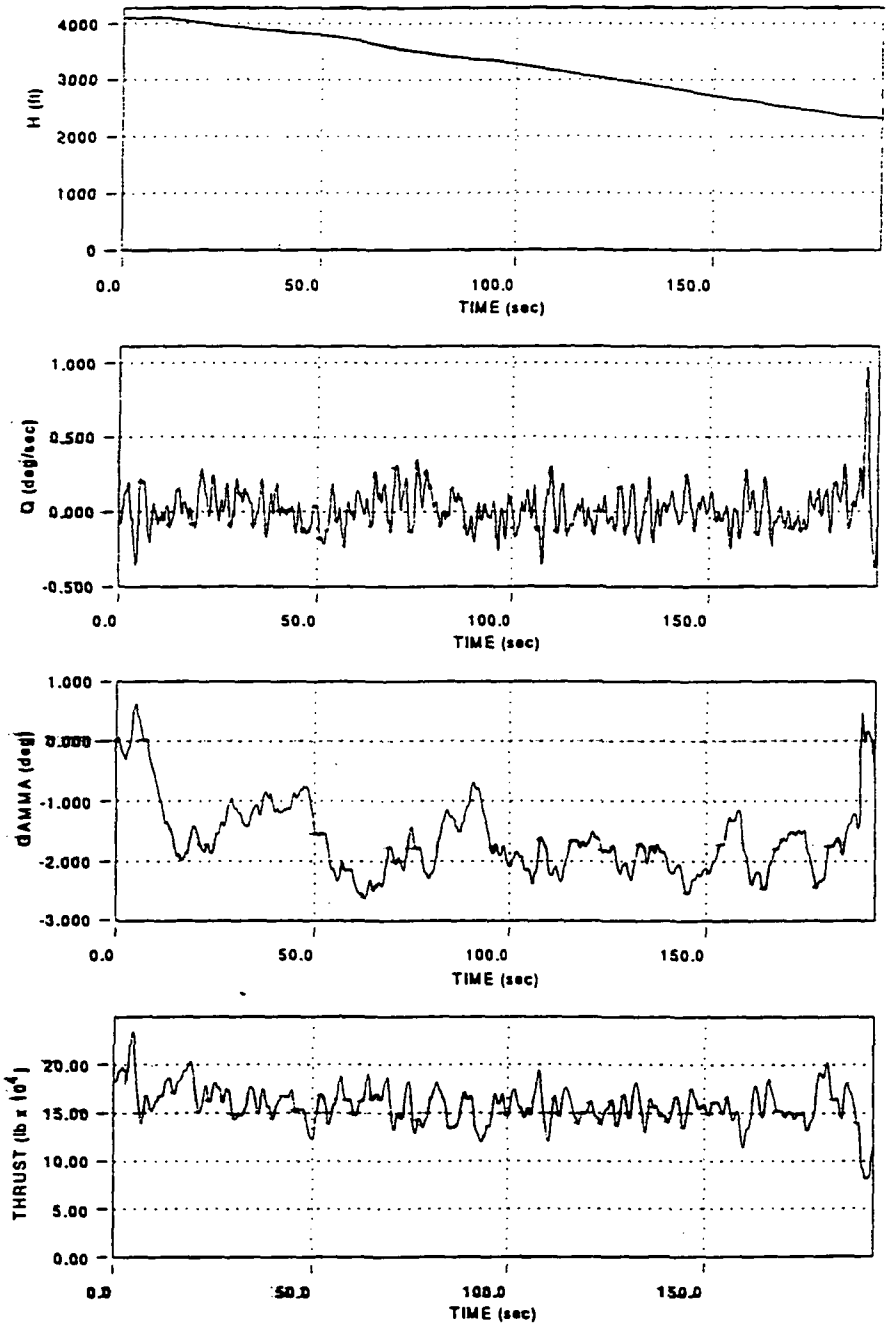

Figure G8(a) Longitudinal Flight Variables for Test Flight A9: Intermediate Turbulence with PCA

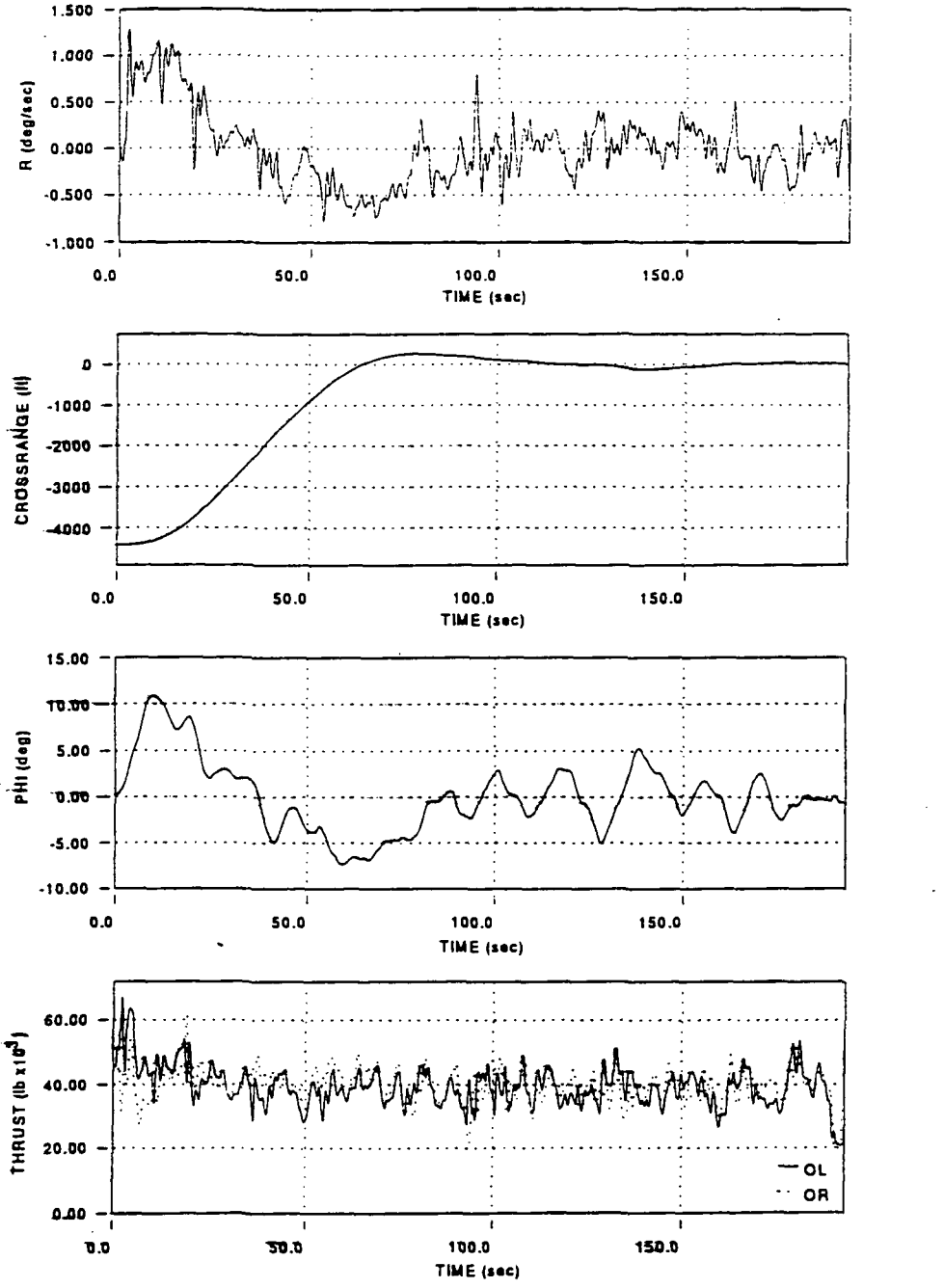

Figure G8(b) Lateral-Directional Flight Variables for Test Flight A9: Intermediate Turbulence with PCA

Test Point A10

Outboard Engine Inoperative With PCA

(Repeat Of Test Point A6)

Comments During Flight

Test Pilot A: Okay. Well, I didn't do as well as I thought I could, but . . . it's more difficult.

Post-Flight Comments

none

Pilot Comment Card

I. Longitudinal Configuration

Cooper-Harper pilot rating - 6

II. Lateral-Directional Configuration

Cooper-Harper pilot rating - 5

III. Summary (Brief)

Comments -

a) slow pitch response

b) slightly slow roll response

Overall Cooper-Harper pilot rating - 7

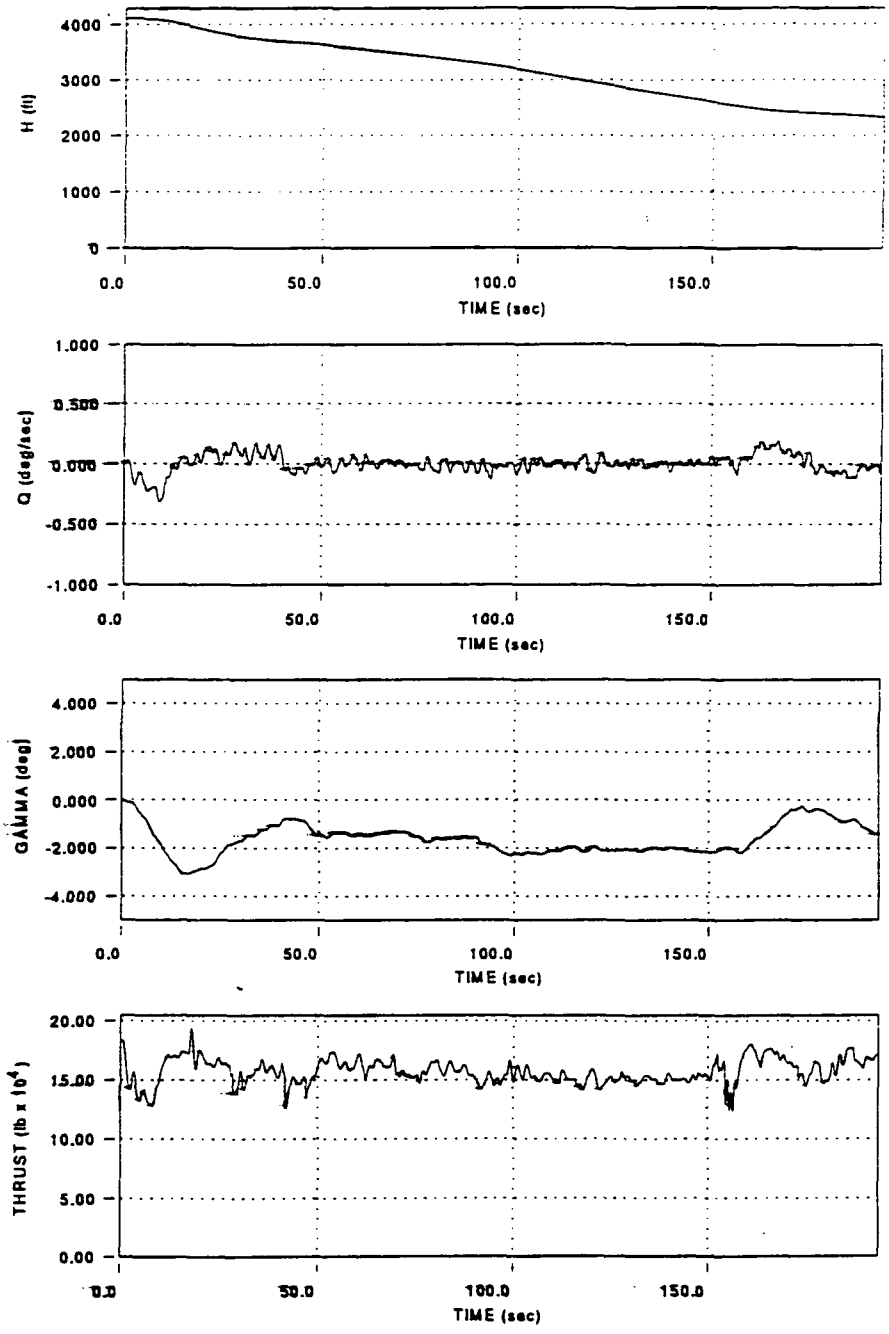

Figure G9(a) Longitudinal Flight Variables for Test Flight A10: Outboard Engine Inoperative with PCA

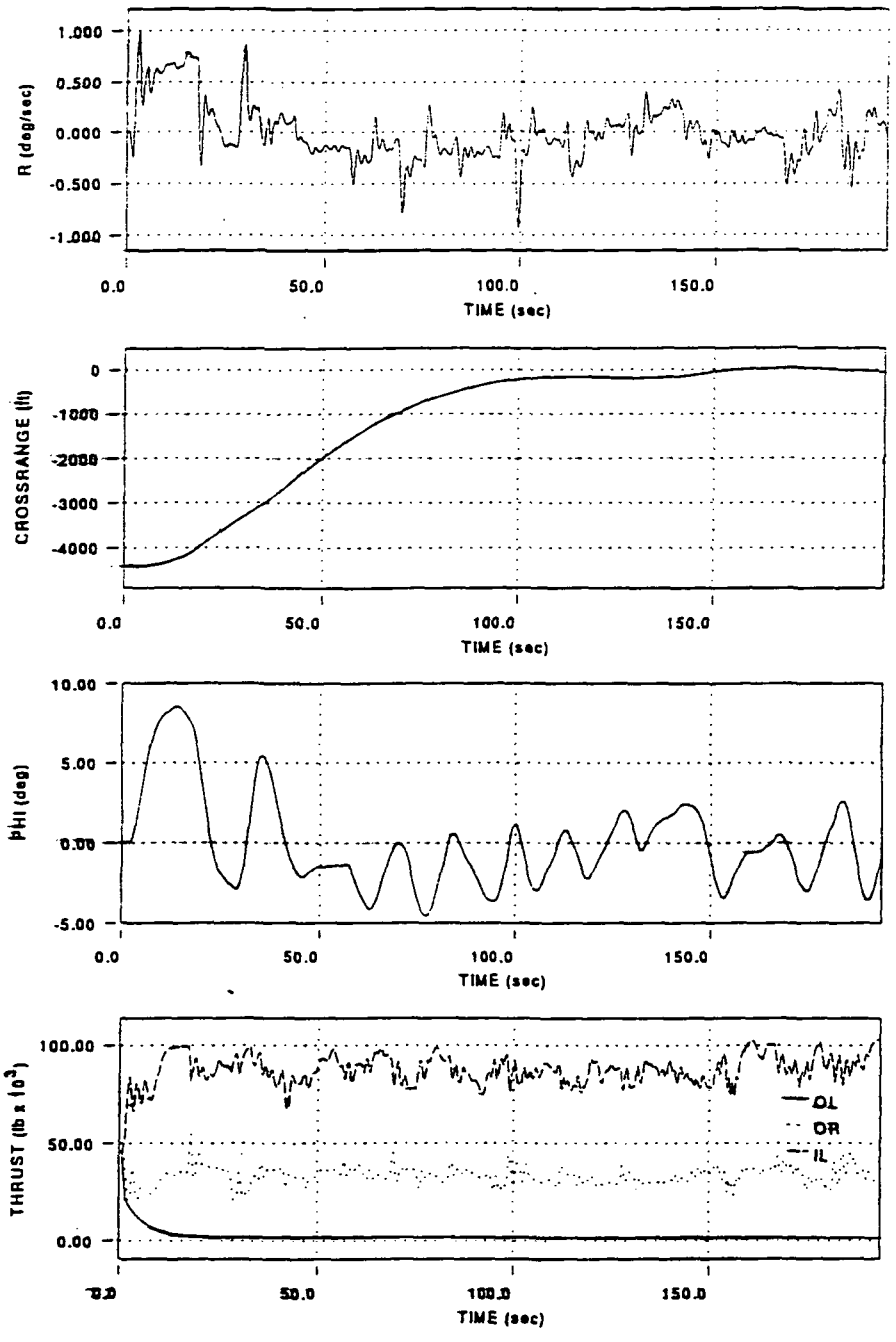

Figure G9(b) Lateral-Directional Flight Variables for Test Flight A10: Outboard Engine Inoperative with PCA

Test Point A11

Manual Throttles - No PCA

Comments During Flight

Test Pilot A: Okay, I have no idea how to do this. This is going to be really interesting. Whew. Well, we'd better just try it again. I didn't make it (the landing). Maybe I'll just go around manually. Okay, let's start a turn here. Okay, let's take a turn here and see if we can find the runway. Is that my runway? That could be my runway. That could be a lakebed runway. Well, we'll see. That's lakebed 23. I'm just about lined up here but I think I'm too high and too close in, so I'll have to reset (the program). Let's go ahead and reset.

Post-Flight Comments

none

Pilot Comment Card

I. Summary (Brief)

Comments - unsuccessful approach with okay go-around

[Pilot ratings were not given on this test point because the pilot did not complete a successful approach and landing.]

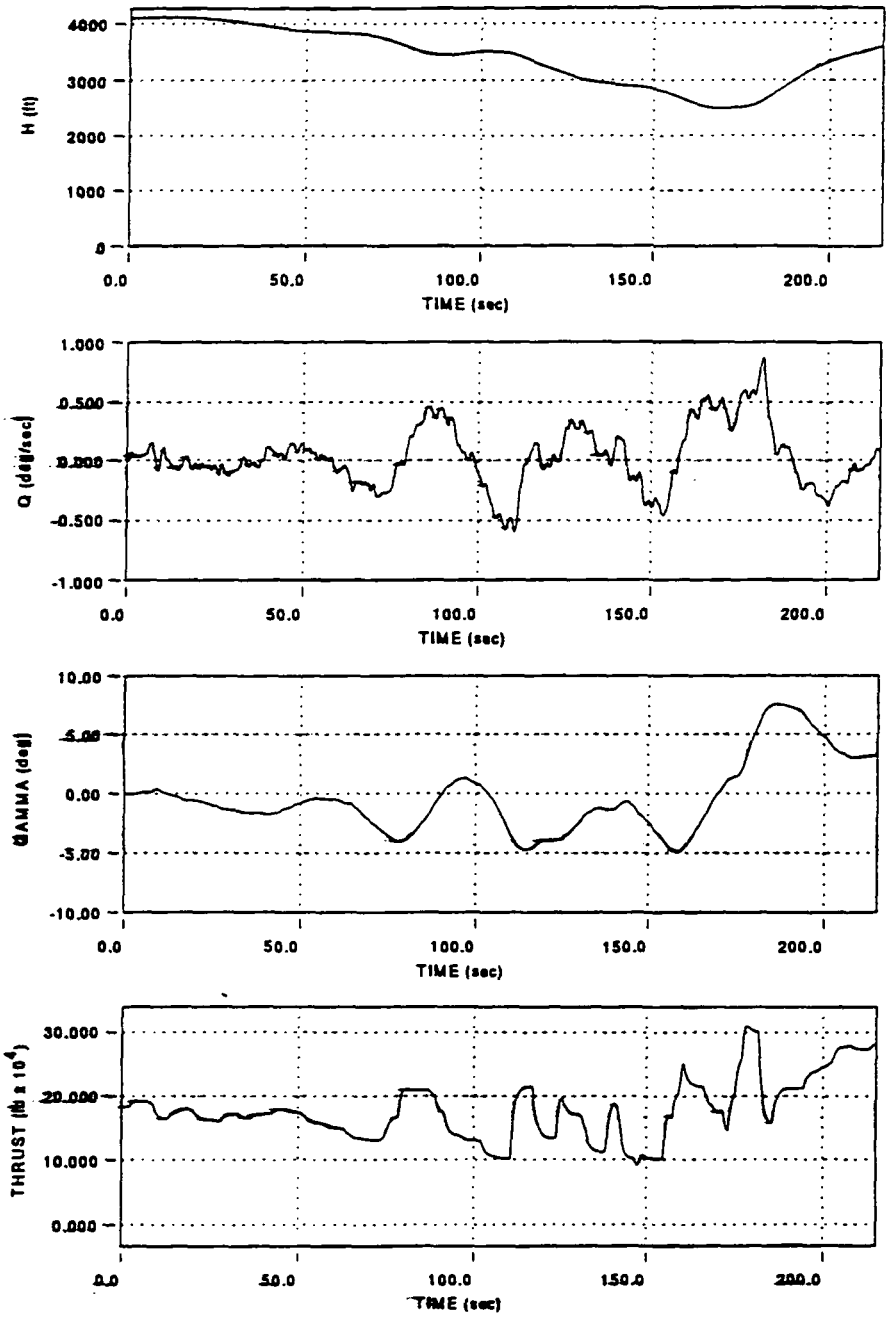

Figure G10(a) Longitudinal Flight Variables for Test Flight A11: Manual Throttles - No PCA

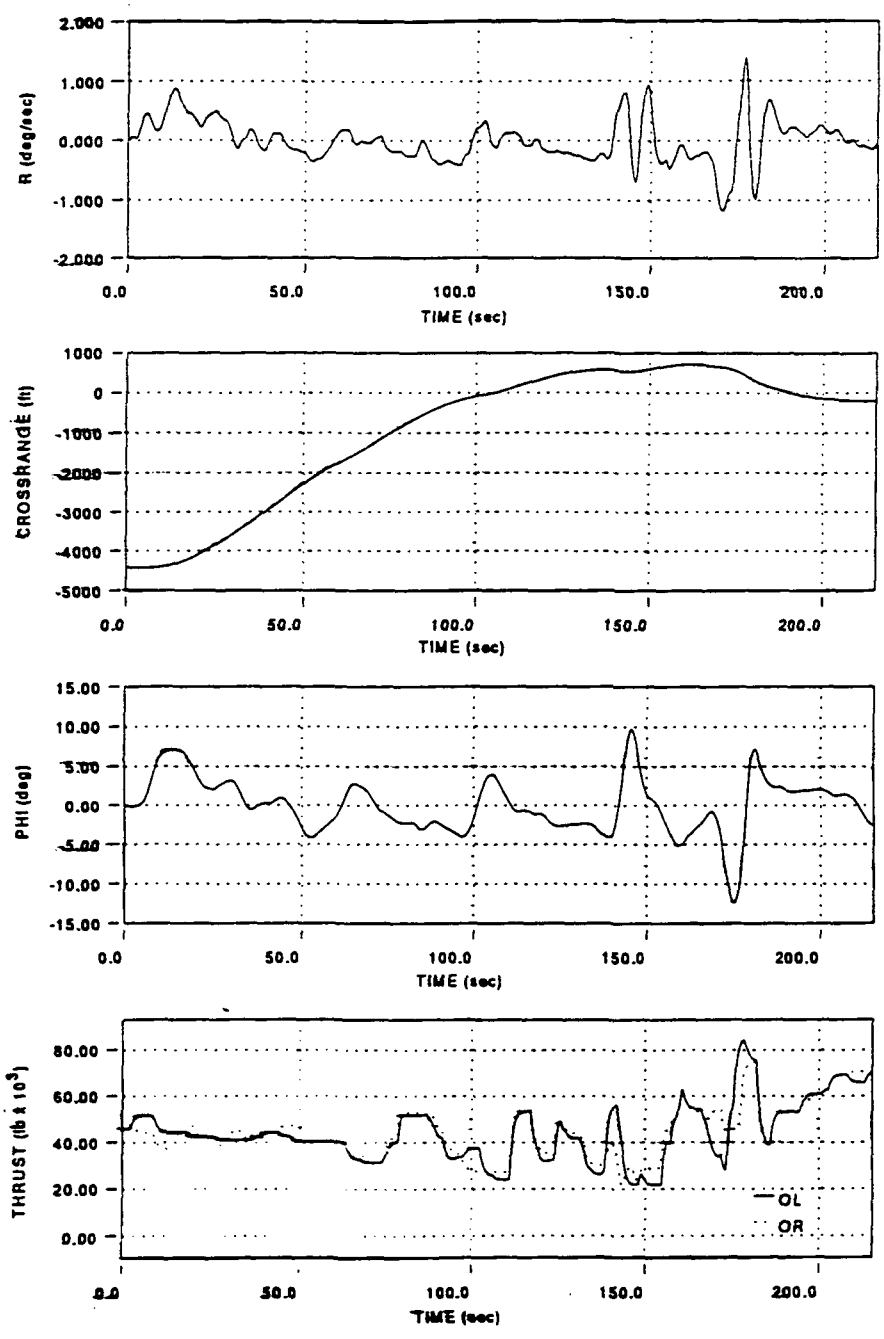

Figure G10(b) Lateral-Directional Flight Variables for Test Flight A11: Manual Throttles - No PCA

Test Point A12

Manual Throttles - No PCA

(Repeat Of Test Point A11)

Comments During Flight

Test Pilot A (TPA): Okay, all clear on that one (landing). I can't believe that - purely by accident.

Post-Flight Comments

TPA: I was really amazed to arrive on the runway. It actually got there. I guess the practice does help. I imagine the guy (pilot flying manual throttles to control crippled aircraft) will have some time to practice typically, but still, the system is nice. It's really a good idea.

Pilot Comment Card

I. Longitudinal Configuration

Cooper-Harper pilot rating - 7

II. Lateral-Directional Configuration

Cooper-Harper pilot rating - 7

III. Summary (Brief)

Comments - only by good luck arrived for satisfactory landing

Overall Cooper-Harper pilot rating - 7

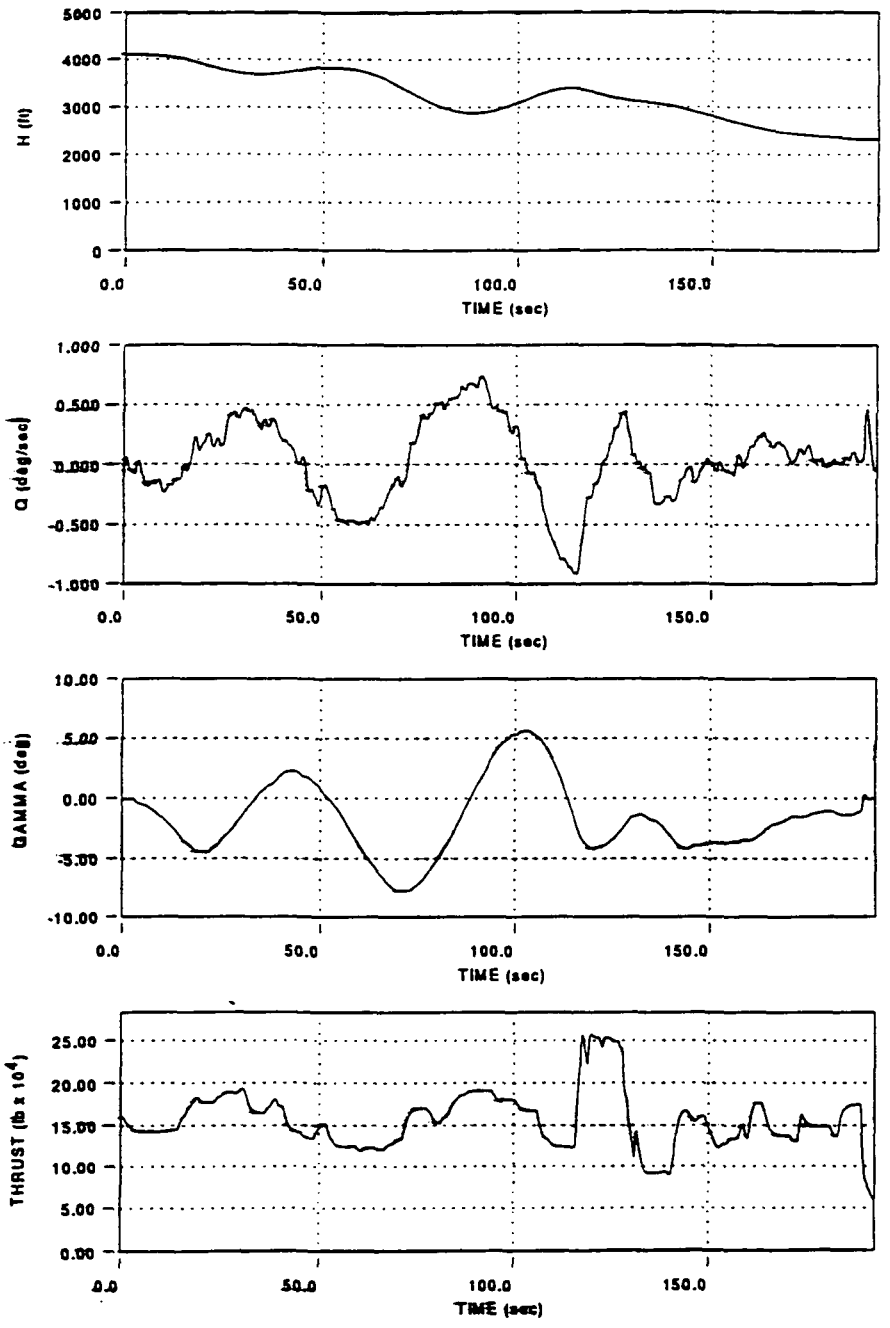

Figure G11(a) Longitudinal Flight Variables for Test Flight A12: Manual Throttles - No PCA

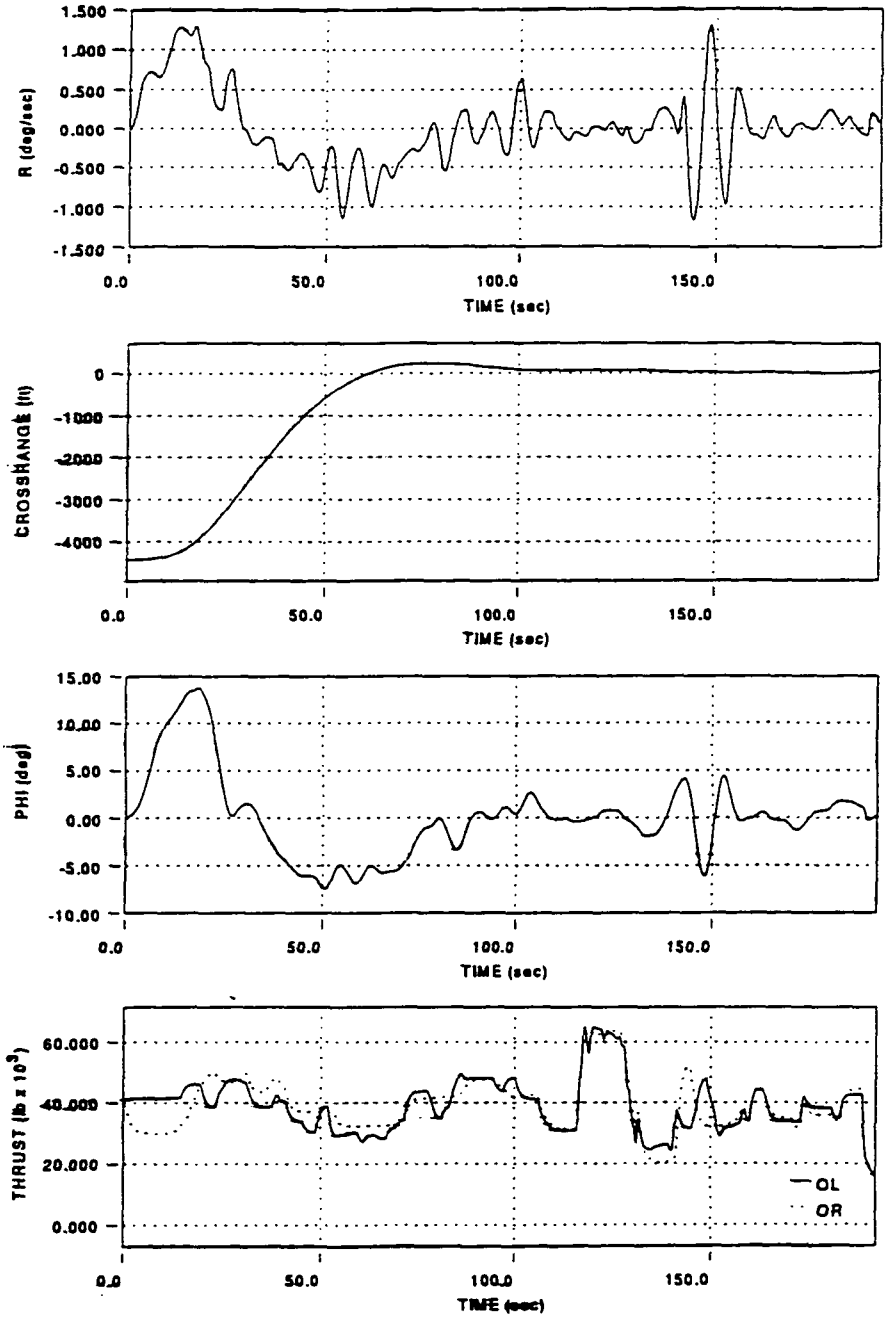

Figure G11(b) Lateral-Directional Flight Variables for Test Flight A12: Manual Throttles - No PCA

Test Point A13

Conventional Control Surfaces Operational - No PCA

Comments During Flight

Test Pilot A: Did we decide that 150 (knots) is a pretty good approach speed for this airplane?

Author: With flaps, I think so.

[At this point during the testing, the video recording tape ran out. Therefore, further comments of the test pilot were not recorded during the remainder of this test session.]

Pilot Comment Card

I. Longitudinal Configuration

Pitch attitude response in general - good

Predictability of final response - very good

Cooper-Harper pilot rating - 3

II. Lateral-Directional Configuration

Roll response in general - good

Roll tendency to overshoot - moderate

Tendency to maintain bank angle - good

Heading response in general - good

Cooper-Harper pilot rating - 5

III. Summary (Brief)

Problems - tendency for bank PIO (pilot induced oscillations) near ground

Any special control techniques - I tried various lateral position control strategies without much success:

a) smooth aileron control

b) pulsed aileron

c) coordinated aileron and rudder

d) mostly rudder

e) wings level - rudder to Δy near ground

- nothing helped much

Good features - good pitch control

Comments - very high degree of front-sidedness

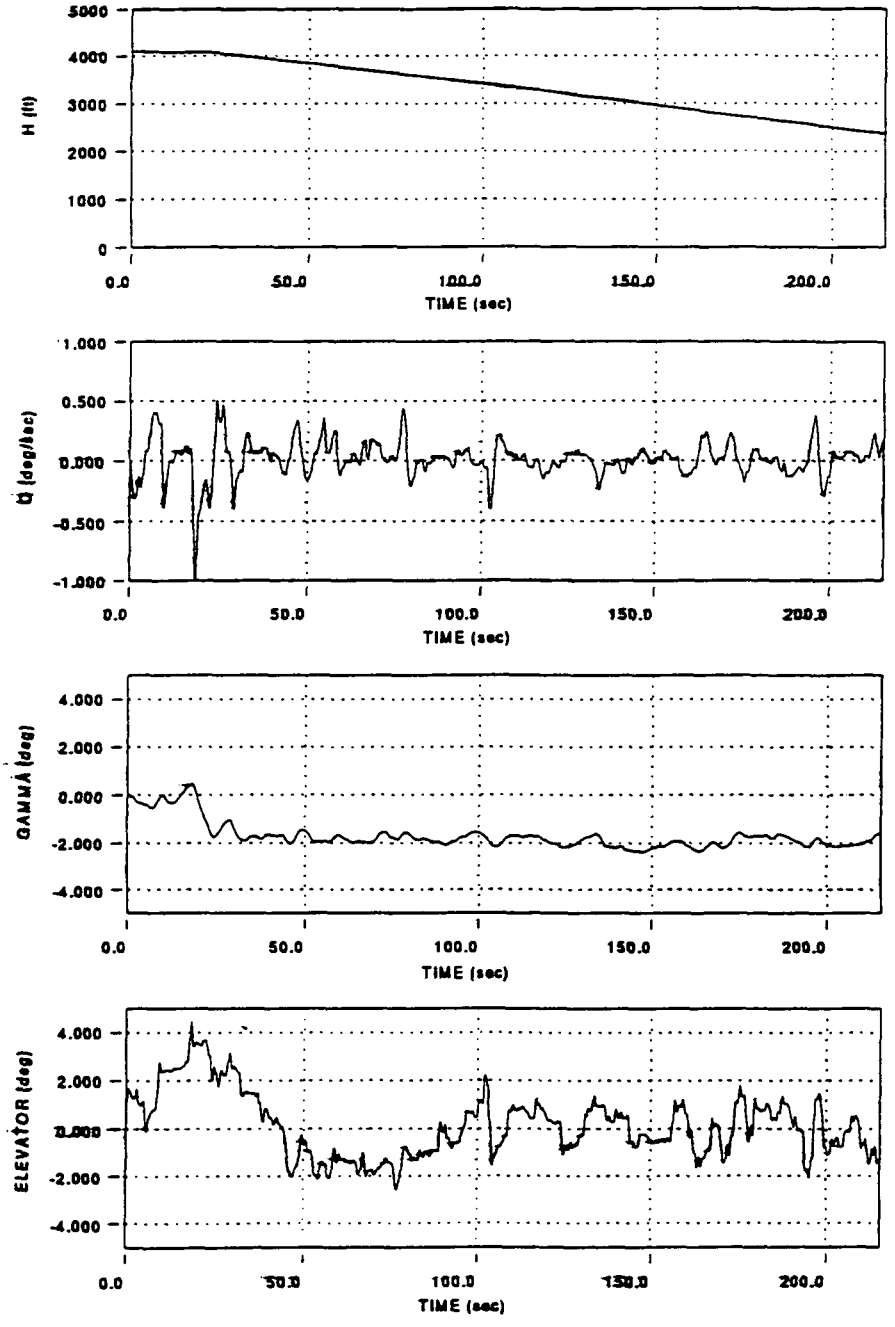

Figure G12(a) Longitudinal Flight Variables for Test Flight A13: Conventional Control Surfaces Operational - No PCA

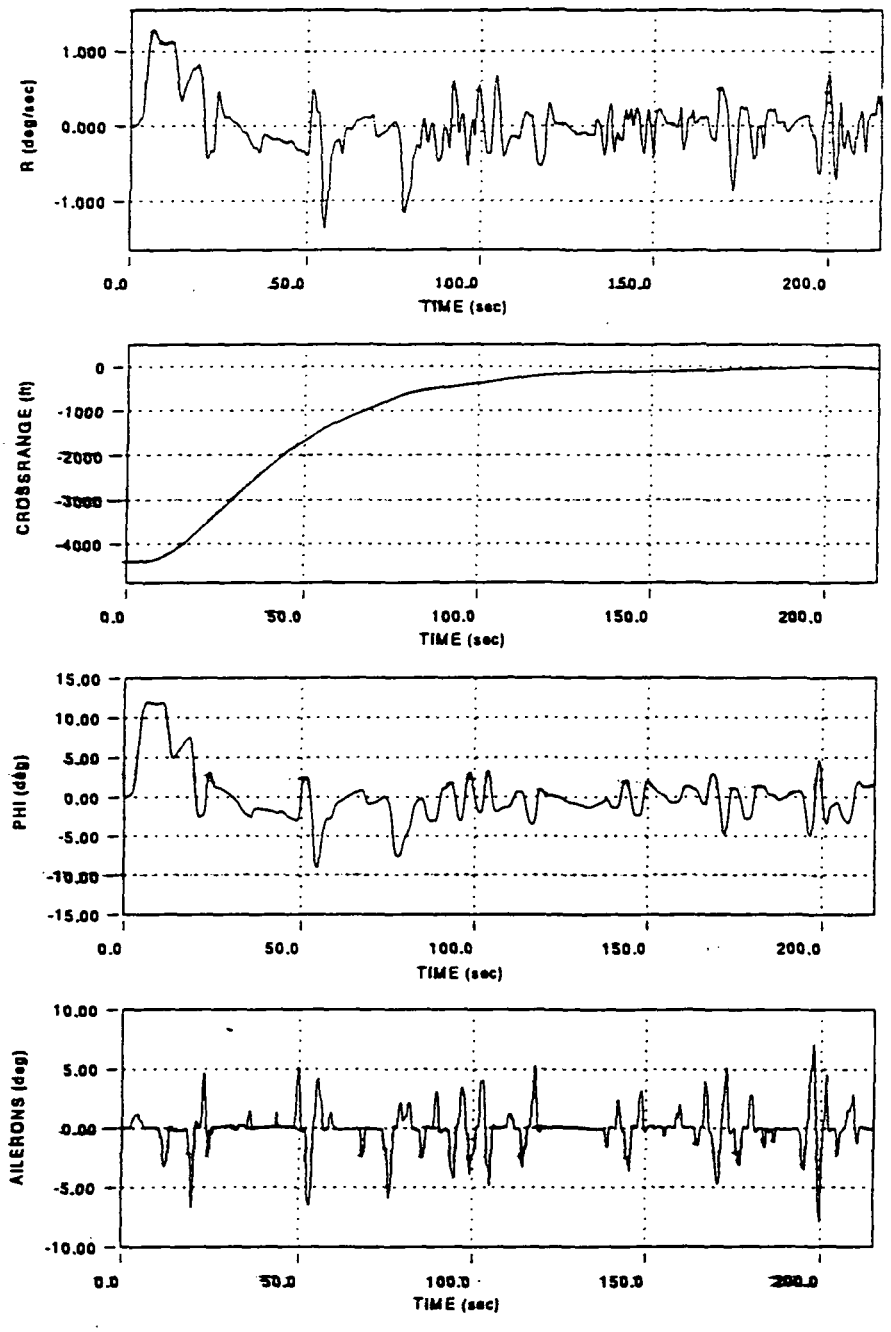

Figure G12(b) Lateral-Directional Flight Variables for Test Flight A13: Conventional Control Surfaces Operational - No PCA

Test Point A14

Baseline Configuration With PCA

(Repeat Of Test Point A1)

Pilot Comment Card

I. Longitudinal Configuration

Pitch attitude response in general - good, quite slow

Predictability of final response - very good

Cooper-Harper pilot rating - 3

II. Lateral-Directional Configuration

Roll response in general - very good

Roll tendency to overshoot - very good

Tendency to maintain bank angle - very good

Heading response in general - very good

Cooper-Harper pilot rating - 4

III. Summary (Brief)

Problems - slow response

Any special control techniques - watch for very small errors, correct early

Good features - very good predictability of final state

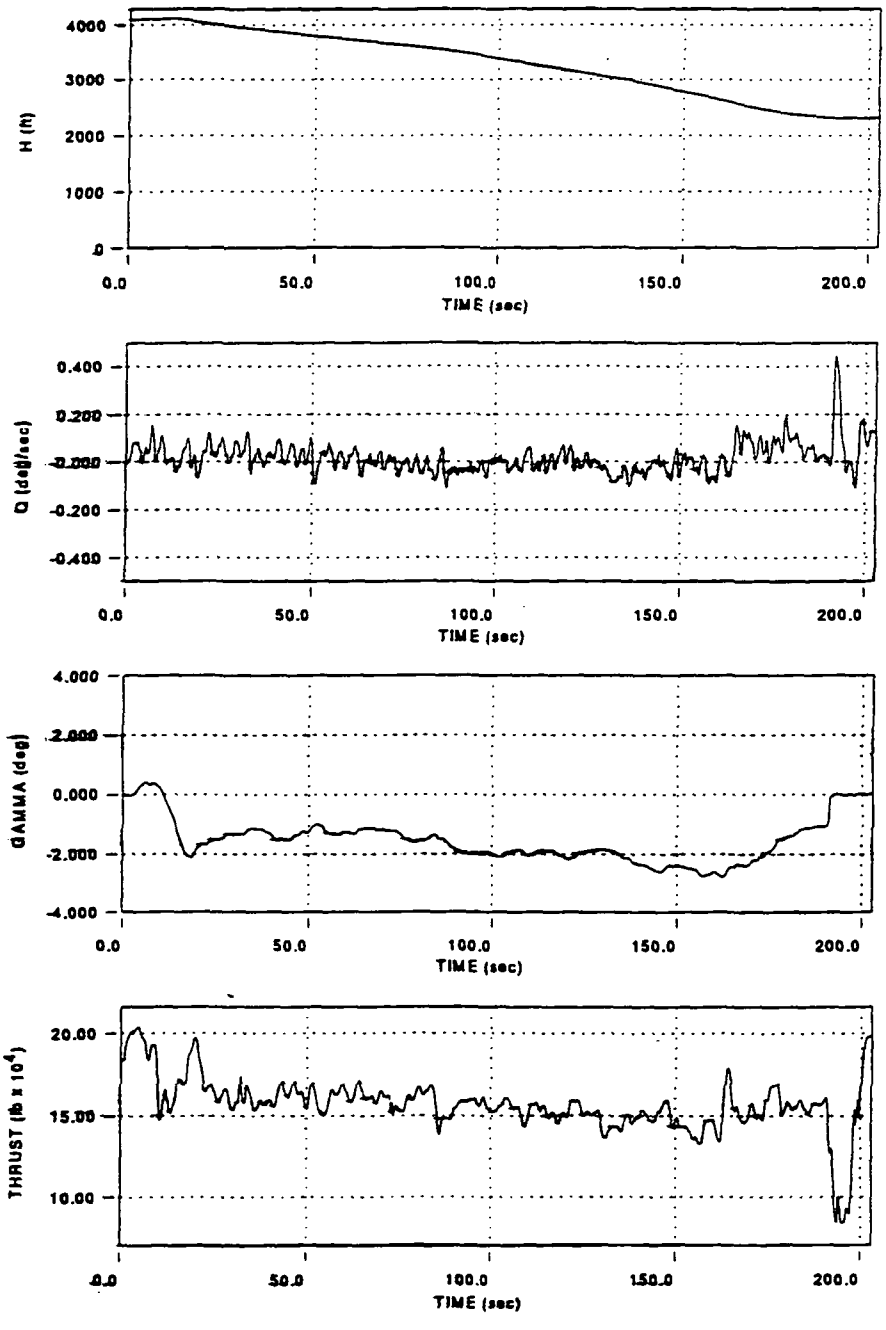

Figure G13(a) Longitudinal Flight Variables for Test Flight A14: Baseline Configuration with PCA

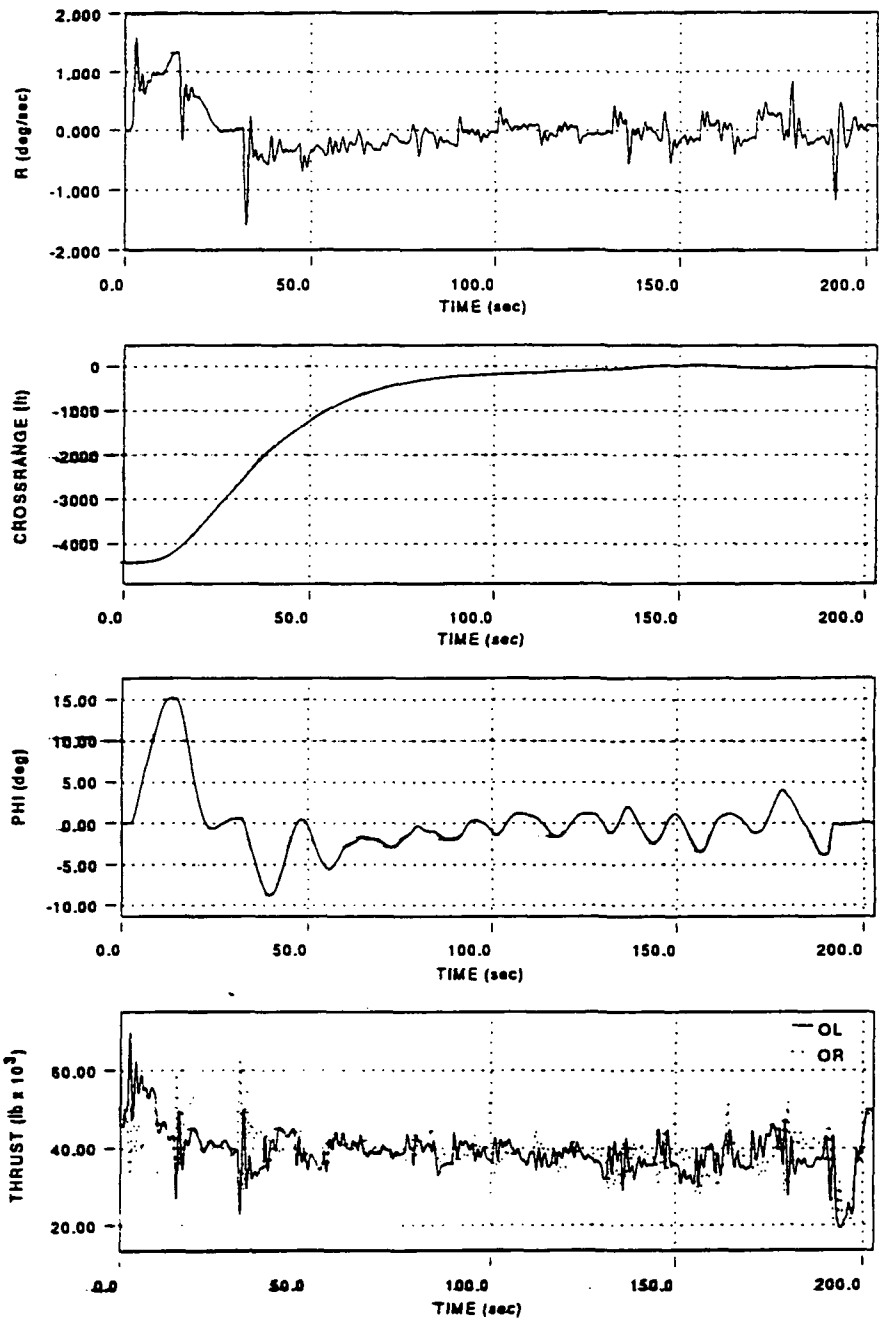

Figure G13(b) Lateral-Directional Flight Variables for Test Flight A14: Baseline Configuration with PCA

Test Point A15

Engines Moved Vertically Upward Into Wing With PCA (Inboard Engines Below Megatransport C.G. And Outboard Engines Above Megatransport C.G.)

Pilot Comment Card

I. Longitudinal Configuration

Cooper-Harper pilot rating - 3

II. Lateral-Directional Configuration

Cooper-Harper pilot rating - 4

III. Summary (Brief)

Comments - could not see a difference from test point 14

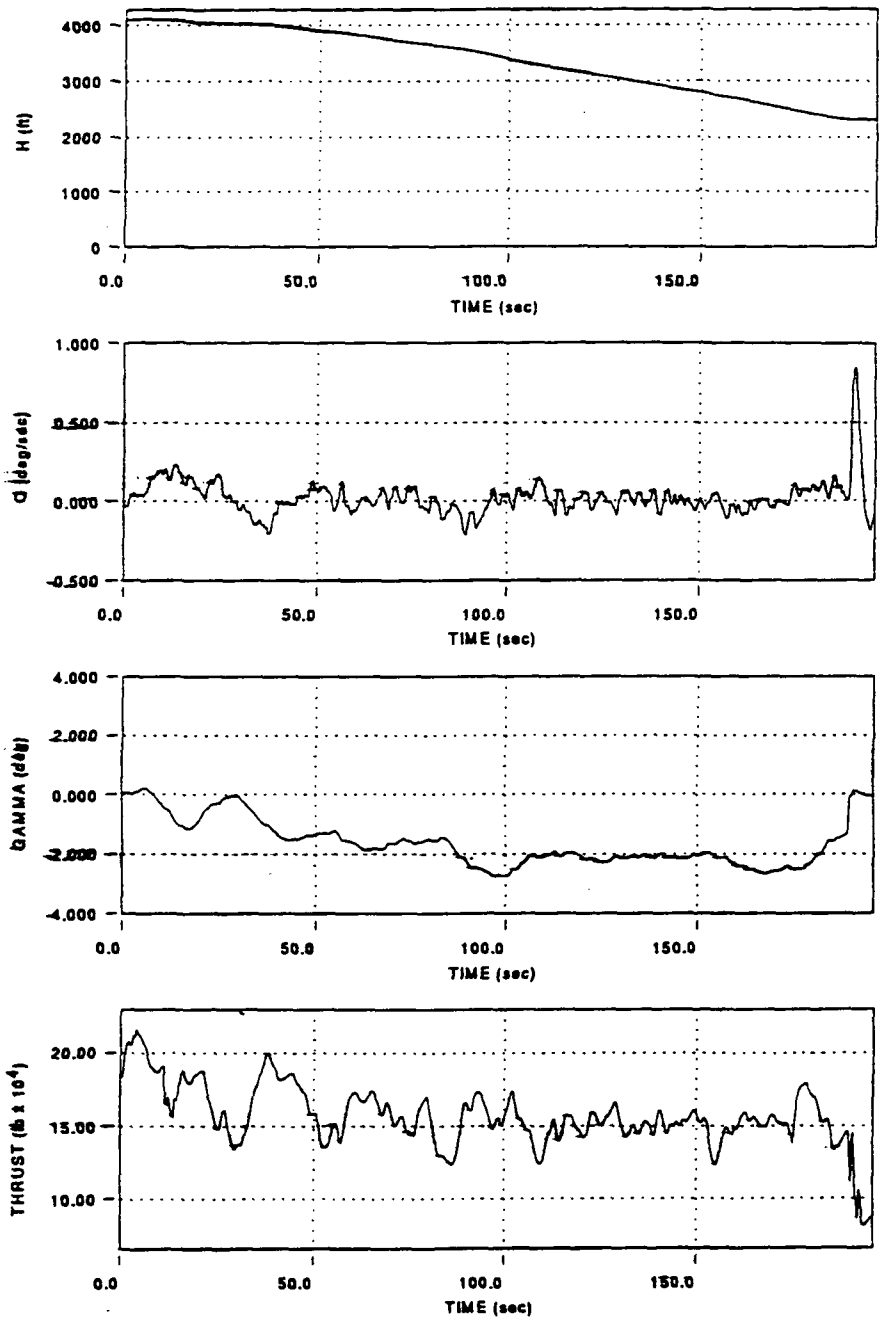

Figure G14(a) Longitudinal Flight Variables for Test Flight A15: Engines Moved Vertically Upward into Wing with PCA

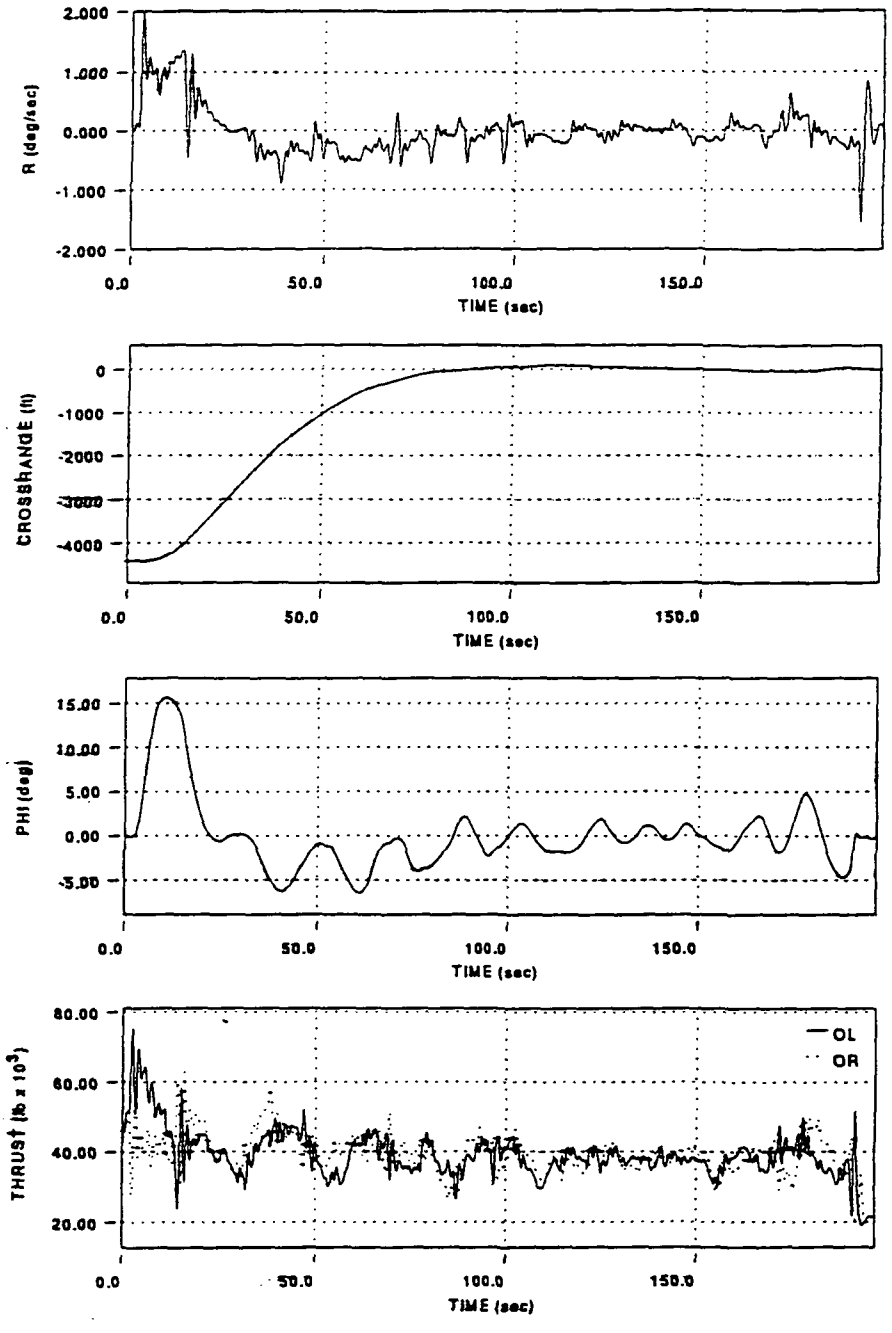

Figure G14(b) Lateral-Directional Flight Variables for Test Flight A15: Engines Moved Vertically Upward into Wing with PCA

Test Point A16

Engines Moved Vertically Upward 2.5 Feet Above Wing With PCA (Inboard And Outboard Engines Above Megatransport C.G.)

Pilot Comment Card

I. Longitudinal Configuration

Pitch attitude response in general - slow, moderate to light damping (for flare and short final)

Predictability of final response - good, but path to final response a little harder to anticipate

Cooper-Harper pilot rating - 5

II. Lateral-Directional Configuration

Roll response in general - very good

Roll tendency to overshoot - very good

Tendency to maintain bank angle - very good

Heading response in general - very good

Cooper-Harper pilot rating - 4

III. Summary (Brief)

Comments - significantly slower, less-damped response in pitch

Any special control techniques - try to arrive on a shallow (2 degree) glide slope before final flare, so smaller flare maneuver required

Good features - predictability of final pitch attitude is good, and very useful

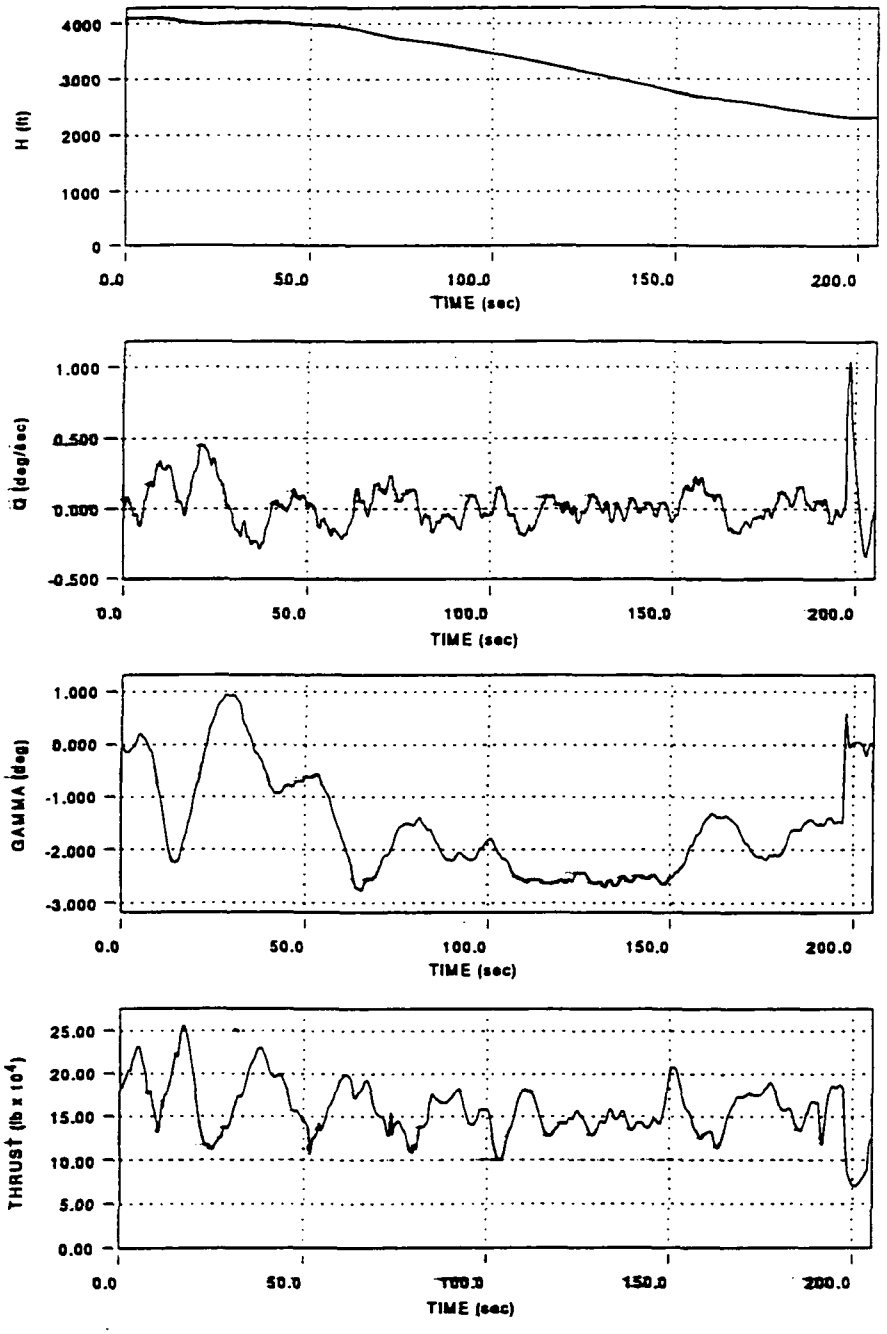

Figure G15(a) Longitudinal Flight Variables for Test Flight A16: Engines Moved Vertically Upward 2.5 Feet Above Wing with PCA

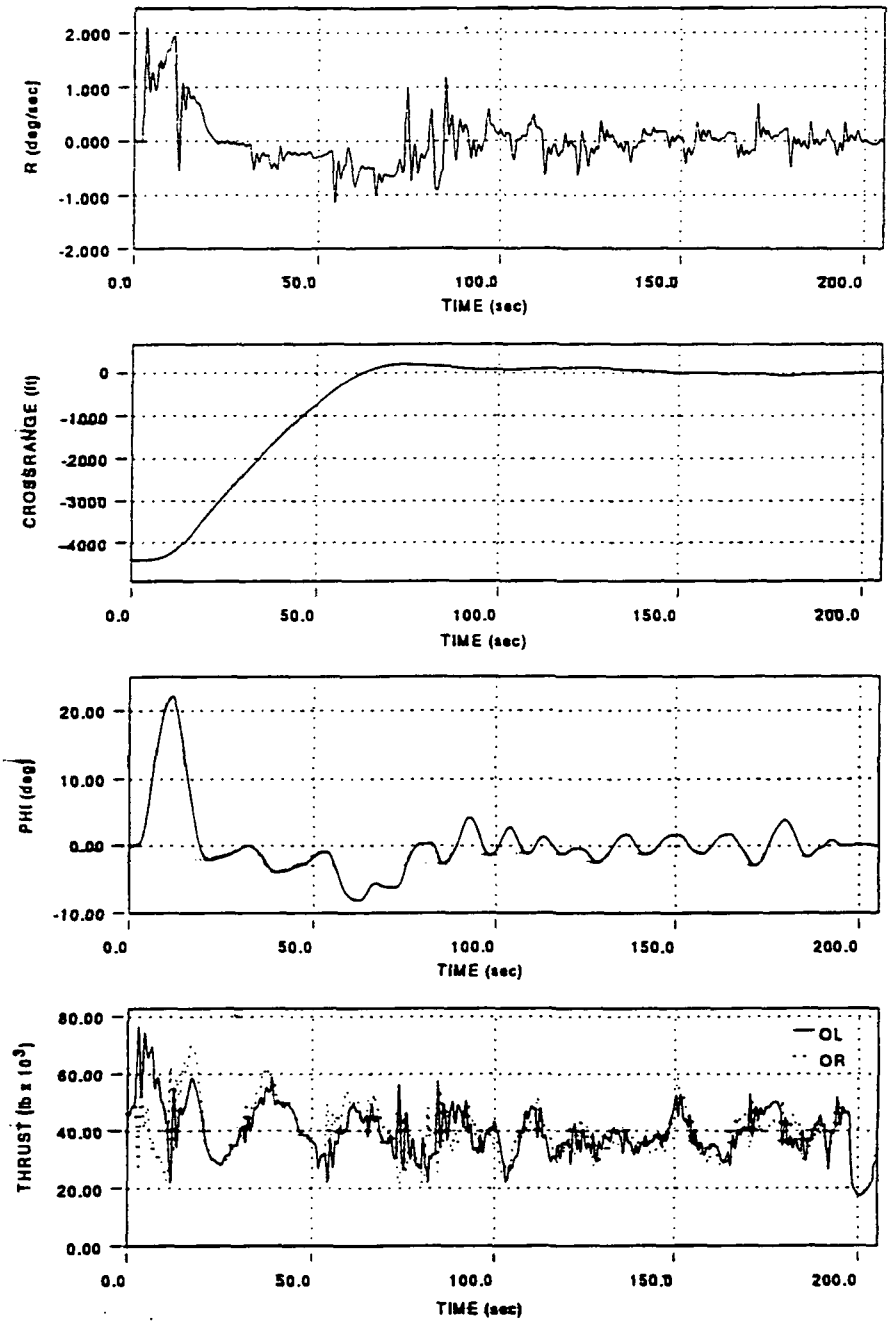

Figure G15(b) Lateral-Directional Flight Variables for Test Flight A16: Engines Moved Vertically Upward 2.5 Feet Above Wing with PCA

Test Point A17

Engines Moved 20 Feet Outboard With PCA

(Repeat Of Test Point A2)

Pilot Comment Card

I. Longitudinal Configuration

Cooper-Harper pilot rating - 3

II. Lateral-Directional Configuration

Cooper-Harper pilot rating - 4

III. Summary (Brief)

Comments - seemed very similar to baseline

Problems – did not achieve as good lateral lineup as baseline but thought cause was pilot thinking about pitch response and not attending lineup task

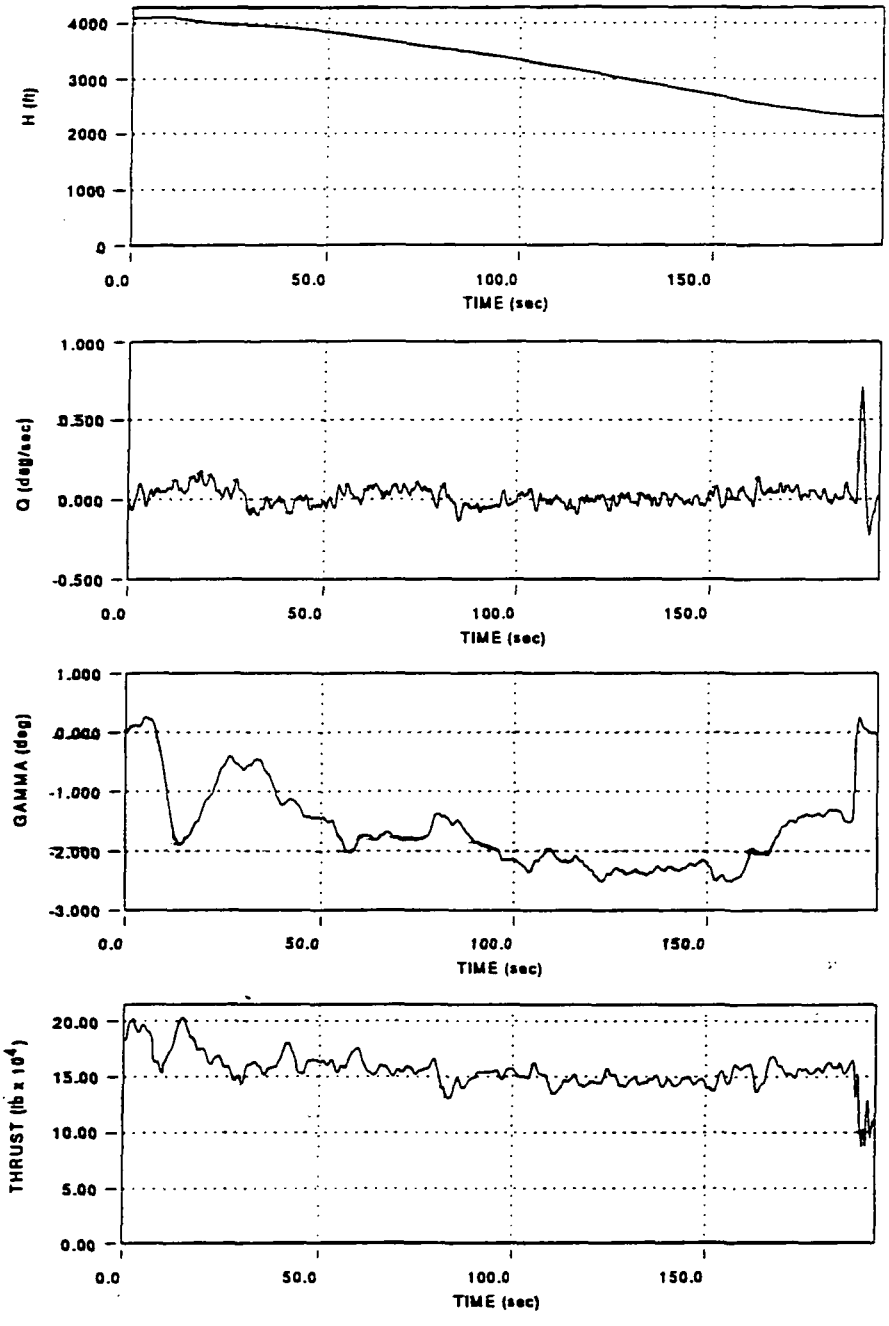

Figure G16(a) Longitudinal Flight Variables for Test Flight A17: Engines Moved 20 Feet Outboard with PCA

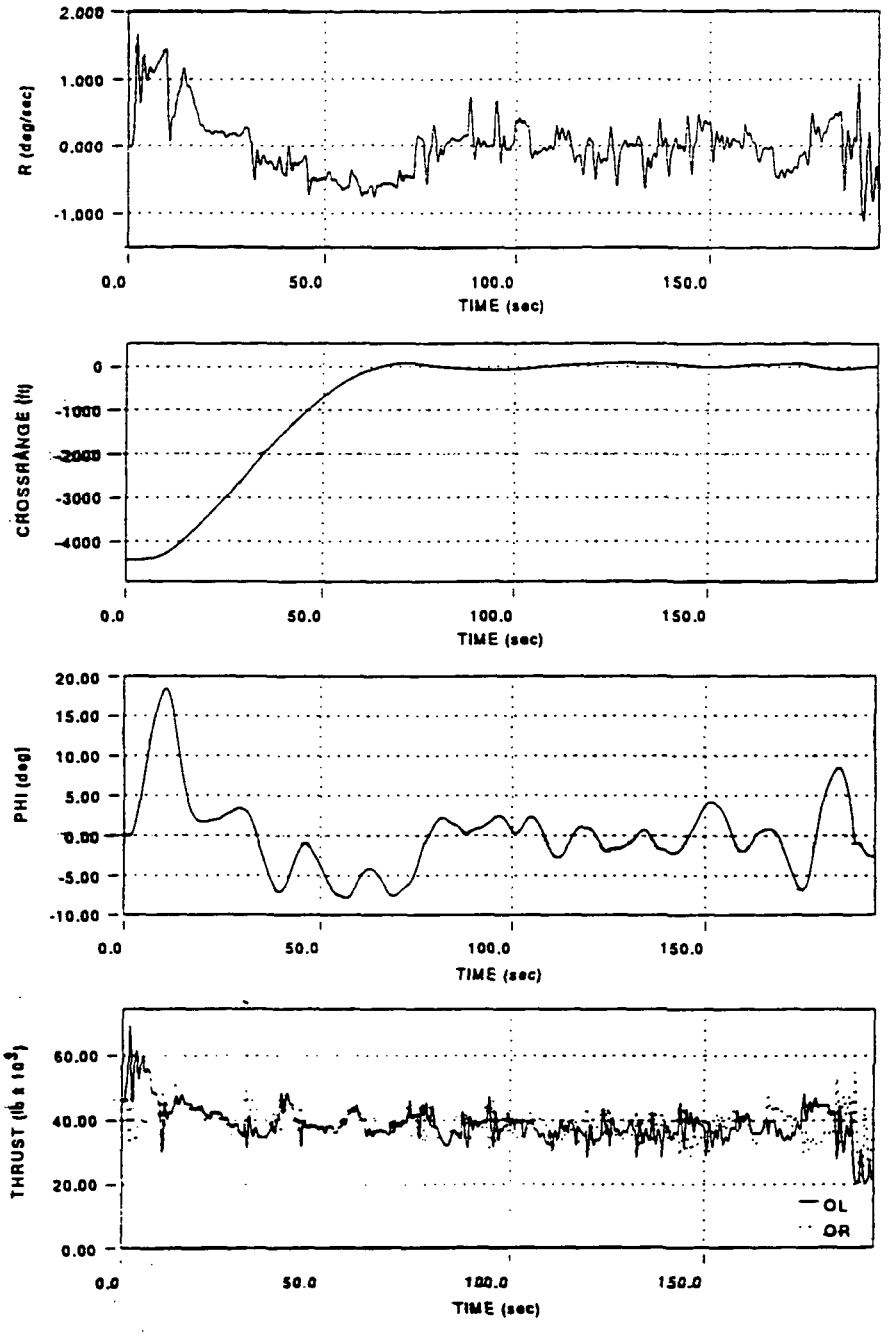

Figure G16(b) Lateral-Directional Flight Variables for Test Flight A17: Engines Moved 20 Feet Outboard with PCA

Test Point A18

Engines Moved 20 Feet Outboard With PCA

With 10 Knot Crosswind From The Right

Pilot Comment Card

I. Longitudinal Configuration

Cooper-Harper pilot rating - 3

II. Lateral-Directional Configuration

Cooper-Harper pilot rating - 4

III. Summary (Brief)

Comments -

a) similar to baseline - lateral Cooper-Harper same as baseline

b) verified that pilot inattention probably caused problem for test point 17

Suggestions - suggest further test topic to study flight in crosswinds diminishing near ground as is normally the case

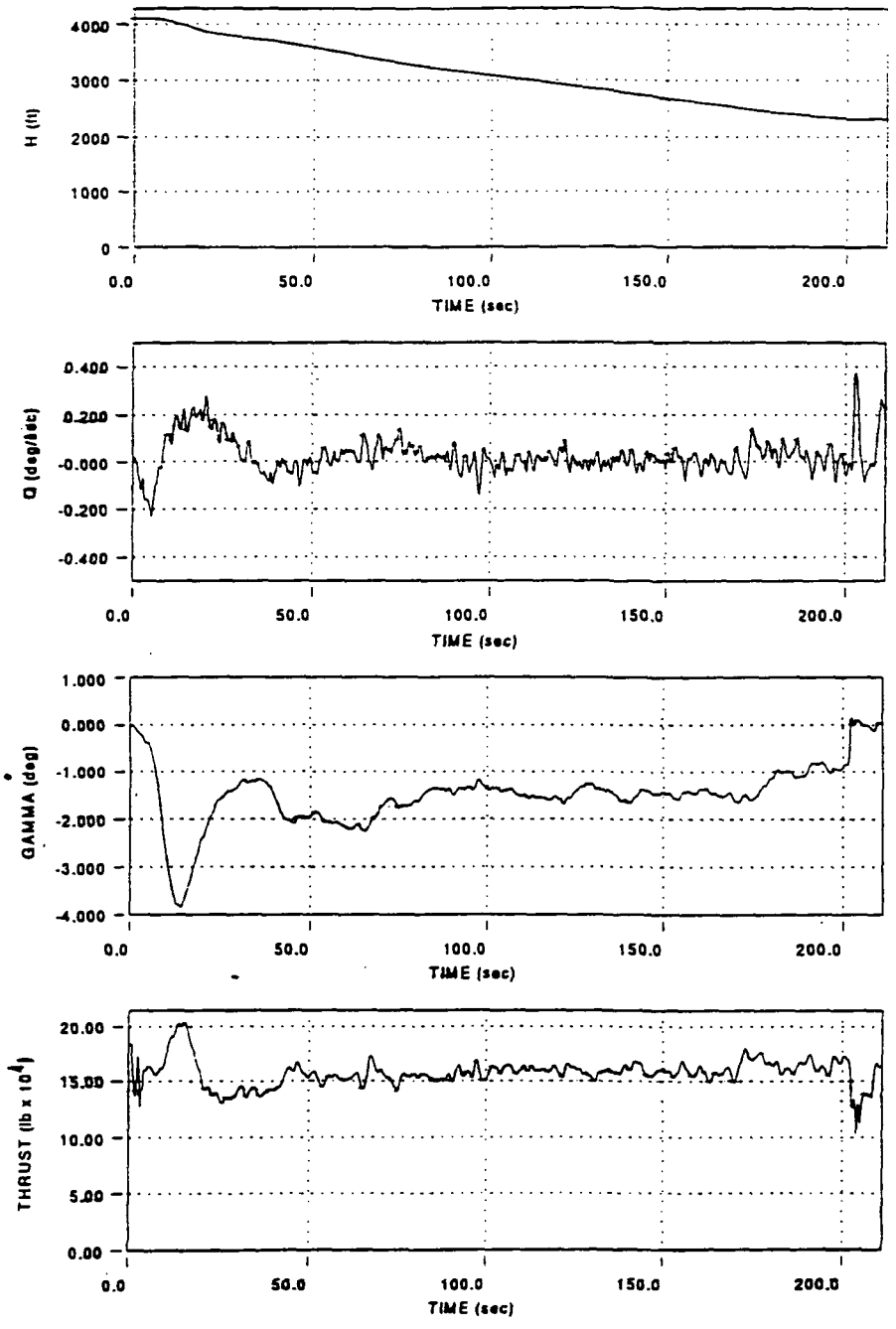

Figure G17(a) Longitudinal Flight Variables for Test Flight A18: Engines Moved 20 Feet Outboard with PCA with 10 Knot Crosswind from the Right

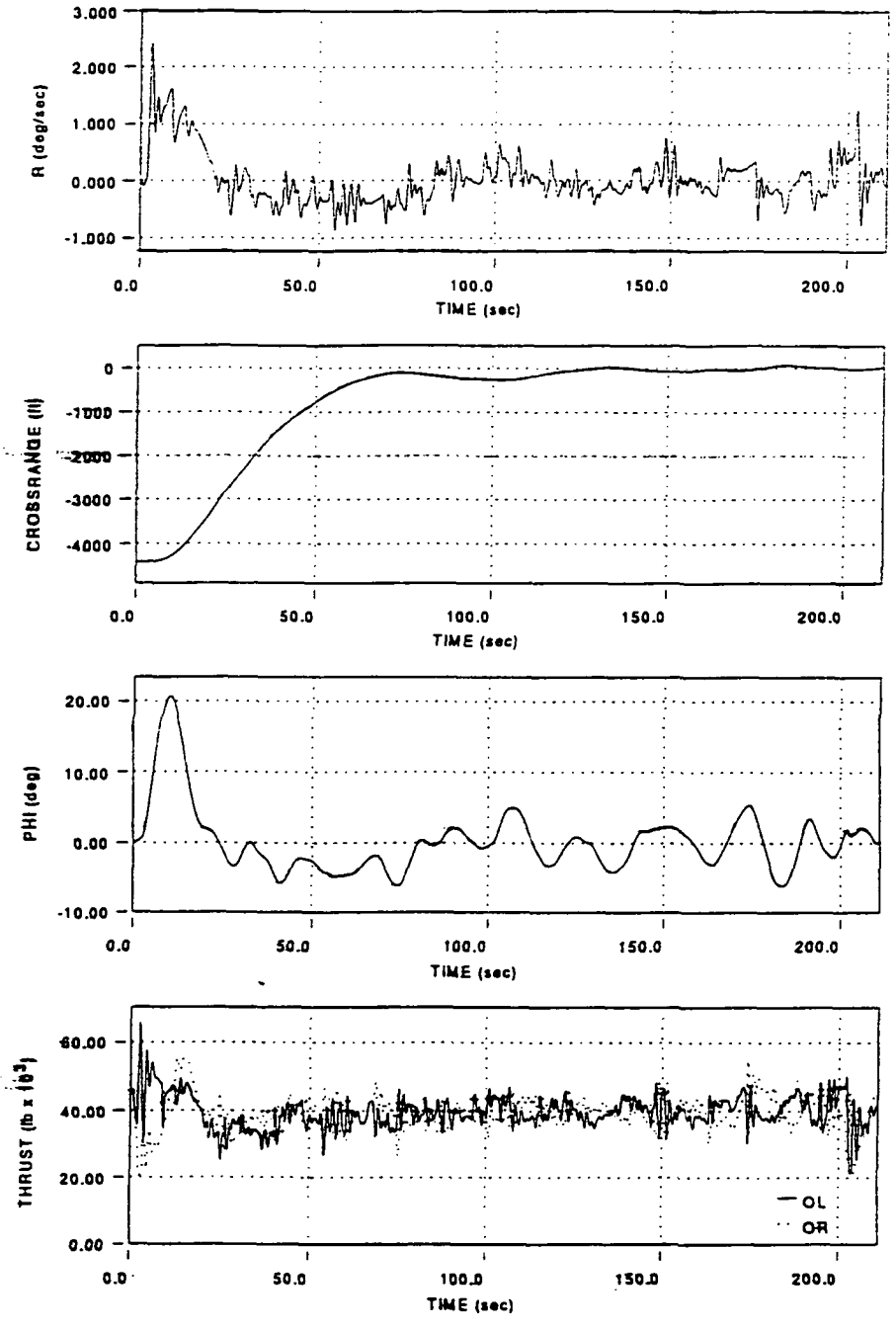

Figure G17(b) Lateral-Directional Flight Variables for Test Flight A18: Engines Moved 20 Feet Outboard with PCA with 10 Knot Crosswind from the Right

TEST PILOT B

TEST POINTS B1 - B18

Test Point B1

Baseline Configuration With PCA

Okay, this is initial try. I don't know what Donna's got set for geometry, but I'm going to start the approach here by correcting lineup and I notice that I already have the IC (initial conditions) below the glide path defined by the telephone poles there so I'll just hold level flight for a little while.

I'm going to crank in about 3 clicks--4 clicks- down and let the airplane start down. Coming up on the east shore at 4,000 feet and 180 knots. Okay, I'll start turning left to roll out on the centerline here. Used a very gentle bank of about 5 degrees and response seems good so far. Well, I've overshot a little bit so I'll have to use a little more bank to turn back and get back on centerline.

The velocity vector is very stable in pitch. It's right . . . only about 2 1/2 degree glide slope. Vectors . . . well, as I spoke it drifted up a little bit but it's still very stable, so it's sitting here right on the end of the runway right where I want it.

The lineup is my current problem - I've got to get back to the left now. Okay, approaching centerline. So, this PCA is flying well. I've got a fairly low workload here, just tiny little corrections. I think most of my overshoots are due to the inherent lack of visual acuity with the visual that makes you overcorrect.

Pitch attitude here is rock solid - just coming right down here. Okay, I'm about 200 feet in the air. I'm going to roll back a couple clicks. I'm on

centerline, not doing anything to correct - maybe a little right wing down now and there's touchdown. Just landed left of centerline - firm, but acceptable.

Okay, so that's from a Cooper-Harper rating - pretty good. The pitch attitude response is fine. I mean, I only made one correction and it was right where I wanted all the way down until the final flare and that was good response and predictable and so, in pitch, I'd give it a 2 for the task and the situation.

Roll is also good but you can see the yaw - a little bit of tendency to overshoot - very small. It maintained bank angle well - very few upsets so heading control was good and I'd give that a 3. My overshoot was my problem, not the system's problem, of starting the correction back left to line up too late - just getting used to the visual again, so, no real problems.

The bank control is sensitive. All that was necessary for this test was very small displacements from the detent on the bank knob. If there's any deficiency here it's the gains are high enough that you have to be ginger with the bank - pitch is just fine. Overall, we've got a Cooper-Harper of 3, Level 1, for that one.

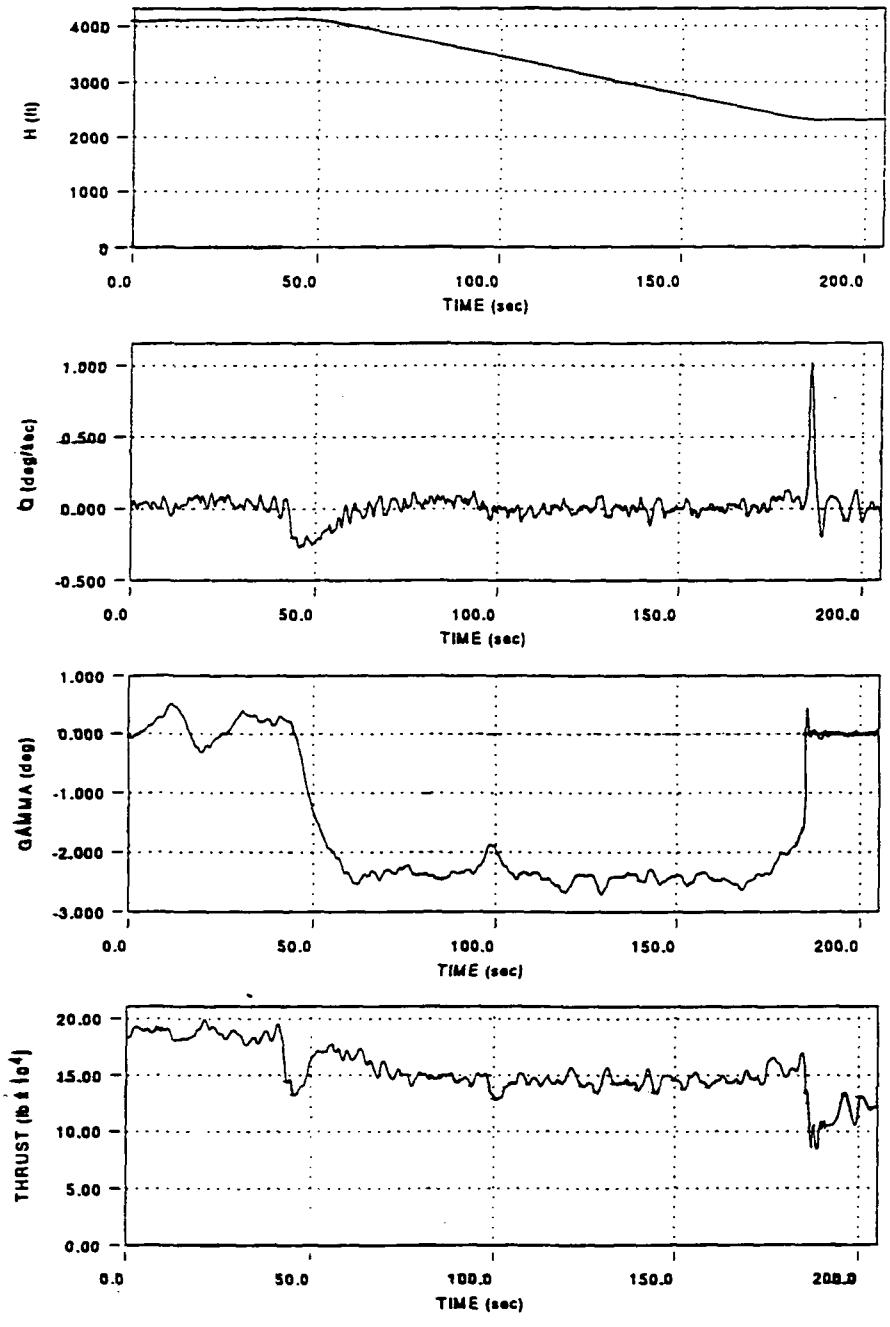

Figure G18(a) Longitudinal Flight Variables for Test Flight B1: Baseline Configuration with PCA

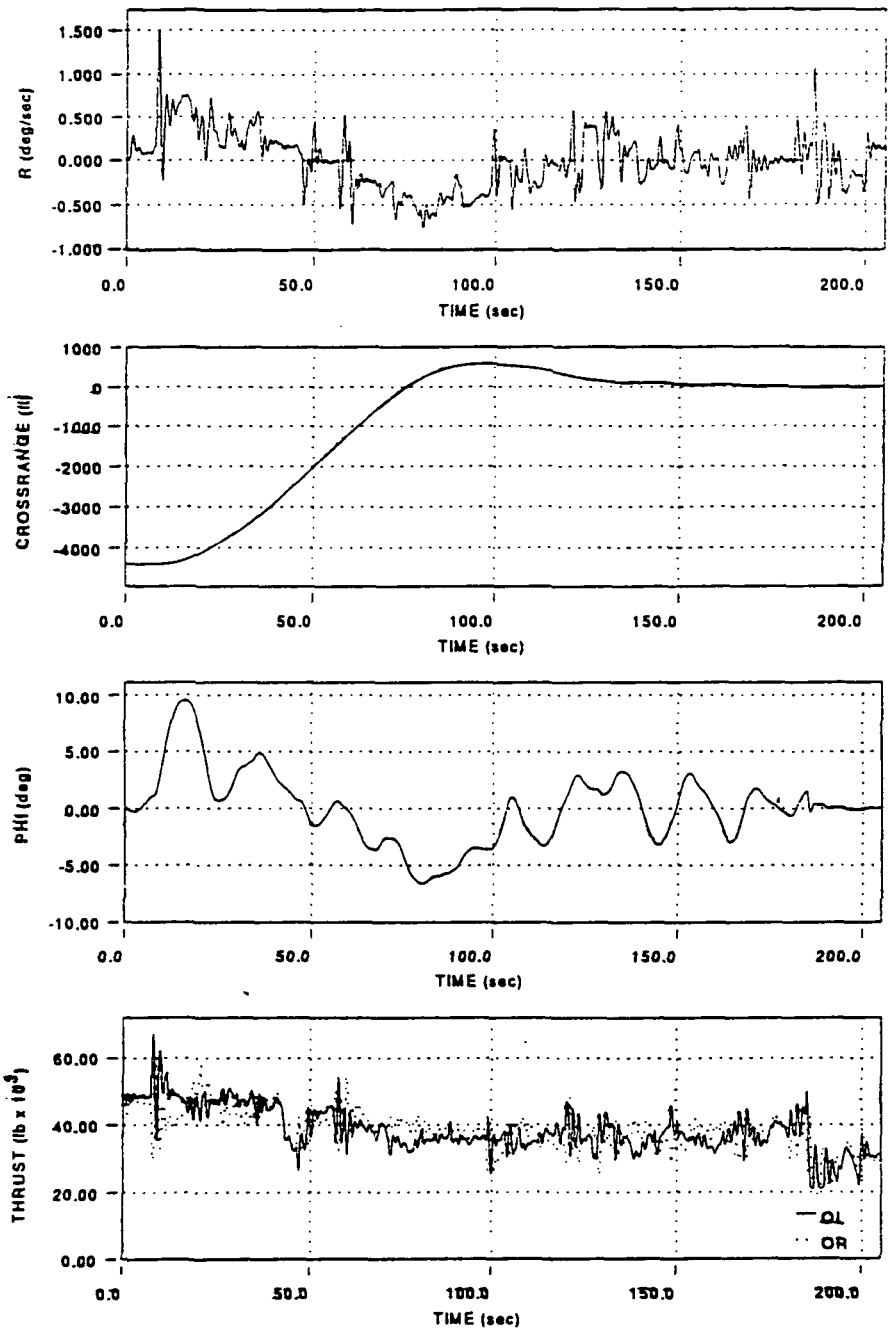

Figure G18(b) Lateral-Directional Flight Variables for Test Flight B1: Baseline Configuration with PCA

Test Point B2

Engines Moved 20 Feet Outboard With PCA

We're on run number 2. This is flaps up again, roughly 180 knots. Same IC (initial conditions) - I'll start my correction to the right. The velocity vector, I guess that's where I left it last time, is already in a descent. I'll take a couple clicks out for a little bit, bring us back up a degree or so of descent which ... man, that system is just nailing it. Whatever you want it goes there and stays.

It's up to level flight. Okay, down 2 clicks. It seems a little looser in bank control than last run - maybe it's my imagination. Another click down - another click down. Okay, looking for about 2 - 2 1/2 degrees of descent now. Put the vector on the end of the runway and starting a left turn to come back to centerline heading. You can see the yaw preceding the roll. Turbulence is very light. You can see little variations around smooth air trajectory but not much.

Okay, just about on the centerline. I'll turn a little more to get the vector over there. Once again, pitch is rock solid. It's just sitting there - piece of cake. It's sitting right on the end right where I want it. One more click nose down. Okay, I'm going to shallow a click. Drifting right a little.

We're at 300 feet (AGL). One click nose down again to get closer to the end. 200 feet. Just little lineup corrections in most of my workload. 100 feet. Put a couple more clicks to try to soften the blow here.

Touchdown just a hair right of centerline and prior to the last hash mark or prior to the last telephone pole. There's no runway markers so it's hard to tell exactly how far down we are.

I really didn't see any difference. I think pitch was solid all the way so I'll give it a 2 and lateral-directional about the same. It's higher workload, more compensation to keep everything nailed there so it gets a 3, but Level 1 all the way and no problems.

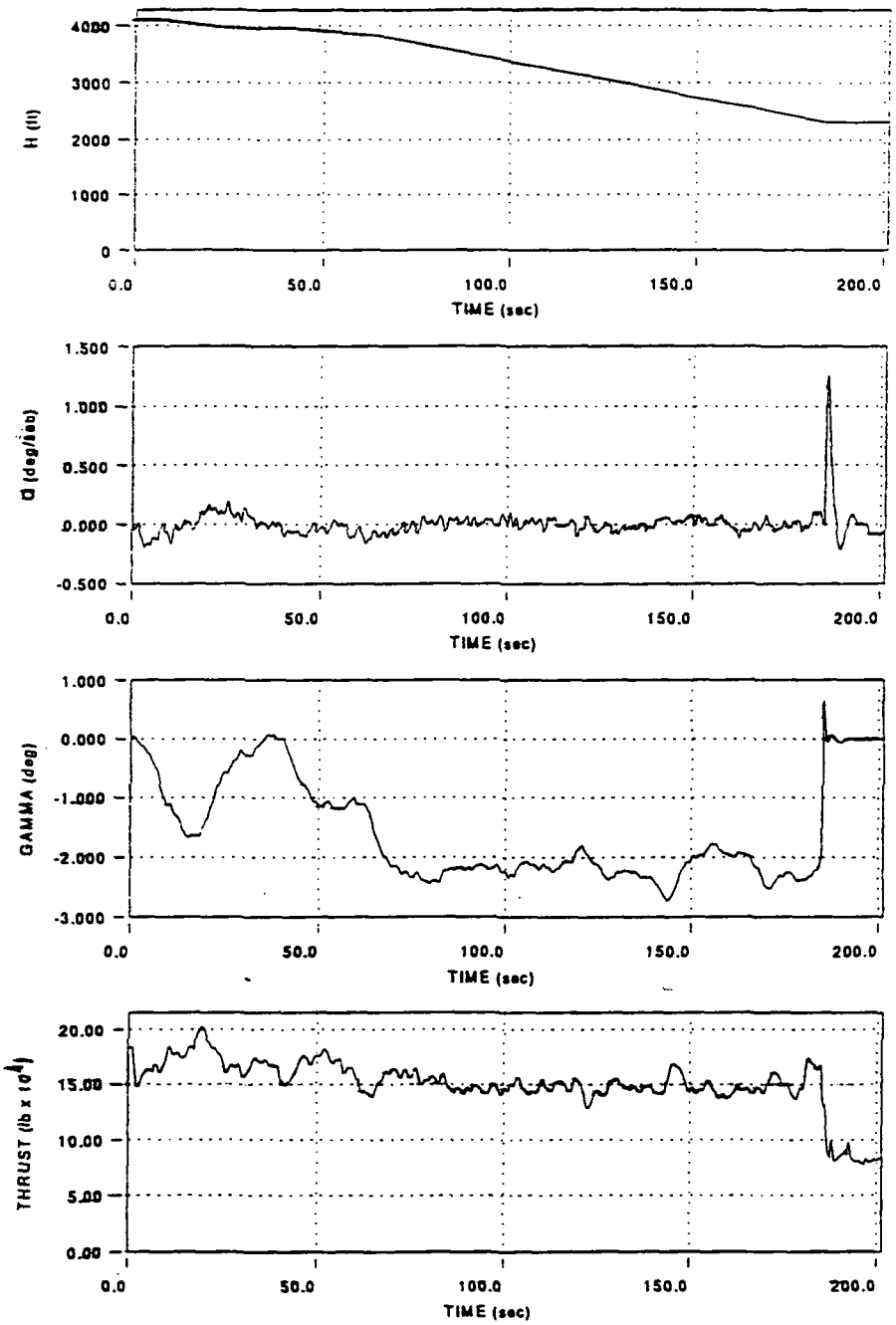

Figure G19(a) Longitudinal Flight Variables for Test Flight B2: Engines Moved 20 Feet Outboard with PCA

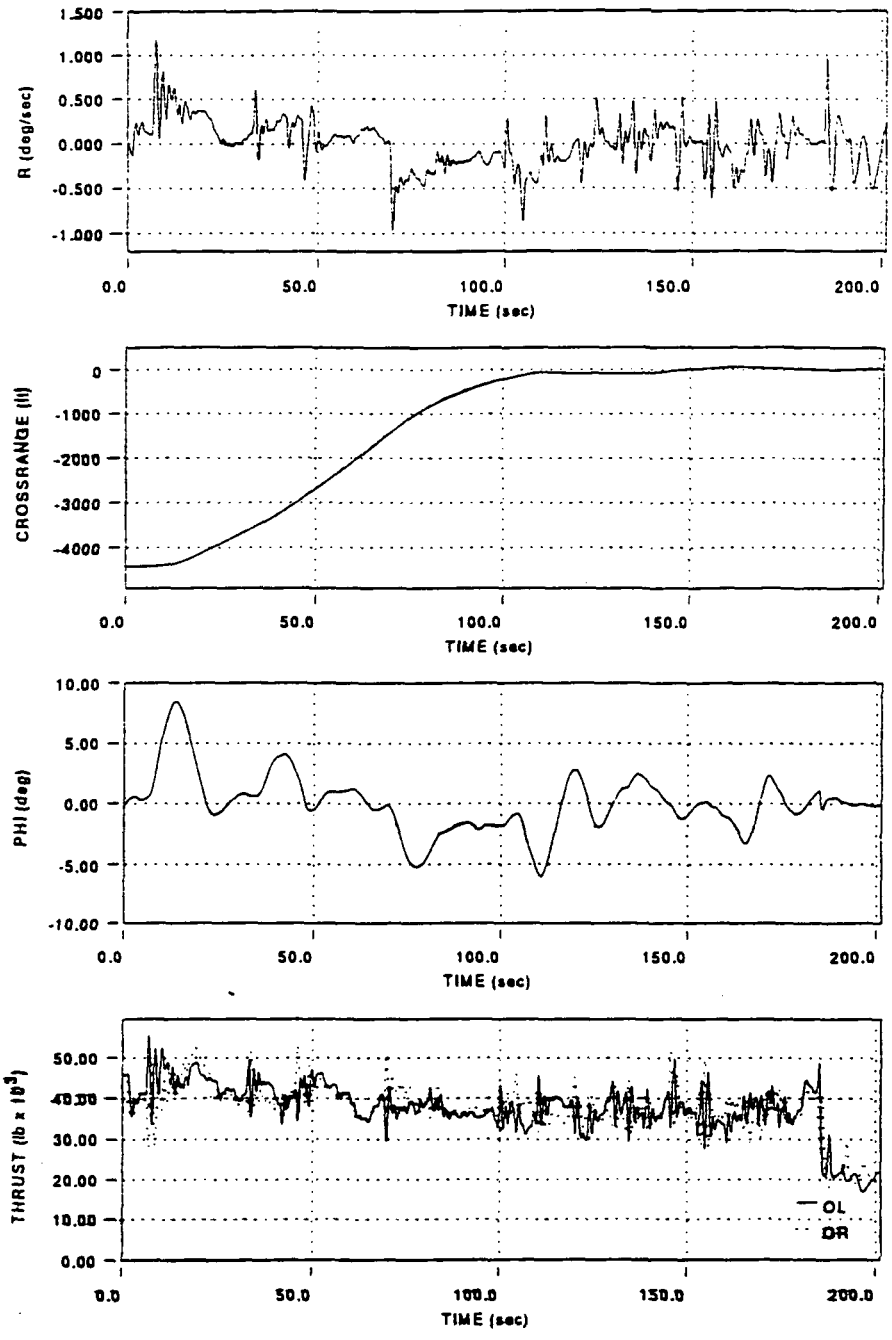

Figure G19(b) Lateral-Directional Flight Variables for Test Flight B2: Engines Moved 20 Feet Outboard with PCA

Test Point B3

Engines Moved 20 Feet Inboard With PCA

Okay, starting run number 3 and start my right turn to correct. Roll in a couple clicks down to get started down. Bank response is good - deadbeat - no overshoots as is pitch. I don't see any difference right now. So, a couple more clicks down . . .

I'm starting a left turn – a very shallow left turn. Another click down. I'm not saying much because I don't see much difference. So far, all the runs are very, very similar as far as the response goes. So, whatever you're doing to the engine geometry, PCA is absorbing it well.

I'm a hair right of center - I'll just let it drift over here a little. I haven't touched the pitch thumbwheels - it's just nailing it. Coming right down - one more click down. Okay, where are we? 2,800 feet (MSL) - 500 feet (AGL). Click up - 2 clicks up. Shallow out here a little - go for a nice, smooth landing.

There's 300 feet - 200 feet - 100. One click nose up - there's 80 feet. Another click nose up - on centerline. I don't see any ground effect - it just flies right down there and lands. A hair right of center and about a degree gamma (flight path angle) at touchdown.

These are all firm landings but I would guess . . . all I can say is, ditto for the last two. It felt the same - the same numbers - I'm not seeing any difference. It's a very good system. I'm landing it where I want to every time.

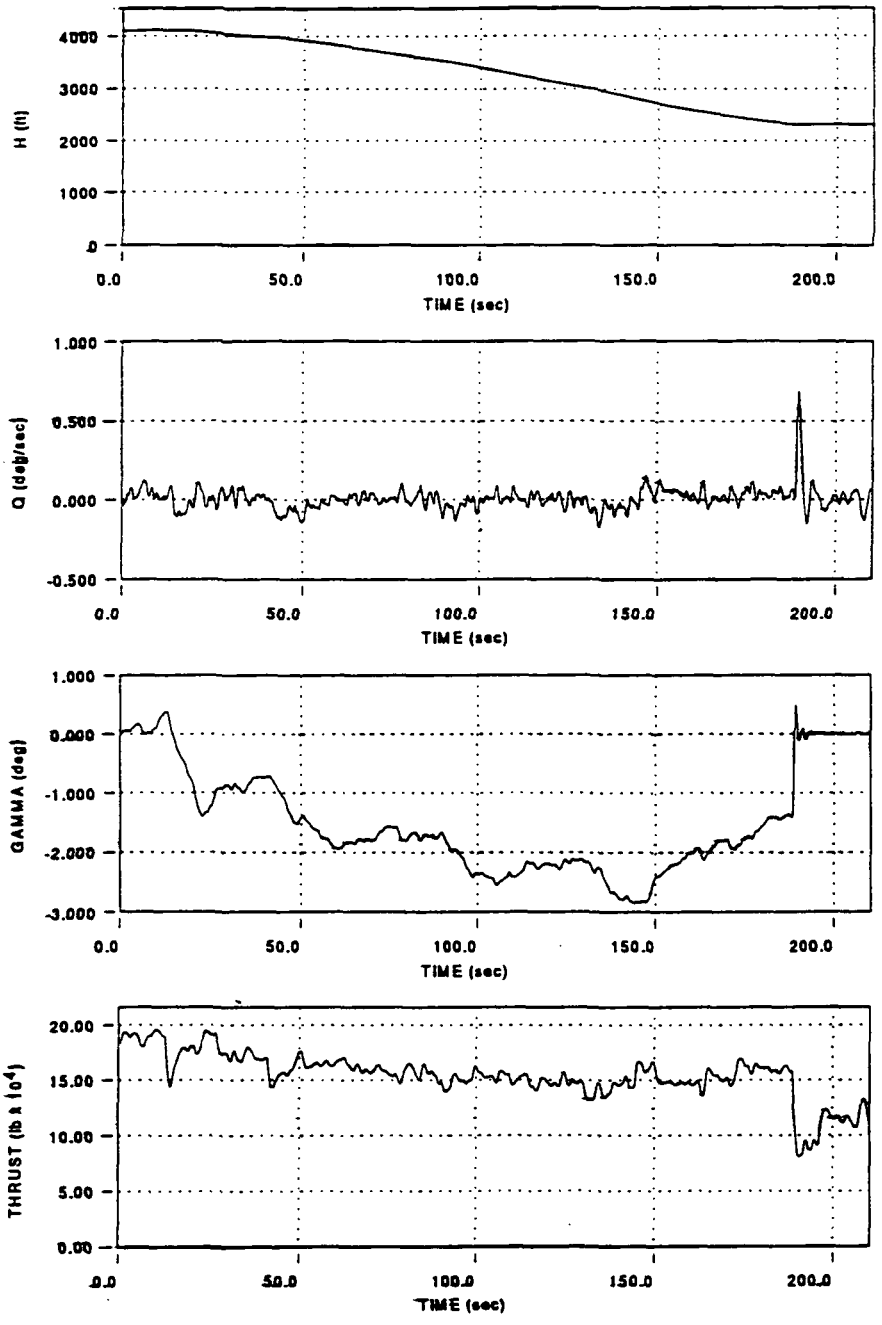

Figure G20(a) Longitudinal Flight Variables for Test Flight B3: Engines Moved 20 Feet Inboard with PCA

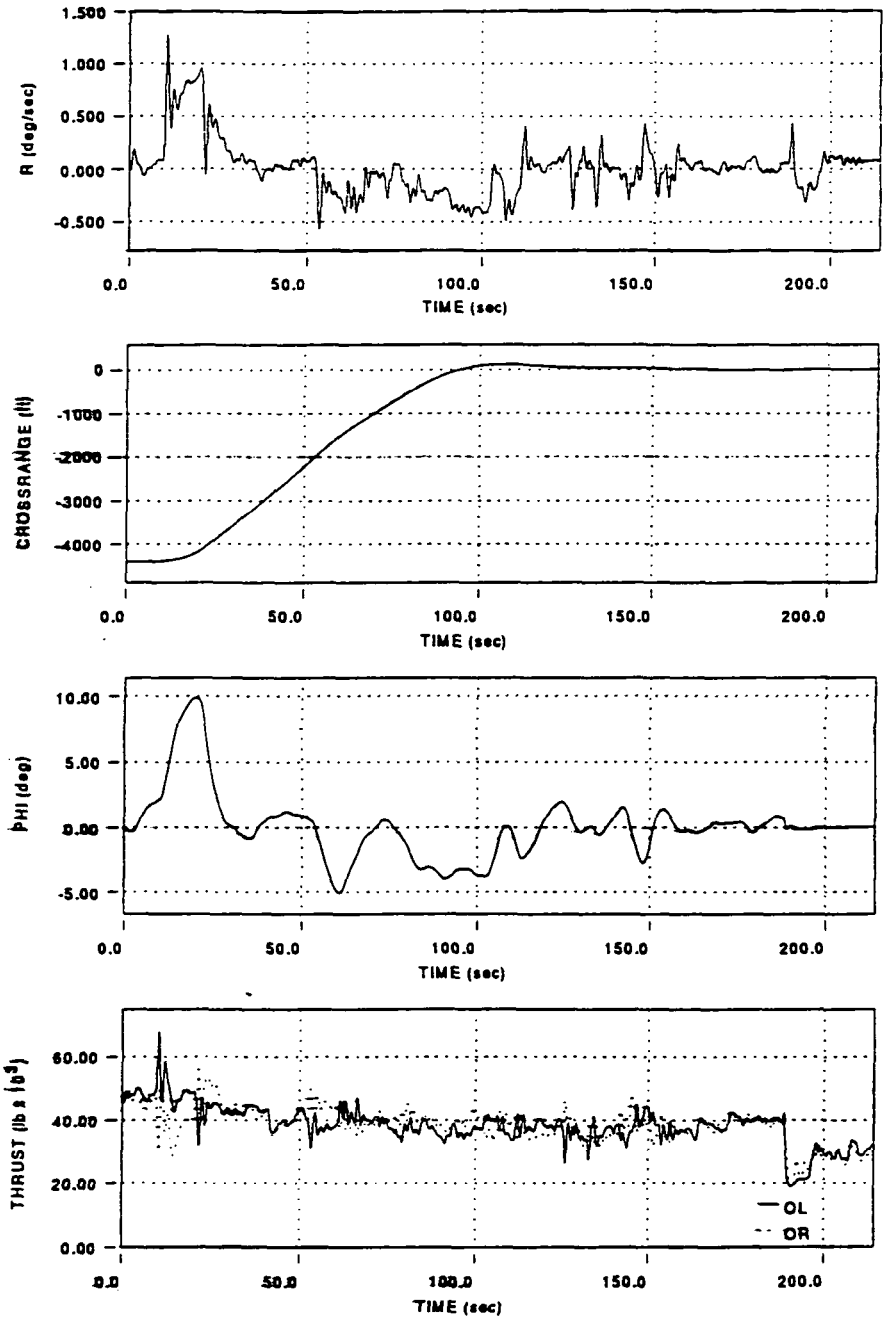

Figure G20(b) Lateral-Directional Flight Variables for Test Flight B3: Engines Moved 20 Feet Inboard with PCA

Test Point B4

Engines Moved 5 Feet Vertically Downward With PCA

Okay, run number 4. The old, standard reset point - starting a right turn. I give it 3 clicks nose down and immediately the bank angle response seems to be exactly as before. Deadbeat - back to detent rolls right out and maintains exactly wings level. I mean, you couldn't ask for more. There seems to be maybe a slight overshoot of a half a degree or so in pitch, but now it's very stable.

I'll give it one more click down while we're angling in here. A pretty hefty correction angle - I'll start taking it out to some extent. Looking for about a 5 degree bank angle or so as we come on around on centerline. Pitch is rock solid, as usual. One more nose down click for now. Overshot slightly, so I'll have to correct back left a little - get that vector on the left side.

Okay, approach gamma's (flight path angle's) 2 degrees. That's good - just what I wanted and right for the end of the under run - also what I wanted. Lineup is correcting very slowly. Okay, I'm on centerline. Correct right a hair - just a tweak of the knob is all it takes. Back in detent. Tweak left a little here to get the wing up.

Okay, there's 2,700 (MSL) - that's 500 feet (AGL). Correct left a little. I'm right on the threshold with the vector. There's 200 feet - I'm down to 12, 13 (rate of descent in feet per second) and I'm going to shallow a little now here at 100 feet. Coming down to 10, 9 - shallow another couple clicks.

Coming on in here at 30 feet - 6 feet per second, 5 - touchdown. 5 - I'll take it. Just left of center and correcting.

Well, Donna, if you're changing anything I can't tell. It's the same airplane all four, so same numbers and I'll just leave it at that.

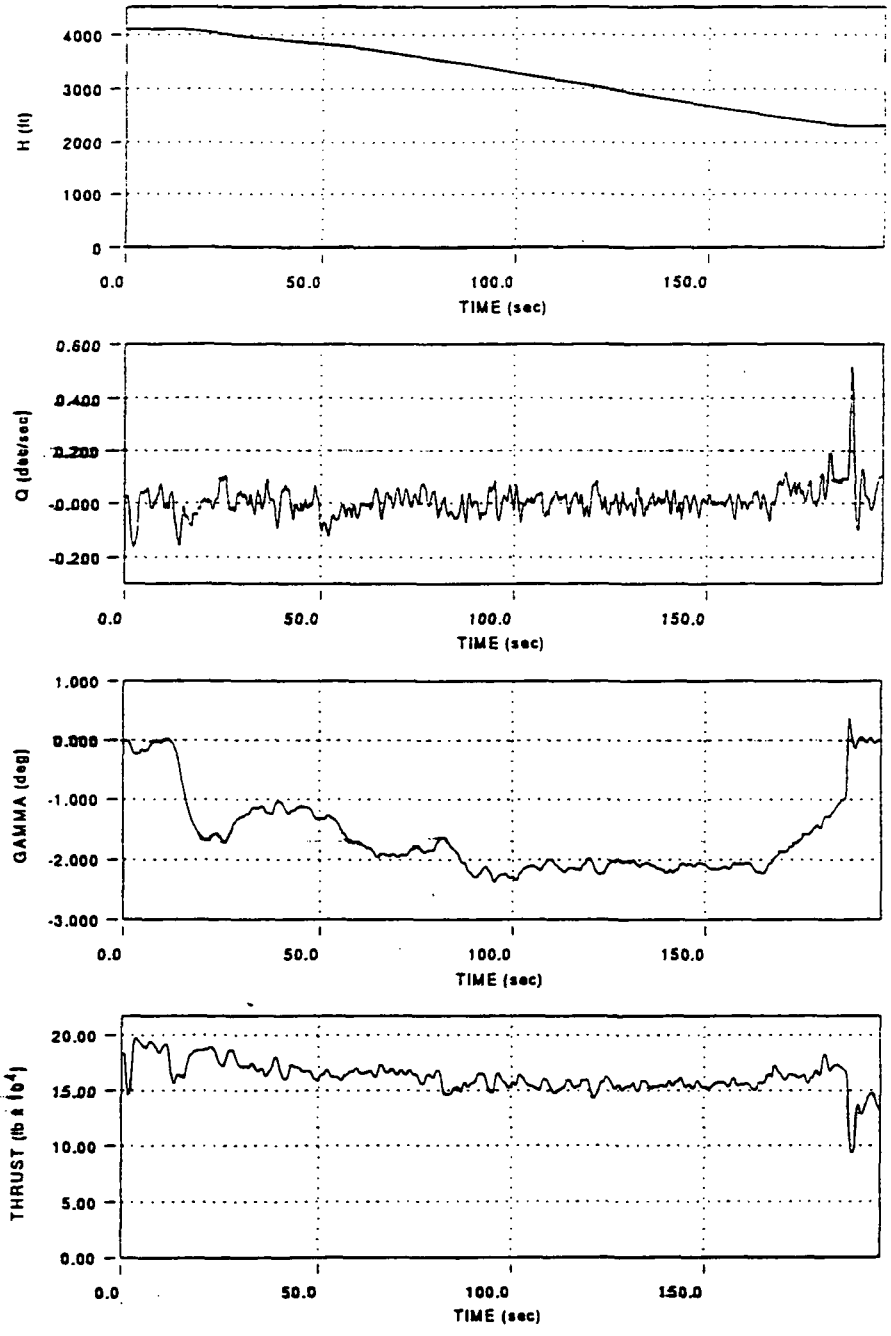

Figure G21(a) Longitudinal Flight Variables for Test Flight B4: Engines Moved 5 Feet Vertically Downward with PCA

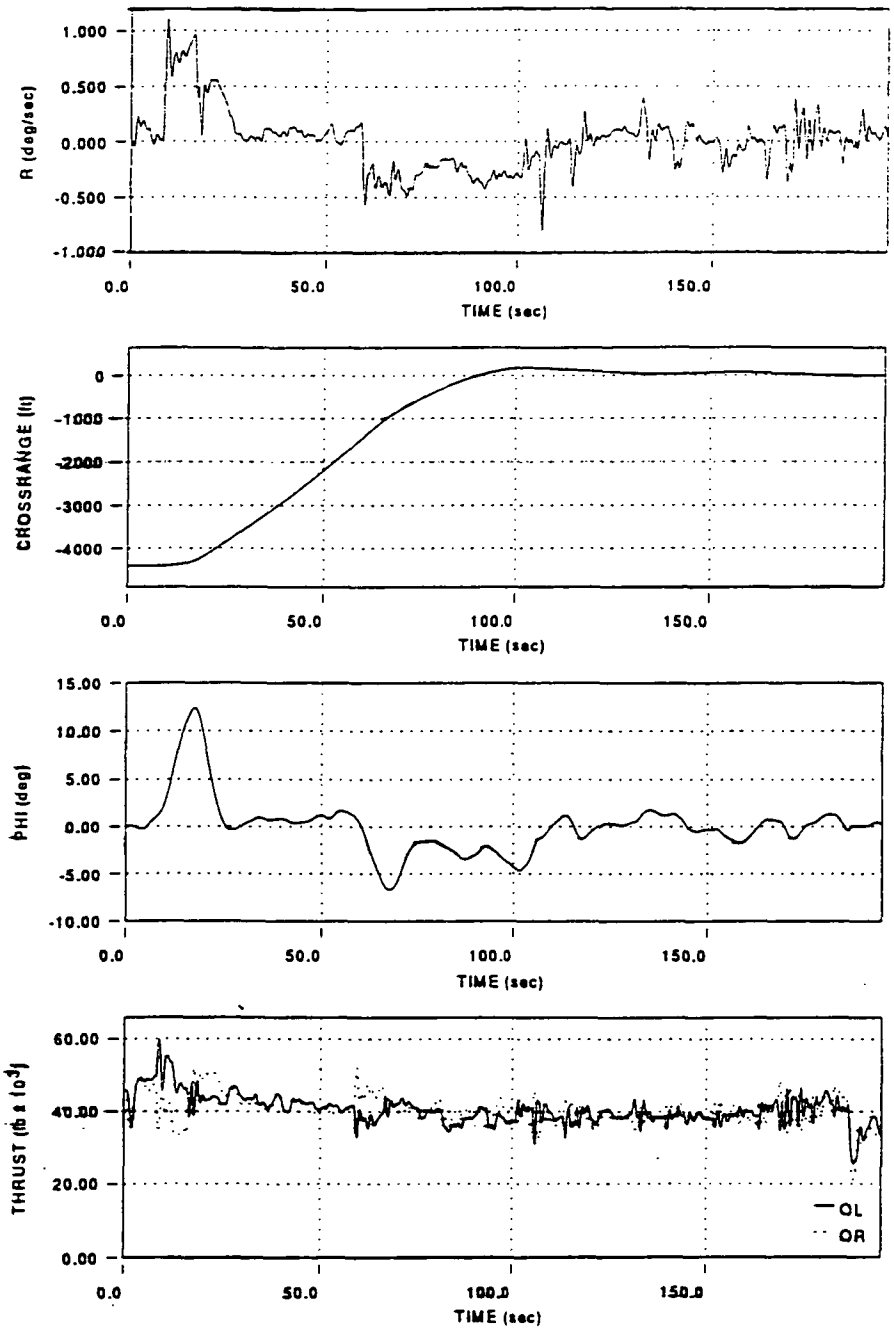

Figure G21(b) Lateral-Directional Flight Variables for Test Flight B4: Engines Moved 5 Feet Vertically Downward with PCA

Test Point B5

Full (50 Degrees) Flaps With PCA

This is run number 5, right? This is desired to be done with flaps down and as I crank it down through 30 (degrees) I see the airplane pitching up slightly. I'll put in about 4 - 5 clicks nose down to get it started down here. Flaps are full down now and let's see how the system does.

I've got to start my lineup correction. I see no change in lateral response with flap position and it looks like we're settled out solid at 2 1/2 degrees descent which is equivalent to 5 clicks. So once that flap transient's over, it feels like the same old airplane so far, anyway.

Bring it up one click. Okay, starting a shallow left bank - a little more left bank. Very solid - steady. I'm trying to think of something to say about this. Certainly not much difference with flaps. Okay, a click nose up. We're on centerline and we're holding a constant degree and a half here - one more click nose down to keep it coming down.

I'm making hardly any inputs - I'm just kind of sitting here watching. Over to the left - left bank - back to detent here. One click nose down to get a little closer to the end. Okay, we're right at 500 (AGL). What it ought to be - steady. There's 300 feet - no, there's 300 feet. Okay, at 200 feet I click to shallow. There's 100 feet - another click. 50 - another click. Now we'll just see how we touchdown here.

I'm drifting a little right. There's 5 feet per second - we'll just let her come on in there - 4, 3. That's a good touchdown - a little right of center. I

didn't watch the lineup - I was kind of hung up on the h dot (rate of descent) there and let the lineup drift on me. I could have done better if I'd paid more attention because the system is very responsive, very stable and every run has felt the same so I don't see any difference in flaps down other than we're flying slower - but it flies just fine. Cooper-Harpers remains at a 2 to 3 - Level 1 definitely.

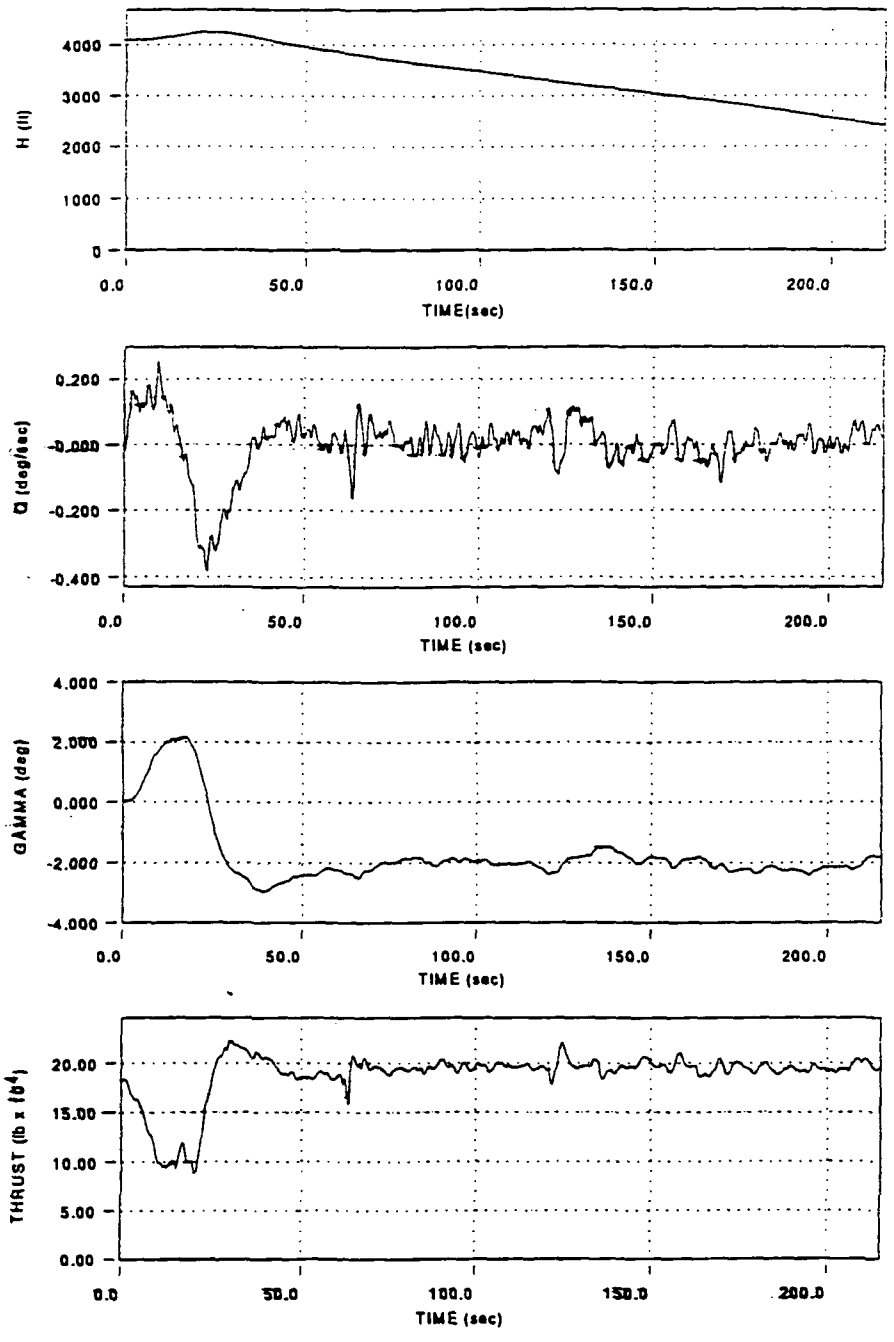

Figure G22(a) Longitudinal Flight Variables for Test Flight B5: Full (50 Degrees) Flaps with PCA

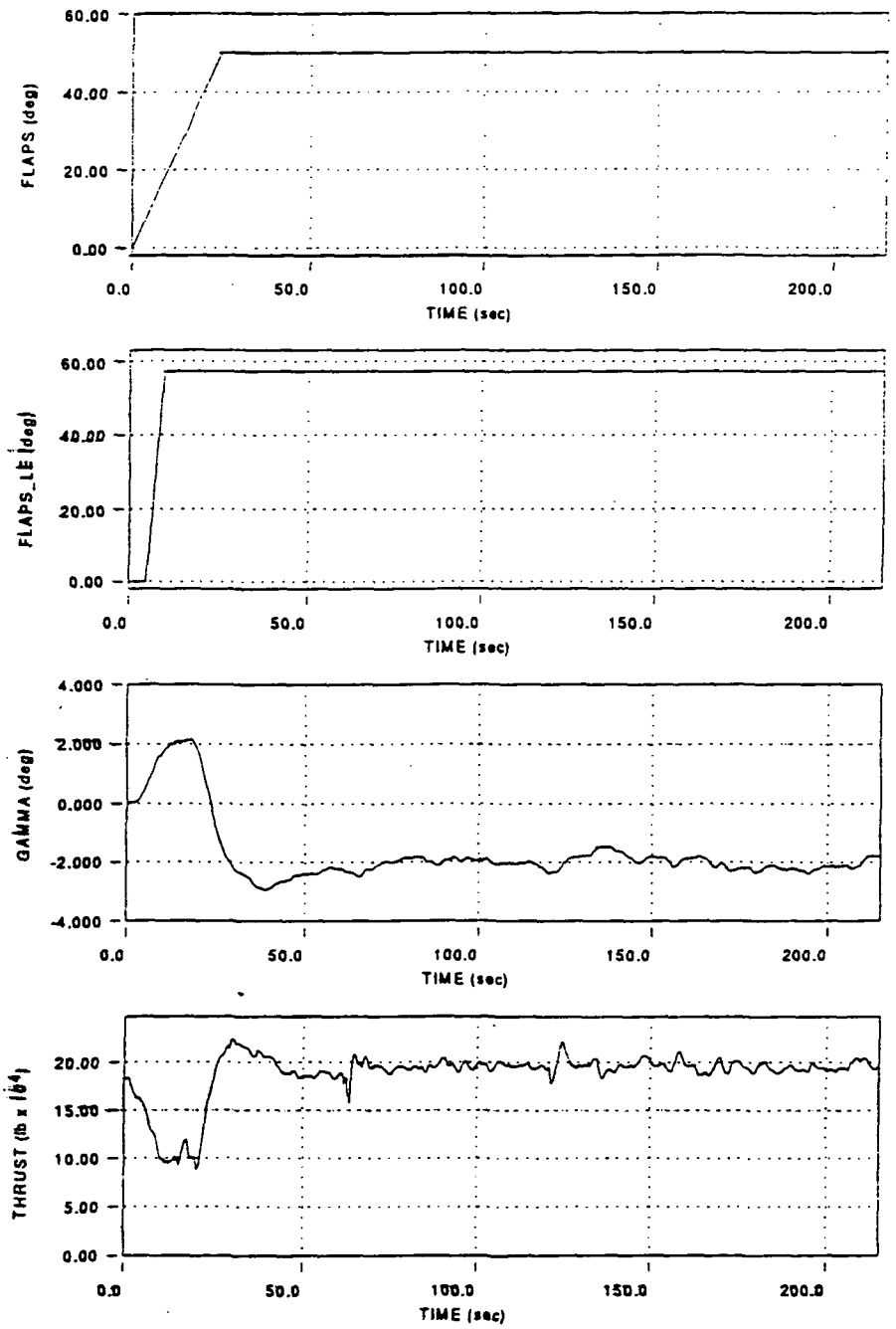

Figure G22(a) Longitudinal Flight Variables for Test Flight B5: Full (50 Degrees) Flaps with PCA (cont.)

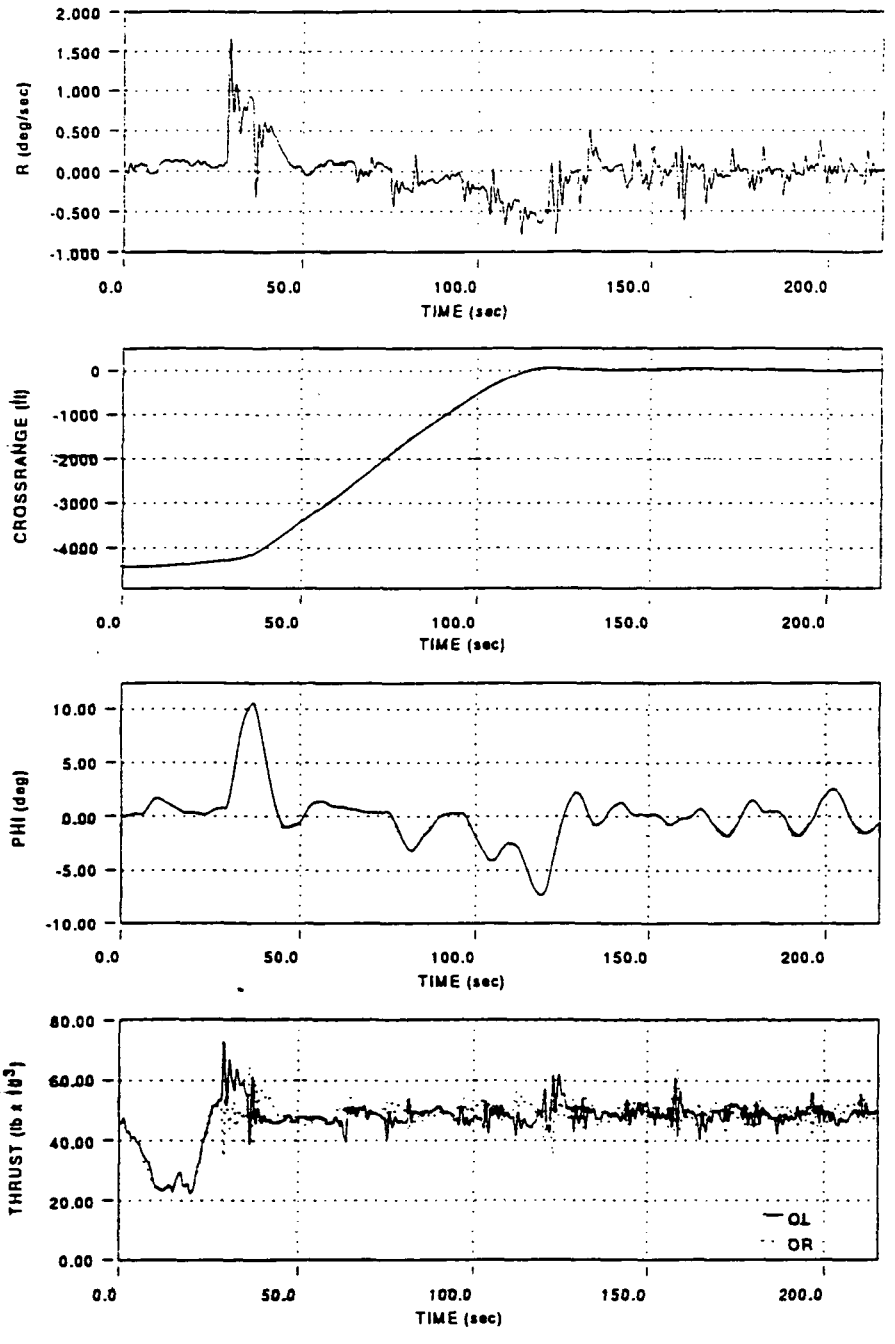

Figure G22(b) Lateral-Directional Flight Variables for Test Flight B5: Full (50 Degrees) Flaps with PCA

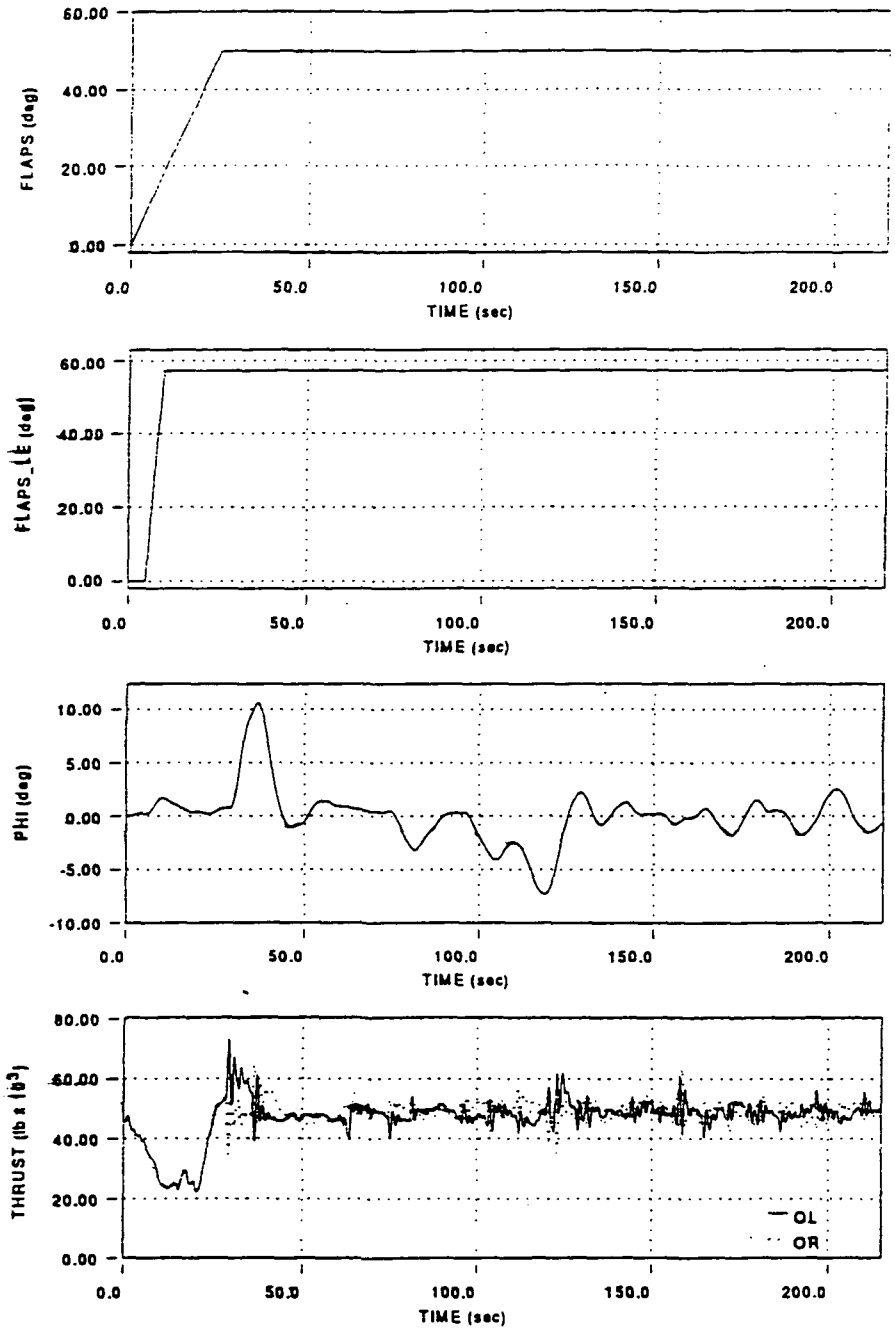

Figure G22(b) Lateral-Directional Flight Variables for Test Flight B5: Full (50 Degrees) Flaps with PCA (cont.)

Test Point B6

Outboard Engine Inoperative With PCA

Here we go with number 6. This will be with flaps up, right? Start the lineup correction - 2 clicks nose down. Two clicks gave me an overshoot of a degree or two. Well, it's just kind of hanging down there. Two clicks - it's like this may be a little looser in pitch. Not quite so absolutely responsive to the pitch. I'm back to only one click nose down and it's sagging on me. I'm going to have to go another, well, another click nose up which is back to zero to hold this 2 degree descent. It's drifted back toward one degree so I'll go one click nose down.

Bank response . . . oh yeah, it's having a lot more trouble with pitch now than the others. I'm having to compensate a little there working the pitch knob. It's drifting up and down from the commanded, so it's not near 'sit there and just watch it' as the previous runs have been. If I had to guess I'd say you've raised the engines a bit.

Okay, try to get this lineup killed and keep our eye on pitch so it doesn't get away from me. Click nose down now and it's fairly stable - still where I want it now. Okay, we're on centerline - back in detent - have to correct right a little. Okay, it's a good, flat approach.

Pitch is fairly stable now to a degree and a half to 2 degrees. Try to keep correcting the lineup. Coming down at 9 feet per second down to 300 feet (AGL). It's drifting nose up which is what I want. I'm kind of nervous about changing anything. It's acceptable - I'm not going to mess with that

pitch thumbwheel for awhile. You know, I'm going a little bit longer than I would be optimum and it's still pretty good.

There's a hundred feet - the nose is tending to drift up which is kind of what you want here in the last 50 feet. H dot (rate of descent in feet per second) - 9. I don't know, give it a click up - 8. Okay, there's a firm landing at 8 feet per second but just left of center. So, my last little click nose up didn't really take. However, because I was in fairly good shape it's an acceptable landing.

So, here a definite degradation in pitch attitude response - slower, looser, and I give it a . . . I think we're getting to the desired performance okay but, well, I'd give pitch in this case a 5 just because it's not dramatically obvious on the screen that there's a lot more worry about keeping the nose where you want it.

Lateral-directional, maybe a little looser than before. I'd give it a 4 and we'll call the whole thing here a Level 2. Still adequate, if you work at it, to get it on the ground within the desired parameters.

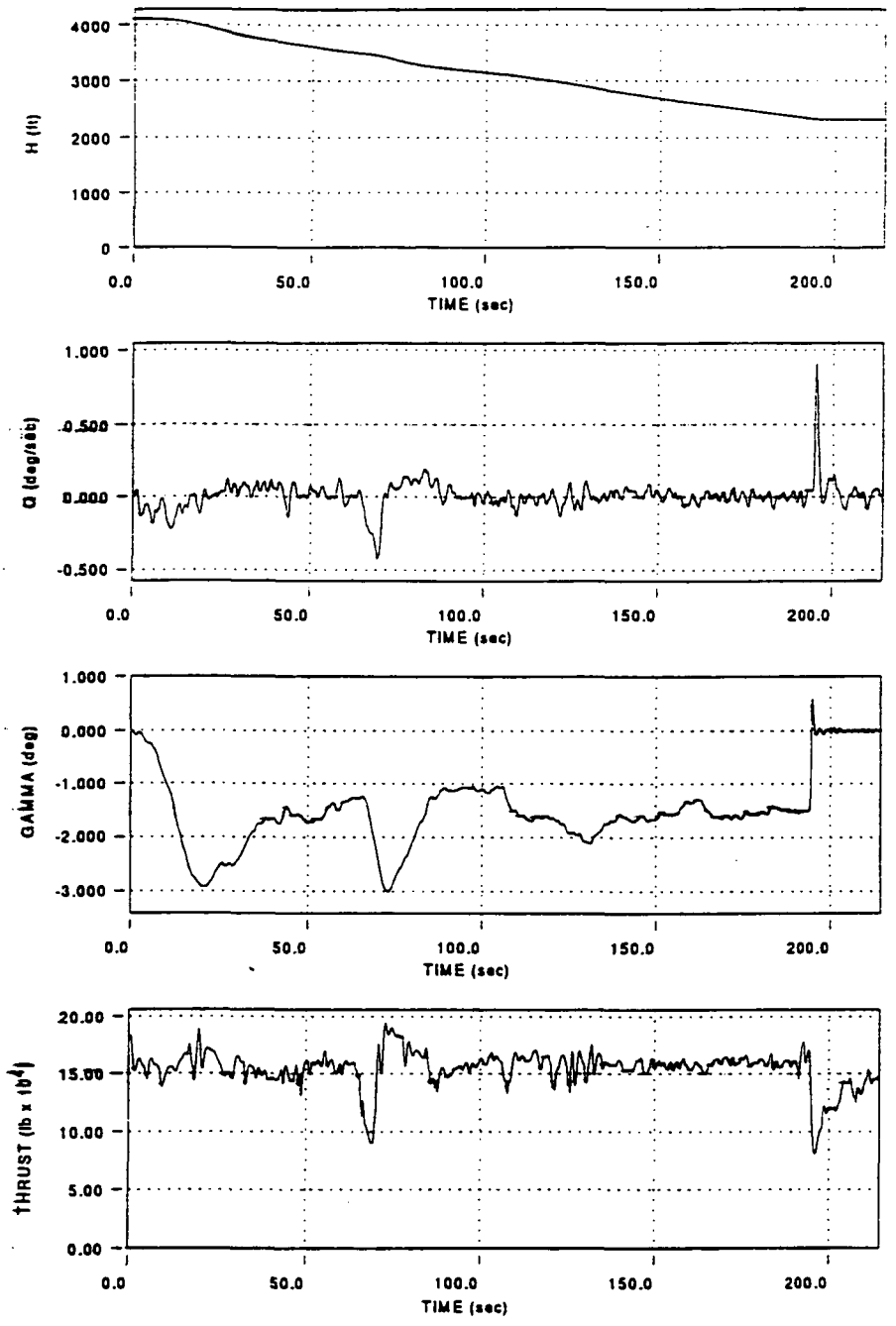

Figure G23(a) Longitudinal Flight Variables for Test Flight B6: Outboard Engine Inoperative with PCA

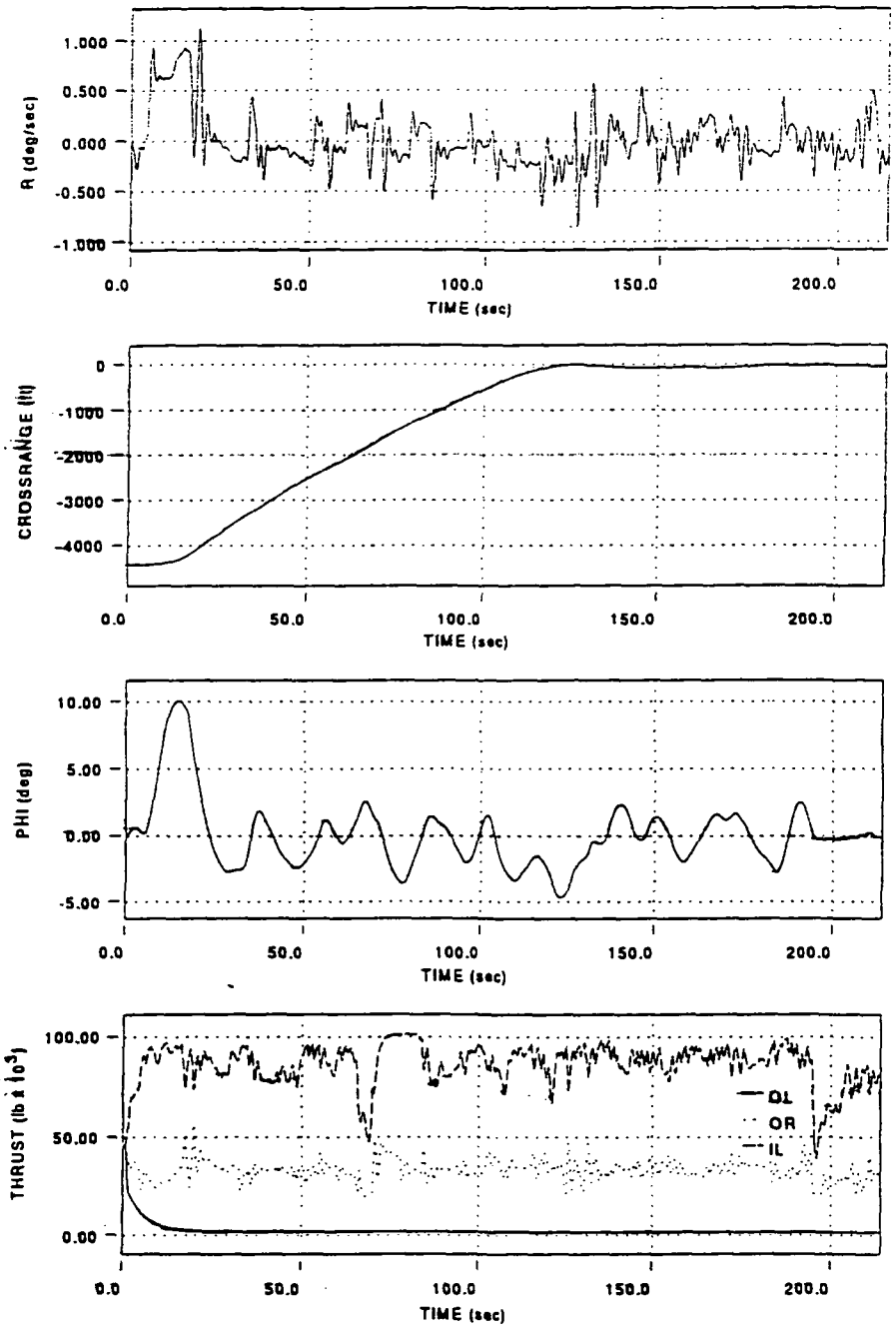

Figure G23(b) Lateral-Directional Flight Variables for Test Flight B6: Outboard Engine Inoperative with PCA

Test Point B7

Engine Time Constant Of Three Seconds With PCA

Here we go on number 7. Start my correction - already pitch has drifted a little, although the bank response is snappy. Okay, we've got our lineup correction in there - back in detent - it's rolling out and wings level. Okay, I'm going to give it about 3 clicks nose down to get it started down here and see what happens. Laterally - just fine. Pitch is a little 'wandery' but it's coming down gradually.

Now make it 4 clicks. Okay, starting a left turn. Two more clicks down - I'm sighting down the top of the phone poles right now. I've overshot it - line up again and set there. I've got 2 more clicks - 2 clicks nose up now. Let's see how that takes.

I've got to get this lineup back on - 2 nose down. The pitch response is just slower. It seems relatively deadbeat, stable, but it's slower. Well, there's kind of an overshoot in the nose down direction. One click nose up. This would be a lot tougher without a HUD (heads up display) because that velocity vector really shows you what it's doing and I think it'd take a lot longer to figure that out without the HUD.

Okay, there's 500 feet (AGL). Try to get the lineup fixed here. 300 feet - lineup's good. In detent - 200 feet. Okay, couple clicks nose up to shallow things out. Longitudinal placement's great. We're coming across the threshold here at about 50 feet and h dot's (rate of descent's) pretty good. We'll give it a couple more clicks to try and soften it.

Here's touchdown at - what was it - 6 (rate of descent in feet per second) or so, 5. I haven't gotten one right on centerline yet - I'm always within 10 feet left or right. Okay, this is very similar to the last run. The pitch attitude is degraded from the earlier ones - pitch attitude control. A 5 in pitch - it's compensation or attention is maybe just a general tendency to wander from where you asked and a 4 laterally.

There's similarities to the last run there - a little looser, a little more corrections required a little more often. But still, a Level 2 to do the task as acceptably completed.

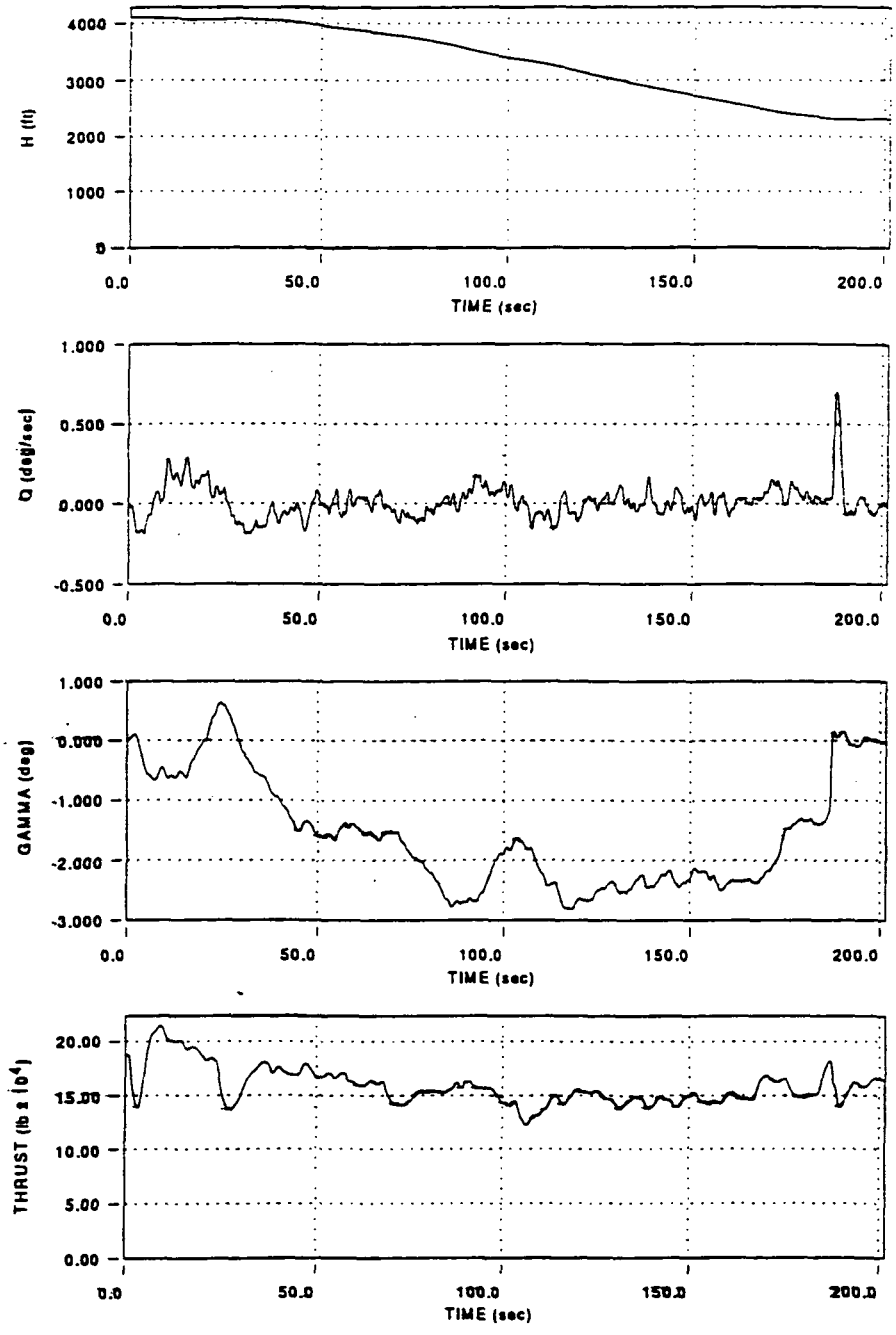

Figure G24(a) Longitudinal Flight Variables for Test Flight B7: Engine Time Constant of 3.0 Seconds with PCA

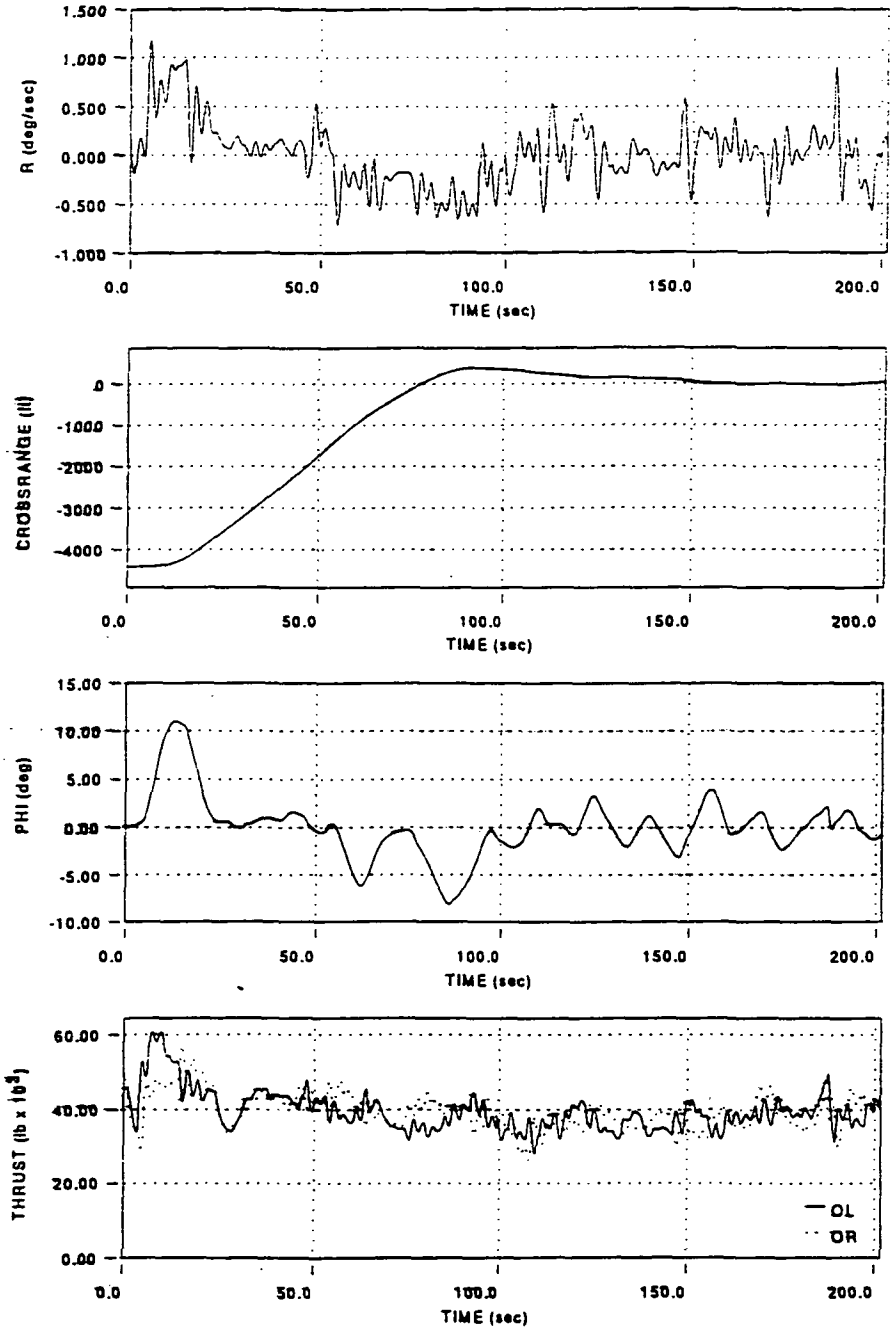

Figure G24(b) Lateral-Directional Flight Variables for Test Flight B7: Engine Time Constant of 3.0 Seconds with PCA

Test Point B8

Engine Time Constant Of One-Half Second With PCA

This is number 8. Okay, breaking right. Bank response is instantaneous. I go 3 clicks nose down to get started down. Okay, there's a good correction angle - I'm going to go back to detent and bank. And it rolls out slow, but deadbeat. Holding good wings level. Pitch is wandering around one degree which is about what I gave it. Make it a degree and a half here - 2 degrees - down to 4 clicks total. Starting a left turn back - very shallow. Now we'll just stop it for awhile.

Okay, back into a little left bank and bring that vector on over. A slight overshoot, not bad. Now looking down the right hand runway boundary. Okay, we'll just use this very gradual return to centerline. That's good - right on. The pitch is fine. I've figured out the right number of clicks and I'm just leaving it there so it's right where I want it.

Just sitting here ginning down final. 600 feet (AGL). Okay, 400 feet. 200 feet - better start shallowing. One hundred feet - just keep it coming down, work on the lineup. That was 50 feet - another click. 7 (rate of descent in feet per second), 6, . . . about 5 or 6 and once again, off centerline, but not by . . . 10 or 15 feet is all.

Okay, it didn't quite seem quite as bad although maybe I'm just learning to play the game a little bit. I didn't have to work pitch as hard that time so I'd probably bring the pitch rating up to 4 as was the lateral-directional for Level 2 and a Cooper-Harper of 4 overall, also.

There are no biases, no crosswinds or anything, so it's really . . . once you get it nailed, it's really happy to stay there even with this very light turbulence as evident by small variations in attitude, but it certainly isn't any problem.

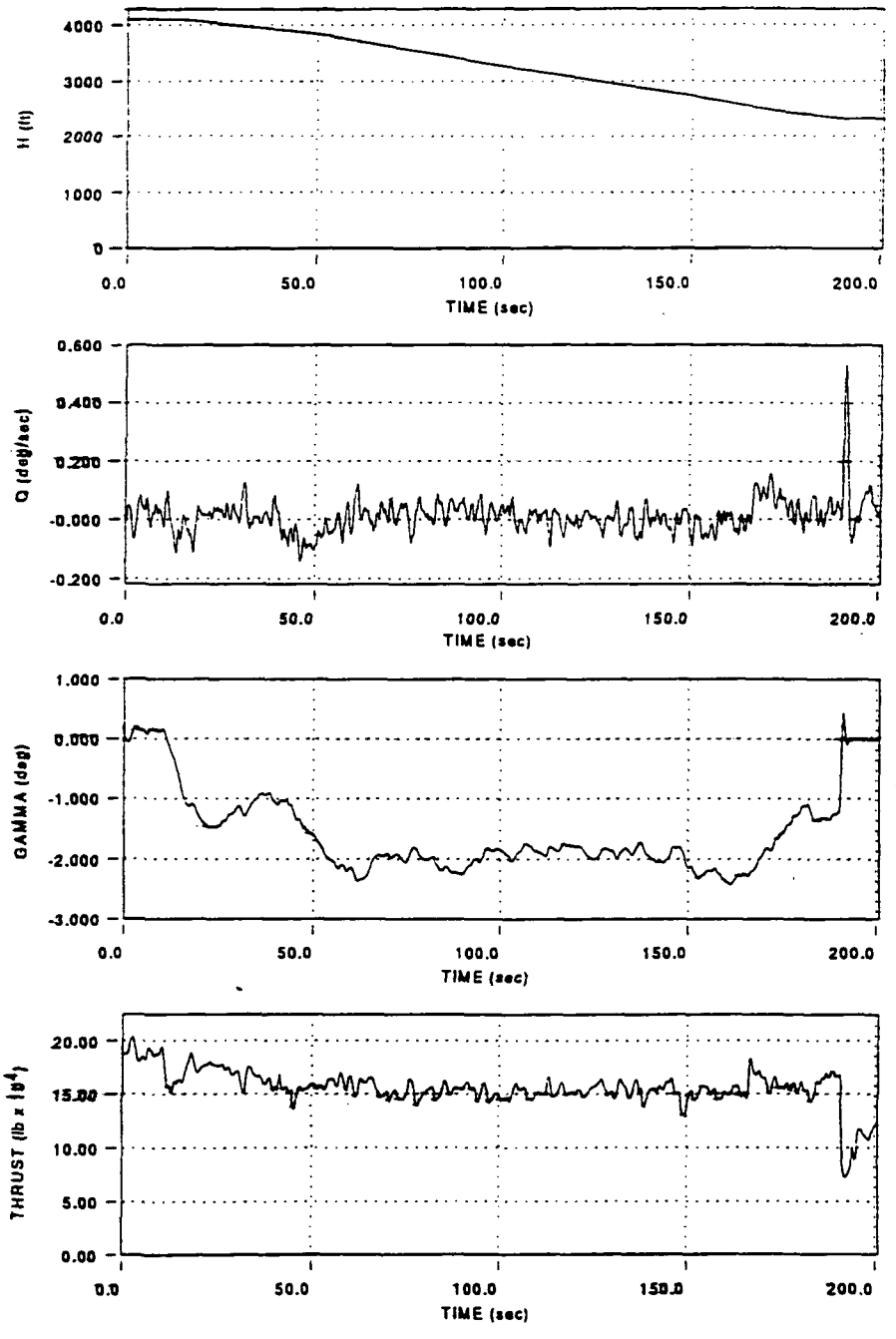

Figure G25(a) Longitudinal Flight Variables for Test Flight B8: Engine Time Constant of 0.5 Seconds with PCA

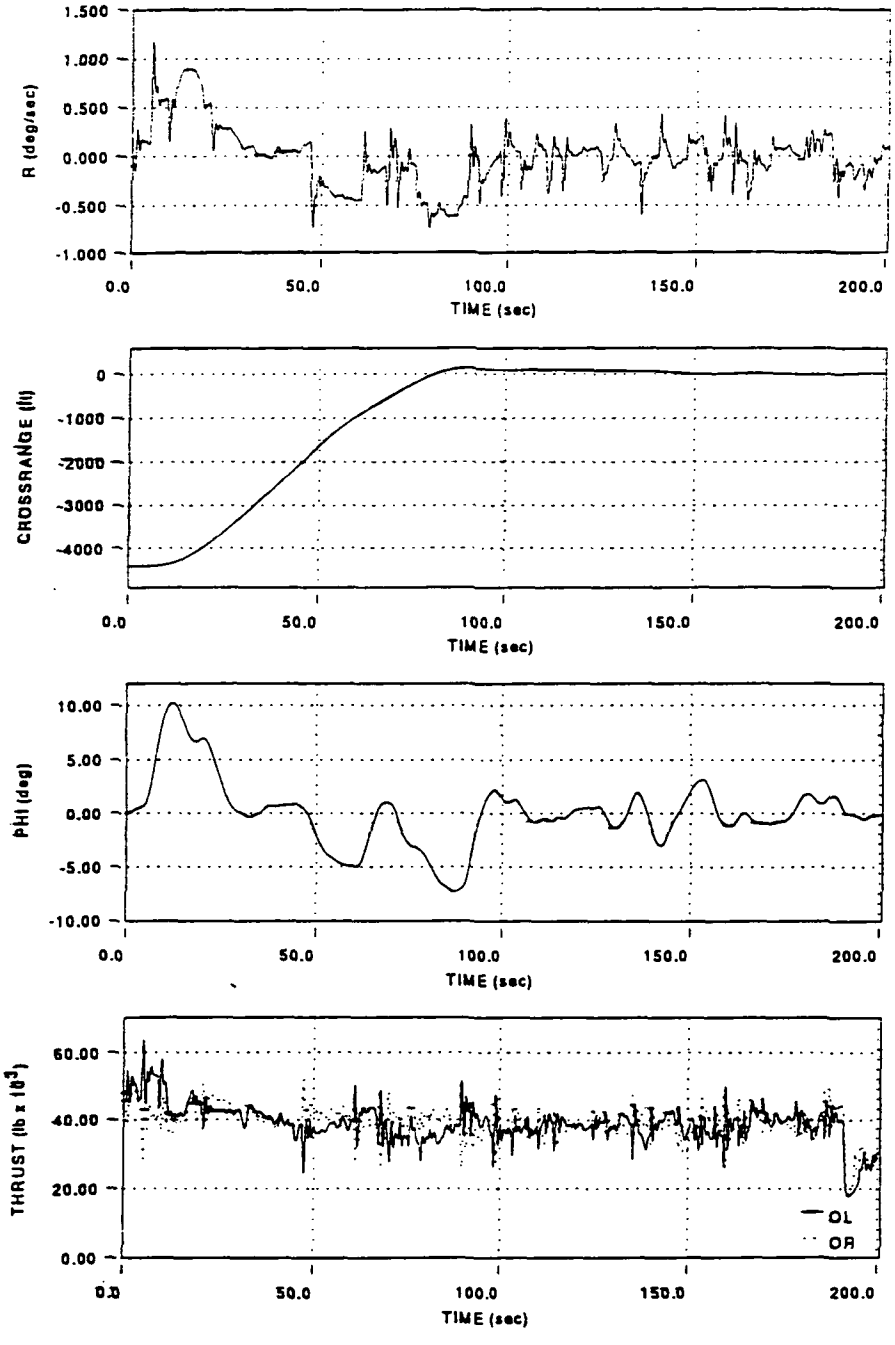

Figure G25(b) Lateral-Directional Flight Variables for Test Flight B8: Engine Time Constant of 0.5 Seconds with PCA

Test Point B9

Intermediate Turbulence With PCA

Whoa, a little transient here. Something's definitely different here laterally. Is this the engine out case? Anyway, there was something causing a left roll transient. Watching the throttles - it's hard to tell whether they happen to carry a bias to hold wings level or not. Anyway, we rapidly corrected the transient - straightened up - and it seems to be flying right right now because with the bank control in detent, the wings are more or less level anyway.

There seems to be a looseness in yaw and in pitch - kind of a much higher frequency. I don't know whether that's more gusts or turbulence or what, but it seems to be just generally more nervous.

It's still flying about as I'm asking it to. Start correcting back left and heading. Couple more clicks down because I am going high. Toward the 2 1/2 (degree) telephone pole slope right now. Slight overshoot in lineup. Okay, lineup's right on. Let me get the vector over there so it'll stay there. Okay, it's drifting nose high. It's taken me . . . I've got to compensate for that. Roll in the thumbwheels. Maybe I'll just dive at the ground.

Okay, we're at 300 feet (AGL). There, a couple clicks up - good show, here. 200 feet. I'm having to work harder. 50 feet - a couple clicks - start a last minute save. This is going to be a firm touchdown, but in a good position. Hit at 10 (rate of descent in feet per second) or 11. I don't know if it would have responded better in pitch if I'd thrown that correction. I was a little late

getting the nose up clicks in there so that was why the firm one. It was just more inattention than anything but it was definitely looser.

I don't know what the early transient was - it handled that well and there was never any problem later but this has been less satisfactory flying - more compensation required. We got there within the adequate, but certainly not desired (performance). I'd go 6 and 6 for the ratings. So we made it, but just barely.

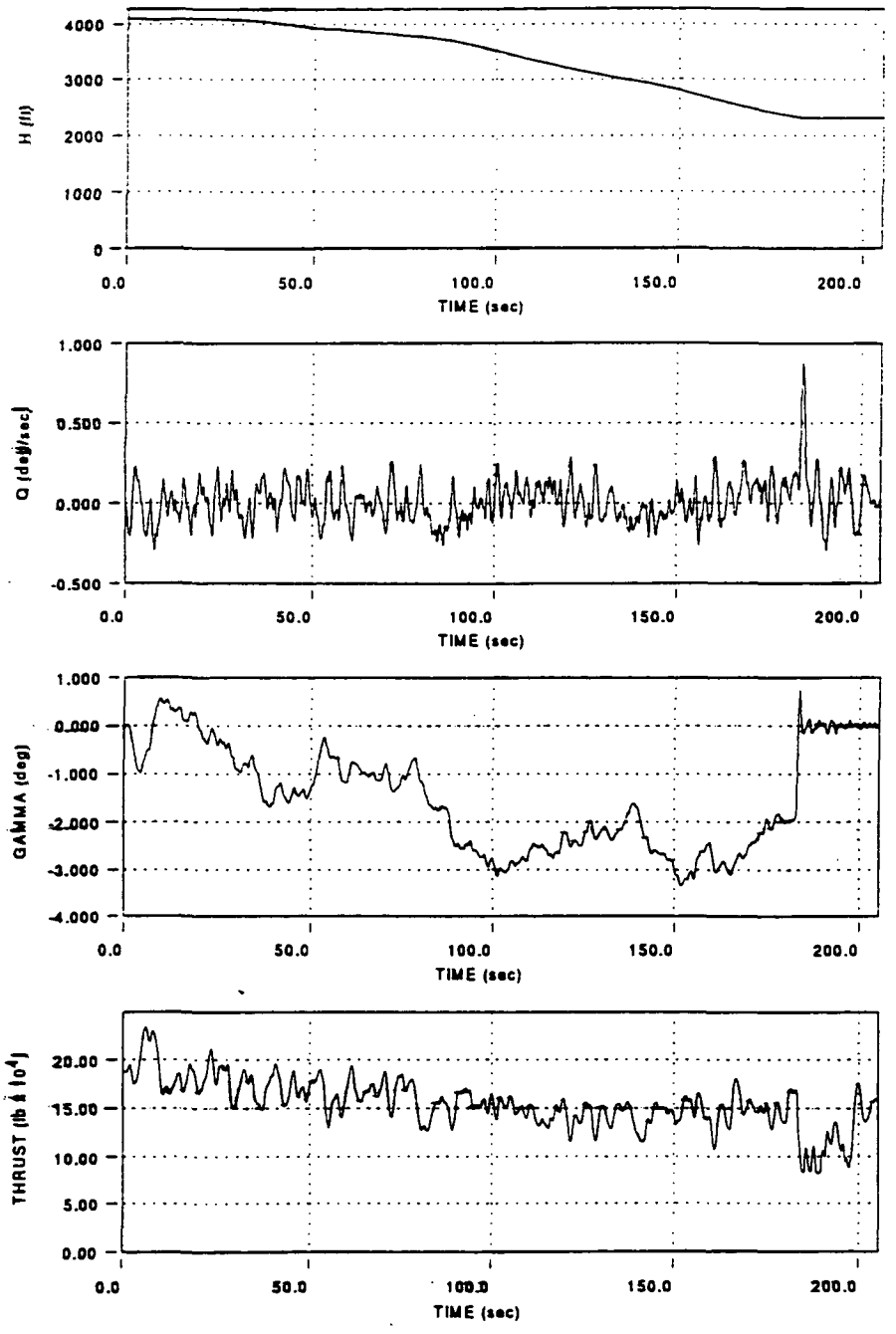

Figure G26(a) Longitudinal Flight Variables for Test Flight B9: Intermediate Turbulence with PCA

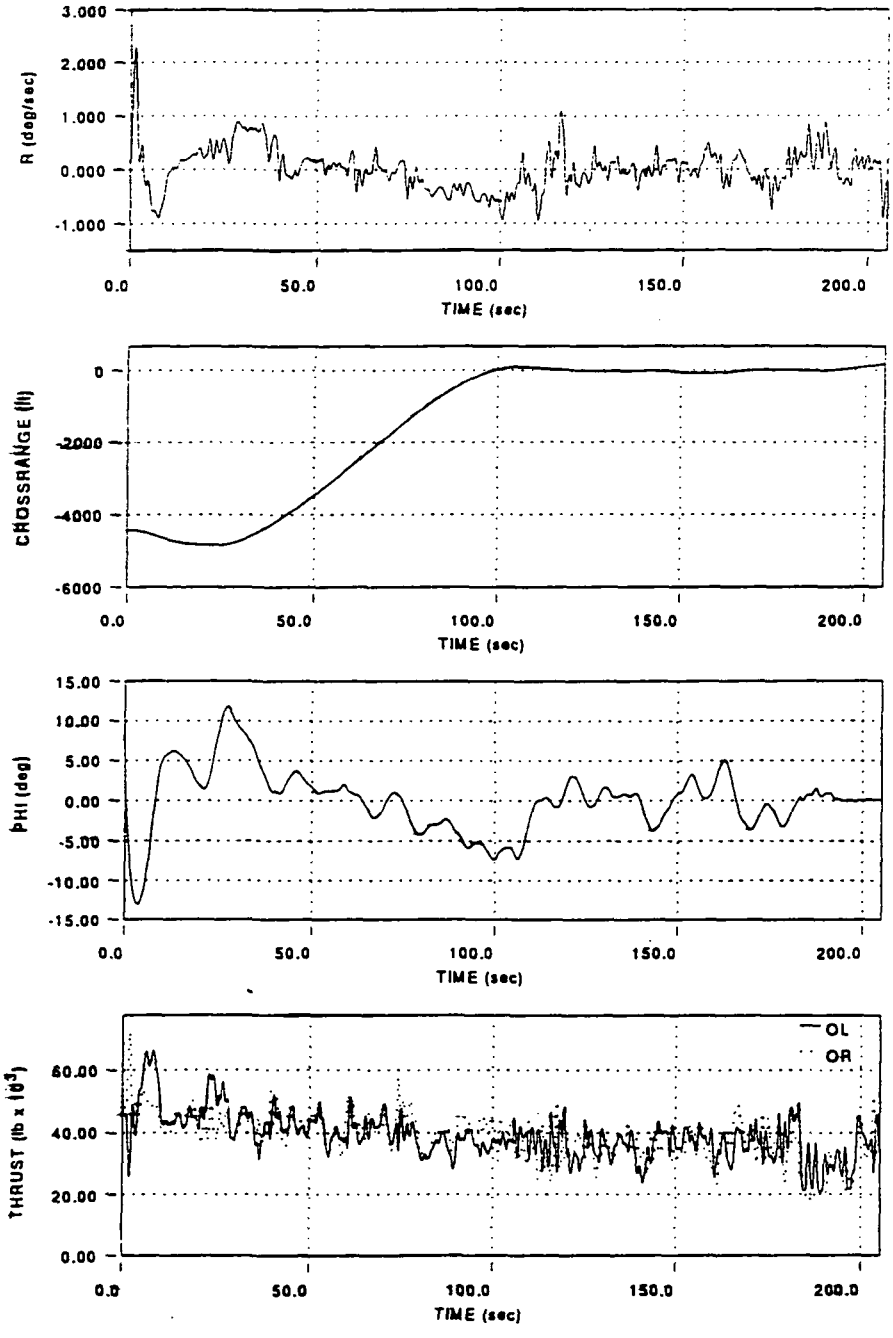

Figure G26(b) Lateral-Directional Flight Variables for Test Flight B9: Intermediate Turbulence with PCA

Test Point B10

Manual Throttles - No PCA

This is manual. Get the friction off of the throttles here. Manual PCA. So we've got to watch the airspeed close. Starting a correction - no response laterally. No problem - just sort of split the throttles briefly. Get the airspeed at 184 (knots) - I'm going to get it back down now so the nose doesn't come up too much. Takes a little more speed to get the nose up. 187 just isn't bringing the nose up. There, 190 is. 187, 6 seems to be a good trim speed.

Okay, it's kind of 'wallowy' in roll but I need to get more of a correction here and get flattened out - I'm getting low. Okay, I'm not doing nearly as good a job on lining up, so I'm just aiming for the end rather than getting over on centerline. This is better. 187. Okay, I'm saving my lineup until the bitter end here so it's going to take a last minute correction here. 181, okay it's coming over.

Okay, velocity setting is good - I don't want to change that. 187, 6 - keep it slower - 5. Lineup's good now - keep it there. Okay, a little slow. I need to get most of the knots back. 184 - watch your lineup. 183 - I need to get the speed up. Okay, feels good right now - just keep it coming down here at one hundred feet.

Okay, 185, good. Pitch is good. Lineup's fine, acceptable. Now we can find the ground - that's probably the best landing of them all as far as sink rate and . . . so, it's not a bad flying machine.

It's pretty responsive. You know, you've got short-period response in pitch. A little throttle keeps that nose from drifting off which is nice to have. So, even though the speed's not exactly on you can stop the little motions which is the key to good landings.

Laterally, you have to keep working at it, but it's controllable and straight forward. So I guess on that one sample I'd say we're still getting adequate performance. I'd say a 5 on both axes for right now. You've got to work at it but again, I've had a lot of practice at this so it's doable.

Test Point B11

Engines Moved Vertically Upward With PCA

(Inboard Engines Below Megatransport C.G.

And Outboard Engines At Megatransport C.G.)

This is an add-on run here now with the engines severely raised and I start my lineup correction here and we'll just see what the ol' pitch does. The nose went down at first but it may be because my throttles were left over from the last manual run. So far, not too bad.

Let me throw in a couple of nose up clicks here to try to shallow out a bit. I don't see any very quick response. The airplane's stable but 'drifty' in pitch. Alright - not too bad. So far it's doing what I want to do which is just sort of drift on down here. Holding here about one degree gamma (flight path angle).

Okay, we'll start the lineup turn here and I put 2 clicks nose down to see if I can drop the nose a degree - it's going down and it's pretty stable. I don't know - I don't know why but it is. You ought to put a patent on this control law because it's unphased by engine position.

Okay, lineup's good - 2 clicks nose up to shallow. We're out about 500 feet (AGL). Well, I'll put 2 clicks back in. That response is good - I thought it might be real sluggish but it's not, it started up there. Okay, we're at 400 feet and looking good. 300 feet - 200 feet - nose up click. 100 feet - another click and the response is good. It's going right up where I asked. 6 feet per second (rate of descent) - I'll just let it land.

Well, so much for the vertical position theory. Try one more - let's really make sure that the system is working on this vertical position. Well, we haven't found the limit yet. Obviously it copes with that and that's Level 2 or 1 and it landed just fine. Let's really overdo it here.

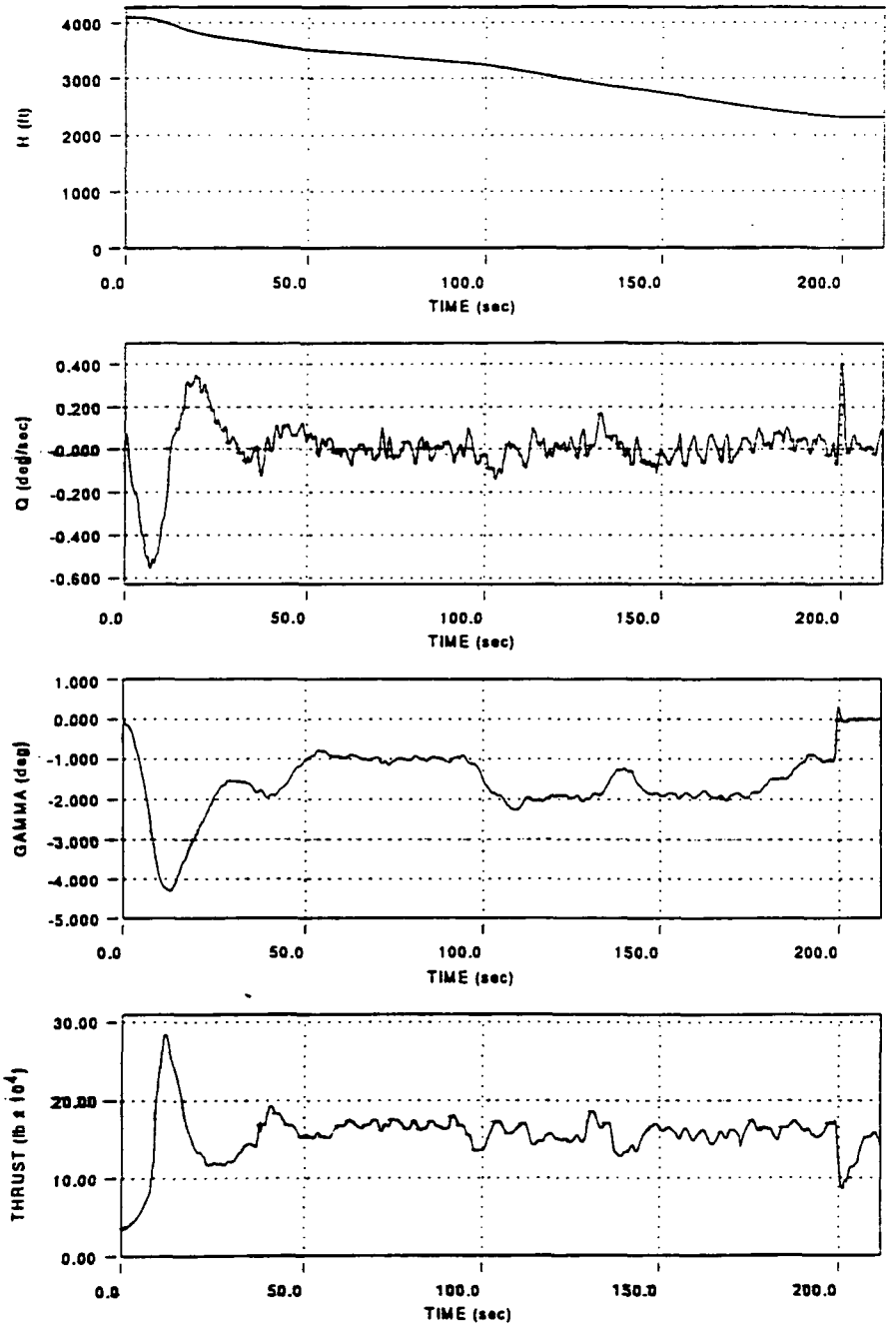

Figure G27(a) Longitudinal Flight Variables for Test Flight B11: Engines Moved Vertically Upward with PCA

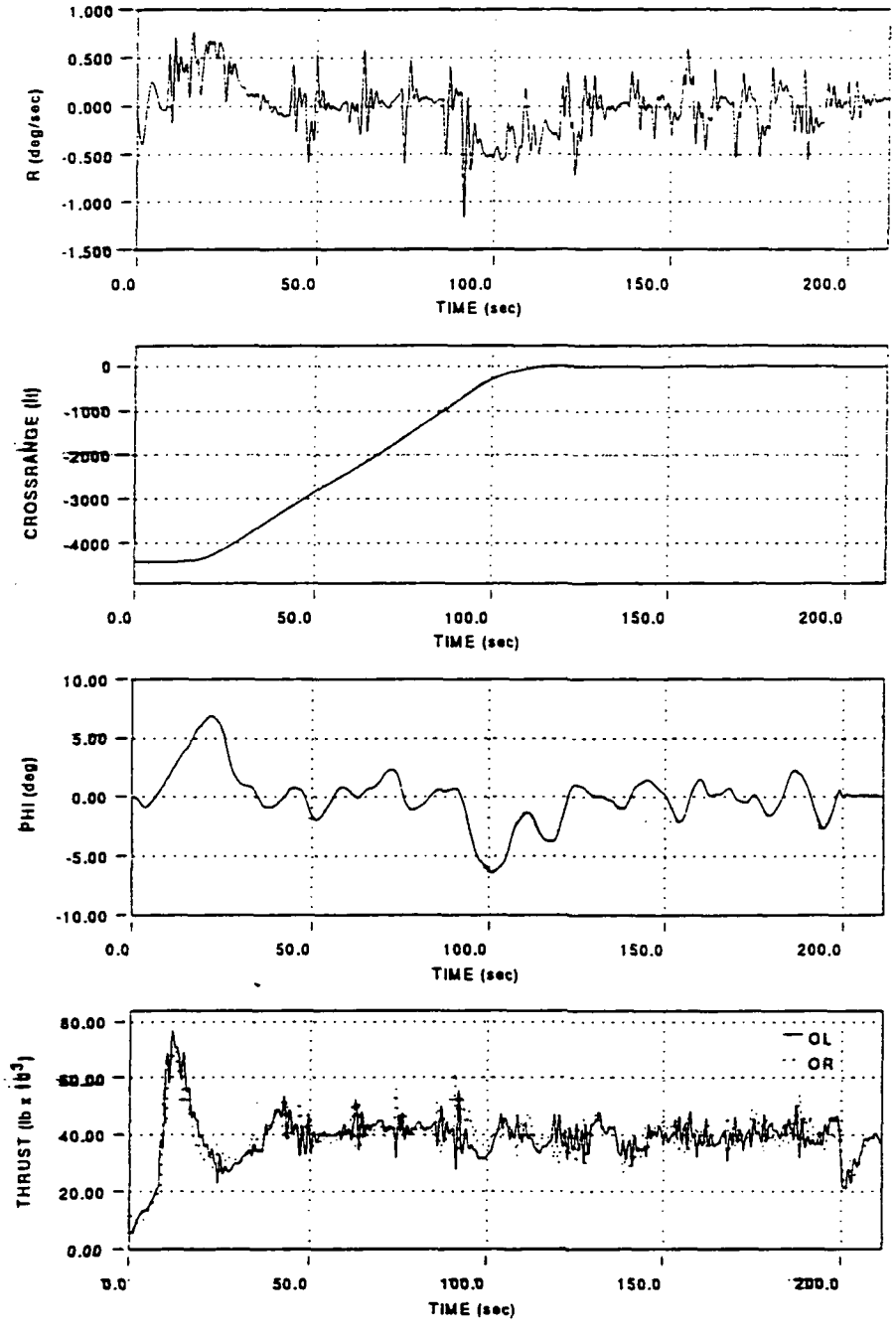

Figure G27(b) Lateral-Directional Flight Variables for Test Flight B11: Engines Moved Vertically Upward with PCA

Test Point B12

Engines Moved Vertically Upward Above Wing With PCA (Inboard And Outboard Engines Above Megatransport C.G.)

Okay, we're on run number 12, I think. In this case, we have put the engines way up there and, yup, the system is going unstable. Airspeed's up to 210 knots and it's finally coming up here and I think we've . . . well, we'll see what happens.

It's having trouble. See, it's real slow. It's got to come in with a lot of thrust - it's pushing it down. I think we're in big trouble - this is a [specific airplane named here].

Well, we're within 30 feet of the ground. This is not good news. Now, see, you've got to get a lot of power on there and get it off again. [Crash.] I think we've proved a point there.

Test Point B13

Conventional Control Surfaces Operational - No PCA

[The video recorder was inadvertently turned off during this test point. Therefore, the comments of the test pilot were not recorded during this flight.

The pilot commented after the test run that he assigned a Cooper-Harper pilot rating of 2 to the baseline megatransport aircraft without use of the PCA system with the conventional control surfaces operational.

The pilot stated that the megatransport was slightly sluggish in pitch but that it was stable, well-damped, and responsive in general.]

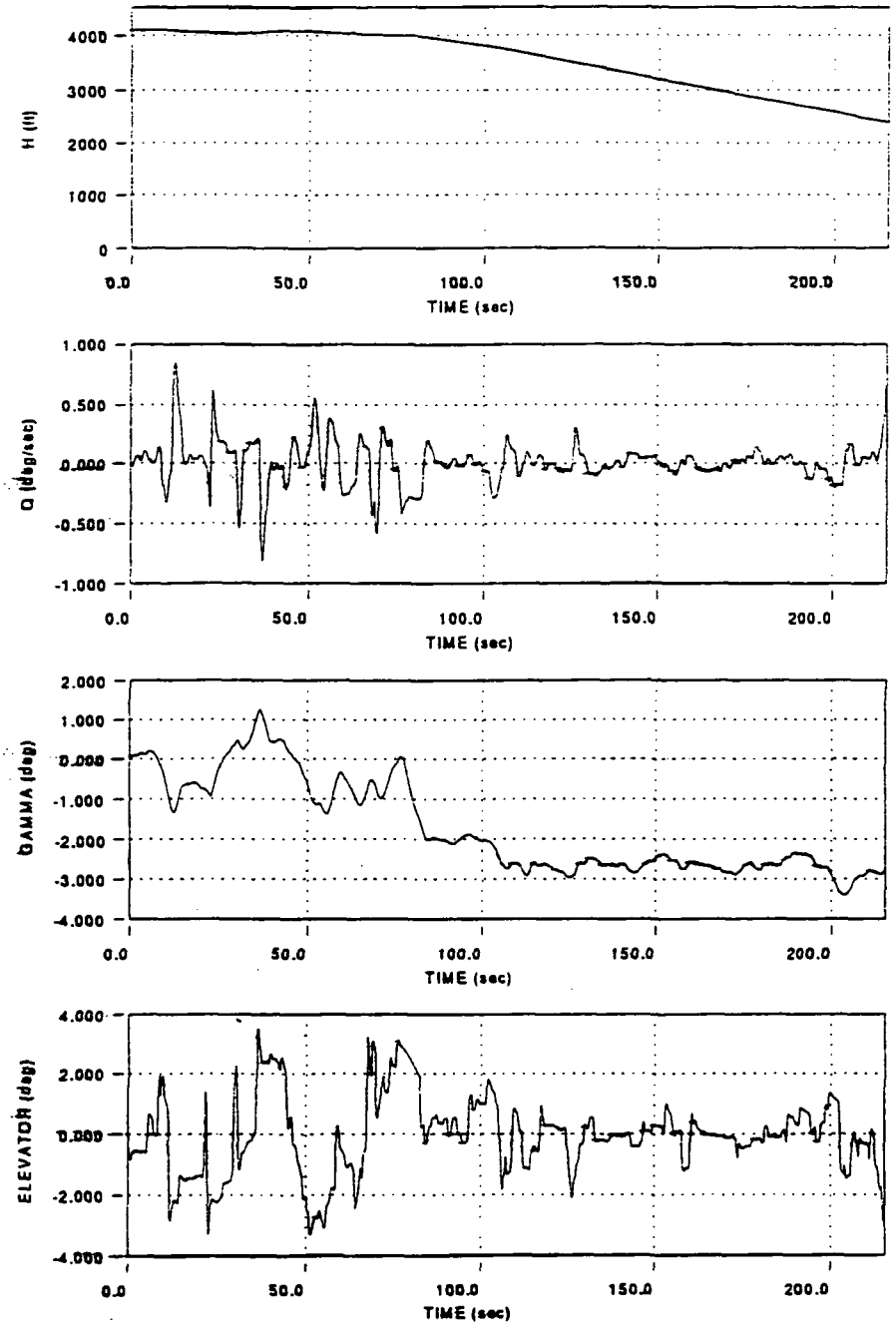

Figure G28(a) Longitudinal Flight Variables for Test Flight B13: Conventional Control Surfaces Operational - No PCA

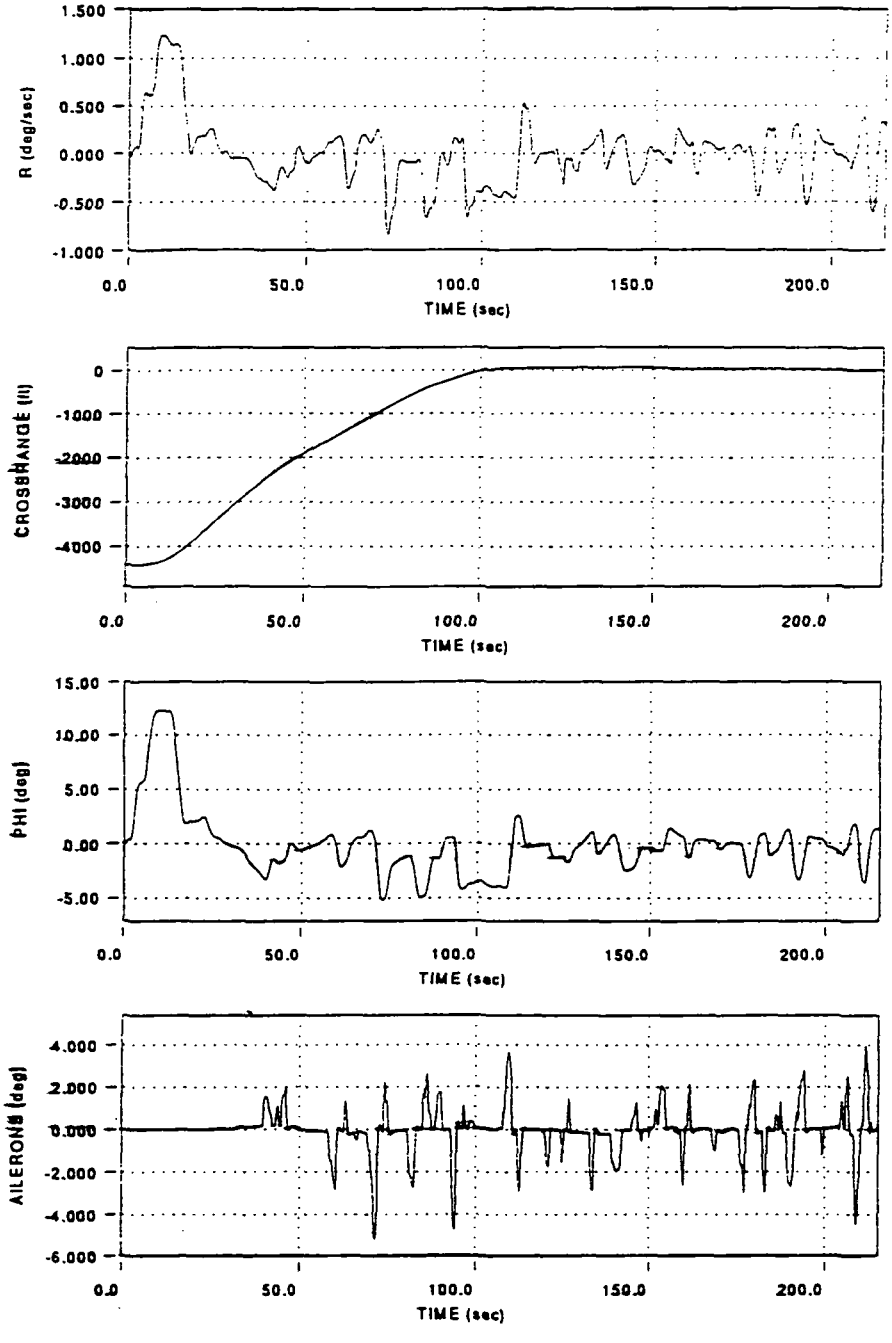

Figure G28(b) Lateral-Directional Flight Variables for Test Flight B13: Conventional Control Surfaces Operational - No PCA

Test Point B14

Manual Throttles - No PCA

(Repeat Of Test Point B10)

Okay, this is manual throttles only. Looks like the trim speed start was 182 (knots). I'm going to start a slow descent and get my right turn going here to correct to lineup. Do we have any turbulence, light turbulence? Looks like there's some. Okay, now I've got to really watch the airspeed here. There was lots of looseness in yaw - not much roll due to yaw, but a lot of nose wandering.

I can tell the engines are underslung just by the fact that when I reduce power to go down, the trim speed increases somewhat. I'm going to need more like 190 here to keep the nose from falling too far. I've overshot final - see if I can get back. Okay, nose wander in yaw is the most disconcerting thing here. Bank angle control is slow, but well-damped so it's not too much of a problem so far.

Okay, I've got pitch attitude about where I want it now if I can keep it there and correct this little bit of alignment discrepancy. Well, the pitch is . . . no, that's good, right there. Need a couple more knots to hold it. Okay, good flight path, right where I want it. Lineup's acceptable - still need a little bit of a right turn. And through about 300 feet (AGL).

Okay, lineup's good - still got that nose wander. Okay, where am I? A hundred feet. On the right side, but still on the runway. Add power. Looks like there's a little ground effect, maybe not - I don't know. Anyway, the touchdown was firm - must have been up around 8 (rate of descent in feet per

second) or 9, I wasn't looking. More than reasonable, both in longitudinal position and lateral position. I'm off on the right side, but still on the concrete. So it's . . . right out of the box.

First approach, I let myself overshoot - made the lineup task more difficult having to come back. However, bank angle's easy to put where you want to. The nose slopping around side to side - there doesn't seem to be much you can do about that. It's damped, but it's very loose and pitch response is not bad for throttles-only. It's relatively easy to keep the airspeed within a couple knots of where I want it and then the airplane's attitude followed that fairly well.

So, I guess we're looking for Cooper-Harpers in pitch, longitudinally, given the sort of acceptable 3,000 foot touchdown box and all (see Figure 5.1) - I made that - I'd say 5 and laterally I had more trouble, maybe a little more than . . . I forget what you had proposed for a criteria laterally, 50 feet or something? I'm probably on the outside edge of that, I think I could do better. Arbitrarily a 6, laterally, 5, longitudinally.

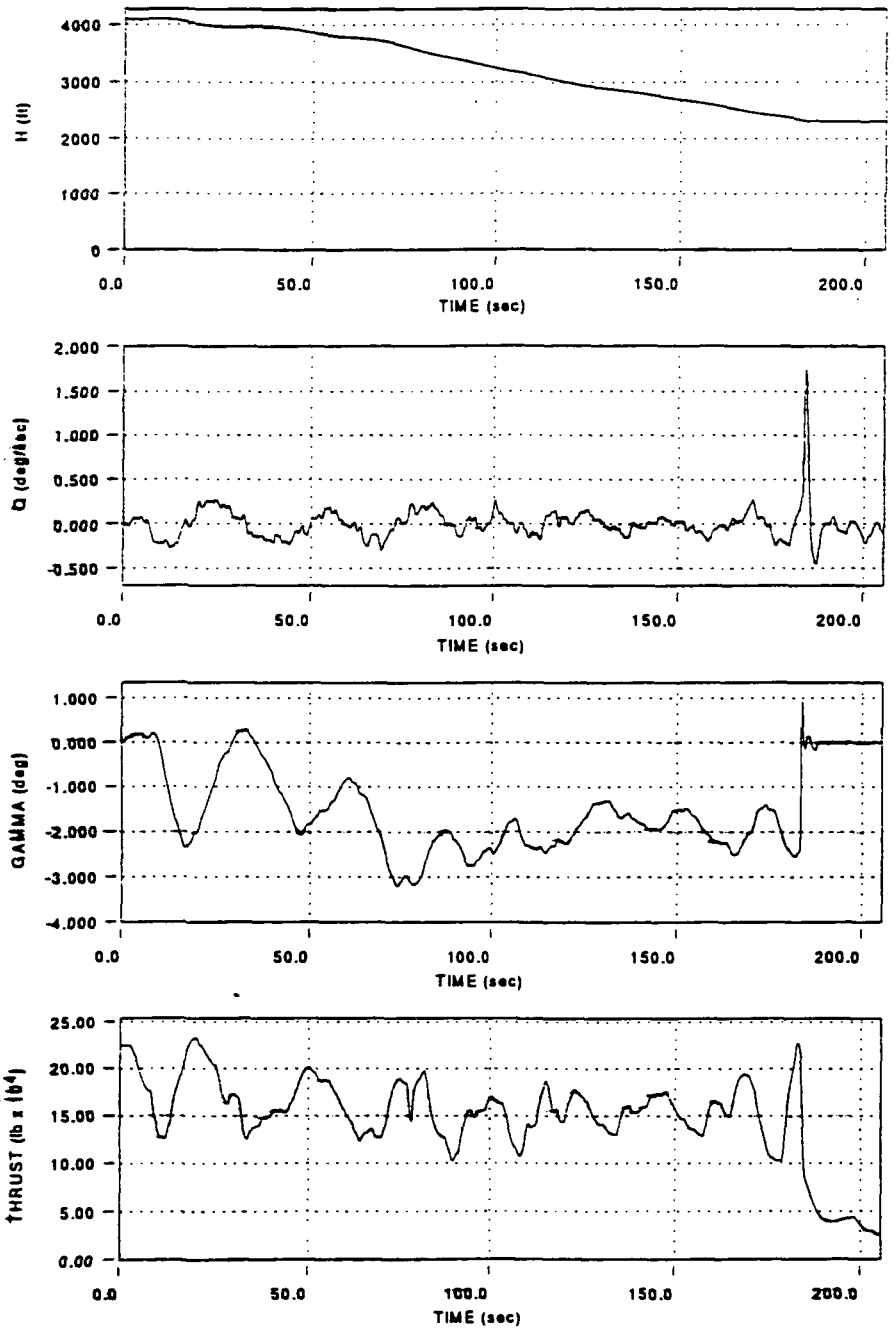

Figure G29(a) Longitudinal Flight Variables for Test Flight B14: Manual Throttles - No PCA

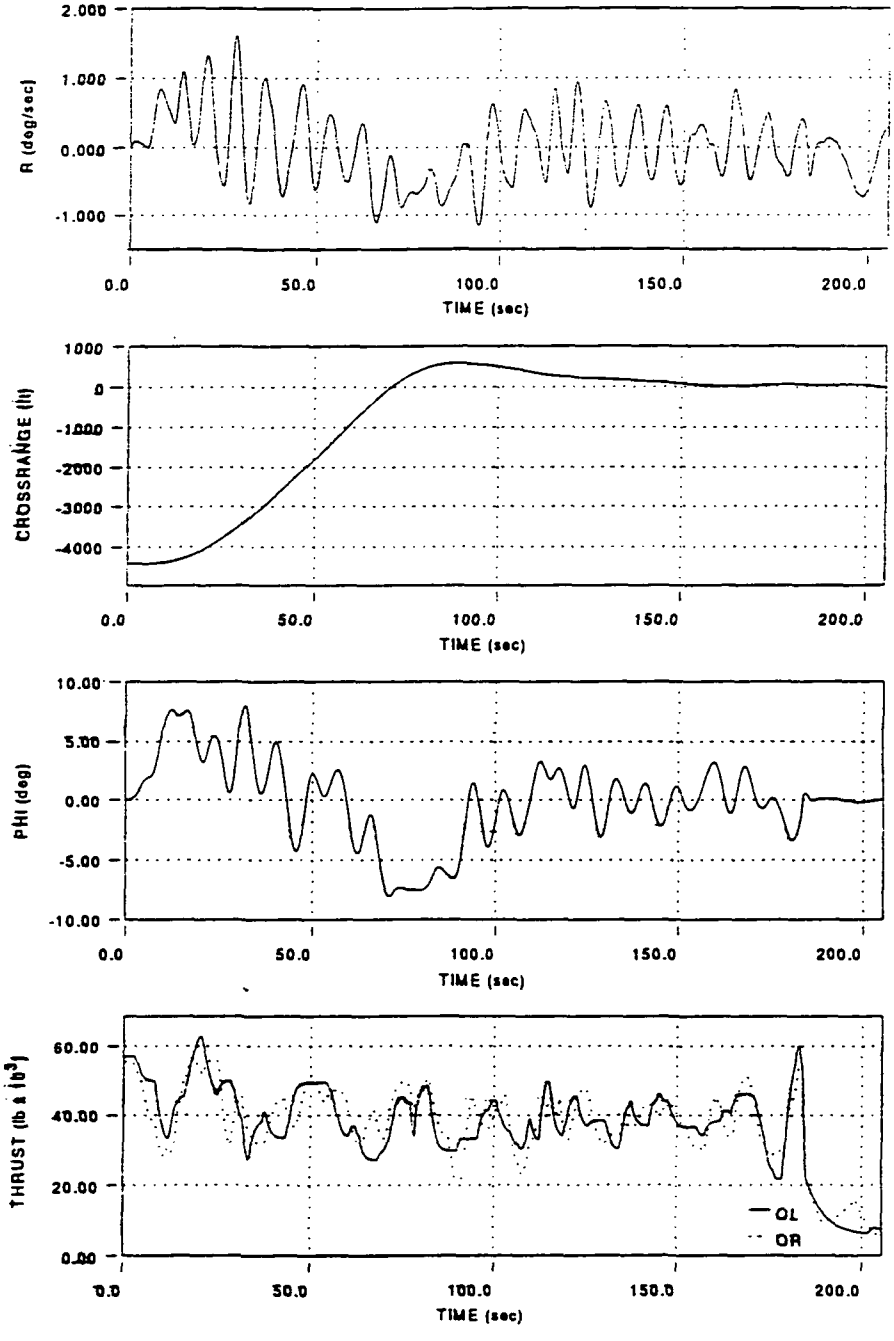

Figure G29(b) Lateral-Directional Flight Variables for Test Flight B14: Manual Throttles - No PCA

Test Point B15

Baseline Configuration With PCA

(Repeat Of Test Point B1)

Okay, now we're flying baseline airplane with PCA. Let's start the right turn - lower the nose down. What is it - 2 clicks per degree, something like that? Okay, got my correction in. Lateral response is great - just twist this turn knob and it starts moving right away.

Let's start a slow bank back toward . . . I'm in a little early with this. Okay, so I'm holding now one degree descent and correcting and it's holding it dead on - no problem, very good performance.

Okay, approaching centerline, start to left bank. Response is immediate, deadbeat, and PCA is able to avoid all this nose wander that I had lots of. And, going down 2 more clicks, so the PCA is doing a lot smoother job. It's excellent control - just coming right down the pipe now. So, I'm just sitting here kind of waiting 'til we get there.

Correcting left, slightly. There's 700 feet (AGL) - one more nose down click. Just little tiny clicks barely out of detent in bank is all that's needed here to kind of try to keep the centerline straight. There, we're at 200 feet. Here at 100 feet I'm going to come back 2 clicks.

Keep correcting on the lineup - wandering right, for some reason. Two more clicks back to try to flare here. The sink rate's real good - there's around . . . I don't know what it was. It was better than my manual landing - in about the same place.

So, the baseline is very good. Rock steady in pitch. A little bit of wander - much less than the manual - in yaw. The workload still is, the majority of it, at least three-quarters of the workload is keeping the lineup straight. Pitch was simply dialing in an initial 2 degrees and then taking it out as it got closer to the ground and landing was fine.

So, on a Cooper-Harper, I'd call it a 3 in pitch, a 4 laterally, mainly because of the workload and anticipation required laterally.

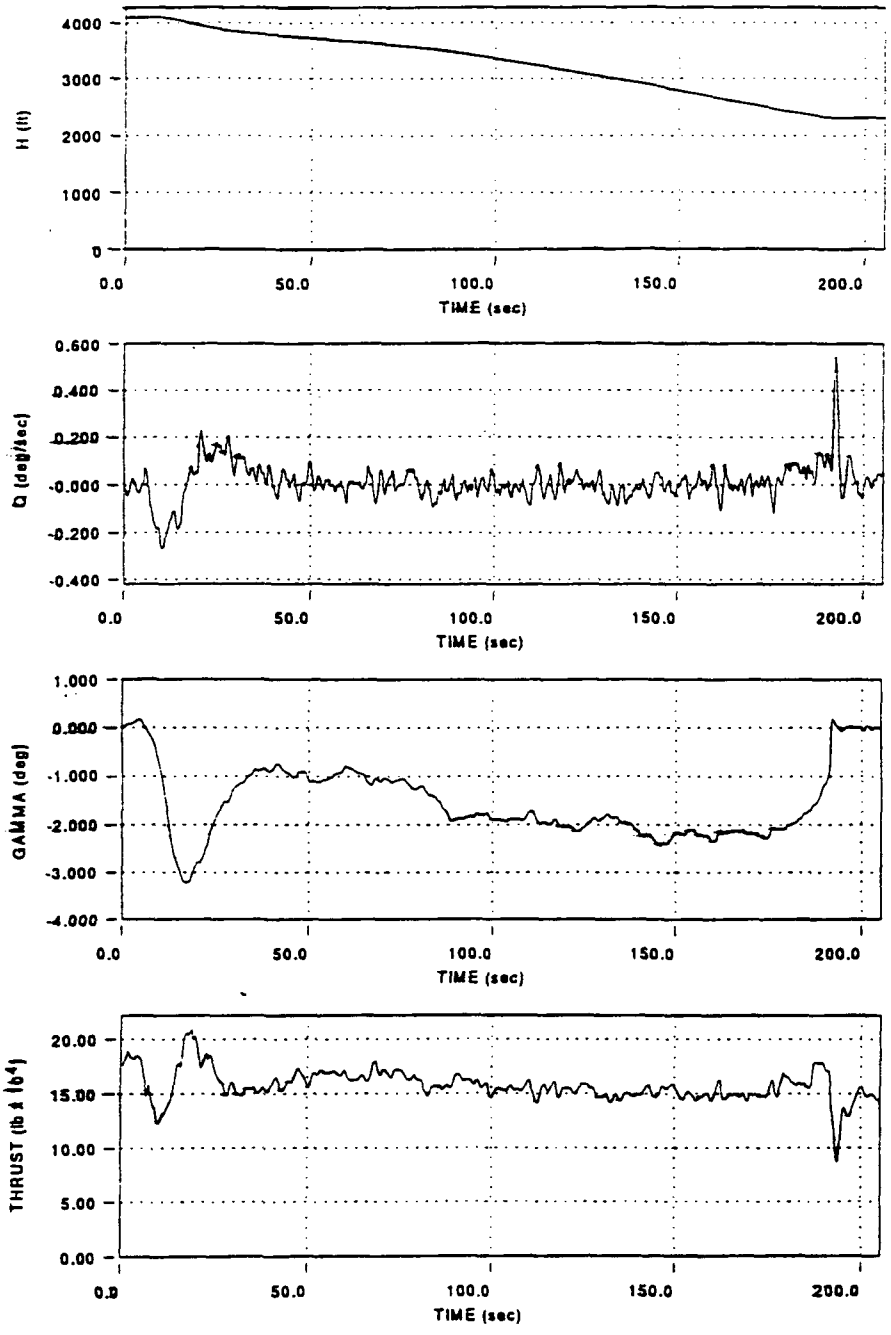

Figure G30(a) Longitudinal Flight Variables for Test Flight B15: Baseline Configuration with PCA

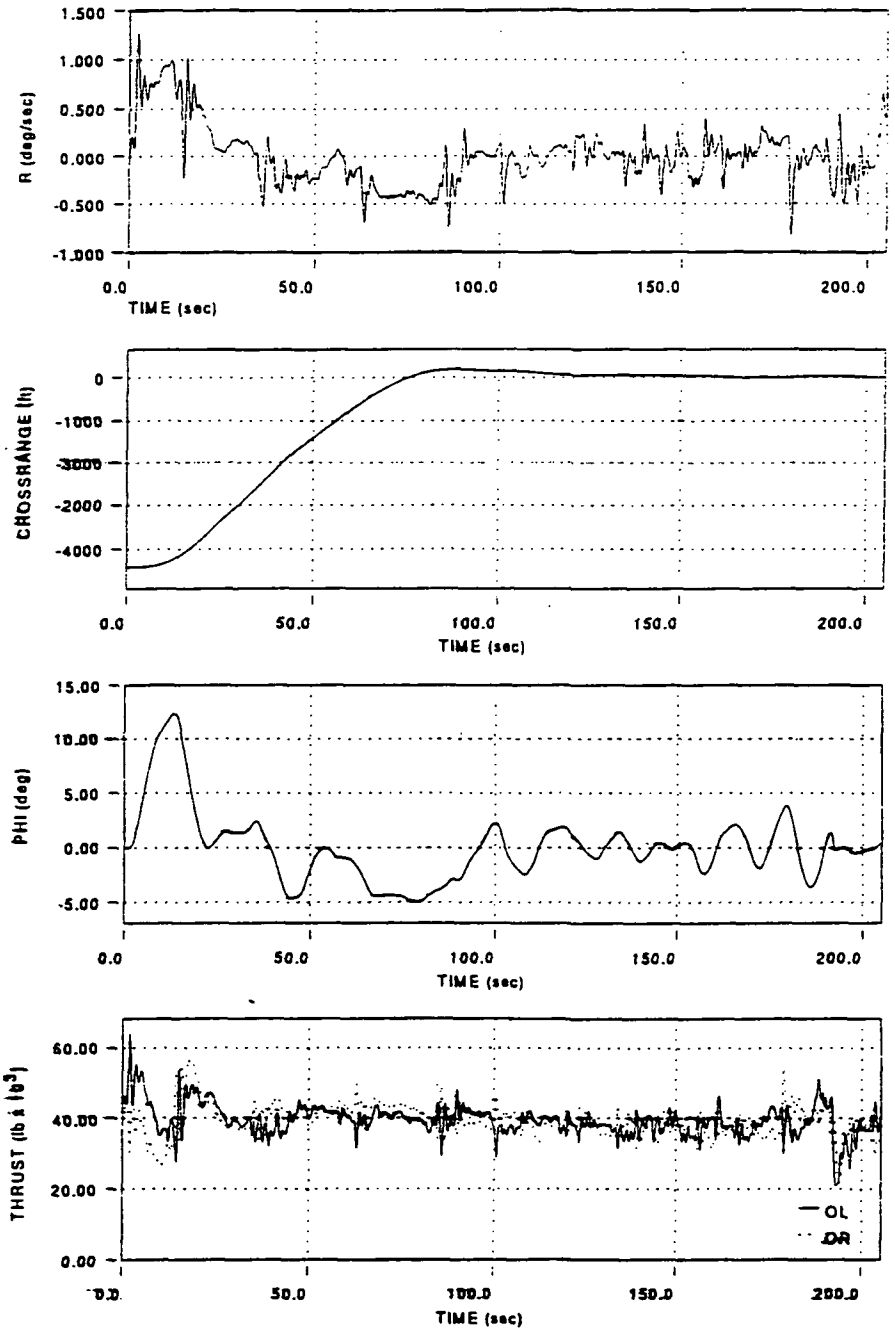

Figure G30(b) Lateral-Directional Flight Variables for Test Flight B15: Baseline Configuration with PCA

Test Point B16

Engines Moved Vertically Upward Into Wing With PCA (Inboard Engines Below Megatransport C.G. And Outboard Engines Above Megatransport C.G.)

Okay, the third approach today and this is PCA - I'll roll in 4 clicks down - PCA with the engine position changed. I may go back to 2 clicks down. Already I notice a bit of an overshoot on the commanded pitch. Directionally, it seems about the same. Bank control is fine. I see no change lateral-directionally and, right now, we're stable so there's good performance in pitch.

Let's start turning left, very gently, back. Wait a little longer here. Okay, coming on centerline - going past centerline a little bit. We're in pretty good shape. Okay, now the nose has kind of wandered up on its own to a degree and a half, or so. I'm going to put a click or two down and that hasn't excited much of an overshoot.

The response is fine - it went down just about a degree, as I requested. Okay, I'm going to put a click up and response is appropriate. So now we're settled in here at about a degree and a half. Well, it's not as right in pitch - it's wandered up a little bit, but still reasonable. I'm not going to disturb it.

Coming down the phone poles through 300 feet (AGL). Now, I'm going a little bit long, but it's still an acceptable part of the runway. Now we'll see how it does in the flare here. Click nose up at a hundred feet - another click at 50 feet - and that's a good sink rate. I'll just let her go. Good touchdown just right of center.

So, the overall performance is no worse than the baseline. I did have the feeling, though, that the pitch is not as tight - had a tendency to wander off a little. A little slower responding, or a little less precise, but again by very carefully not really making very many inputs, I didn't really stress it very much.

I'm going to move pitch rating to a 5 and, lateral-directionally, the same as before - whatever I said, 4 or 5, somewhere in there - really no change there.

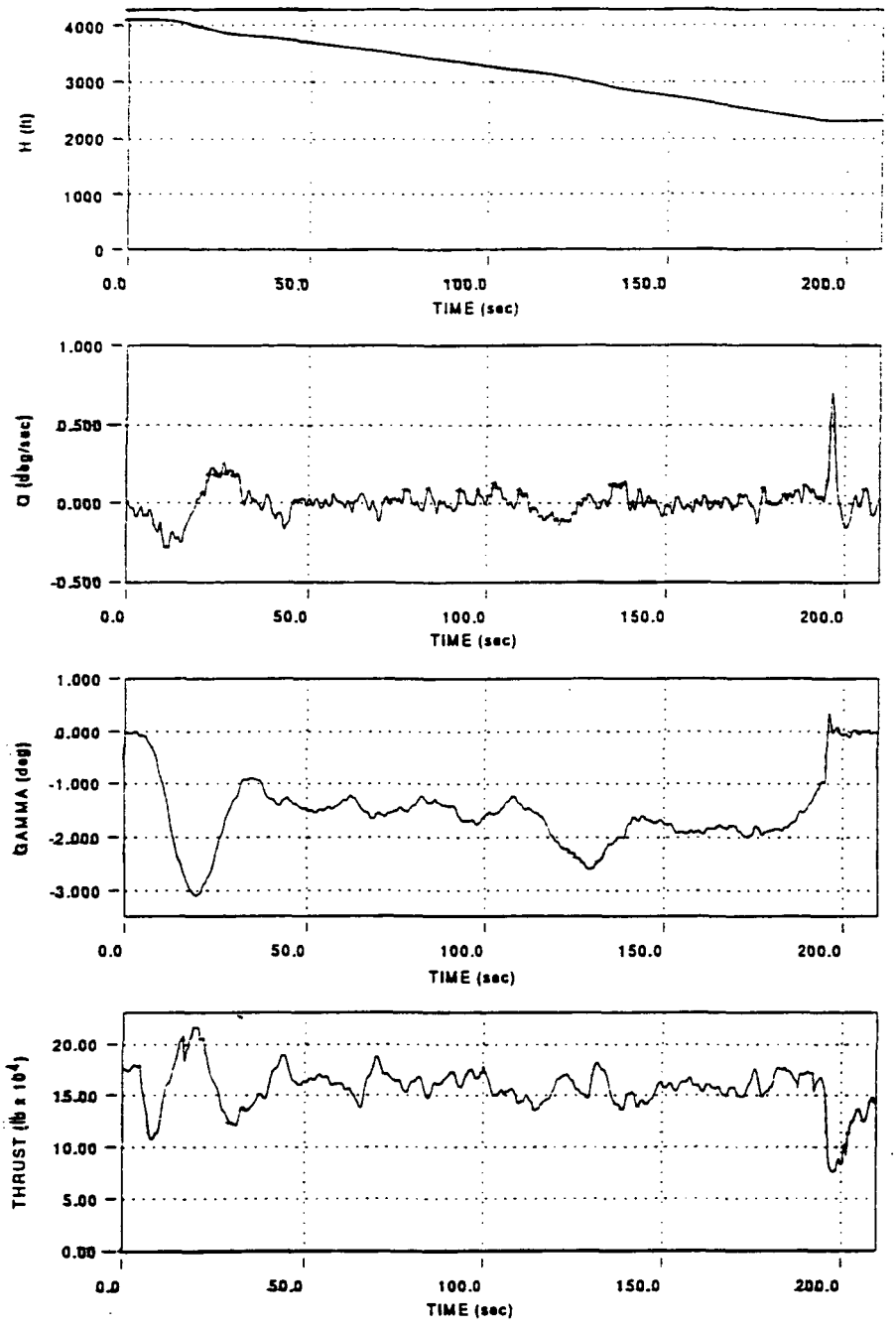

Figure G31(a) Longitudinal Flight Variables for Test Flight B16: Engines Moved Vertically Upward into Wing with PCA

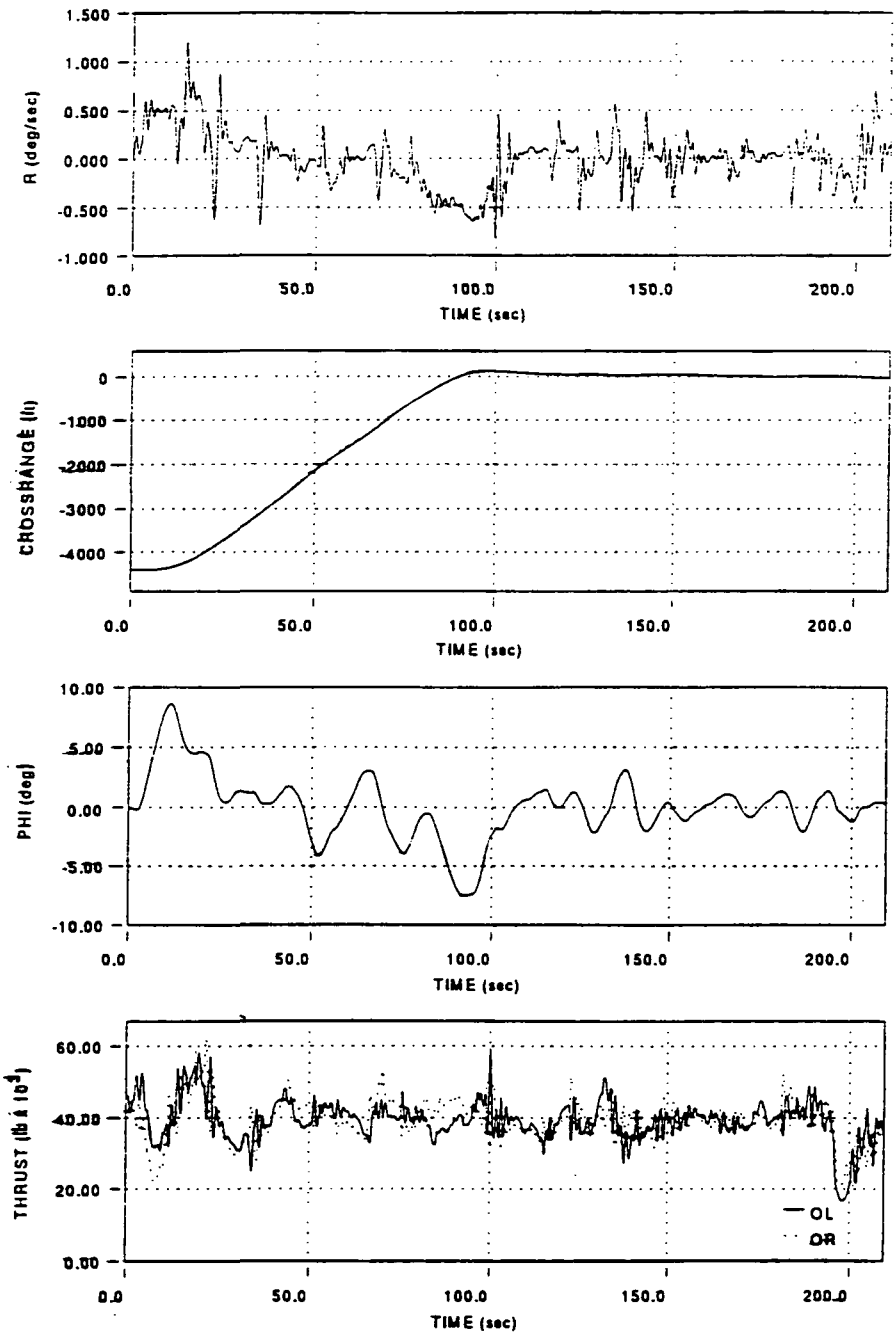

Figure G31(b) Lateral-Directional Flight Variables for Test Flight B16: Engines Moved Vertically Upward into Wing with PCA

Test Point B17

Engines Moved Vertically Upward 2.5 Feet Above Wing With PCA (Inboard And Outboard Engines Above Megatransport C.G.)

Okay, I don't know what this is but I'm going to fly it and see. PCA - start to turn - 2 clicks nose down. Rolling out - bank response is identical - quick and well-damped. So, I'm just sitting here with my one degree descent going. I'm going to put in 2 more clicks - get the nose down - start the left turn to line up. The nose response is good. Come on down to the 2 degrees that I'd asked for.

Okay, we're on centerline now and just driving on down. Steady in pitch and I'm aiming a little shorter this time trying to get near the end of the runway. Okay, where are we? 600 feet (AGL). It's steady. I don't know if I'm testing the system much because I'm just sitting here, I'm not doing hardly anything even . . . just occasional lineup correction is all.

Let's see how it responds in the flare. There's 400 feet - 300 - everything's right where I want it. 200 - 2 clicks nose up and is it going to do it? Yeah, nose coming up nicely. Down one degree gamma (flight path angle) and just driving down here. I'm happy - one more click to try to make a grease job out of it here.

Okay, well for once I landed left of center instead of right. Well, I honestly can't see much difference than the baseline here in handling - seemed like a repeat to me. It certainly responded. It nosed right over and then it flared fine. I mean it's nailed - you can't ask for more than that. So

certainly it's got enough control to land the airplane as happened on the last approach. It's doing fine . . . nothing wrong with that.

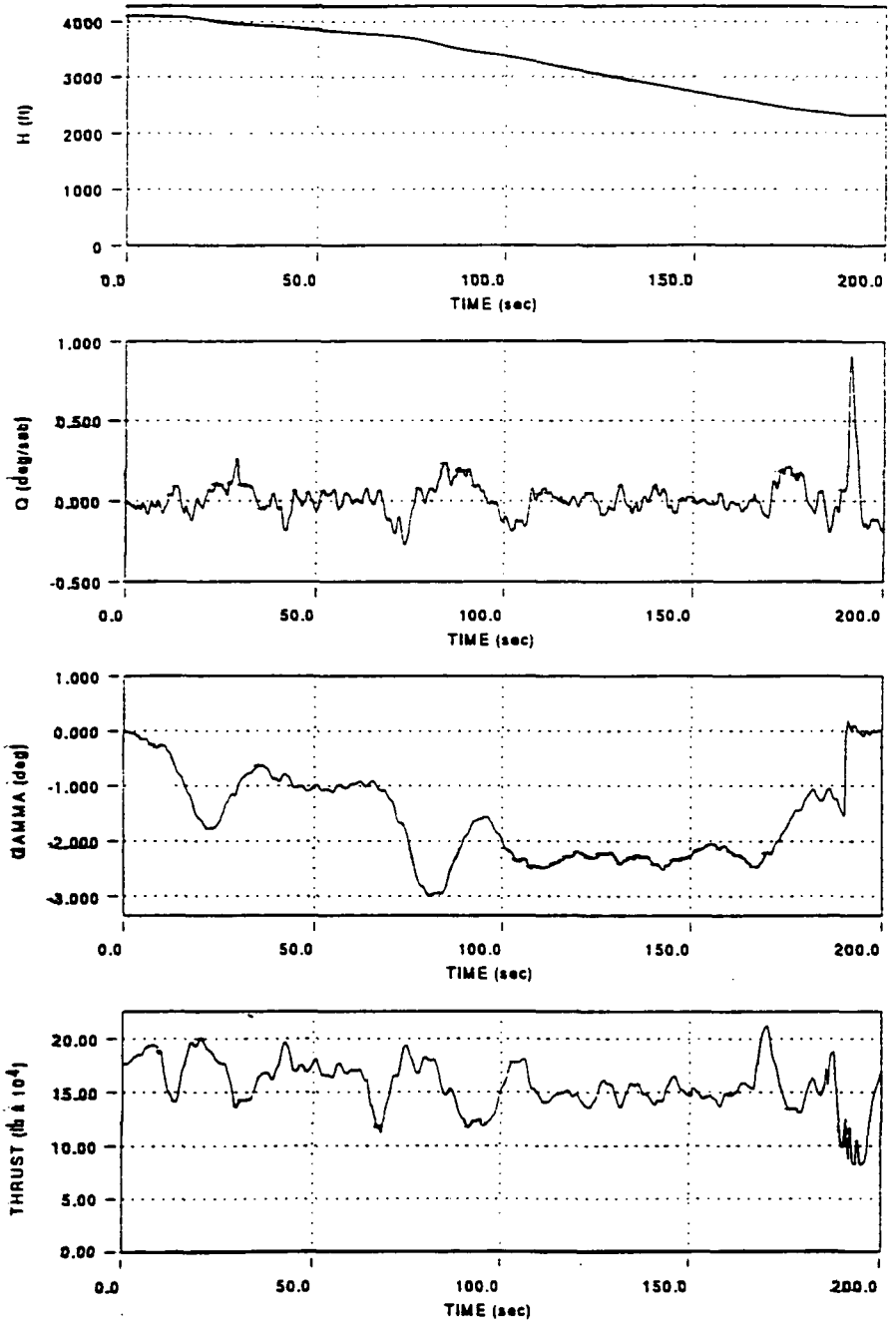

Figure G32(a) Longitudinal Flight Variables for Test Flight B17: Engines Moved Vertically Upward 2.5 Feet Above Wing with PCA

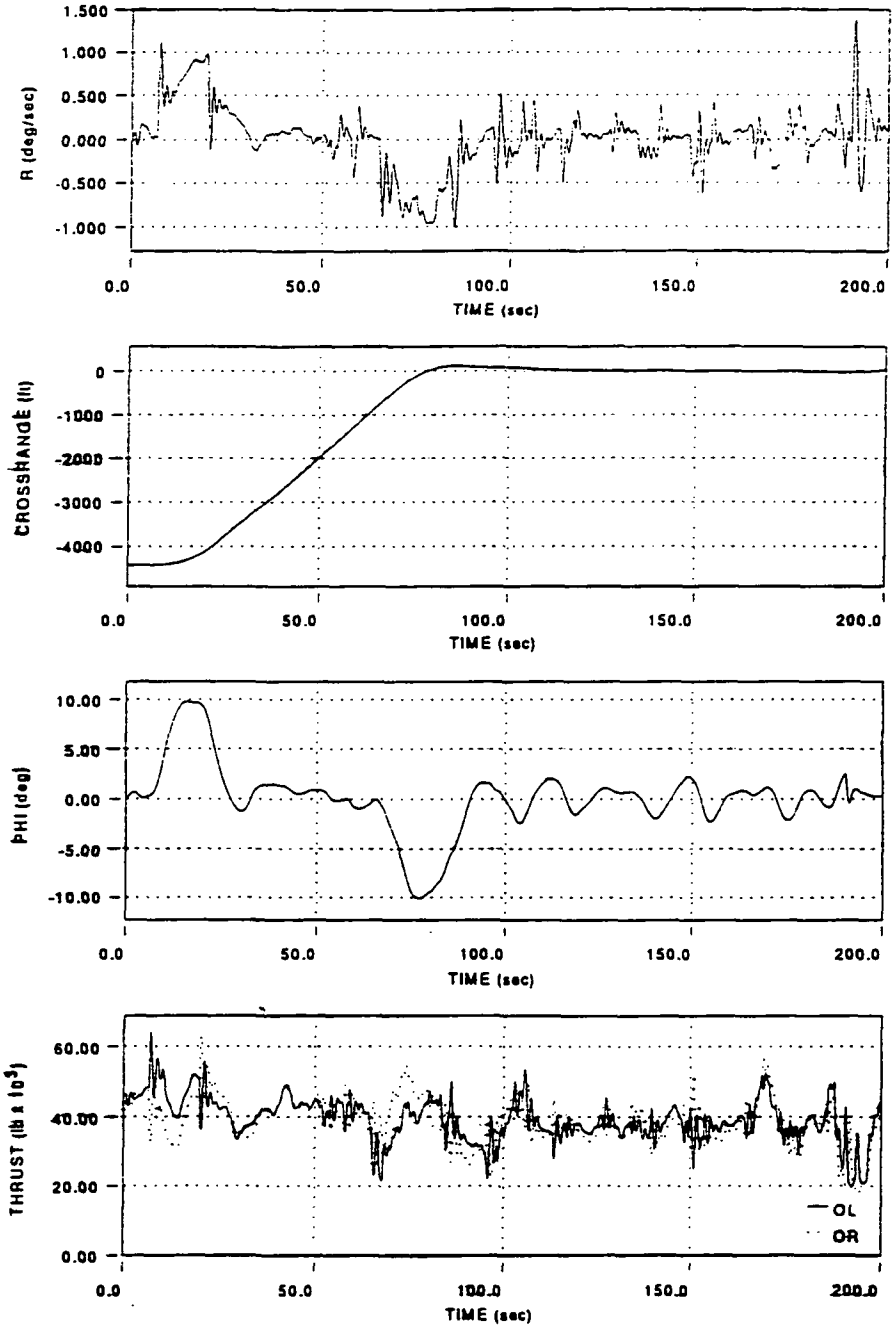

Figure G32(b) Lateral-Directional Flight Variables for Test Flight B17: Engines Moved Vertically Upward 2.5 Feet Above Wing with PCA

Test Point B18

Engines Moved Vertically Upward 2.5 Feet Above Wing

Manual Throttles - No PCA

Let me try a manual approach here with it. Can you just turn the PCA off? This is the same airplane except I'm doing it (controlling the throttles). Now it's a lot tougher to fly manually - I'm really having to . . . I'm getting in an airspeed PIO here trying to make it settle down.

There's a lot of wander in the nose through big airspeed changes so you've got all that speed deficit there. You've got to get some speed on the airplane or it's going to dive into the lakebed. Just like the other manual approach, the nose is slopping all around. I'm obviously overcontrolling. See, it's going to really go down on me. Don't get back up to the 188 (knots) or so.

Yeah, this is reminiscent of the [specific airplane named here] I flew where everything you do, you get the wrong thing in the short term. It really requires a lot of anticipation. A lot of body english required here. Get some speed on there and hope it flares for me before I hit.

Well, a little short - I accepted that considering I knew I'd mess it up if I tried to correct that. Well, interesting and clearly, degraded. You can really see it manually.

APPENDIX H

LONGITUDINAL AND LATERAL-DIRECTIONAL TRANSFER FUNCTION EQUATIONS FOR THE MEGATRANSPORT USING ENGINE THRUST FOR FLIGHT CONTROL

[Ref. 18]

H.1. INTRODUCTION

The aircraft dynamics transfer function of an aircraft controlled by conventional control surfaces can be found by substituting the appropriate values of mass, geometry, velocity, inertias, and stability derivatives into the lateral-directional and longitudinal transfer function equations as described in Reference 18.

The longitudinal and lateral-directional transfer functions for the megatransport were developed in Sections 3.9.2 and 3.9.3, respectively, and are presented in Tables 3.12 and 3.13. The denominators of these two transfer functions are independent of the method being used for flight control, whether conventional control surfaces or engine thrust, but the numerators are not.

The numerators for these transfer functions contain control surface dimensional derivatives such as $X_{\delta E}$, $Z_{\delta E}$, $M_{\delta E}$, $Y_{\delta A}$, $L_{\delta A}$, $N_{\delta A}$, $Y_{\delta R}$, $L_{\delta R}$, and $N_{\delta R}$. For aircraft motions commanded not by control surface deflections but by changes in engine thrust, however, these control surface derivatives are not

applicable. A numerator which contains thrust control derivatives must be developed.

H.2. LONGITUDINAL THRUST NUMERATOR

A longitudinal thrust numerator relating the flight path angle to a change in thrust was developed for the megatransport based upon a conventional control surface numerator model.

Conventional longitudinal transfer function numerators relate either speed (N_u), angle of attack (N_α), or pitch attitude (N_θ) to a control surface deflection, but do not relate flight path angle directly to control surface deflection. However, since flight path angle is equal to the difference between the pitch attitude and the angle of attack, a numerator for the flight path angle, (N_γ), was developed as follows using the linearity property of Laplace transforms:

$$N_\gamma = N_\theta - N_\alpha \qquad \text{[Eqn. H1]}$$

where:

$$N_\theta = A_\theta s^2 + B_\theta s + C_\theta \qquad \text{[Eqn. H2]}$$

$$N_\alpha = A_\alpha s^3 + B_\alpha s^2 + C_\alpha s + D_\alpha \qquad \text{[Eqn. H3]}$$

These numerators, as described in Reference 18, contain control surface dimensional derivatives $X_{\delta E}$, $Z_{\delta E}$, and $M_{\delta E}$. These terms must be replaced by thrust dimensional derivatives $X_{\delta T}$, $Z_{\delta T}$, and $M_{\delta T}$, respectively, to enable these modified longitudinal numerators to be used for thrust-controlled aircraft.

H.2.1. DERIVATION OF $X_{\delta T}$

As shown in Figure H1, the engines of the megatransport are installed on the wing at a slight cant angle, η, thereby imparting a thrust in both the x- and z-directions.

The force produced along the x-axis due to a change in engine thrust is:

$$F_{X_{\delta T}} = \Delta\text{Thrust} \cdot \cos(\eta) \quad \text{per engine} \qquad \text{[Eqn. H4]}$$

$$F_{X_{\delta T}} = \Delta T_{OL} \cdot \cos(\eta) + \Delta T_{IL} \cdot \cos(\eta) + \Delta T_{IR} \cdot \cos(\eta) + \Delta T_{OR} \cdot \cos(\eta) \qquad \text{[Eqn. H5]}$$

The equation for the conventional control derivative, $X_{\delta E}$, divides the force term by the aircraft mass, thereby giving $X_{\delta E}$ the dimension of ft sec^{-2}. Similarly, dividing $F_{X_{\delta T}}$ by the mass of the megatransport gives:

$$\left(F_{X_{\delta T}}/m\right) = (1/m) \cdot \left[\Delta T_{OL} + \Delta T_{IL} + \Delta T_{IR} + \Delta T_{OR}\right] \cdot \cos(\eta) \qquad \text{[Eqn. H6]}$$

The force imparted to the megatransport by the engine thrust will be in the +x-direction. Therefore the thrust stability derivative, $X_{\delta T}$, is:

$$X_{\delta T} = \left(F_{X_{\delta T}} / m \right) \qquad \text{[Eqn. H7]}$$

$$X_{\delta T} = (1/m) \cdot \left[\Delta T_{OL} + \Delta T_{IL} + \Delta T_{IR} + \Delta T_{OR} \right] \cdot \cos(\eta) \qquad \text{[Eqn. H8]}$$

H.2.2. DERIVATION OF $Z_{\delta T}$

Referring again to Figure H1, it can be seen that the force produced along the z-axis due to a change in engine thrust is:

$$F_{Z_{\delta T}} = \Delta \text{Thrust} \cdot \sin(\eta) \quad \text{per engine} \qquad \text{[Eqn. H9]}$$

$$F_{Z_{\delta T}} = \Delta T_{OL} \cdot \sin(\eta) + \Delta T_{IL} \cdot \sin(\eta) + \Delta T_{IR} \cdot \sin(\eta) + \Delta T_{OR} \cdot \sin(\eta) \qquad \text{[Eqn. H10]}$$

Similarly to $X_{\delta E}$, the equation for $Z_{\delta E}$ divides the force term by the aircraft mass, thereby giving $Z_{\delta E}$ the dimension of ft sec^{-2}. Dividing $F_{Z_{\delta T}}$ by the mass of the megatransport gives:

$$\left(F_{Z_{\delta T}} / m \right) = (1/m) \cdot \left[\Delta T_{OL} + \Delta T_{IL} + \Delta T_{IR} + \Delta T_{OR} \right] \cdot \sin(\eta) \qquad \text{[Eqn. H11]}$$

The force imparted to the megatransport by the engine thrust will be in the -z-direction. Therefore the thrust stability derivative, $Z_{\delta T}$, is:

$$Z_{\delta T} = -\left(F_{Z_{\delta T}} / m \right) \qquad \text{[Eqn. H12]}$$

$$Z_{\delta T} = -(1/m) \cdot \left[\Delta T_{OL} + \Delta T_{IL} + \Delta T_{IR} + \Delta T_{OR} \right] \cdot \sin(\eta) \qquad \text{[Eqn. H13]}$$

H.2.3. DERIVATION OF $M_{\delta T}$

The pitching moment of the megatransport due to a change in engine thrust can be divided into two parts:

- the pitching moment due to the thrust along the x-axis with a z-axis moment-arm from the engine to the center of gravity of the megatransport
- the pitching moment due to the thrust along the z-axis with an x-axis moment-arm from the engine to the center of gravity of the megatransport.

H.2.3.1. $M_{\delta T}$ DUE TO THRUST ALONG X-AXIS

A front view of the megatransport is shown in Figure H2, along with the z-axis moment-arms from each engine to the center of gravity.

The pitching moment due to the change in thrust along the x-axis from all four engines is given below:

$$\begin{aligned} M_{X_{\delta T}} = {} & \Delta T_{OL} \cdot \cos(\eta) \cdot z_1 + \Delta T_{IL} \cdot \cos(\eta) \cdot z_2 \\ & + \Delta T_{IR} \cdot \cos(\eta) \cdot z_2 + \Delta T_{OR} \cdot \cos(\eta) \cdot z_1 \end{aligned} \qquad \text{[Eqn. H14]}$$

$$M_{X_{\delta T}} = \left[\left(\Delta T_{OL} + \Delta T_{OR}\right)\cdot z_1 + \left(\Delta T_{IL} + \Delta T_{IR}\right)\cdot z_2\right]\cdot\cos(\eta) \qquad \text{[Eqn. H15]}$$

The conventional control derivative, $M_{\delta E}$, divides the moment term by the aircraft pitch inertia, I_{yy}, giving $M_{\delta E}$ the dimension of sec^{-2}. Dividing $M_{X_{\delta T}}$ by the megatransport pitch inertia gives:

$$M_{\delta T_1} = \left(M_{X_{\delta T}} / I_{yy}\right) \qquad \text{[Eqn. H16]}$$

$$M_{\delta T_1} = \left(1/I_{yy}\right)\cdot\left[\left(\Delta T_{OL} + \Delta T_{OR}\right)\cdot z_1 + \left(\Delta T_{IL} + \Delta T_{IR}\right)\cdot z_2\right]\cdot\cos(\eta) \qquad \text{[Eqn. H17]}$$

H.2.3.2. $M_{\delta T}$ DUE TO THRUST ALONG Z-AXIS

Figure H3 shows a side view of the megatransport, along with the x-axis moment-arms from each engine to the center of gravity. The pitching moment due to the change in thrust along the z-axis from all four engines is given below:

$$M_{Z_{\delta T}} = \Delta T_{OL}\cdot\sin(\eta)\cdot x_1 + \Delta T_{IL}\cdot\sin(\eta)\cdot x_2 + \Delta T_{IR}\cdot\sin(\eta)\cdot x_2 + \Delta T_{OR}\cdot\sin(\eta)\cdot x_1 \qquad \text{[Eqn. H18]}$$

$$M_{Z_{\delta T}} = \left[\left(\Delta T_{OL} + \Delta T_{OR}\right)\cdot x_1 + \left(\Delta T_{IL} + \Delta T_{IR}\right)\cdot x_2\right]\cdot\sin(\eta) \qquad \text{[Eqn. H19]}$$

Dividing $M_{Z_{\delta T}}$ by the megatransport pitch inertia gives:

$$M_{\delta T_2} = \left(M_{Z_{\delta T}} / I_{yy} \right) \qquad \text{[Eqn. H20]}$$

$$M_{\delta T_2} = \left(1/I_{yy}\right) \cdot \left[\left(\Delta T_{OL} + \Delta T_{OR}\right) \cdot x_1 + \left(\Delta T_{IL} + \Delta T_{IR}\right) \cdot x_2 \right] \cdot \sin(\eta) \qquad \text{[Eqn. H21]}$$

Combining the two parts of the pitching moment derivative, $M_{\delta T}$:

$$M_{\delta T} = M_{\delta T_1} + M_{\delta T_2} \qquad \text{[Eqn. H22]}$$

$$M_{\delta T} = \left(1/I_{yy}\right) \cdot \left\{ \left[\left(\Delta T_{OL} + \Delta T_{OR}\right) \cdot z_1 + \left(\Delta T_{IL} + \Delta T_{IR}\right) \cdot z_2 \right] \cdot \cos(\eta) + \left[\left(\Delta T_{OL} + \Delta T_{OR}\right) \cdot x_1 + \left(\Delta T_{IL} + \Delta T_{IR}\right) \cdot x_2 \right] \cdot \sin(\eta) \right\} \qquad \text{[Eqn. H23]}$$

H.2.4. CALCULATION OF THE LONGITUDINAL THRUST NUMERATOR

For the megatransport, the engines are canted at an angle of 2 degrees:

- η = 2 degrees

The x-axis moment-arms from each engine to the center of gravity, x_1 and x_2, along with the z-axis moment-arms from each engine to the center of gravity, z_1 and z_2, are given below:

- x_1 = -4.51 ft
- x_2 = 23.51 ft
- z_1 = 6.44 ft
- z_2 = 10.29 ft

The weight of the megatransport in the approach flight condition is:

- W = 948,650 lb

Therefore:

- m = (W/g) = (948,650/32.17) = 29,488.65 slugs

The pitch inertia was calculated in Chapter 3 to be:

- I_{yy} = 59,538,365 sl-ft^2

In the approach condition, each engine was trimmed at 44,000 pounds of thrust apiece. To generate a longitudinal frequency sweep, each engine contributed an average change in thrust of +/-9,500 pounds from the trimmed flight condition.

For the longitudinal case, thrust was either sinusoidally increased or decreased simultaneously on all four engines to generate the longitudinal frequency sweep. Therefore, the change in thrust output on all four engines was identical:

$$\Delta T_{OL} = \Delta T_{IL} = \Delta T_{IR} = \Delta T_{OR} = \pm 9{,}500 \text{ lb} \qquad \text{[Eqn. H24]}$$

Substituting the previously mentioned numerical values into Equations H8, H13, and H23:

$$X_{\delta T} = (1/29{,}488.65)\cdot[9{,}500 + 9{,}500 + 9{,}500 + 9{,}500]\cdot\cos(2^\circ) \qquad \text{[Eqn. H25]}$$

$$X_{\delta T} = 1.2878 \text{ ft sec}^{-2} \qquad \text{[Eqn. H26]}$$

$$Z_{\delta T} = -(1/29{,}488.65)\cdot[9{,}500 + 9{,}500 + 9{,}500 + 9{,}500]\cdot\sin(2^\circ) \qquad \text{[Eqn. H27]}$$

$$Z_{\delta T} = -0.0450 \text{ ft sec}^{-2} \qquad \text{[Eqn. H28]}$$

$$M_{\delta T} = (1/59{,}538{,}365)\{[(9{,}500 + 9{,}500)\cdot(6.44) + (9{,}500 + 9{,}500)\cdot(10.29)]\cdot\cos(2^\circ) + [(9{,}500 + 9{,}500)\cdot(-4.51) + (9{,}500 + 9{,}500)(23.51)]\cdot\sin(2^\circ)\} \qquad \text{[Eqn. H29]}$$

$$M_{\delta T} = 0.0055 \text{ sec}^{-2} \qquad \text{[Eqn. H30]}$$

As can be seen from these values, $X_{\delta T}$ is several orders of magnitude larger than $Z_{\delta T}$. This result is not surprising considering the fact that the thrust in the z-direction is very small compared to the thrust along the x-axis. For an engine trimmed at 44,000 pounds thrust, the thrust along the x-axis is 43,973 pounds, while the thrust along the z-axis is only 1,536 pounds.

The pitching moment due to thrust, although small, is seen to be positive. This is due primarily to the fact that the engines are below the center of gravity of the megatransport as can be seen in Equation H29. An increase in thrust results in a desirable pitch-up of the aircraft, a decrease in thrust results in a desirable pitch-down moment. For engines above the center of gravity of the aircraft, however, an increase in thrust would result in a pitch-down of the aircraft and a decrease in thrust would result in a pitch-up moment, both undesirable reactions.

The numerical values for $X_{\delta T}$, $Z_{\delta T}$, and $M_{\delta T}$ are substituted for the values of $X_{\delta E}$, $Z_{\delta E}$, and $M_{\delta E}$, respectively, into the equations for N_θ and N_α as described in Reference 18. After substituting in values for all the variables, the equations for N_θ, N_α, and N_γ become:

$$N_\theta = 1.711s^2 + 1.157s - 0.241 \qquad \text{[Eqn. H31]}$$

$$N_\alpha = -0.045s^3 + 1.915s^2 + 0.492s + 0.053 \qquad \text{[Eqn. H32]}$$

$$N_\gamma = 0.045s^3 - 0.204s^2 + 0.665s - 0.294 \qquad \text{[Eqn. H33]}$$

Combining the flight path angle numerator, N_γ, with the megatransport longitudinal transfer function denominator calculated in Chapter 3, the transfer function equation which relates the flight path angle to a symmetric change in the actual engine thrust is:

$$\left(\gamma/\delta T_{actual}\right)_{sym} = \frac{0.045s^3 - 0.204s^2 + 0.665s - 0.294}{308.516s^4 + 613.116s^3 + 505.415s^2 + 29.798s + 8.475} \qquad \text{[Eqn. H34]}$$

H.3. LATERAL-DIRECTIONAL THRUST NUMERATOR

A lateral-directional thrust numerator relating the bank angle to a change in thrust was developed for the megatransport based upon a conventional control surface numerator model.

Conventional lateral-directional transfer function numerators relate either sideslip angle (N_β), bank angle (N_ϕ), or heading angle (N_ψ) to a control surface deflection.

The numerator which relates the bank angle to a change in control surface deflection, N_ϕ, is described in Reference 18 and contains control surface dimensional derivatives $Y_{\delta A}$, $L_{\delta A}$, $N_{\delta A}$, $Y_{\delta R}$, $L_{\delta R}$, and $N_{\delta R}$. These terms must be replaced by thrust dimensional derivatives $Y_{\delta T}$, $L_{\delta T}$, and $N_{\delta T}$ to enable these modified lateral-directional numerators to be used for thrust-controlled aircraft.

H.3.1. DERIVATION OF $Y_{\delta T}$

As was seen in Figure H1, the engines of the megatransport are installed on the wing at a slight cant angle, η, thereby imparting a thrust in both the x- and z-directions. The engines have no 'toe-in' angle, however, so there is no force produced in the y-direction due to engine thrust. Therefore the thrust stability derivative, $Y_{\delta T}$, is:

$$Y_{\delta T} = 0 \qquad \text{[Eqn. H35]}$$

H.3.2. DERIVATION OF $L_{\delta T}$

A front view of the megatransport is shown in Figure H4, along with the y-axis moment-arm of each engine. As can be seen in Figure H4, a rolling moment due to thrust occurs when the thrust in the downward direction on one side of the aircraft exceeds the downward thrust on the other side. The rolling moment of the megatransport due to asymmetric thrust is:

$$L_{Z_{\delta T}} = \Delta T_{OL} \cdot \sin(\eta) \cdot y_1 + \Delta T_{IL} \cdot \sin(\eta) \cdot y_2 - \Delta T_{IR} \cdot \sin(\eta) \cdot y_2 - \Delta T_{OR} \cdot \sin(\eta) \cdot y_1 \qquad \text{[Eqn. H36]}$$

$$L_{Z_{\delta T}} = \left[\left(\Delta T_{OL} - \Delta T_{OR} \right) \cdot y_1 + \left(\Delta T_{IL} - \Delta T_{IR} \right) \cdot y_2 \right] \cdot \sin(\eta) \qquad \text{[Eqn. H37]}$$

The conventional control derivatives, $L_{\delta A}$ and $L_{\delta R}$, divide the moment term by the aircraft stability-axis roll inertia, I_{xx_S}, giving $L_{\delta A}$ and $L_{\delta R}$ the

dimension of sec^{-2}. Dividing $L_{Z_{\delta T}}$ by the megatransport roll inertia gives the thrust stability derivative, $L_{\delta T}$:

$$L_{\delta T} = \left(L_{Z_{\delta T}} / I_{xx_S} \right) \qquad \text{[Eqn. H38]}$$

$$L_{\delta T} = \left(1/I_{xx_S} \right) \cdot \left[\left(\Delta T_{OL} - \Delta T_{OR} \right) \cdot y_1 + \left(\Delta T_{IL} - \Delta T_{IR} \right) \cdot y_2 \right] \cdot \sin(\eta) \qquad \text{[Eqn. H39]}$$

H.3.3. DERIVATION OF $N_{\delta T}$

A top view of the megatransport is shown in Figure H5, along with the y-axis moment-arm of each engine. A yawing moment due to thrust will occur when the thrust along the x-axis on one side of the aircraft exceeds the x-axis component of thrust on the other side. The yawing moment of the megatransport due to asymmetric thrust is:

$$N_{X_{\delta T}} = \Delta T_{OL} \cdot \cos(\eta) \cdot y_1 + \Delta T_{IL} \cdot \cos(\eta) \cdot y_2 - \Delta T_{IR} \cdot \cos(\eta) \cdot y_2 - \Delta T_{OR} \cdot \cos(\eta) \cdot y_1 \qquad \text{[Eqn. H40]}$$

$$N_{X_{\delta T}} = \left[\left(\Delta T_{OL} - \Delta T_{OR} \right) \cdot y_1 + \left(\Delta T_{IL} - \Delta T_{IR} \right) \cdot y_2 \right] \cdot \cos(\eta) \qquad \text{[Eqn. H41]}$$

The conventional control derivatives, $N_{\delta A}$ and $N_{\delta R}$, divide the moment term by the aircraft stability-axis yaw inertia, I_{ZZ_S}, giving $N_{\delta A}$ and $N_{\delta R}$ the

dimension of sec^{-2}. Dividing $N_{X_{\delta T}}$ by the megatransport yaw inertia gives the thrust stability derivative, $N_{\delta T}$:

$$N_{\delta T} = \left(N_{X_{\delta T}} / I_{zz_S} \right) \qquad \text{[Eqn. H42]}$$

$$N_{\delta T} = \left(1 / I_{zz_S} \right) \cdot \left[\left(\Delta T_{OL} - \Delta T_{OR} \right) \cdot y_1 + \left(\Delta T_{IL} - \Delta T_{IR} \right) \cdot y_2 \right] \cdot \cos(\eta) \qquad \text{[Eqn. H43]}$$

H.3.4. CALCULATION OF THE LATERAL-DIRECTIONAL THRUST NUMERATOR

Again, the megatransport engines have a cant angle of 2 degrees:

- η = 2 degrees

The y-axis moment-arms from each engine to the center of gravity, y_1 and y_2, are given below:

- y_1 = 103.35 ft
- y_2 = 59.63 ft

The roll and yaw inertias used were:

- I_{xx_S} = 57,874,253 sl-ft^2

- $I_{ZZS} = 114{,}275{,}412$ sl-ft^2

These stability-axis inertias were calculated for a 5 degree angle of attack using the body-axis inertias calculated in Chapter 3.

In the approach condition, each engine was trimmed at 44,000 pounds of thrust apiece. To generate a lateral-directional frequency sweep, each engine contributed an average change in thrust of +/-4,000 pounds from the trimmed flight condition.

For the lateral-directional case, if thrust was increased on both engines on the left side of the aircraft, it was decreased the same amount on the other two engines on the right side of the aircraft. The thrust was then decreased on the left side of the aircraft and increased on the right side of the aircraft.

This differential thrust was pulsed sinusoidally to generate the lateral-directional frequency sweep. Therefore, the change in thrust output of the engines on the same side of the aircraft is equal but opposite in sign to the change in thrust output of the engines on the other side of the aircraft:

$$\Delta T_{OL} = \Delta T_{IL} = \pm 4{,}000 \text{ lb} \qquad \text{[Eqn. H44]}$$

$$\Delta T_{OR} = \Delta T_{IR} = \mp 4{,}000 \text{ lb} \qquad \text{[Eqn. H45]}$$

Substituting the previously mentioned numerical values into Equations H39 and H43:

$$L_{\delta T} = (1/57{,}874{,}253)\cdot\left[\left(4{,}000-(-4{,}000)\right)\cdot(103.35) + \left(4{,}000-(-4{,}000)\right)\cdot(59.63)\right]\cdot\sin(2^\circ) \quad \text{[Eqn. H46]}$$

$$L_{\delta T} = 0.0008 \text{ sec}^{-2} \quad \text{[Eqn. H47]}$$

$$N_{\delta T} = (1/114{,}275{,}412)\cdot\left[\left(4{,}000-(-4{,}000)\right)\cdot(103.35) + \left(4{,}000-(-4{,}000)\right)\cdot(59.63)\right]\cdot\cos(2^\circ) \quad \text{[Eqn. H48]}$$

$$N_{\delta T} = 0.0114 \text{ sec}^{-2} \quad \text{[Eqn. H49]}$$

As can be seen from these values, $N_{\delta T}$ is several orders of magnitude larger than $L_{\delta T}$. Again, this result is not surprising considering the fact that the thrust in the z-direction is very small compared to the thrust along the x-axis. These values confirm the fact that differential thrust primarily generates yaw, not roll. Roll is generated indirectly due to the dihedral of the wing rather than directly by a large thrust rolling moment.

The numerical values for $Y_{\delta T}$, $L_{\delta T}$, and $N_{\delta T}$ are substituted for the values of $Y_{\delta A}$, $L_{\delta A}$, $N_{\delta A}$, $Y_{\delta R}$, $L_{\delta R}$, and $N_{\delta R}$ into the equation for N_ϕ as described in Reference 18. After substituting in values for all the variables, the equation for N_ϕ becomes:

$$N_\phi = 0.137s^2 + 3.793s + 9.244 \quad \text{[Eqn. H50]}$$

Combining the bank angle numerator, N_ϕ, with the megatransport lateral-directional transfer function denominator calculated in Chapter 3, the

transfer function equation which relates the bank angle to an asymmetric change in the actual engine thrust is:

$$\left(\phi/\delta T_{actual}\right)_{asym} = \frac{0.137s^2 + 3.793s + 9.244}{303.662s^4 + 746.104s^3 + 496.103s^2 + 489.681s - 7.061} \qquad \text{[Eqn. H51]}$$

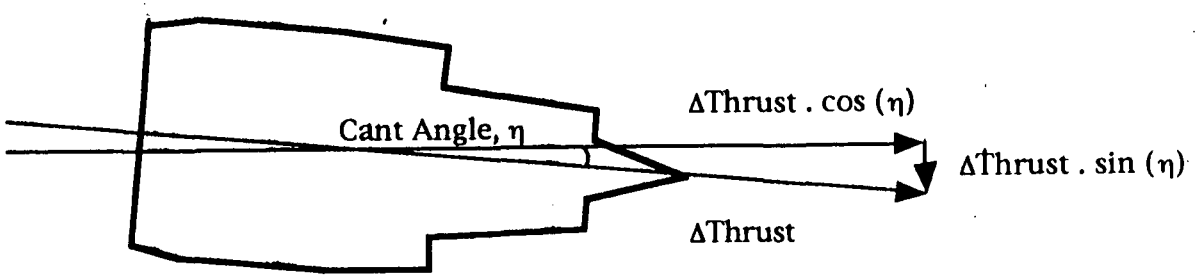

Figure H1 Side View of the Megatransport Engine

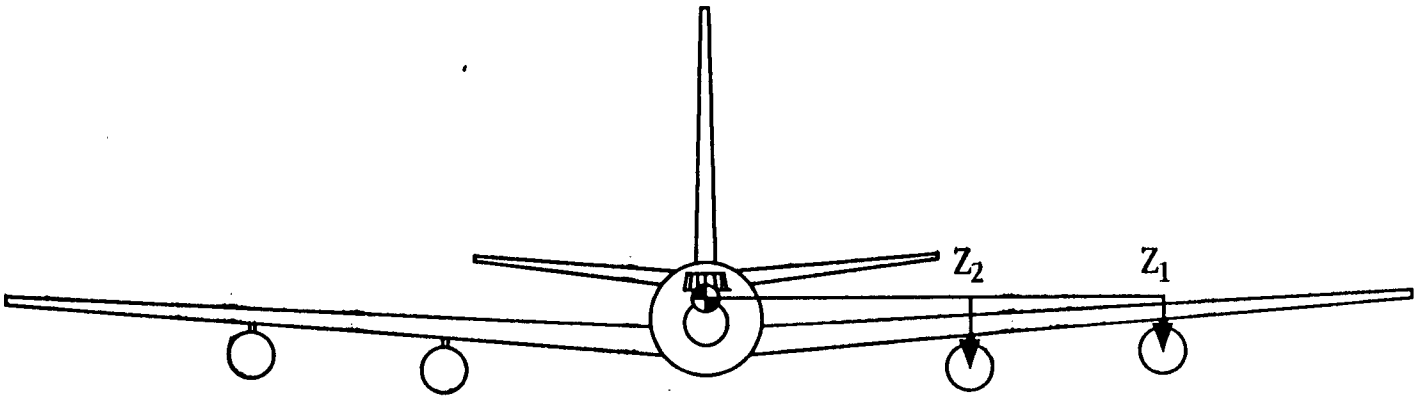

Figure H2 Z-Axis Moment-Arms from the Center of Gravity of the Megatransport to the Center of the Engine

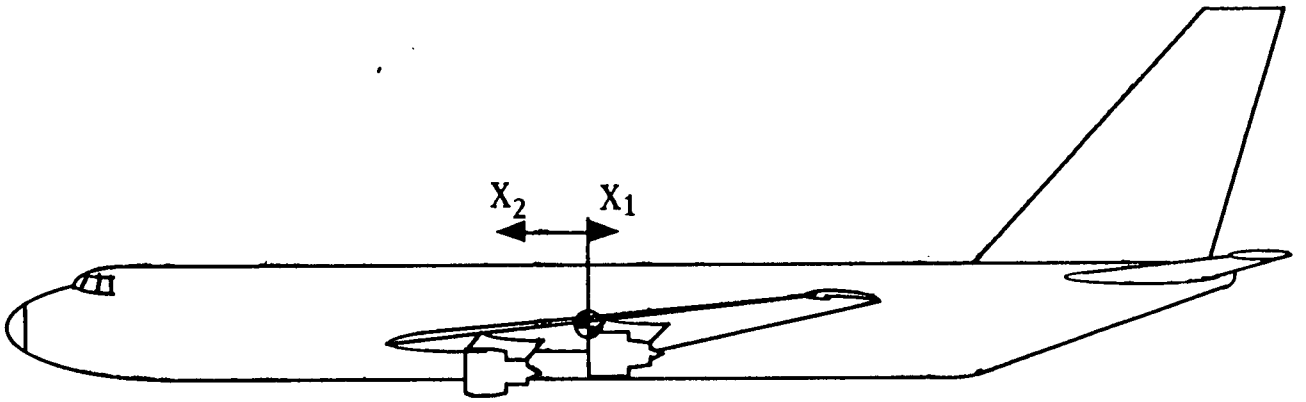

Figure H3 X-Axis Moment-Arms from the Center of Gravity of the Megatransport to the Center of the Engine

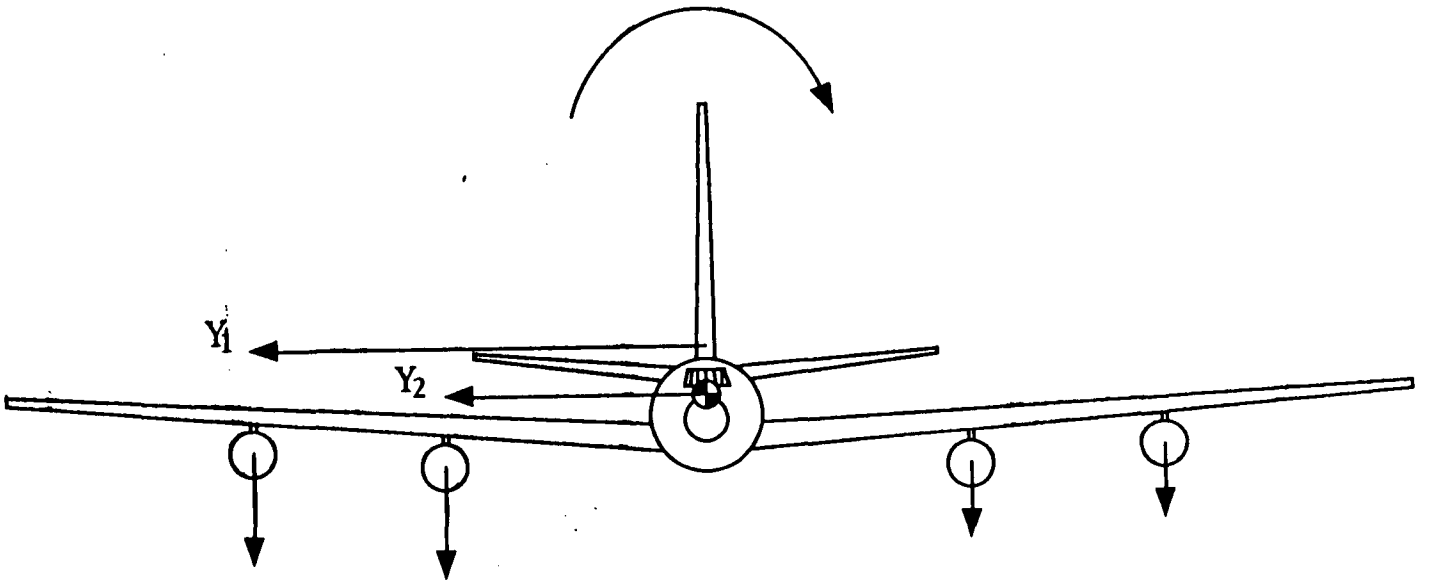

Figure H4 Rolling Moment Due to Downward Component of Asymmetric Thrust

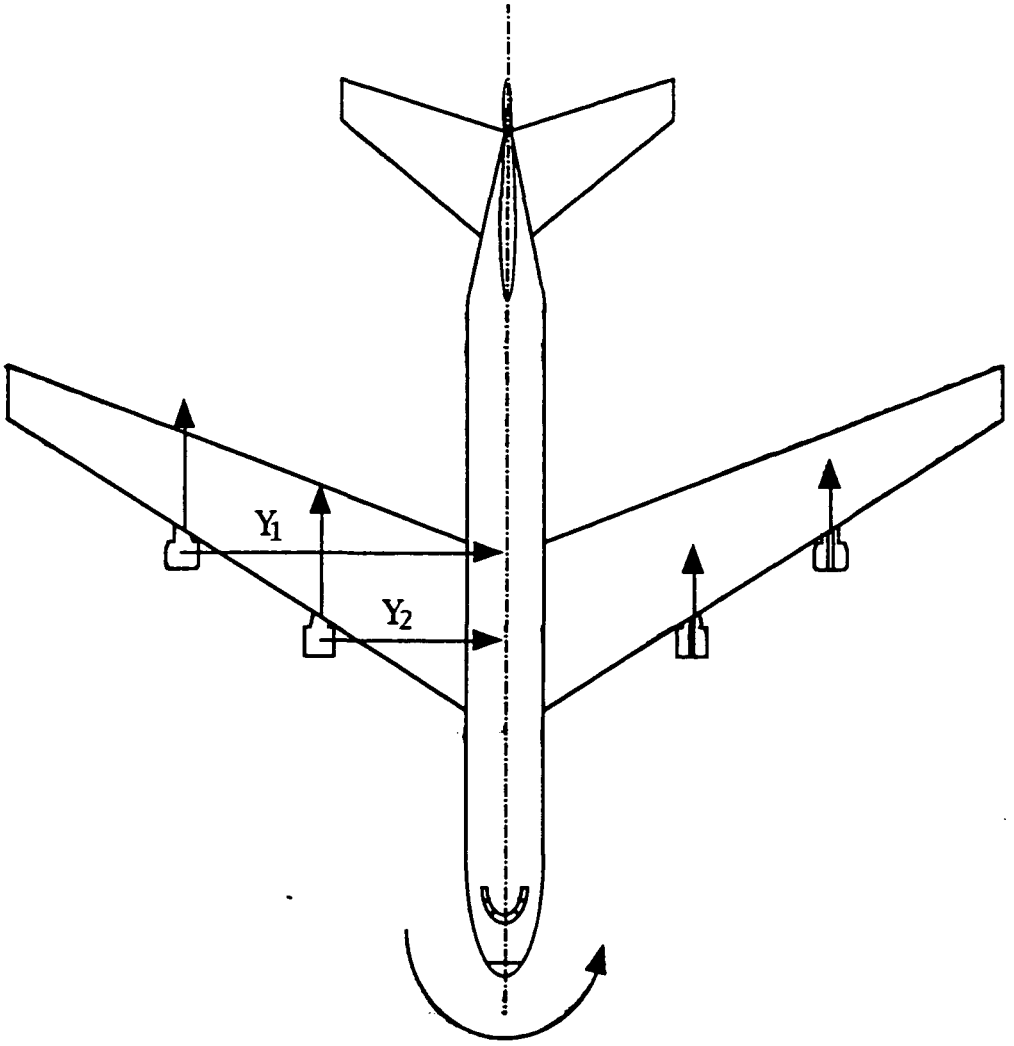

Figure H5 Yawing Moment Due to Axial Component of Asymmetric Thrust

REFERENCES

1. Taylor, J.W.R. , Jane's All the World's Aircraft, Jane's Information Group, Sentinel House, 163 Brighton Rd., Coulsdon, Surrey, CR5 2NH, UK, 1984 - 1985.

2. National Transportation Safety Board, Aircraft Accident Report, PB90-910406, NTSB/AAR-90/06, United Airlines Flight 232, McDonnell Douglas DC-10-10, Sioux Gateway Airport, Sioux City, Iowa, July 19, 1989.

3. Hughes, David, and Michael A. Dornheim, *United DC-10 Crashes in Sioux City, Iowa,* Aviation Week & Space Technology: Vol. 131, No. 4, 96 - 97, July 24, 1989.

4. Ott, James, *Probe Focuses on Failure of Fan Disk in DC-10 Crash,* Aviation Week & Space Technology: Vol. 131, No. 5, 30 - 31, July 31, 1989.

5. Ott, James, *Investigators Find Reconstructed Tail of DC-10 Riddled with Damage,* Aviation Week & Space Technology: Vol. 131, No. 6, 22 - 23, August 7, 1989.

6. Lacagnina, Mark, *Locked Controls at 37,000 Feet in a DC-10,* Aviation Safety: Vol. XI, No. 7, 4 - 6, April 1, 1991.

7. Burcham, F., Jr., C. Fullerton, G. Gilyard, T. Wolf, and J. Stewart, "A Preliminary Investigation of the Use of Throttles for Emergency Flight Control", NASA TM-4320, 1991.

8. Dornheim, Michael A., *NASA Develops Software to Control Aircraft With Throttles Alone,* Aviation Week & Space Technology: Vol. 134, No. 25, 42, June 24, 1991.

9. Gilyard, Glenn B., Joseph L. Conley, Jeanette L. Le, and Frank W. Burcham, Jr., "A Simulation Evaluation of a Four-Engine Jet Transport Using Engine Thrust Modulation for Flightpath Control", NASA TM-4324, September 1991.

10. Burcham, Frank W., Jr., and C. Gorden Fullerton, "Controlling Crippled Aircraft - With Throttles", NASA TM-104238, 1991.

11. Burcham, Frank W., Jr., Trindel Maine, and Thomas Wolf, "Flight Testing and Simulation of an F-15 Airplane Using Throttles for Flight Control", NASA TM-104255, August 1992.

12. Shifrin, Carole A., *New Jumbos, SSTs Face Tough Hurdles,* Aviation Week & Space Technology: Vol. 141, No. 21, 42 - 43, November 21, 1994.

13. Mecham, Michael, and James T. McKenna, *Cost, Not Size, To Drive Success Of Superjumbo,* Aviation Week & Space Technology: Vol. 141, No. 21, 45 - 46, November 21, 1994.

14. Casad, Michael, artist's rendering of Boeing New Large Airplane (NLA) concept, Aviation Week & Space Technology: Vol. 141, No. 21, cover page, November 21, 1994.

15. Proctor, Paul, *Boeing Refines Designs For 600-Seat NLA,* Aviation Week & Space Technology: Vol. 141, No. 21, 48 - 53, November 21, 1994.

16. Sparaco, Pierre, *Airbus Weighs Four A3XX Versions,* Aviation Week & Space Technology: Vol. 141, No. 21, 54, November 21, 1994.

17. Gerren, Donna S., "Design, Analysis, and Control of Large Transport Aircraft Utilizing Engine Thrust as a Backup System for the Primary Flight Controls", University of Kansas, Department of Aerospace Engineering, NASA CR-192938, February 1993.

18. Roskam, Jan, Airplane Flight Dynamics and Automatic Flight Controls: Part I, Roskam Aviation and Engineering Corporation, 120 East Ninth, Suite 2, Lawrence, Kansas, Second Printing, 1982.

19. NASA Dryden Flight Research Center F-15 Simulation Data

20. Taylor, J.W.R. , Jane's All the World's Aircraft, Jane's Information Group, Sentinel House, 163 Brighton Rd., Coulsdon, Surrey, CR5 2NH, UK, 1993 - 1994.

21. Propulsion Controlled Aircraft (PCA) MD-11 Simulator Demonstration briefing at Douglas Aircraft Company, Long Beach, California, August 6, 1992.

22. Internal memo at NASA Dryden Flight Research Center, Edwards, California, from Bill Burcham concerning MD-11, Ship 506, Flight 51, September 13, 1992.

23. Internal memo at NASA Dryden Flight Research Center, Edwards, California, from Bill Burcham concerning first PCA flight, January 25, 1993.

24. Internal memo at NASA Dryden Flight Research Center, Edwards, California, from Bill Burcham concerning PCA progress, January 27, 1993.

25. Internal memo at NASA Dryden Flight Research Center, Edwards, California, from Bill Burcham concerning F-15 PCA status, February 16, 1993.

26. Internal memo at NASA Dryden Flight Research Center, Edwards, California, from Bill Burcham concerning PCA flight to 10 feet, February 5, 1993.

27. Internal memo at NASA Dryden Flight Research Center, Edwards, California, from Bill Burcham concerning PCA news, April 21, 1993.

28. Internal memo at NASA Dryden Flight Research Center, Edwards, California, from Bill Burcham concerning PCA guest pilot, September 1, 1993.

29. Internal memo at NASA Dryden Flight Research Center, Edwards, California, from Bill Burcham concerning PCA USAF guest pilot, September 17, 1993.

30. Internal memo at NASA Dryden Flight Research Center, Edwards, California, from Bill Burcham concerning PCA to M=0.87 at 37,000 feet, October 26, 1993.

31. *F-15 Highly Integrated Digital Electronic Control Aircraft Retires,* The X-Press, NASA Ames Research Center/Dryden Flight Research Facility: Vol. 35, Issue 22, 2, December, 1993.

32. FAR 25, Airworthiness Standards: Transport Category Airplanes, Federal Aviation Agency, Washington, D.C., November 1984.

33. FAR 121, Certification and Operations: Domestic, Flag, and Supplemental Air Carriers and Commercial Operators of Large Aircraft, Federal Aviation Agency, Washington, D.C., October 1985.

34. Roskam, Jan, Airplane Design - Part I: Preliminary Sizing of Airplanes, Roskam Aviation and Engineering Corporation, 120 East Ninth, Suite 2, Lawrence, Kansas, Second Printing, 1989.

35. Roskam, Jan, Airplane Design - Part II: Preliminary Configuration Design and Integration of the Propulsion System, Roskam Aviation and Engineering Corporation, 120 East Ninth, Suite 2, Lawrence, Kansas, Second Printing, 1989.

36. Roskam, Jan, Airplane Design - Part III: Layout Design of Cockpit, Fuselage, Wing and Empennage: Cutaways and Inboard Profiles, Roskam Aviation and Engineering Corporation, 120 East Ninth, Suite 2, Lawrence, Kansas, Second Printing, 1989.

37. Roskam, Jan, Airplane Design - Part IV: Layout Design of Landing Gear and Systems, Roskam Aviation and Engineering Corporation, 120 East Ninth, Suite 2, Lawrence, Kansas, Second Printing, 1989.

38. Roskam, Jan, Airplane Design - Part V: Component Weight Estimation, Roskam Aviation and Engineering Corporation, 120 East Ninth, Suite 2, Lawrence, Kansas, Second Printing, 1989.

39. Roskam, Jan, Airplane Design - Part VI: Preliminary Calculation of Aerodynamic, Thrust and Power Characteristics, Roskam Aviation and Engineering Corporation, 120 East Ninth, Suite 2, Lawrence, Kansas, Second Printing, 1990.

40. Roskam, Jan, Airplane Design - Part VII: Determination of Stability, Control and Performance Characteristics: FAR and Military Requirements, Roskam Aviation and Engineering Corporation, 120 East Ninth, Suite 2, Lawrence, Kansas, First Printing, 1988.

41. MIL-F-8785C (USAF), Military Specification - Flying Qualities of Piloted Airplanes, November 5, 1980.

42. User's Manual for Steady State Performance: Customer Computer Deck - PW4084 Study Simulation, Pratt & Whitney Division of United Technologies Corporation, May 15, 1993.

43. Torenbeek, E., "Development and Application of a Comprehensive, Design-Sensitive Weight Prediction Method for Wing Structures of Transport Category Aircraft", Report LR-693, Delft University Press, Delft, The Netherlands, September 1992.

44. Heffley, Robert K., and Wayne F. Jewell, "Aircraft Handling Qualities Data", STI Technical Report 1004-1, Systems Technology, Inc., Hawthorne, California, May 1972.

45. Teper, Gary L., "Aircraft Stability and Control Data", STI Technical Report 176-1, Systems Technology, Inc., Hawthorne, California, April 1969.

46. Advanced Aircraft Analysis (AAA) Computer Program, Version 1.4, Design, Analysis and Research Corporation, 120 East Ninth, Suite 2, Lawrence, Kansas, 1993.

47. Propulsion Controlled Aircraft - Critical Design Review, McDonnell Douglas Corporation, 3 - 4 June, 1992.

48. Kandebo, Stanley W., *Higher Thrust PW4000 Planned For 1996,* Aviation Week & Space Technology: Vol. 141, No. 6, 32, August 8, 1994.

49. Roskam, Jan, Airplane Flight Dynamics and Automatic Flight Controls: Part II, Roskam Aviation and Engineering Corporation, 120 East Ninth, Suite 2, Lawrence, Kansas, First Printing, 1979.

50. Hoak, D. E., et al, USAF Stability and Control Datcom, Flight Control Division, Air Force Flight Dynamics Laboratory, Wright Patterson Air Force Base, Ohio, 1978, revised.

51. Weingarten, Norman C., and Charles R. Chalk, "In-Flight Investigation of Large Airplane Flying Qualities for Approach and Landing", Technical Report AFWAL-TR-81-3118, Calspan, Buffalo, New York, September 1981.

52. Little, John N., and Loren Shure, Signal Processing Toolbox for Use with MATLAB, The Math Works, Inc., 1993.

53. Bendat, Julius S., and Allan G. Piersol, Engineering Applications of Correlation and Spectral Analysis, John Wiley & Sons, Inc., Second Edition, 1993.

54. Hoh, Roger H., et al, "Proposed MIL Standard and Handbook - Flying Qualities of Air Vehicles: Volume II", Technical Report AFWAL-TR-82-3081, Vol. II, Systems Technology, Inc., Hawthorne, California, and McDonnell Aircraft Co., St. Louis, Missouri, November 1982.

55. Bauerfeind, Klaus, "Some General Topics in the Field of Engine Handling", AGARD Conference Proceedings No. 324 - Engine Handling, Paper No. 1, October 11 - 14, 1982.

56. Koff, Bernard L., "Designing For Fighter Engine Transients", AGARD Conference Proceedings No. 324 - Engine Handling, Paper No. 2, October 11 - 14, 1982.

57. Patterson, Grant T., "Techniques For Determining Engine Stall Recovery Characteristics", AGARD Conference Proceedings No. 324 - Engine Handling, Paper No. 28, October 11 - 14, 1982.

58. Conversation with Dr. Jan Roskam, University of Kansas, November 17, 1992.

59. Conversation with NASA propulsion engineer Tim Conners, November 19, 1992.

60. Conversation with Lt. Coyne, Wright Patterson Air Force Base, November 1992.

61. Kandebo, Stanley W., *Pratt Engine Meets Phase 1 IHPTET Goals,* Aviation Week & Space Technology: Vol. 141, No. 20, 38 - 39, November 14, 1994.

62. Presentation given by Mike Robinson at NASA Dryden on thrust vectoring, Rockwell International, May 27, 1993.

63. Grantham, William D., et al, "Simulator Study of Flight Characteristics of Several Large, Dissimilar, Cargo Transport Airplanes During Approach and Landing", NASA Technical Paper 2357, 1984.

64. *NTSB Probes DC-10 Cargo Door Devices,* Aviation Week & Space Technology: Vol. 96, No. 25, 23, June 19, 1972.

65. *Cargo Door Focus of Paris Crash Study,* Aviation Week & Space Technology: Vol. 100, No. 10, 198 - 199, March 11, 1974.

66. *DC-10 Evidence Points to Cargo Door,* Aviation Week & Space Technology: Vol. 100, No. 13, 26 - 27, April 1, 1974.

67. *C-5 Crash Cause Sought,* Aviation Week & Space Technology: Vol. 102, No. 15, 18, April 14, 1975.

68. Internal memo at NASA Dryden Flight Research Center, Edwards, California, from Bill Burcham concerning C-5 loss of flight control, May 29, 1992.

69. McMahan, Jack, *Flight 1080,* Air Line Pilot , July 1978.

70. *Japan Orders Checks of 747 Tail Sections After JAL Crash,* Aviation Week and Space Technology: Vol. 123, No. 7, 30, August 19, 1985.

71. *JAL Crash Inquiry Team Examining Damage in Aft Pressure Bulkhead,* Aviation Week and Space Technology: Vol. 123, No. 8, 28 - 30, August 26, 1985.

72. *JAL Crash Investigators Set to Transfer Wreckage,* Aviation Week and Space Technology: Vol. 123, No. 9, 33, September 2, 1985.

73. *Inquiry Committee Analyzes JAL 747 Flight Data Recorder,* Aviation Week and Space Technology: Vol. 123, No. 10, 97, September 9, 1985.

74. *747 Inquiry Team Examines Repaired Bulkhead Replicas,* Aviation Week and Space Technology: Vol. 123, No. 11, 31, September 16, 1985.

75. *Limited Repairs to Follow 747 Bulkhead Review,* Aviation Week and Space Technology: Vol. 123, No. 12, 28, September 23, 1985.

76. Handout of engine information from Bill Burcham, August 12, 1992.

77. NASA biographical data on Gordon Fullerton, NASA Dryden Flight Research Center, March 1991.